HIGH THROUGHPUT EXPERIMENTATION AS A GUIDE TO THE CONTINUOUS FLOW SYNTHESIS OF ACTIVE PHARMACEUTICAL INGREDIENTS

by

Zinia Jaman

A Dissertation

Submitted to the Faculty of Purdue University

In Partial Fulfillment of the Requirements for the degree of

Doctor of Philosophy

Department of Chemistry

West Lafayette, Indiana

May 2019

THE PURDUE UNIVERSITY GRADUATE SCHOOL
STATEMENT OF COMMITTEE APPROVAL

Dr. David H. Thompson, Chair
Department of Chemistry
Dr. Mingji Dai
Department of Chemistry
Dr. R. Graham Cooks
Department of Chemistry
Dr. Christopher Uyeda
Department of Chemistry

Approved by:
Dr. Christine Hrycyna
Head of the Graduate Program

To Almighty

ACKNOWLEDGMENTS

At first, I would like to express my sincere gratitude to my advisor Prof. David H. Thompson for his continuous support on my Ph.D. study and related research, for his patience, motivation, and immense knowledge. His guidance helped me in all the time of research and writing of this thesis. He is also exceptionally generous and would frequently take us for outings to let us know our work is appreciated. I would like to thank my advisor one more time for giving me a home in his lab and support over the years. I could not have imagined having a better advisor and mentor for my Ph.D. study. His advice on presentation skills, and being confident in myself will be something that I will always remember in the rest of my life. I would also like to thank my committee members Prof. Mingji Dai, and Prof. Christopher Uyeda for all of their support. Special thanks to Prof. R. Graham Cooks, who is not only my committee member but also the principal investigator of the DARPA project, for his insightful comments and encouragement.

I am especially thankful to my fellow members of Thompson Lab. There is no way to express how much it meant to me to have been a member of this lab. I got the best possible support from them. This is my another sweet, cute family. I will definitely miss them when I leave Purdue, especially our lunch time. I would particularly like to acknowledge Dr. Vivek D. Badwaik, Dr. Yawo A. Mondjinou, Dr. Christopher J. Benjamin for welcoming me into the lab and provided guidance on all the problems of my first year. Special thanks to a great friend, Dr. Vivek D. Badwaik for your continuous support and guidance in all aspects. I would also like to thank Dr. Kyle J. Wright, Ross VerHeul, Minji Ha, Scott Bolton, Shayak Samaddar, Craig Sweet, Terry Villarreal, Rejaul Hoq, Zachary Struzik, Aayush, Kiera Estes, and Robert Nicholas for all their help and support.

I would like to express my very great appreciation to everybody of the DARPA Make-It project, which is a collaboration between members of the Thompson, Cooks, and Nagy groups, where I have worked with as a part. Working on such a large collaboration was the best part of my Ph.D. thesis and I had an incredibly rewarding experience. Dr. Bradley Loren, Dr. Seok-Hee Hyun, Sam Ewan, and Shruti Biyani, I couldn't have asked for better group members to work on this project with. Dr. Bradley Loren, Dr. Michael Wleklinski and Dr. Andy Koswara, are the most encouraging and helpful persons in this project. Brad and Mike, you have been my great mentors

and true friends. I am grateful to Dr. Larisa Avramova, Dr. Christina R. Ferreira, Dr. Tiago J. P. Sobreira, and Dr. Botond Szilagy for their great help and support during working in this DARPA project. Thanks go to Caitlin Falcone, and David Logsdon, who contributed great effort to the atropine and S_NAr projects respectively.

I am grateful to all the talented undergraduate researchers throughout my time at Purdue. Samyukta Sah, Jia Xu, Yuta Moriuchi, Deborah Aremu, and Ahmad Mufti, I am very happy and glad to work with you as a mentor. You have done a lot for me and working with all of you has been a great pleasure, thank you! Mufti, I will always remember your tremendous help and enthusiasm in the continuous flow synthesis part.

I am also grateful to the following university staff: Ann Cripe, Debbie Packer, Lynn Rider, Betty Hatfield, Robert Reason, Brandy McMasters, and Susan McCreery for their unfailing support and assistance and the DARPA for funding the Ph.D. research.

I am extremely grateful to my life-coach, my deceased father Zahiduzzaman: because I owe it all to you. Many Thanks! I miss you a lot, Abbu. Also, I want to thank my mother who is by far the kindest and most reliable person for me. She has done everything she can do and supported mentally a lot. I also want to thank my brother, sister-in-law and the rest of my family members for their unconditional love and support during this journey. I owe thanks to a very special person, my husband, Monzurul Alam, for his continued and unfailing love, support and understanding during my pursuit of a Ph.D. degree that made the completion of thesis possible. You were always around at times I thought that it is impossible to continue, you helped me to keep things in perspective. My heartfelt regard goes to my father-in-law, mother-in-law for their love and moral support. I consider myself the luckiest in the world to have such a lovely and caring family, standing beside me with their love and unconditional support.

Words are not enough to say thank to the Almighty for giving me the strength and patience to work through all these years so that today I can finish my Ph.D.

TABLE OF CONTENTS

LIST OF TABLES 10
LIST OF FIGURES 12
ABSTRACT 15
CHAPTER 1. INTRODUCTION 17
1.1 Introduction 17
1.2 References 18
CHAPTER 2. REACTION SCREENING AND OPTIMIZATION OF CONTINUOUS FLOW ATROPINE SYNTHESIS BY PREPARATIVE ELECTROSPRAY MASS SPECTROMETRY 21
2.1 Introduction 21
2.1.1 Continuous Flow Synthesis 21
2.1.2 Accelerated Reaction Screening using Electrospray Ionization (EESI) Technique 22
2.1.3 Brief Summary of this Chapter 22
2.2 Results and Discussion 23
2.2.1 Preparation of Atropine Intermediate by Electrospray 23
2.2.2 Synthesis of Atropine Intermediate in Flow 25
2.2.3 Preparation of Atropine by Electrospray 26
2.2.4 Preparation of Atropine in Flow in Two Chips 27
2.2.5 Preparation of Atropine by Extractive Electrospray 31
2.2.6 Continuous Microfluidic Synthesis of Atropine 32
2.2.7 Comparison of Preparative ES and Microfluidics 33
2.3 Experimental 35
2.3.1 Chemicals 35
2.3.2 Mass Spectrometer 35
2.3.3 Microfluidics 35
2.3.4 HPLC-MS Analysis 36
2.3.5 RP-UPLC Analysis 36
2.3.6 NMR Analysis 37
2.3.7 Preparative Electrospray 37

2.3.8 Preparative Reactive EES 37
2.3.9 Synthesis of Intermediates in Preparative ES 38
2.3.10 Synthesis of Intermediates in Microfluidics 38
2.3.11 Synthesis of Atropine in Preparative ES 38
2.3.12 Synthesis of Atropine in Preparative EES 39
2.3.13 Synthesis of Atropine **1** in Microfluidics in Two Chips 39
2.3.14 Continuous Microfluidic Synthesis of Atropine 39
2.4 Conclusion 39
2.5 Acknowledgements 40
2.6 References 41
CHAPTER 3. HIGH THROUGHPUT EXPERIMENTATION AND CONTINUOUS FLOW VALIDATION OF SUZUKI-MIYAURA CROSS-COUPLING REACTIONS 45
3.1 Introduction 45
3.1.1 Brief Summary of this Chapter 47
3.2 Results and Discussion 47
3.2.1 High Throughput Experimentation 47
3.2.2 Microfluidic Evaluation of HT Experimentation Leads 53
3.3 Experimental 56
3.3.1 Chemicals 56
3.3.2 Liquid Handling Robot 56
3.3.3 Customized Heating Block 57
3.3.4 Mass Spectrometry 57
3.3.5 Microfluidics 57
3.3.6 HPLC/MS-MS Analysis 57
3.3.7 High Throughput Bulk Screening 58
3.3.8 MS data analysis procedure 59
3.3.9 Microfluidic Reactions 59
3.4 Conclusion 60
3.5 Acknowledgements 60
3.6 References 61

CHAPTER 4. ON-DEMAND RAPID SYNTHESIS OF LOMUSTINE UNDER CONTINUOUS FLOW CONDITIONS 64
4.1 Introduction 64
4.1.1 Brief Summary of this Chapter 66
4.2 Results and Discussion 66
4.2.1 Continuous Synthesis of 1-(2-Chloroethyl)-3-cyclohexylurea, **3** 66
4.2.2 Synthesis of Lomustine, Guided by DESI-MS High Throughput Experimentation... 69
4.2.3 Nitrosation Reaction Optimization in Continuous Flow 70
4.2.4 Telescoped synthesis of Lomustine 74
4.3 Experimental 76
4.3.1 Chemicals 76
4.3.2 Liquid Handling Robot 77
4.3.3 Mass Spectrometer 77
4.3.4 Microfluidics 77
4.3.5 HPLC-MS Analysis 78
4.3.6 DESI-MS Analysis 78
4.3.7 NMR Analysis 79
4.3.8 Carbamylation of Cyclohexylamine 79
4.3.9 Preparation of Reaction (Master) Plates and Stamping on DESI-MS Slides 82
4.3.10 Nitrosation of 1-(2-chloroethyl)-3-cyclohexylurea, **3** 83
4.3.11 Telescoped Synthesis of Lomustine 86
4.4 Conclusion 89
4.5 References 89
CHAPTER 5. HIGH THROUGHPUT EXPERIMENTATION AND CONTINUOUS FLOW VALIDATION OF NUCLEOPHILIC AROMATIC SUBSTITUTION REACTIONS 94
5.1 Introduction 94
5.1.1 Brief Summary of this Chapter 95
5.2 Results and Discussion 95
5.2.1 High throughput experimentation (HTE) 95
5.2.2 Microfluidic Evaluation. 104

5.3 Experimental 107
5.3.1 Chemicals 107
5.3.2 Liquid Handling Robot 107
5.3.3 Customized Heating Block 108
5.3.4 DESI-MS Analysis 108
5.3.5 DESI-MS Analysis Software (CHRIS) 109
5.3.6 Mass Spectrometer 109
5.3.7 Microfluidics 109
5.3.8 High Throughput Experimentation: 109
5.3.9 Microfluidic Validation 110
5.4 Conclusion 110
5.5 References 111
APPENDIX A 116
APPENDIX B 141
APPENDIX C 155
APPENDIX D 174
VITA 186
LIST OF PUBLICATIONS 191

LIST OF TABLES

Table 2.1 Comparison of percent conversion to atropine and byproducts 29

Table 2.2 Comparison of conversion of atropine in different base..... 30

Table 2.3 Comparison of percent conversion of byproducts in different bases..... 30

Table 3.1 HTE outcomes as a function of reagent addition order and substrate concentration in the reaction mixture. Each quantity is an average of two experimental measurements. Each set of similar substrates and stoichiometries appears as a set of four conditions wherein the top left, top right, bottom left and bottom right entries are reactions run at 200 °C, 150 °C, 100 °C and 50 °C, respectively. The first two columns (St. = **1**:0) and last four columns (St. = (R'X:0 and 0:0) are the negative controls. Sub = substrates; St = stoichiometry. 49

Table 3.2 Product peak intensities observed for 504 unique S-M reactions run in bulk mode with the order of addition of base solution after the catalyst. Each quantity is an average of two experimental measurements. Each row indicates reactions of nine ratios of substrates including the control reactions at two different temperatures. Each set of similar substrates and stoichiometries appears as a set of four conditions wherein the top left, top right, bottom left and bottom right entries are reactions run at 200 °C, 150 °C, 100 °C and 50 °C, respectively. The first two columns (St. = **1**:0) and last four columns (St. = (R'X:0 and 0:0) are the negative controls. Sub = substrates; St = stoichiometry. 52

Table 3.3 Comparison of microfluidic and bulk screening outcomes for S-M reactions performed under similar conditions using 200 mmol substrate loading and a 1:1 4-hydroxyphenylboronic acid:aryl halide stoichiometry. In the microfluidic reaction tables, time is reported in min and temperature in °C. 54

Table 3.4: Comparison of microfluidic and bulk screening outcomes for S-M reactions that gave negative bulk reaction results. The same reaction conditions were used in each case with 200 mmol substrate loading and 1:20 4-hydroxyphenylboronic acid:aryl halide stoichiometry. In the microfluidic reaction tables, the units are time in min and temperature in °C. 55

Table 3.5 Quantified yields of some S-M microfluidic reactions using HPLC/MS-MS. The same reaction conditions were used in each case (i.e., 200 mmol substrate loading and 1:1 4-hydroxyphenylboronic acid:aryl halide stoichiometry). Peak intensity values are multiples of 1×10^6..... 55

Table 4.1: Reaction conditions evaluated for the synthesis of **3** in flow using a Chemtrix S1 glass system fitted with a 3225 SOR reactor chip. 68

Table 4.2 Isolated yields of lomustine under different reaction conditions using **4** as the nitrosation reagent. Temperture = 0 °C, solvent = MeOH:H_2O (4:1)..... 72

Table 4.3 Synthesis of lomustine under at different reaction conditions using **5** as the nitrosation reagent. 73

Table 4.4 Lomustine synthesis yields for telescoped reactions under different reagents, residence time, stoichiometry, and temperature conditions. 75

Table 5.1: A) The DESI and B) bulk HTE result of the same set of reaction condition. The conditions are, spray solvent: methanol; reaction solvent: NMP; base: DIPEA. C) Same B

condition but the spray solvent is methanol with 1% formic acid, FA D) Same condition as C, but the solvent is 1,4 dioxane. 97

Table 5.2: Summary of Round 1 S_NAr reaction. FA=formic acid 100

Table 5.3. Summary of Round 2 S_NAr HTE reactions. The bulk reaction results are reported for three different the time points. 104

LIST OF FIGURES

Figure 2.1 Preparative ES. A high voltage is applied to the solvent through a syringe and the use of nitrogen nebulizes the liquid sample. The spray droplets are deposited on the glass wool for analysis. 24

Figure 2.2 Mass spectra of preparative ES deposited material. a) The full scan positive ion mode spectrum of the deposited material from the preparative ES reaction of tropine **2**, phenylacetyl chloride **5** and HCl in dioxane yielding a percent conversion to intermediate of 29.5%. b) The full scan positive ion mode spectrum of the deposited material from the preparative ES reaction of tropine **2**, and phenylacetyl chloride **5** in DMA yielding a percent conversion to intermediate of 55.3%. 25

Figure 2.3 Synthesis of Atropine in flow in two chips. A=Tropine; B=Phenylacetyl chloride, D=Base + Formaldehyde; E=Water 28

Figure 2.4 Preparative reactive EES. A high voltage is applied to the solvent through a platinum electrode and the use of nitrogen nebulizes the liquid sample. The ES emitters are positioned at an angle of 22.5^0 and the point of intersection for the spray plumes is 4 cm. The spray droplets are deposited on the glass wool for analysis. 31

Figure 2.5 Mass spectrum of preparative ES deposited material. The full scan positive ion mode spectrum of the deposited material from the preparative reactive EES synthesis of atropine. 32

Figure 2.6 Continues flow synthesis of atropine in separate reactors..... 33

Figure 2.7 Mass spectra of microfluidic and preparative ES products using 3 different bases. a) The full scan positive ion mode spectrum of atropine synthesis using 1,5-diazabicyclo[4.3.0]non-5-ene in microfluidics. b) The full scan positive ion mode spectrum of atropine synthesis using 1,5-diazabicyclo[4.3.0]non-5-ene in preparative ES. c) The full scan positive ion mode spectrum of atropine synthesis using potassium methoxide in microfluidics. d) The full scan positive ion mode spectrum of atropine synthesis using potassium methoxide in preparative ES. e) The full scan positive ion mode spectrum of atropine synthesis using sodium hydroxide in microfluidics. f) The full scan positive ion mode spectrum of atropine synthesis using sodium hydroxide in preparative ES. 34

Figure 3.1 Biologically and materially important synthons containing common [1,1'-biphenyl]-4-ol cores. 46

Figure 3.2 Comparative coupling efficiencies for anisole-type biphenyl products formed under different temperature, and stoichiometric conditions. Reactant concentrations were 200 mmol except for **1**+**5** that was run at 100 mmol, 400 mmol DBU, and 10% XPhosPdG3. A = **1**+**2**; B = **1**+**3**; C = **1**+**4**; D = **1**+**5**. 50

Figure 3.3 Comparative coupling efficiencies for aniline-type biphenyl products formed under different temperature and stoichiometric conditions. Reactant concentrations were 200 mmol, 400 mmol DBU, and 10% XPhosPdG3. A = **1**+**6**; B = **1**+**7**; C = **1**+**8**; D = **1**+**10**, E = **1**+**9**, F = **1**+**11**, G = **1**+**12**. 51

Figure 3.4 Chemtrix reactor and fluid handling for continuous flow synthesis of S-M cross coupling reactions. A = 1:1 mixture of 4-hydroxyphenylboronic acid and aryl halide; B = DBU, C = XPhosPdG3. 53

Figure 3.5 Schematic flow of preparation and analysis of microtiter plates for bulk screening of S-M reaction. 59

Figure 3.6 Schematic flow of 384-well plate preparation for MS and analysis using an auto-sampler. 59

Figure 4.1 Microfluidic synthesis of intermediate **3** in a glass reactor chip (Chemtrix SOR 3225). A = **1** in THF; B = **2** in THF, C = TEA in THF. 67

Figure 4.2 DESI-MS plate maps showing the presence or absence of expected ions at each spot where the nitrosation reaction conditions were tested using different stoichiometries and with commercially available standards. Blue dots indicate the presence of the *m/z* 169 expected stable fragment for the reaction product (successful reaction), Red dots indicate that the expected *m/z* for the reaction product was not present at the reaction spot (unsuccessful reaction condition). A: Concentration screening using the lomustine ion (*m/z* 169) intensity and $NaNO_2$ as nitrosation reagent; B: Solvent screening using the lomustine ion (*m/z* 169) intensity and $NaNO_2$ as nitrosation reagent; C: Solvent screening using the lomustine ion (*m/z* 169) intensity and tBuONO as nitrosation reagent. 70

Figure 4.3 Microfluidic synthesis of lomustine using $NaNO_2/HCO_2H$ as nitrosation reagent in a Chemtrix 3225 SOR glass reactor chip. A = **3** in THF; B = HCO_2H (neat), C = $NaNO_2$ in MeOH:H_2O (4:1). 71

Figure 4.4 Microfluidic synthesis of lomustine using **5** as nitrosation reagent in a Chemtrix 3223 SOR glass reactor chip. A = **3** in ACN:EtOH (3.7:1) ; B = **5** in ACN. 73

Figure 4.5 Schematic for the telescoped synthesis of lomustine using $NaNO_2/HCO_2H$ (**4**) as nitrosation reagent. 74

Figure 4.6 Schematic for the final telescoped synthesis of lomustine using **5** as a nitrosation reagent. 76

Figure 4.7 Total ion chromatogram (TIC) from HPLC-MS/MS and comparison between synthesized lomustine (top, red) and commercially available lomustine (bottom, black).76

Figure 4.8 Set up of continuous flow synthesis of **3**, using chemtrix S1 system..... 80

Figure 4.9 Fragments from 1-(2-chloroethyl)-3-cyclohexylurea, **3.**..... 81

Figure 4.10 Full ESI-MS scan of commercially available **3** and synthesized **3** derived from flow under the reaction conditions of 50 °C, 1 min. 81

Figure 4.11 MS/MS of m/z=205 from commercially available **3** and synthesized **3** derived from flow under the reaction conditions of 50 °C, 1 min. 82

Figure 4.12 (left & center) Direct DESI-MS data comparison between the two nitrosation reactions in different solvents. (right) DESI-MS data of commercially available 3 and lomustine standards. The data was analyzed using BioMAP imaging software. 83

Figure 4.13 Comparison of 1H NMR of lomustine synthesized by continuous flow for different methods of purification. Method 1: extraction with Et_2O; method 2: recrystallization from CAN; method 3: hot filtration and recrystallization from petroleum ether 84

Figure 4.14 Fragments of lomustine in MS 84

Figure 4.15 Full MS scan of commercially available lomustine and synthesized lomustine from flow. Reaction conditions were 25 °C, 8 min. 85

Figure 4.16 MS/MS of m/z=169 from commercially available lomustine and synthesized lomustine from flow. Reaction conditions were 25 °C, 8 min. 86

Figure 4.17 TLC monitoring during lomustine synthesis in flow. 88

Figure 4.18 Comparison of TLC of telescoped lomustine synthesis using different equivalents of base 88

Figure 5.1. Heat map of 1,536 reactions of R-1 S_NAr HTE using MeOH with 1% FA as spray solvent under DESI-MS or bulk microtiter plate conditions at 150°C with four different basic condition. A) reaction solvent: NMP; B) reaction solvent: 1,4-dioxane. 99

Figure 5.2. Heat map of 1,536 reactions (768 in DESI and 768 in bulk at three time points) of R-2 S_NAr HTE using MeOH with 1% FA as spray solvent in NMP at A) 150 °C; B) 200 °C. 103

Figure 5.3. Continuous flow synthesis of S_NAr reactions in a glass chip reactor, SOR 3225. A = amine; B=aryl halide; C = DIPEA 105

ABSTRACT

Author: Jaman, Zinia. Ph.D.
Institution: Purdue University
Degree Received: May 2019
Title: High Throughput Experimentation as A Guide to The Continuous Flow Synthesis of Active Pharmaceutical Ingredients.
Committee Chair: David H. Thompson

Continuous flow chemistry for organic synthesis is an emerging technique in academia and industry because of its exceptional heat and mass transfer ability and, in turn, higher productivity in smaller reactor volumes. Preparative electrospray (ES) is a technique that exploits reactions in charged microdroplets that seeks to accelerate chemical synthesis. In Chapter 2, the flow synthesis of atropine, a drug which is included in the WHO list of essential of medicines and currently in shortage according to the U.S Food and Drug Administration (FDA) is reported. The two steps of atropine synthesis were initially optimized separately and then continuously synthesized using two microfluidic chips under individually optimized condition. The telescoped continuous-flow microfluidics experiment gave a 55% conversion with an average of 34% yield in 8 min residence time. In Chapter 3, a robotic HTE technique to execute reactions in 96-well arrays was coupled with fast MS analysis. Palladium-catalyzed Suzuki-Miyaura (S-M) cross-coupling reactions were screened in this system and a heat map was generated to identify the best reaction condition for downstream scale up in continuous flow.

In Chapter 4, an inexpensive and rapid synthesis of an old anticancer drug, lomustine, was synthesized. Using only four inexpensive commercially available starting materials and a total residence time of 9 min, lomustine was prepared via a linear sequence of two chemical reactions performed separately in two telescoped flow reactors. Sequential offline extraction and filtration resulted in 63% overall yield of pure lomustine at a production rate of 110 mg/h. The primary advantage of this approach lies in the rapid manufacture of lomustine with two telescoped steps to avoid isolation and purification of a labile intermediate, thereby decreasing the production cost significantly. A high throughput reaction screening approach based on desorption electrospray ionization mass spectrometry (DESI-MS) is described in Chapter 4 and 5 for finding the heat-map from a set of reaction conditions. DESI-MS is used to quickly explore a large number of reaction

conditions and guide the efficient translation of optimized conditions to continuous flow synthesis that potentially accelerate the process of reaction optimization and discovery. Chapter 5 described HTE of S_NAr reactions using DESI-MS and bulk techniques with 1536 unique reaction conditions explored using both in DESI-MS and bulk reactors. The hotspots from the HTE screening effort were validated using a microfluidic system that confirmed the conditions as true positives or true

INTRODUCTION

1.1 Introduction

Traditionally, organic synthesis is performed in round-bottomed flasks which allows for limited control with lengthy reaction times. Recently continuous flow reactors are gaining traction in the pharmaceutical and fine chemistry industries for the preparation of small and large molecules including active pharmaceutical ingredients (APIs). [1,2] Enhanced heat and mass transfer, controlled flow, ease of integration, flow chemistry on the micro scale, offers precise control of reaction time, efficiency and safety are the key advantages for continuous flow synthesis.[3,4] Generally, reaction optimization and screening require significant investments in time and material.[5,6] Pharmaceutical production still depends on multipurpose batch reactors that requires months to isolate and investigate of the intermediates in several steps.[7] Microreactors can greatly accelerate rapid scanning[8] of reactions and combined with quick analysis using nESI-MS, [9] reduce significant amount of material needed to perform screening, and optimize reaction conditions at higher temperature and pressure that cannot be possible in conventional glassware.[10,11] Microreactors allow these reactions to be screened and optimized at reduced cost due to low material requirements and waste generation.[12,13] The reduced channel widths, together with the exceptional mass-and heat transfer capacity of these reactors, enhance the reaction rate as fast that it is capable to occur a reaction in second.[14] Therefore, it is predictable that continuous flow processes should emerge as an important technique for APIs synthesis.[15,16]. Chapter 1 & 3 describe the design and development of continuous-flow synthesis of APIs, atropine,[17] and lomustine,[18] respectively, which includes small scale synthesis to large scale synthesis in flow system.

High throughput experimentation (HTE) techniques allows the implementation of a large numbers of experiments in parallel spending minimum amount of compounds and time, involving less labor per experiment.[19, 20] The technique can change the lab productivity by rapid generation of comprehensive data and knowledge, both in academic and industry.[19, 21] HTE based on the screening of compounds across a range of settings have spread in the area of not only in biology, drug discovery[22], and medicinal chemistry,[23, 24] but also in other fields such as catalysis.[20, 25, 26] Originally these tools and techniques were used in the field of biology in the 1950s, but are routinely performed for HTE in 1,534 or 3,456-well microtiter plates.[19] However, the analysis is

always a bottleneck because of significantly large time requirement and expenses. HTE coupled with MS analysis speeds up both the discovery and the optimization of reaction conditions, specially in the field of chemical process development.[25, 27, 28] These impacts are particularly evident in the fields of pharmaceutical and biopharmaceutical industries where reduction in the time of experimental cycle is a necessity due to the higher importance of the reaction class.[8, 14] However, HTE is always a challenge in case of organic synthesis because of the presence of solid or volatile organic solvents.[26, 27] Recently, our group reported the high throughput reaction screening using bulk microtiter[20] and desorption electrospray ionization mass spectrometry (DESI-MS) to guide scalable syntheses in continuous flow reactors at scale.[28] DESI is an MS technique that analyses reaction results in droplets within about 1 s. [28] A reliable approach con be able to reduce the analysis time from 2 months to about a day. [28] Bulk microtiter HTE of Suzuki-Miyura cross-coupling reactions are described in Chapter 3 to inform the continuous flow synthesis. An expansion of the HTE studies were used to guide the flow synthesis of lomustine in Chapter 4. A further investigation to find the scope of chemistry explored using both bulk microtiter and DESI-MS HTE techniques for nucleophilic aromatic substitution (S_NAr) is described in Chapter 5.

1.2 References

1. Hessel, V.; Kralisch, D.; Kockmann, N.; Noël, T.; Wang, Q., Novel process windows for enabling, accelerating, and uplifting flow chemistry. *ChemSusChem* **2013,** *6*, 746-789.

2. Yoshida, J.-i.; Takahashi, Y.; Nagaki, A., Flash chemistry: flow chemistry that cannot be done in batch. *ChemComm* **2013,** *49*, 9896-9904.

3. Wegner, J.; Ceylan, S.; Kirschning, A., Ten key issues in modern flow chemistry. *Chem Commun (Camb)* **2011,** *47*, 4583-92.

4. Webb, D.; Jamison, T. F., Continuous flow multi-step organic synthesis. *Chem. Sci.* **2010,** *1*, 675-680.

5. Geyer, K.; Gustafsson, T.; Seeberger, P. H., Developing continuous-flow microreactors as tools for synthetic chemists. *Synlett* **2009**, 2382-2391.

6. Jensen, K. F., Silicon-based microchemical systems: Characteristics and applications. *MRS Bull.* **2006,** *31*, 101-107.

7. Adamo, A.; Beingessner, R. L.; Behnam, M.; Chen, J.; Jamison, T. F.; Jensen, K. F.; Monbaliu, J. C.; Myerson, A. S.; Revalor, E. M.; Snead, D. R.; Stelzer, T.; Weeranoppanant, N.; Wong, S. Y.; Zhang, P., On-demand continuous-flow production of pharmaceuticals in a compact, reconfigurable system. *Science* **2016,** *352*, 61-7.

8. Snead, D. R.; Jamison, T. F., A three-minute synthesis and purification of ibuprofen: pushing the limits of continuous-flow processing. *Angew. Chem. Int. Ed. Engl.* **2015,** *54*, 983-7.

9. Sun, S.; Kennedy, R. T., Droplet electrospray ionization mass spectrometry for high throughput screening for enzyme inhibitors. *Anal. Chem.* **2014,** *86*, 9309-9314.

10. Marre, S.; Adamo, A.; Basak, S.; Aymonier, C.; Jensen, K. F., Design and packaging of microreactors for high pressure and high temperature applications. *Industrial & Engineering Chemistry Research* **2010,** *49*, 11310-11320.

11. Trachsel, F.; Hutter, C.; von Rohr, P. R., Transparent silicon/glass microreactor for high-pressure and high-temperature reactions. *Chem. Eng. J.* **2008,** *135*, S309-S316.

12. Kralisch, D.; Kreisel, G., Assessment of the ecological potential of microreaction technology. *Chem. Eng. Sci.* **2007,** *62*, 1094-1100.

13. Hartman, R. L.; Jensen, K. F., Microchemical systems for continuous-flow synthesis. *Lab Chip* **2009,** *9*, 2495-507.

14. Kim, H.; Min, K. I.; Inoue, K.; Im, D. J.; Kim, D. P.; Yoshida, J., Submillisecond organic synthesis: outpacing Fries rearrangement through microfluidic rapid mixing. *Science* **2016,** *352*, 691-694.

15. Malet-Sanz, L.; Susanne, F., Continuous flow synthesis. A pharma perspective. *J. Med. Chem.* **2012,** *55*, 4062-98.

16. Baxendale, I. R.; Braatz, R. D.; Hodnett, B. K.; Jensen, K. F.; Johnson, M. D.; Sharratt, P.; Sherlock, J. P.; Florence, A. J., Achieving continuous manufacturing: technologies and approaches for synthesis, workup, and isolation of drug substance May 20-21, 2014 continuous manufacturing symposium. *J. Pharm. Sci.* **2015,** *104*, 781-791.

17. Falcone, C. E.; Jaman, Z.; Wleklinski, M.; Koswara, A.; Thompson, D. H.; Cooks, R. G., Reaction screening and optimization of continuous-flow atropine synthesis by preparative electrospray mass spectrometry. *Analyst* **2017,** *142*, 2836-2845.

18. Jaman, Z.; Sobreira, T. J. P.; Mufti, A.; Ferreira, C. R.; Cooks, R. G.; Thompson, D. H., Rapid on-demand synthesis of lomustine under continuous flow conditions. *Org. Process Res. Dev.* **2019**, DOI: 10.1021/acs.oprd.8b00387.

19. Shevlin, M., Practical high-throughput experimentation for chemists. *ACS Med. Chem. Lett.* **2017,** *8*, 601-607.

20. Zinia, J.; Ahmed, M.; Samyukta, S.; Larisa, A.; H., T. D., High throughput experimentation and continuous flow validation of Suzuki–Miyaura cross-coupling reactions. *Chem. Eur. J.* **2018,** *24*, 9546-9554.

21. Selekman, J. A.; Qiu, J.; Tran, K.; Stevens, J.; Rosso, V.; Simmons, E.; Xiao, Y.; Janey, J., High-throughput automation in chemical process development. *Annual Review of Chemical and Biomolecular Engineering* **2017,** *8*, 525-547.

22. Ichiishi, N.; Caldwell, J. P.; Lin, M.; Zhong, W.; Zhu, X.; Streckfuss, E.; Kim, H.-Y.; Parish, C. A.; Krska, S. W., Protecting group free radical C–H trifluoromethylation of peptides. *Chem. Sci.* **2018,** *9*, 4168-4175.

23. Macarron, R.; Banks, M. N.; Bojanic, D.; Burns, D. J.; Cirovic, D. A.; Garyantes, T.; Green, D. V. S.; Hertzberg, R. P.; Janzen, W. P.; Paslay, J. W.; Schopfer, U.; Sittampalam, G. S., Impact of high-throughput screening in biomedical research. *Nature Reviews Drug Discovery* **2011,** *10*, 188.

24. Liu, M.; Chen, K.; Christian, D.; Fatima, T.; Pissarnitski, N.; Streckfuss, E.; Zhang, C.; Xia, L.; Borges, S.; Shi, Z.; Vachal, P.; Tata, J.; Athanasopoulos, J., High-throughput purification platform in support of drug discovery. *ACS Combinatorial Science* **2012,** *14*, 51-59.

25. Chen, P., Electrospray ionization tandem mass spectrometry in high-throughput screening of homogeneous catalysts. *Angew. Chem. Int. Ed.* **2003,** *42*, 2832-2847.

26. Buitrago Santanilla, A.; Regalado, E. L.; Pereira, T.; Shevlin, M.; Bateman, K.; Campeau, L.-C.; Schneeweis, J.; Berritt, S.; Shi, Z.-C.; Nantermet, P.; Liu, Y.; Helmy, R.; Welch, C. J.; Vachal, P.; Davies, I. W.; Cernak, T.; Dreher, S. D., Nanomole-scale high-throughput chemistry for the synthesis of complex molecules. *Science* **2015,** *347*, 49-53.

27. Troshin, K.; Hartwig, J. F., Snap deconvolution: An informatics approach to high-throughput discovery of catalytic reactions. *Science* **2017,** *357*, 175-181.

28. Wleklinski, M.; Loren, B. P.; Ferreira, C. R.; Jaman, Z.; Avramova, L.; Sobreira, T. J. P.; Thompson, D. H.; Cooks, R. G., High throughput reaction screening using desorption electrospray ionization mass spectrometry. *Chem. Sci.* **2018,** *9*, 1647-1653.

CHAPTER 2. REACTION SCREENING AND OPTIMIZATION OF CONTINUOUS FLOW ATROPINE SYNTHESIS BY PREPARATIVE ELECTROSPRAY MASS SPECTROMETRY

Reproduced (adapted) from Jaman, Z.; Falcone, C. E.; Wleklinski, M.; Koswara, A.; Thompson, D. H.; Cooks, R. G. 'Reaction screening and optimization of continuous-flow atropine synthesis by preparative electrospray mass spectrometry' *Analyst* **2017**, 142, 2836 with permission from The Royal Society of Chemistry.

2.1 Introduction

2.1.1 Continuous Flow Synthesis

Traditionally, organic synthesis is performed in round-bottomed flasks which allow for limited control with lengthy reaction times. Continuous flow reactors are gaining traction in pharmaceutical and fine chemistry for the preparation of small and large molecules including Active Pharmaceutical Ingredients (APIs).[1- 2] Key advantages of continuous flow are enhanced heat and mass transfer, controlled flow, ease of integration, precise control of reaction time, efficiency and safety.[3-4] Generally, reaction optimization and screening take significant investments in time and material.[5,6] Pharmaceutical production still utilizes a supply chain network where shortages often appear due to dependence on multipurpose batch reactors that require months for synthesis, isolation and validation of intermediates.[7] Microreactors in conjunction with nESI-MS can accelerate optimization[8] of reactions, while allowing reactions to be screened and optimized at reduced cost due to low material requirements and waste generation. [9,10] The reduced channel widths, together with the exceptional mass-and heat transfer capacity of these reactors can lead to enhanced reaction rate.[11] With all of these advantages, continuous flow processes are emerging as an important new technique to synthesis APIs.[12-13] APIs have been synthesized continuously by incorporating reaction telescoping and continuous work up techniques. Continuous flow synthesis of the APIs efaproxial, rimonabant[14], imatinib[15,16], ibuprofen[8], rufinamide[17], diphenhydramine hydrochloride[18], (E/Z)-tamoxifen[19] have been reported.

2.1.2 Accelerated Reaction Screening Using Electrospray Ionization Technique

In electrospray, accelerated chemical reactions occur in charged microdroplets that can accelerate reaction times.[20] These accelerated reactions have been studied in the ambient ionization techniques like desorption electrospray ionization (DESI),[21] paper spray[22] and electrospray ionization (ESI).[23] Accelerated reactions in charged microdroplets have been employed for derivatizing analytes for improved MS analysis[20], mechanistic studies of reactions[24-26], identifying reaction intermediates[25, 27, 28] and the collection of products generated via microscale synthesis.[29, 30] Accelerated droplet reactions can be used to prepare milligram quantities of material in minutes in preparative electrospray (ES).[29] Preparative ES is a method where a reaction mixture is electrosprayed onto a surface and the deposited material is washed for chemical analysis. Extractive electrospray ionization (EESI) is an ionization technique that utilizes two intersecting ESI emitters. One emitter nebulizes the sample in a complex matrix and the other produces charged microdroplets of solvent.[31] The colliding microdroplets leads to the liquid–liquid extraction of the analytes from the complex matrix to a solvent amenable for on-line mass spectromic analysis. A technique similar to EESI, droplet fusion, uses two separate ESI emitters where two plumes of microdroplet reagents collide to form fused droplets consisting of both reagents. The reagents are mixed in the fused droplets and the reaction proceeds. Microdroplet fusion has been used to study the kinetics of phenolindophenol reduction by ascorbic acid, acid-induced cytochrome c unfolding, and HDX in Bradykinin.[32] In a third multi ESI emitter technique, multichannel rotating electrospray ionization (MRESI), ESI emitters nebulize volatile reagents that induce reactions in the gas phase and the resulting products are extracted by droplets from another ESI emitter.[33]

2.1.3 Brief Summary of this Chapter

Atropine is traditionally manufactured industrially from natural products extraction[34]. Atropine, a natural tropane alkaloid, exists as a racemic mixture of D-hyoscyamine and L-hyoscyamine and has both anticholinergic and antiparasympathetic properties[35]. The U.S Food and Drug Administration (FDA) has reported a shortage drugs during 2011-2014 that include atropine salt[36]. The total synthesis of atropine has previously been published using a batch process[37, 38, 39] and has recently been published in continuous flow[36]. The previously published continuous flow process required multiple steps of purification by liquid-liquid extraction due to a variety of byproducts which in turn reduced the overall yield of atropine. Reported herein is a rapid screening

technique that utilizes preparative ES to screen pathways and microfluidics to optimize the pathway to produce a synthesis of atropine with an average yield of 33.45. This pathway has a 4.34 fold increase in percent yield and a 1.9 fold reduction in reaction time in microfluidics, compared to the previously published continuous flow paper[36].

2.2 Results and Discussion

2.2.1 Preparation of Atropine Intermediate by Electrospray

Pathways for the synthesis of atropine were explored in preparative ES (Figure 2.1). Preparative ES fundamentally gives a binary response of whether a synthetic route did or did not yield product. A successful reaction in spray guides which reactions should be pursued in microfluidics. Four synthetic routes (scheme 2.1) were screened in preparative ES for the fabrication of the atropine intermediate. The first pathway (scheme 2.1 a) explored the use of tropine **2**, phenyl acetic acid **3** and HCl in both water and dioxane. The use of aqueous HCl yielded no intermediate **4** in the full scan, however it was present in low abundance in MS/MS of the protonated intermediate m/z 260. Using HCl in dioxane yielded low abundance of the intermediate **4** in the full scan with a percent conversion of 1.4%. The second pathway (scheme 2.1 b) of tropine **2** and phenyl acetic acid **3** yielded no intermediate **4** in the full scan in a solvent screen of acetonitrile (ACN), dichloromethane (DCM), dimethylacetamide (DMA), dimethylformamide (DMF), dimethyl sulfoxide (DMSO), ethanol, methanol, tetrahydrofuran (THF), and toluene. The third pathway (scheme 2.1 c), tropine **2**, phenylacetyl chloride **5** and HCl in dioxane yielded a percent conversion of 29.5% (figure 2.2 a). The fourth pathway (scheme 2.1 d) eliminated the use of acid, with only tropine **2** and phenylacetyl chloride **5** in a solvent. A solvent screen was conducted in the fourth pathway for the esterification of tropine **2** and phenylacetyl chloride **5** testing the 9 solvents previously discussed. The intermediate was produced in DMA, DMF, ethanol and methanol, however the highest percent conversion was from DMA with a percent conversion of 55.3% (figure 2.2 b). The percent conversion increased with each permutation of the pathway leading to the determination that tropine **2** and phenylacetyl chloride **5** with the addition of a solvent produced the highest percent conversion of the four pathways and was a promising pathway to carry forward for testing in microfluidics. The solvents ethanol and methanol will lead to byproducts in the aldol condensation reaction, therefore, only the solvents DMA and DMF were

examined in microfluidics. Full scan MS of the first step of the atropine synthesis by preparative ES were shown in APPENDIX A (Fig A1-A8).

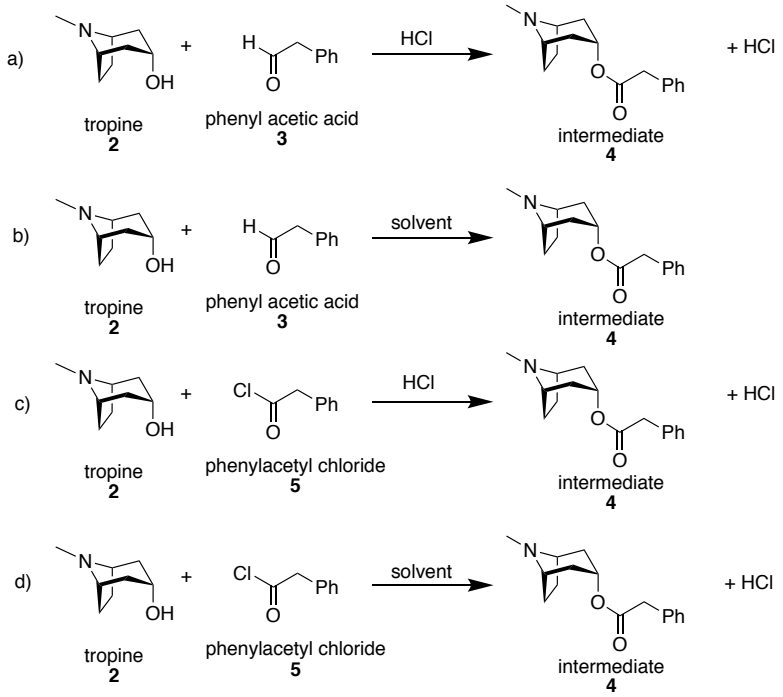

Scheme 2.1 Atropine intermediate routes

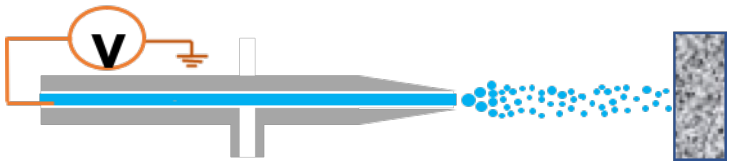

Figure 2.1 Preparative ES. A high voltage is applied to the solvent through a syringe and the use of nitrogen nebulizes the liquid sample. The spray droplets are deposited on the glass wool for analysis.

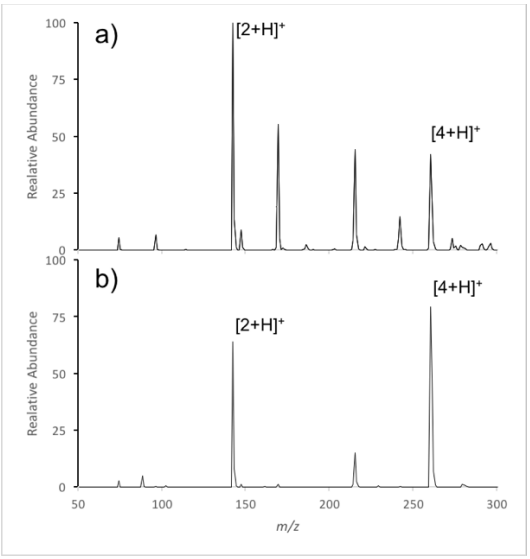

Figure 2.2 Mass spectra of preparative ES deposited material. a) The full scan positive ion mode spectrum of the deposited material from the preparative ES reaction of tropine **2**, phenylacetyl chloride **5** and HCl in dioxane yielding a percent conversion to intermediate of 29.5%. b) The full scan positive ion mode spectrum of the deposited material from the preparative ES reaction of tropine **2**, and phenylacetyl chloride **5** in DMA yielding a percent conversion to intermediate of 55.3%.

2.2.2 Synthesis of Atropine Intermediate in Flow

The two best pathways (Scheme 2.1: c & d**)** and solvents, DMA and DMF, for the synthesis of the intermediates **4** from preparative ES were examined in microfluidics. The flow reaction between tropine **2** (1 equivalent) and phenylacetyl chloride **5** (1.1 equivalent) in the presence of HCl in dioxane in DMA (Scheme 2.1, c) showed 85% conversion by LC-MS of intermediate salt **4** at 100 °C in 2 minutes. The second pathway of tropine **2** (1 equivalent) and phenylacetyl chloride **5** (1.1 equivalent) (Scheme 2.1, d) in DMA (Scheme 2) at 100 °C in 2 minutes gave 62% conversion of the intermediate **4** along with quaternary ammonium salts byproducts (Scheme 2.2). The quaternary ammonium salts were produced from the reaction between ester intermediate and phenylacetyl chloride. The presence of solvent associated byproducts was noted at 150 °C and 200 °C (Scheme 2.3). The microfluidic reaction using DMF as the solvent showed more solvent associated byproduct than DMA. For both of these processes, no quenching was performed.

Reducing the quaternary ammonium salt byproducts are important to reduce the probability of producing further byproducts in the next step of the atropine synthesis. For this, equimolar (1:1) amounts of tropine **2** and phenylacetyl chloride **5** were taken that gave 89% conversion of

intermediate **4** with less quaternary ammonium byproducts at the same reaction conditions. The latter route eliminates the step of producing tropine salt using hydrochloric acid with a similar percent conversion to intermediate. This route is 3.8 fold faster than the reported flow synthesis of atropine.[36] Preparative ES and microfluidics both agreed that the highest percent conversion pathway to the production of intermediate **4** was tropine **2** and phenylacetyl chloride **5** in DMA. APPENDIX A has all the tables in details (Table A1 & A2).

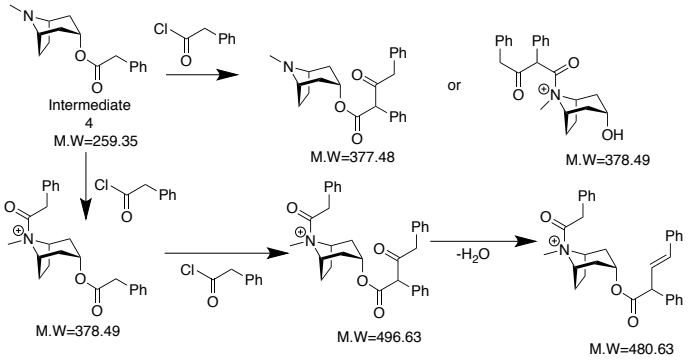

Scheme 2.2 Quaternary ammonium byproducts from first step

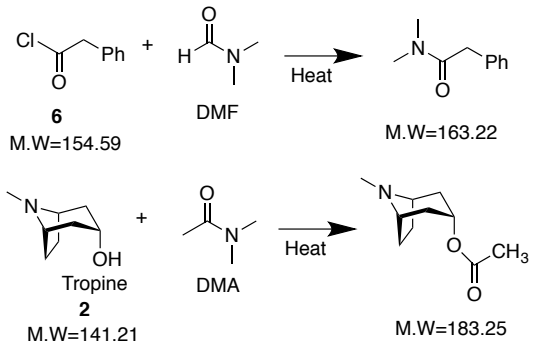

Scheme 2.3 Byproduct associated with solvent DMF and DMA

2.2.3 Preparation of Atropine by Electrospray

The second step in the synthesis of atropine is a base catalyzed aldol condensation with the addition of formaldehyde and base to the step 1 intermediate. The crude product from the preparative ES reaction of tropine **2** and phenylaceyl chloride **5** in DMA, was telescoped with aqueous formaldehyde 37% and 1M base in DMA to form atropine. Twenty-two bases were

screened in preparative ES to determine the base that yielded the highest percent conversion to atropine with the least amount of byproduct formation. This methodology quickly screened different bases to determine which bases yield the highest conversion to atropine and examined the byproducts produced by each base. Out of the 22 bases screened (APPENDIX A), 7 bases had a percent conversion to atropine larger than 5%. The percent conversion accounted for byproducts previously identified in the continuous flow synthesis of aldol condensation to atropine using aqueous formaldehyde and both sodium hydroxide and pH 10 buffer. Seven bases successfully produced atropine, therefore, the best bases for the aldol condensation were determined by both the percent conversion to atropine and the percent conversion to byproducts. The bases 1,8-diazabicyclo[5.4.0]undec-7-ene, potassium ethoxide, potassium methoxide, sodium ethoxide, sodium hydroxide and sodium methoxide had a higher percent yield of apoatropine **6** the E1 elimination byproduct, than atropine. The base 1,5-diazabicyclo[4.3.0]non-5-ene was the screened base with the highest percent conversion of 44.5% to atropine, but was the only base with nominal production of byproducts. The preparative ES suggestion for the best base for the synthesis of atropine in microfluidics is 1,5-diazabicyclo[4.3.0]non-5-ene. APPENDIX A (Fig A6-A26) shows the full scan MS of the second step base screen by preparative ES.

2.2.4 Preparation of Atropine in Flow in Two Chips

The hydroxymethylation step (aldol condensation, 2nd step) was examined in different reaction conditions using the intermediate from the first step in microfluidics without any further purification (Figure 2.3). Nine bases were screened, which encompassed both successful and unsuccessful reactions in preparative ES. Their percent conversions are summarized in table 2.1. Apoatropine **6** (E1 eliminated byproduct) was produced in all conditions as the E1 elimination reaction is accelerated by temperature and base. Sodium ethoxide in ethanol produced solid during the microfluidic reaction leading to a clogged chip because the byproduct sodium chloride has a low solubility in ethanol forming transient solids during the reaction.

The pH 10 buffer had an overall conversion to atropine of 34% and this condition produced byproducts **6** and **8** (Scheme 2.4). Increasing the temperature led to more elimination byproduct **7** as the higher temperatures helped to eliminate water from the atropine. Increasing the amount of formaldehyde or the residence time increased the second aldol byproduct **8.** Further decreases in temperature did not lead to the production of atropine. Sodium methoxide and potassium

methoxide had similar overall percent conversions, 26% and 23%, respectively, however increasing residence time and temperature increased the production of byproduct **6.** A new byproduct **7** was found due to the Michael addition of methanol present in the base as well as formaldehyde solutions. Trimethylamine and DABCO showed poor conversion to atropine even at higher temperature and longer residence time.

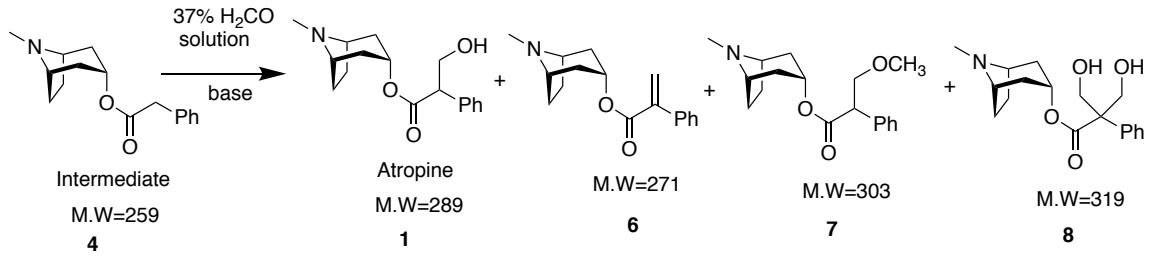

Scheme 2.4 Possible byproducts from second step reaction

Tetramethylammonium hydroxide took less than a minute to convert all intermediate to product and byproducts. The maximum conversion of atropine (37%) produced high amounts of byproducts **6, 7.** The best condition for tetramethylammonium hydroxide with the highest percent conversion (32%) and the smallest percent conversion of byproducts was found at 100 °C in 8.6-seconds. Sodium hydroxide showed 13% maximum overall conversion of atropine in a 6-minute residence time with hydrolyzed tropine and byproducts **6, 8**.

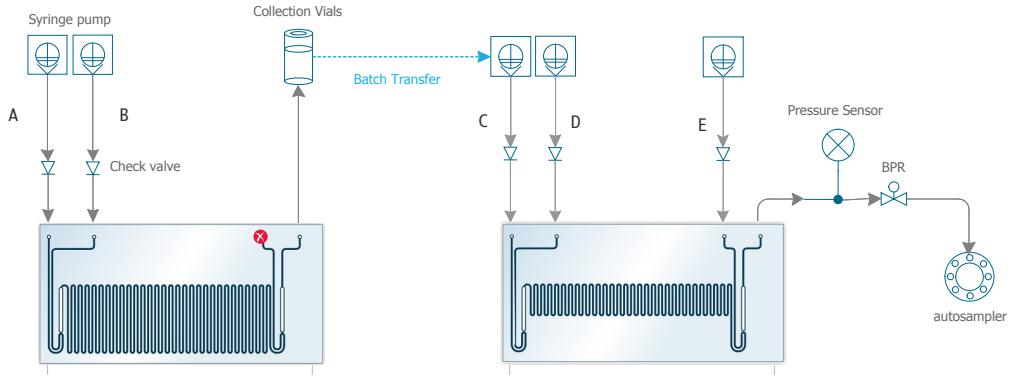

Figure 2.3 Synthesis of Atropine in flow in two chips. A=Tropine; B=Phenylacetyl chloride, D=Base + Formaldehyde; E=Water

Table 2.1 Comparison of percent conversion to atropine and byproducts

Base	Maximum conversion of atropine (%)	Reaction conditions	Byproducts In flow	Preparative ES percent conversion (%)	Byproducts In ES
pH 10 buffer	34*	150 °C , 2 min	**7, 9**	1.6	**7**
Sodium methoxide in methanol (CH_3ONa)	26	150 °C , 2.9 min	**7, 8**	9.9	**7**
Potassium methoxide in methanol (CH_3OK)	23*	70 °C , 2 min	**7, 8**	7.6	**7, 9**
Tetramethyl ammonium hydroxide	36*	100 °C , 21.4 sec	**7, 8**	1.6	**7, 9**
Sodium hydroxide	13*	22 °C , 6 min	**7, 9**	15.4	**7**
1,5-Diazabicyclo[4.3.0]non-5-ene	42*	70 °C , 4 min	**7**	47.5	**7**

Maximum percent conversion of atropine in two steps in two different chips. The percent conversion was determined by calculated by nESI-MS and * percent conversion was determined by LC-MS. The reaction conditions describe the temperature and residence time in the second chip.

The 1,5-diazabicyclo[4.3.0]non-5-ene base was the most effective base for the aldol condensation reaction in microfluidics, which correlates to the preparative ES data. The maximum overall conversion of atropine using 1,5-diazabicyclo[4.3.0]non-5-ene base was 42% (Table 2.1) at 70 °C in 4 and 6 minutes residence time with minimum amount of byproduct **6**. Increasing residence time and temperature increased byproduct **6**. The maximum yield of atropine was 30.3% at 70 °C with a 6 minutes residence time.

Table 2.2 Comparison of conversion of atropine in different base

Base	Overall Conversion of Atropine by LC/MS (%)			
	2 min	4 min	6 min	8 min
1,5-diazabicyclo[4.3.0]non-5-ene	39.61	42.42	42.25	37.83
CH_3OK	23.20	19.89	16.07	18.36
NaOH	10.80	6.8	5.78	5.1
pH 10 Buffer	<1	<1	<1	<1

Table 2.3 Comparison of percent conversion of byproducts in different bases

Byproduct	Method	Percent Conversion of Byproducts (%)		
		1,5-diazabicyclo[4.3.0]non-5-ene	CH_3OK	NaOH
6	ES	11.4	45.1	40.3
	Flow	3.8	20.2	65.8
7	ES	<1	<1	<1
	Flow	<1	44.8	<1
8	ES	2.2	31.1	1.4
	Flow	1.5	4.1	13.4

The base 1,5-diazabicyclo[4.3.0]non-5-ene had the smallest percent conversion to byproducts and had only 3.8% of the byproduct **6** in 6 min residence time (Table 2.3). The best base for the aldol condensation was 1,5-diazabicyclo[4.3.0]non-5-ene in both preparative ES and microfluidics.

The reaction conditions (chip 3227, 4 equiv of formaldehyde, 4 equiv base, 70 °C, P = 9 bar) for the highest percent conversion of 1,5-diazabicyclo[4.3.0]non-5-ene were used to compare the relative conversion of atropine in 1,5-diazabicyclo[4.3.0]non-5-ene, potassium methoxide, sodium hydroxide and pH 10 buffer (Table 2.2). The overall percent conversion of atropine using 1,5-diazabicyclo[4.3.0]non-5-ene in two steps was almost identical in 4 and 6 minutes. Atropine conversion decreased with increasing residence time for both potassium methoxide and sodium

hydroxide bases. The pH 10 buffer did not lead to the production of atropine in this reaction condition.

2.2.5 Preparation of Atropine by Extractive Electrospray

The multi-step synthesis of atropine was prepared continuously using a derivative of extractive electrospray (EES) (figure 2.4). This technique utilized two electrospray emitters where the first ESI emitter produced the intermediate **4** and the second ESI emitter nebulized the hydroxymethylation reagents for the second and final step of the atropine synthesis. The reactive EES setup differs from traditional EES. In traditional EES the angle of intersection of the two ES emitters is 90, with a few variations using angles of 40-60 degrees.[40, 41] For reactive EES, the angle of intersection is shallower (<22.5%), which allows for longer and more inclusion of the droplets from both ES emitters, allowing for a less extractive method. The second variation is distance where the distance of intersection is greater at 4 cm. This allows for adequate reaction time for the first step of the reaction to proceed before interacting with droplets from the second step reagents. The setup was optimized by different angles of emitters, distance of the emitters to droplet intersection and droplet intersection to the glass wool, and polarities applied (APPENDIX A, Fig A30-A33).

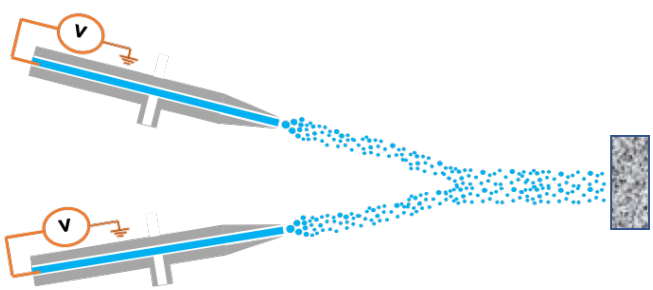

Figure 2.4 Preparative reactive EES. A high voltage is applied to the solvent through a platinum electrode and the use of nitrogen nebulizes the liquid sample. The ES emitters are positioned at an angle of 22.5^0 and the point of intersection for the spray plumes is 4 cm. The spray droplets are deposited on the glass wool for analysis.

When the ES emitters were orthogonal, like in traditional EES, the ratio of product to intermediate was less, potentially due to lack of interaction time with the droplets. The highest ratio of product to intermediate occurred when the emitters were placed laterally, with an angle less than 22.5°. A higher ratio of product to intermediate occurred when the point of intersection of the plume from

both emitters and distance from the intersection to the collection surface were greater, however, there was a trade off in quantity of material deposited to the glass wool. In preparative reactive EES, the unreacted phenylacetyl chloride reacted with the water in the aqueous formaldehyde to form $[2M+H]^+$ of phenylacetic acid. This was expected as phenylaceyl chloride is highly reactive with water. Despite this, the percent conversion to atropine was 23.5%, which is similar to the total percent conversion from both steps of the preparative ES of 26.2% (Figure 2.5). Therefore, telescoped preparative EES is a valid microscale synthesis system with similar percent conversions to telescoped preparative ES.

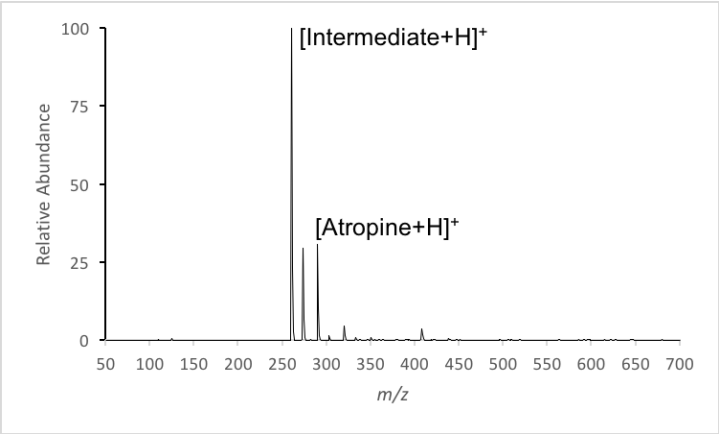

Figure 2.5 Mass spectrum of preparative ES deposited material. The full scan positive ion mode spectrum of the deposited material from the preparative reactive EES synthesis of atropine.

2.2.6 Continuous Microfluidic Synthesis of Atropine

Telescoping in one reactor, 3224 led to more byproducts and less control over reactions, thus encouraging the use of two separate reactors to telescope the atropine synthesis (figure 2.6). The optimized conditions for 1,5-diazabicyclo[4.3.0]non-5-ene base in separate steps (1st step: 2 min, 100 °C and 2nd step: 6 min, 70 °C) were used to telescope the synthesis of atropine at 32.14% and average yield of 33.45%.

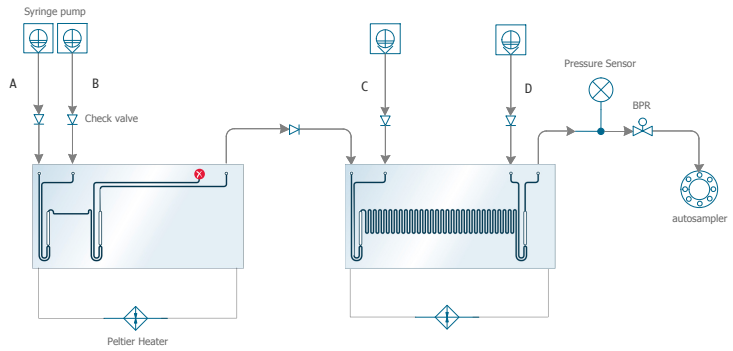

Figure 2.6 Continues flow synthesis of atropine in separate reactors.

2.2.7 Comparison of Preparative ES and Microfluidics

Preparative ES successfully predicted the reaction pathway, solvent and base with the highest percent conversion in microfluidics, however there were noticeable differences from the results of the two techniques in both percent conversion and production of byproducts. The percent conversion from starting material to product was higher in microfluidics than in preparative ES. This can be attributed the greater ability to control reactions in microfluidics. Elevated temperatures were used in microfluidics, which lead to a greater reaction efficiency. Elevated temperatures have been used for preparative ES experiments [42, 43]. The successful synthesis of the intermediate at room temperature deemed heat was unnecessary for the binary reaction screen, however, elevated temperatures may be employed for other reaction screenings. Another factor impacting the percent conversion is the open atmosphere in preparative ES. In microfluidics, the reaction occurs in a closed pressurized system. In preparative ES, the system is open and subjected to the atmospheric environment in a chemical hood. This could be eliminated by preforming preparative ES in a controlled environment like a glove box. The third factor effecting the difference in percent conversion is the vapor pressure of both the reagents and solvents. The reaction acceleration in preparative ESI relies heavily on the evaporation of the charged droplets. When a reagent evaporates and leaves the droplet significantly faster than the solvent, there may not be ample time for the reagents to interact leading to an unsuccessful or diminished reaction. When the solvent does not evaporate from the charged droplet in a timely manner, the reaction will not accelerate solely on volume reduction.

There were differences in the formation of byproducts for the second step of the atropine synthesis in preparative ES and microfluidics (Figure 2.7). While both techniques heavily favored

the E1 eliminated byproduct, byproduct **6**, the major difference occurred in the production of byproducts **7** and **8**. In preparative ES, byproduct **7** was not produced and there was a percent conversion greater than 5% of byproduct **8** in every successful base with the exception of 1,5-diazabicyclo[4.3.0]non-5-ene, sodium hydroxide and sodium methoxide. Conversely, byproduct **7** was produced in the cases in microfluidics with sodium methoxide, potassium methoxide and tetramethyl ammonium hydroxide. The only bases to produce byproduct **8** with a percent conversion greater that 5 was sodium hydroxide and pH 10 buffer. Byproduct **8** is formed when two formaldehyde molecules react with the intermediate **4** and byproduct **7** is a Michael addition of methanol to **6** at high temperature. Byproduct **7** was not formed in preparative ES due to the lack of heat necessary for the Michael addition of methanol. The rest of the figures and datasets related to this chapter are in APPENDIX A.

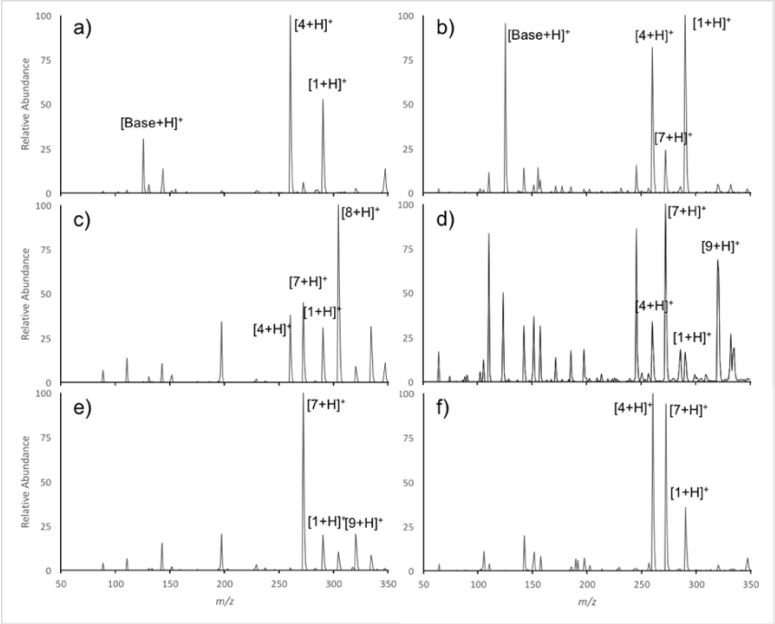

Figure 2.7 Mass spectra of microfluidic and preparative ES products using 3 different bases. a) The full scan positive ion mode spectrum of atropine synthesis using 1,5-diazabicyclo[4.3.0]non-5-ene in microfluidics. b) The full scan positive ion mode spectrum of atropine synthesis using 1,5-diazabicyclo[4.3.0]non-5-ene in preparative ES. c) The full scan positive ion mode spectrum of atropine synthesis using potassium methoxide in microfluidics. d) The full scan positive ion mode spectrum of atropine synthesis using potassium methoxide in preparative ES. e) The full scan positive ion mode spectrum of atropine synthesis using sodium hydroxide in microfluidics. f) The full scan positive ion mode spectrum of atropine synthesis using sodium hydroxide in preparative ES.

2.3 Experimental

2.3.1 Chemicals

All chemicals and solvent were purchased from Sigma-Aldrich (St. Louis, Missouri) and used without any purification. pH=10 buffer was purchased from Macron (Avantor Performance Materials, Center Valley, PA)

2.3.2 Mass Spectrometer

Samples were analyzed on a Thermo LTQ linear ion trap mass spectrometer (ThermoFisher Scientific, San Jose, CA, USA). NanoESI analysis in both positive and negative ion mode were performed with a 2.0 kV spray voltage. Other experimental parameters were: capillary temperature: 200C; tube lens (V): -85 V; capillary voltage: -20 V for positive ion mode and tube lens (V): 85 V; capillary voltage: 20V for negative ion mode. Tandem mass spectrometry was performed with an isolation window of 1.5 (m/z units) and 25% collision energy. The spectra were acquired with automatic gain control while averaging 3 micro-scans for each spectrum. Samples were prepared for nanoESI by diluting 100-fold in acetonitrile.

2.3.3 Microfluidics

Labtrix Start Flex (Chemtrix BV, Labtrix S1, Netherlands) employs custom fabricated parts made of PPS (polyphenylsulfide) and perfluoroelastomer. PPS provides excellent chemical resistance against hydrochloric acid, trifluoroacetic acid, nitrobenzene, acetic acid, sulfuric acid and butyl lithium. It can be used to perform syntheses at temperatures ranging from -20 °C to +195 °C and under pressures of up to 25 bar. The outer diameter of the tube of the flex/ultraflex system is 1/32 inches and inner diameter is 150 μm that is made of *fluorinated ethylene propylene* (FEP). The micro reactors differ in volume and number of connections. The micro reactors are made of glass. All staggered orientated micro reactors (SOR) have width channel 300 μm and depth channel 120 μm. The SOR chips used were: 3221 (three inlets and one outlet, volume 1 μl), 3332 (three inlets and one outlet, volume 2 μl), 3223 (three inlets and one outlet, volume 5 μl), 3224 (four inlets and one outlet, volume 10+5 μl), 3225 (four inlets and one outlet, volume 10 μl), and 3227 (three inlets and one outlet, volume 19.5 μl). The Labtrix unit is enabled to pump five syringes with liquids into the microreactor with a heating and cooling unit. All the gastight glass syringes were bought separately from Innovative Labor System. (ILS, Philadelphia, PA).

The tubing and fittings connect the syringes with the selected connection port on the microreactor. All operations are controlled via a ChemTrix GUI software, which is installed on a laptop and connected to the Labtrix S1 housing with a USB cable.

2.3.4 HPLC-MS Analysis

Separations were performed on an Agilent 1100 HPLC system (Palo Alto, CA) using a Varian C18 Amide column (3 µm, 150 x 2.1 mm i.d) and 10 µL injection volume. A binary mobile phase consisting of solvent systems A and B were used in gradient elution where A was 0.1% formic acid (v/v) in ddH_2O and B was 0.1% formic acid (v/v) in acetonitrile. The mobile phase flow rate was 0.3 mL/min. Initial conditions were set at 90:10 A:B with a linear gradient to 80:20 from 0 to 12 min, conditions were held at 80:20 from 12 to 18 minutes, followed by a linear gradient to 50:50 from 18 to 24 minutes and held at 50:50 until 30 minutes. Gradient conditions were reset to 90:10 A:B from 30 to 32 minutes, and the column was equilibrated for 10 minutes at initial conditions prior to the next run. Following the separation, the column effluent was introduced by negative mode electrospray ionization (ESI) into an Agilent MSD-TOF spectrometer. The parameters were: ESI capillary voltage: −3.5 kV, nebulizer gas: nitrogen at 35 psi and 350 °C, drying gas flow rate: 9.0 L/min, fragmentor voltage: 165 V, skimmer: 60 V and OCT RF V: 250 V. Spectroscopic (UV at 280 nm) and mass data (from m/z 60-1000) were collected and analyzed using MassHunter software. The percent conversion was calculated by integrating the all peaks in the chromatogram.

2.3.5 RP-UPLC Analysis

An isocratic reverse-phase ultra-high performance liquid chromatography method (RP-UPLC) using the PATROL UPLC Process Analysis System (Waters Corp.) was developed to determine the yield of atropine reaction in continuous flow. The method was developed using an ACQUITY BEH C18 (130 Å pore size, 1.7 µm particle size, 2.1 mm ID X 100 mm) as the stationary phase with potassium dihydrogen phosphate:methanol (80:20, v/v) at pH = 3.5 as the mobile phase. The mobile phase was prepared by dissolving potassium dihydrogen phosphate powder (Sigma-Aldrich, CAS: 7778-77-0) in HPLC-grade water (Fisher Scientific, CAS: 7732-18-5), which is pH-adjusted via titration using 85% orthophosphoric acid (Fisher Scientific, CAS: 7664-38-2,7732-18-5). The mobile phase flow rate through the column was 0.4 mL/min and the

column temperature was maintained at 40 °C during the run. The detection of eluted atropine was accomplished using a dual-channel PDA detector at 190 and 225 nm in conjunction with ApexTrack analysis for integrating the atropine peak that was matched with an atropine standard chromatogram. The quantitation was then performed via interpolation using a standard calibration curve at 225 nm. Three standard stock solutions of atropine sulphate were prepared by dissolving atropine sulphate powder (Sigma-Aldrich, CAS: 5908-99-6) in the mobile phase to generate concentrations of 1.20 mg/mL, 1.17 mg/mL, and 0.960 mg/mL. The solutions were used to generate three separate calibration curves by diluting the stock solutions inline to 1X, 2X, 4X, 8X, 16X, and 32X to cover a concentration range of 20-1200 μg/mL; the mean R^2 was 0.9997 (n=5). The mean slope of the curves was used for quantitation. The method's precision was calculated by repeated injections of the same standard solution without any change to the chromatographic methods.

2.3.6 NMR Analysis

^{1}H-NMR and ^{13}C-NMR samples were prepared by dissolving ~10 mg of sample in $CDCl_3$ and spectra were acquired using a Bruker AV-III-500-HD NMR spectrometer (Billerica, Massachusetts, USA). The NMR data was analyzed using MestReNova 10.0 software.

2.3.7 Preparative Electrospray

A homebuilt electrospray source was enclosed in a polypropylene tube (15 mL Falcon tube) with a small piece of glass wool for deposition. The reaction mixture was pumped through a fused silica capillary at a rate of 10 μL/min and a high voltage of 5kV is applied through the stainless steel needle of the 250 μL Hamilton gastight syringe. A nitrogen sheath gas was used at 100 psi. The sprayed droplets were collected on the gas wool and washed with a solvent for analysis by nanoESI or to be telescoped for the next step in the reaction.

2.3.8 Preparative Reactive EES

Two homebuilt electrospray sources were angled at 22.5^o with the intersection of the spray plumes occurring at 4 cm. The deposition surface of glass wool in a polypropylene tube was placed at varying distances from the intersection. Each ES emitter was connected to two syringes via tubing and mixed in line with a mixing T. Each syringe had a flow rate of 5 μL/min with a total

flow rate of 10 μL/min for each ES emitter. The high voltage was applied through a platinum electrode in a T junction. A nitrogen sheath gas was used at 100 psi. The sprayed droplets were collected on the gas wool and washed with a solvent for analysis by nanoESI.

2.3.9 Synthesis of Intermediates in Preparative ES

For the synthesis of intermediate **4**, 0.1 mmoles of solid tropine **2** and 0.1 mmoles of phenylacetic acid or phenylacetyl chloride **5** were added to 100 μL of aqueous 3 M HCl or 100 μL of 4 M HCl in dioxane and sprayed for 5 minutes. For the synthesis of intermediate **4**, 0.1 mmoles of solid tropine **2** and 0.1 mmoles of phenyl acetic acid or phenylacetyl chloride **5** were added to 100 μL of solvent and sprayed for 5 minutes. All deposited products were washed with 500 μL ACN and analyzed via nanoESI-MS.

2.3.10 Synthesis of Intermediates in Microfluidics

A DMF solution of tropine **2,** HCl in dioxane and phenylacetyl chloride **6** were individually loaded into 1 mL ILS gas tight glass syringes. Each solution was in turn dispensed into the SOR 3225 reactor to react and produce intermediate **4**. Similarly, a DMA solution of tropine **2** and phenylacetyl chloride **5** were loaded in a pair of 1 mL syringes and reacted onto the SOR 3227 reactor to prepare for intermediate **4**. The esterification reaction was run at 100 °C, 150 °C and 200 °C and for a residence time of 1 min, 2 min, 5 min, and 8 min. The intermediate was collected without any quenching. The subsequent nESI-MS and HPLC-MS analyses were performed without further purification. In contrast, NMR analysis was performed after neutralization and extraction of the reaction mixture.

2.3.11 Synthesis of Atropine in Preparative ES

The first step product of the atropine synthesis was made by preparative ES spraying 200 μL 1:1 0.5 M tropine in DMA: 0.5 M phenylacetyl chloride in DMA and then washing the deposited product from the glass wool with 500 μL DMA. The second step of the atropine synthesis was prepared by spraying 50 μL of the following solution: 10 μL Step 1 product, 30 μL 36-37% formaldehyde solution in water and 30 μL 1M base in DMA. The glass wool was quenched with 500 μL water and the product was extracted with 100 μL DCM. The preparative ESI product was analyzed via nanoESI.

2.3.12 Synthesis of Atropine in Preparative EES

The first ES emitter sprayed the step 1 reagents to form the intermediate and the first syringe contained 0.1 M tropine in DMA and the second syringe contained 0.1 M phenylacetyl chloride in DMA. The second ES emitter sprayed the second step reagents and the first syringe contained 1 M 1,5-diazabicyclo[4.3.0]non-5-ene in DMA and the second syringe contained 36-37% formaldehyde solution in water. A total of 100 μL of each reagent was sprayed for 20 minutes. The glass wool was quenched with 2 mL water and the product was extracted with 100 μL DCM. For analysis via nanoESI, 10 μL of the DCM extract was diluted in 90 μL of ACN.

2.3.13 Synthesis of Atropine **1** in Microfluidics in Two Chips

The DMA solution of intermediate **4** and aqueous formaldehyde solution with nine bases were loaded onto a pair of 1 mL glass syringes and delivered at temperatures starting from room temperature to 200 °C. All the bases were diluted in DMA. The residence times of the reactions also varied from 10 sec to 8 minutes depending on the base in a Labtrix SOR reactors, such as the 3227, 3225, 3223 or 3222 reactors. Deionized water was loaded into the last 1 mL glass syringe and delivered to quench the reaction.

2.3.14 Continuous Microfluidic Synthesis of Atropine

The DMA solutions of tropine **2** (1.0 equiv) and phenylacetyl chloride **5** (1.0 equiv) were loaded onto a pair of 1 mL glass syringes and delivered to SOR 3221 at 100 °C in 2-min residence time. The solution coming from SOR 3221 was entered to the first inlet of SOR 3223. A DMA solution of 1,5-diazabicyclo[4.3.0] non-5-ene base + formaldehyde solutions (4.0 equiv) and water were loaded onto a pair of 1 mL glass syringes and delivered to SOR 3223 at 70 °C in 6-min residence time.

2.4 Conclusion

Preparative ES was compared with continuous microfluidic synthesis of atropine. Preparative ES was used to explore new pathways for the two steps synthesis of atropine. This investigation led to a highly efficient first step esterification of tropine to intermediate without the use of tropine salt or the additional supplement of an acid, which is a route first published by the

authors in Wleklinski et.al.[42] The first step was optimized in flow utilizing the information obtained in charged microdroplets. The intermediate from the first step in preparative ES was used to screen 22 unique bases for the base catalyzed aldol condensation to form the final product, atropine. Seven bases were shown to yield atropine and with the exception of transient solids, all lead to the production of atropine in flow. In both preparative ES and continuous microfluidics, the base with the highest percent conversion and lowest percent conversion to byproducts was 1,5-diazabicyclo[4.3.0]non-5-ene.

In preparative ES the first step yielded a percent conversion of 55.3% to intermediate and the second step yielded a 47.4% conversion to atropine, with an overall percent conversion of 26.2% to atropine. In flow, the percent yield was 30.3% with a 42.2% percent conversion to atropine. Atropine was continuously synthesized in both preparative EES and microfluidics with a percent conversion of 23.5% in preparative EES and 33.45% yield in flow. This represents an increase in yield a factor of 4.34 and the 8-minute pathway is almost 1.9 times faster than the previously published state-of-the-art flow synthesis. The correlation of the data between preparative ES and microfluidics provides evidence that accelerated reactions in droplets can guide microfluidics. This is the first detailed investigation of spray reactions guiding microfluidic synthesis where preparative ES has been explicitly used for route screening, solvent screening and acid/base screenings on a large scale. Preparative ES was used as a rapid way to discover new synthetic pathways and this methodology led to faster optimization of microfluidic reactions by determining unsuccessful reaction pathways. Pathways discovery to determine new and faster reactions for formulations from raw materials can improve the current workflow and manufacturing in the pharmaceutical and chemical industries.

2.5 Acknowledgements

Financial support from the Department of Defense's Defense Advanced Research Projects Agency (award no. W911NF- 16-2- 0020) is acknowledged.

2.6 References

1. Hessel, V.; Kralisch, D.; Kockmann, N.; Noël, T.; Wang, Q., Novel process windows for enabling, accelerating, and uplifting flow chemistry. *ChemSusChem* **2013,** *6*, 746-789.

2. Yoshida, J.-i.; Takahashi, Y.; Nagaki, A., Flash chemistry: flow chemistry that cannot be done in batch. *ChemComm* **2013,** *49*, 9896-9904.

3. Wegner, J.; Ceylan, S.; Kirschning, A., Ten key issues in modern flow chemistry. *Chem Commun (Camb)* **2011,** *47*, 4583-92.

4. Webb, D.; Jamison, T. F., Continuous flow multi-step organic synthesis. *Chem. Sci.* **2010,** *1*, 675-680.

5. Geyer, K.; Gustafsson, T.; Seeberger, P. H., Developing continuous-flow microreactors as tools for synthetic chemists. *Synlett* **2009**, 2382-2391.

6. Jensen, K. F., Silicon-based microchemical systems: Characteristics and applications. *MRS Bull.* **2006,** *31*, 101-107.

7. Adamo, A.; Beingessner, R. L.; Behnam, M.; Chen, J.; Jamison, T. F.; Jensen, K. F.; Monbaliu, J. C.; Myerson, A. S.; Revalor, E. M.; Snead, D. R.; Stelzer, T.; Weeranoppanant, N.; Wong, S. Y.; Zhang, P., On-demand continuous-flow production of pharmaceuticals in a compact, reconfigurable system. *Science* **2016,** *352*, 61-7.

8. Snead, D. R.; Jamison, T. F., A three-minute synthesis and purification of ibuprofen: pushing the limits of continuous-flow processing. *Angew. Chem. Int. Ed. Engl.* **2015,** *54*, 983-7.

9. Kralisch, D.; Kreisel, G., Assessment of the ecological potential of microreaction technology. *Chem. Eng. Sci.* **2007,** *62*, 1094-1100.

10. Hartman, R. L.; Jensen, K. F., Microchemical systems for continuous-flow synthesis. *Lab Chip* **2009,** *9*, 2495-507.

11. Kim, H.; Min, K. I.; Inoue, K.; Im, D. J.; Kim, D. P.; Yoshida, J., Submillisecond organic synthesis: Outpacing Fries rearrangement through microfluidic rapid mixing. *Science* **2016,** *352*, 691-694.

12. Malet-Sanz, L.; Susanne, F., Continuous flow synthesis. A pharma perspective. *J. Med. Chem.* **2012,** *55*, 4062-98.

13. Baxendale, I. R.; Braatz, R. D.; Hodnett, B. K.; Jensen, K. F.; Johnson, M. D.; Sharratt, P.; Sherlock, J. P.; Florence, A. J., Achieving continuous manufacturing: technologies and approaches for synthesis, workup, and isolation of drug substance May 20-21, 2014 continuous manufacturing symposium. *J. Pharm. Sci.* **2015,** *104*, 781-791.

14. Gustafsson, T.; Ponten, F.; Seeberger, P. H., Trimethylaluminium mediated amide bond formation in a continuous flow microreactor as key to the synthesis of rimonabant and efaproxiral. *ChemComm* **2008**, 1100-1102.

15. Hopkin, M. D.; Baxendale, I. R.; Ley, S. V., An expeditious synthesis of imatinib and analogues utilising flow chemistry methods. *Org Biomol Chem* **2013,** *11*, 1822-39.

16. Deadman, B. J.; Hopkin, M. D.; Baxendale, I. R.; Ley, S. V., The synthesis of Bcr-Abl inhibiting anticancer pharmaceutical agents imatinib, nilotinib and dasatinib. *Org. Biomol. Chem.* **2013,** *11*, 1766-1800.

17. Zhang, P.; Russell, M. G.; Jamison, T. F., Continuous flow total synthesis of rufinamide. *Org. Process Res. Dev.* **2014,** *18*, 1567-1570.

18. Snead, D. R.; Jamison, T. F., End-to-end continuous flow synthesis and purification of diphenhydramine hydrochloride featuring atom economy, in-line separation, and flow of molten ammonium salts. *Chem. Sci.* **2013,** *4*, 2822-2827.

19. Murray, P. R. D.; Browne, D. L.; Pastre, J. C.; Butters, C.; Guthrie, D.; Ley, S. V., Continuous flow-processing of organometallic reagents using an advanced peristaltic pumping system and the telescoped flow synthesis of (E/Z)-Tamoxifen. *Org. Process Res. Dev.* **2013,** *17*, 1192-1208.

20. Espy, R. D.; Wleklinski, M.; Yan, X.; Cooks, R. G., Beyond the flask: Reactions on the fly in ambient mass spectrometry. *TrAC, Trends Anal. Chem.* **2014,** *57*, 135-146.

21. Girod, M.; Moyano, E.; Campbell, D. I.; Cooks, R. G., Accelerated bimolecular reactions in microdroplets studied by desorption electrospray ionization mass spectrometry. *Chemical Science* **2011,** *2*, 501-510.

22. Bain, R. M.; Pulliam, C. J.; Raab, S. A.; Cooks, R. G., Chemical synthesis accelerated by paper spray: the haloform reaction. *Journal of Chemical Education* **2015,** *93*, 340-344.

23. Bain, R. M.; Pulliam, C. J.; Cooks, R. G., Accelerated Hantzsch electrospray synthesis with temporal control of reaction intermediates. *Chem. Sci.* **2015,** *6*, 397-401.

24. Schröder, D., Applications of electrospray ionization mass spectrometry in mechanistic studies and catalysis research. *Acc. Chem. Res.* **2012,** *45*, 1521-1532.

25. Perry, R. H.; Cahill, T. J., 3rd; Roizen, J. L.; Du Bois, J.; Zare, R. N., Capturing fleeting intermediates in a catalytic C-H amination reaction cycle. *Proceedings of the National Academy of Sciences of the United States of America* **2012,** *109*, 18295-18299.

26. Mortensen, D. N.; Williams, E. R., Microsecond and nanosecond polyproline II helix formation in aqueous nanodrops measured by mass spectrometry. *Chemical communications (Cambridge, England)* **2016,** *52*, 12218-12221.

27. Xu, G.; Chen, B.; Guo, B.; He, D.; Yao, S., Detection of intermediates for the Eschweiler–Clarke reaction by liquid-phase reactive desorption electrospray ionization mass spectrometry. *Analyst* **2011,** *136*, 2385-2390.

28. Perry, R. H.; Splendore, M.; Chien, A.; Davis, N. K.; Zare, R. N., Detecting reaction intermediates in liquids on the millisecond time scale using desorption electrospray ionization. *Angew. Chem. Int. Ed.* **2011,** *123*, 264-268.

29. Müller, T.; Badu-Tawiah, A.; Cooks, R. G., Accelerated Carbon-Carbon Bond-Forming Reactions in Preparative Electrospray. *Angewandte Chemie International Edition* **2012,** *51*, 11832-11835.

30. Banerjee, S.; Gnanamani, E.; Yan, X.; Zare, R. N., Can all bulk-phase reactions be accelerated in microdroplets? *Analyst* **2017,** *142*, 1399-1402.

31. Chen, H.; Venter, A.; Cooks, R. G., Extractive electrospray ionization for direct analysis of undiluted urine, milk and other complex mixtures without sample preparation. *Chemical Communications* **2006**, 2042-2044.

32. Lee, J. K.; Kim, S.; Nam, H. G.; Zare, R. N., Microdroplet fusion mass spectrometry for fast reaction kinetics. *Proceedings of the National Academy of Sciences* **2015,** *112*, 3898-3903.

33. Qiu, R.; Zhang, C.; Qin, Z.; Luo, H., A multichannel rotating electrospray ionization mass spectrometry (MRESI): instrumentation and plume interactions. *RSC Advances* **2016,** *6*, 36615-36622.

34. Grynkiewicz, G.; Gadzikowska, M., Tropane alkaloids as medicinally useful natural products and their synthetic derivatives as new drugs. *Pharmacol Rep* **2008,** *60*, 439-463.

35. Gadzikowska, M.; Grynkiewicz, G., Tropane alkaloids in pharmaceutical and phytochemical analysis. *Acta Pol Pharm* **2002,** *59*, 149-60.

36. Dai, C. H.; Snead, D. R.; Zhang, P.; Jamison, T. F., Continuous-Flow Synthesis and Purification of Atropine with Sequential In-Line Separations of Structurally Similar Impurities. *J Flow Chem.* **2015,** *5*, 133-138.

37. Robinson, R., LXIII.-A synthesis of tropinone. *J. Chem. Soc.* **1917,** *111*, 762-768.

38. Schmidt, G. C.; Eling, T. E.; Drach, J. C., Synthesis of tropine-labeled atropine I. Micro methods for the synthesis of tropine and for its esterification with tropic acid. *J. Pharm. Sci.* **1967,** *56*, 215-221.

39. Pfister, J. R., Convenient synthesis of N-noratropine. *J. Org. Chem.* **1978,** *43*, 4373-4374.

40. Zhu, L.; Gamez, G.; Chen, H. W.; Huang, H. X.; Chingin, K.; Zenobi, R., Real-time, on-line monitoring of organic chemical reactions using extractive electrospray ionization tandem mass spectrometry. *Rapid Commun. Mass Spectrom.* **2008,** *22*, 2993-2998.

41. Chen, H.; Yang, S.; Li, M.; Hu, B.; Li, J.; Wang, J., Sensitive Detection of Native Proteins Using Extractive Electrospray Ionization Mass Spectrometry. *Angew. Chem. Int. Ed.* **2010,** *49*, 3053-3056.

42. Wleklinski, M.; Falcone, C. E.; Loren, B. P.; Jaman, Z.; Iyer, K.; Ewan, H. S.; Hyun, S.-H.; Thompson, D. H.; Cooks, R. G., Can accelerated reactions in droplets guide chemistry at scale? *Eur. J. Org. Chem.* **2016,** *2016*, 5480-5484.

43. Chen, H.; Eberlin, L. S.; Nefliu, M.; Augusti, R.; Cooks, R. G., Organic reactions of ionic intermediates promoted by atmospheric-pressure thermal activation. *Angew. Chem. Int. Ed.* **2008,** *47*, 3422-3425.

CHAPTER 3. HIGH THROUGHPUT EXPERIMENTATION AND CONTINUOUS FLOW VALIDATION OF SUZUKI-MIYAURA CROSS-COUPLING REACTIONS

Reproduced (adapted) from Jaman, Z.; Mufti, A.; Sah, S.; Avramova, L.; Thompson, D. H. 'High Throughput Experimentation and Continuous Flow Validation of Suzuki-Miyaura Cross-Coupling Reactions' *Chem. Eur. J* **2018**, 24, 9546-9554 with permission provided by John Wiley and Sons and Copyright Clearance Center.

3.1 Introduction

The development of automated high-throughput (HT) methods has been shown to boost lab productivity by rapid generation of comprehensive reaction data that enriches our understanding of reaction scope and limitations.[1] HT experimentation (HTE) based on the screening of compounds across a range of settings have impacted many areas of biology, drug discovery, medicinal chemistry, [2, 3] and catalysis.[4, 5] Automated reactions can often be run in parallel, but the downstream analysis is typically a bottleneck due to relatively slow chromatographic separation and quantitation. HTE coupled with mass spectrometry (MS) analysis can accelerate both the discovery and optimization of reaction conditions, particularly in the cases of chemical process development[4, 6, 7] and (bio)pharmaceutical drug development where pressures to shorten the time to market are increasing.[8, 9] HTE has been challenging in the case of organic reaction optimization, especially for catalytic reactions that may employ solid catalysts or volatile organic solvents. [5, 6]

The central goal in reaction HTE is the discovery of the best conditions for a given set of precursors to identify reaction hotspots. After HTE, a quick validation of these reaction hotspots is used to build confidence in the hits identified by this method. Microfluidic reaction screening of the HTE hits are an ideal method for validating organic transformations[10] under continuous flow conditions. This has been shown to be especially true for catalytic reactions that can be achieved under faster and greener conditions.[11] Moreover, fast microfluidic synthesis of small organic molecules, coupled with continuous reaction monitoring using electrospray ionization mass spectrometry (ESI-MS) shows even greater promise for rapid optimization of continuous production methodology. [12-15] Here, we report a study of the Suzuki-Miyura (S-M) cross-coupling

reaction as a HTE test bed using ESI-MS as a readout tool. The S-M reaction was chosen because the carbon–carbon bond formation via palladium-catalyzed S-M cross-coupling is an important reaction for small molecule synthesis [16] that has been widely used. [17-19]

A simple, and efficient technique for identifying and optimizing S-M reaction conditions with different functional group tolerance is described. Biologically important synthons were synthesized using S-M cross coupling reaction without protecting the functional groups. The HT screening was used as a faster way of finding best reaction parameters that can lead to faster optimization of microfluidic reactions by eliminating failed reaction conditions. Decreasing the number of unsuccessful opportunities will result in different libraries that has compounds with various physicochemical properties. There is a high chance of finding drug candidates by building such library in a short time.

The S-M reaction has already been reported under some limited ranges of flow conditions [11, 20-22], nonetheless, we explored its utility toward the synthesis of biologically as well as pharmaceutically important synthons[23-29] without protecting groups (Figure 3.1) in a microfluidic reactor using EtOH as the solvent to make broadly explore the utility of this transformation. [11, 19]

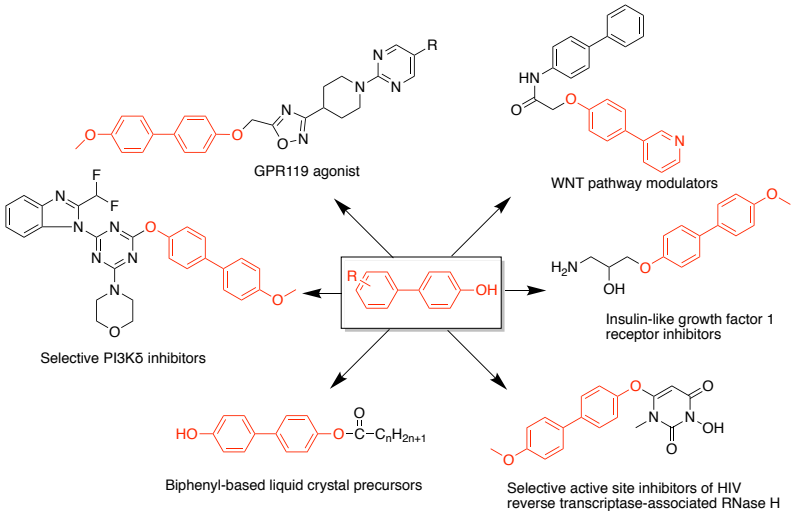

Figure 3.1 Biologically and materially important synthons containing common [1,1'-biphenyl]-4-ol cores.

3.1.1 Brief Summary of this Chapter

An automated HTE of S-M reactions was performed in 96-well plates using 4-hydroxyphenylboronic acid and 11 different aryl halides (Scheme 3.1) with order of addition, stoichiometry, temperature, and concentration as independent variables. These experiments led to the discovery of optimized batch conditions from hundreds of different reaction conditions using XPhosPdG3 catalyst and 1,8-diazabicyclo[5.4.0]undec-7-ene (DBU) as base. A small scale microfluidic reaction employing the best conditions from the batch reaction screening produced up to 98% yield of S-M coupled product by HPLC/MS-MS analysis, thus validating our finding from HT experimentations.

3.2 Results and Discussion

3.2.1 High Throughput Experimentation

A high-precision robot was used for the preparation of nanoliter scale reaction mixtures for automated HT screening of S-M reaction conditions with downstream MS analysis. The reactions were performed in a glass vials sealed within four 96-well aluminum blocks using EtOH as solvent and heating of single block for 1h either at 50 °C,100 °C,150 °C, or 200 °C. A highly sensitive triple quadrupole MS coupled to an autosampler was used for rapid investigation of the reaction product distribution. Full mass spectra in negative ion mode were recorded for each reaction mixture.

The S-M cross-coupling reactions were screened using 4-hydroxyphenylboronic acid, various aryl halides, and a commercially available palladium catalyst, XPhosPdG3 (Scheme 3.1), to explore the impact of different aryl halide substrates on reaction efficiency without the use of additional protection/deprotection steps. Reaction mixtures (45 μL of total volume of each well) were deposited in duplicate in 96 glass-lined Al well plates and the reactions heated at either 50 °C, 100 °C, 150 °C, or 200 °C for 1 h before quenching to 20 °C, centrifuging, and diluting into 384 well plates for MS analysis. Each square in Table 3.1 represents a unique reaction condition. The first two columns and last four columns are negative controls. Although the ionization efficiencies vary for each compound, the outcomes are reported on the basis of reaction product peak intensity to enable a simple and uniform comparison.

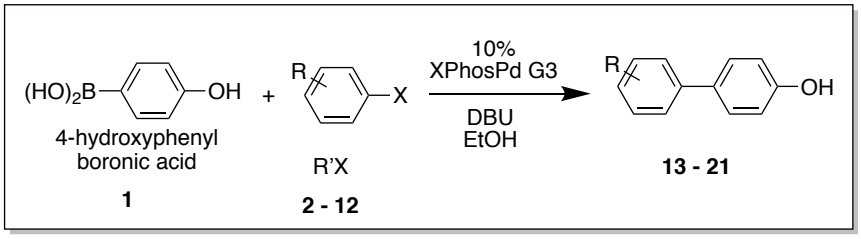

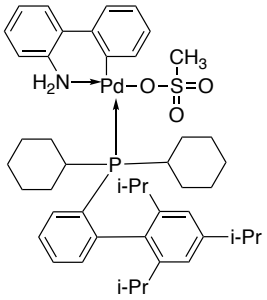

XPhosPd G3

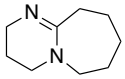

1,8-Diazabicyclo[5.4.0]undec-7-ene (DBU)

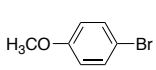

2

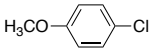

3

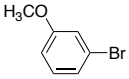

4

5

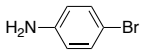

6

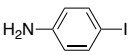

7

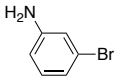

8

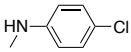

9

10

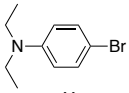

11

12

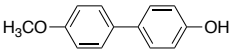

13

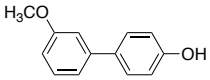

14

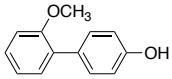

15

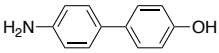

16

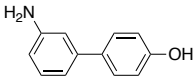

17

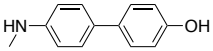

18

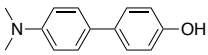

19

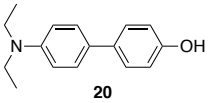

20

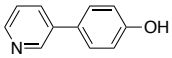

21

Scheme 3.1 scope evaluated in high-throughput experimentation of S-M cross-coupling reactions to generate various biphenyl products.

Table 3.1 HTE outcomes as a function of reagent addition order and substrate concentration in the reaction mixture. Each quantity is an average of two experimental measurements. Each set of similar substrates and stoichiometries appears as a set of four conditions wherein the top left, top right, bottom left and bottom right entries are reactions run at 200 °C, 150 °C, 100 °C and 50 °C, respectively. The first two columns (St. = **1**:0) and last four columns (St. = (R'X:0 and 0:0) are the negative controls. Sub = substrates; St = stoichiometry.

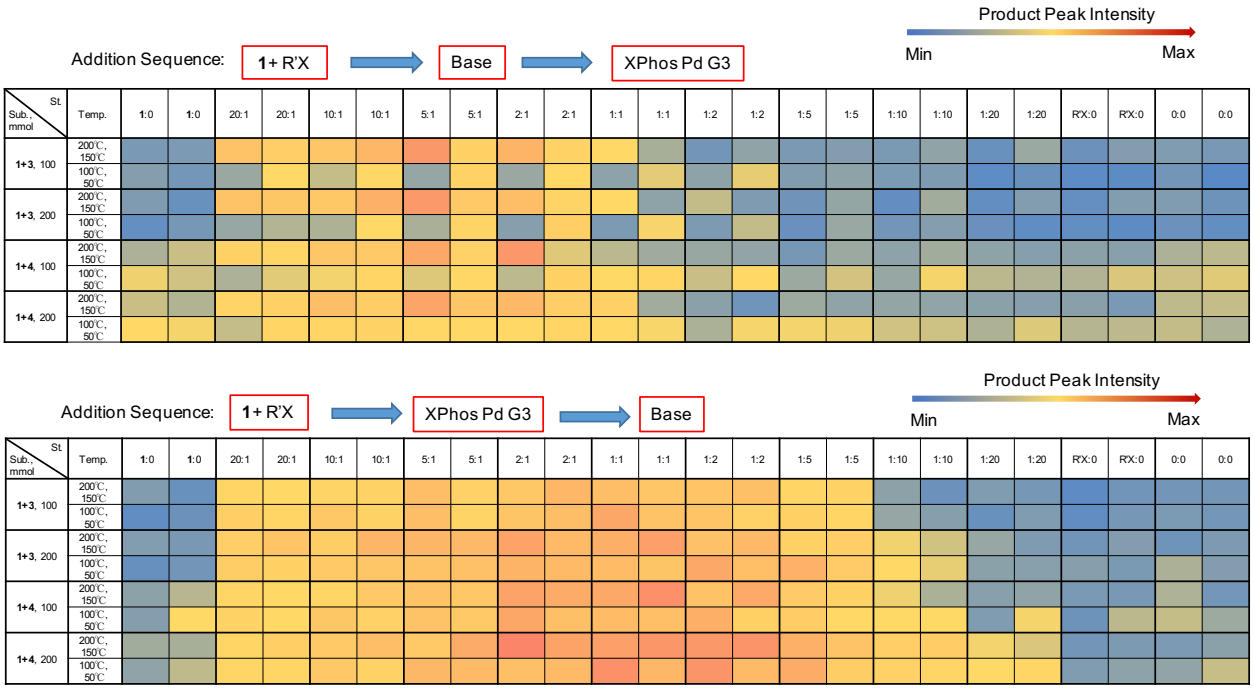

Our initial HTE explored the S-M reaction by adding in sequence a mixture of **1**, base, and catalyst solution in EtOH, followed by aryl halide (**2-12**) addition. Unfortunately, no product peak was detected in MS, although a prominent peak corresponding to the hydrolyzed boronic acid product was observed. These findings suggest that the catalyst was poisoned by the base while sitting idle at 20 °C during subsequent robotic reagent transfers over the intervening period (20 min) before the reaction was initiated by heating. When the order of addition was changed to aryl halide and **1**, followed by base and catalyst in sequence, the product peak was observed in resulting MS, although the product yields were not satisfactory (Table 3.1, A). We attribute these finding to the consumption of **1** by base before catalyst addition such that insufficient boronic acid was available to participate in the catalytic cycle. Nonetheless, when the base solution was added after the catalyst, a significant increase in product conversion was observed (Table 3.1, B) with the accompanied detection of self-coupled **1-1** product by MS.

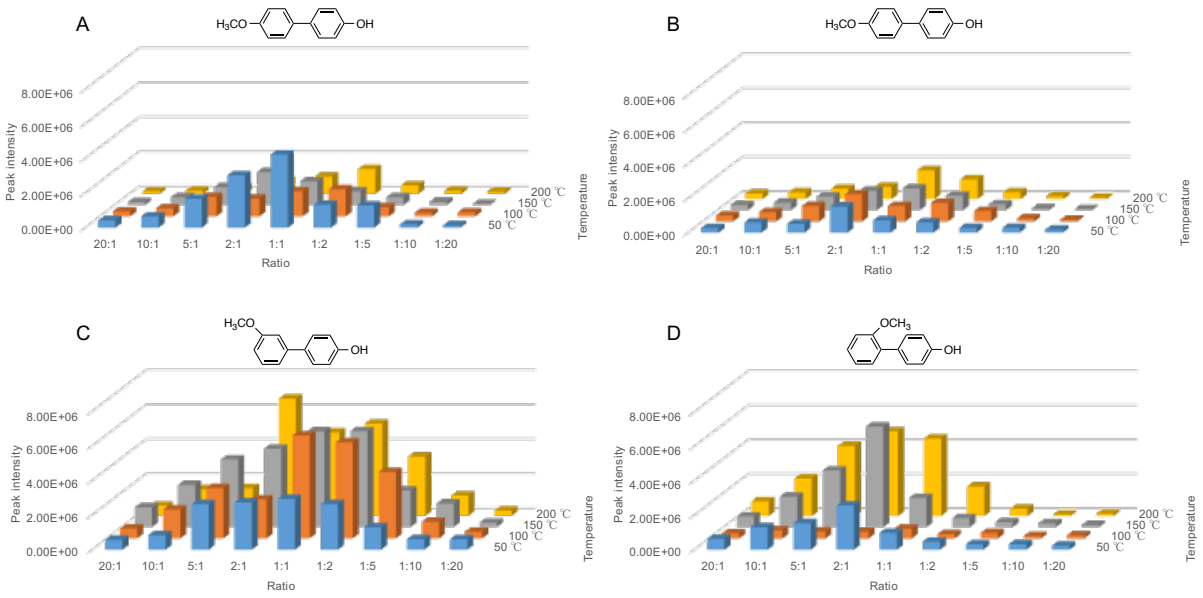

Figure 3.2 Comparative coupling efficiencies for anisole-type biphenyl products formed under different temperature, and stoichiometric conditions. Reactant concentrations were 200 mmol except for **1**+**5** that was run at 100 mmol, 400 mmol DBU, and 10% XPhosPdG3. A = **1**+**2**; B = **1**+**3**; C = **1**+**4**; D = **1**+**5**.

We subsequently utilized the optimal conditions identified in Table 3.1 for a broader screen of aryl halide substrates. Our results show that both electron-rich and electron-deficient aryl halides (**2-12**) were tolerated to produce cross coupled products in moderate to good yield as assessed by product peak intensities (Figure 3.2A-D). Comparison of the anisole family of precursors (**2-5**) revealed that the meta-positioned methoxy group (**4**, Figure 3.2C) provided more desired product than ortho (**5**, Figure 3.2D) or para (**2**&**3**, Figure 3.2A&B) due to the reduced electron donating contribution from the meta placement of this substituent.[30]

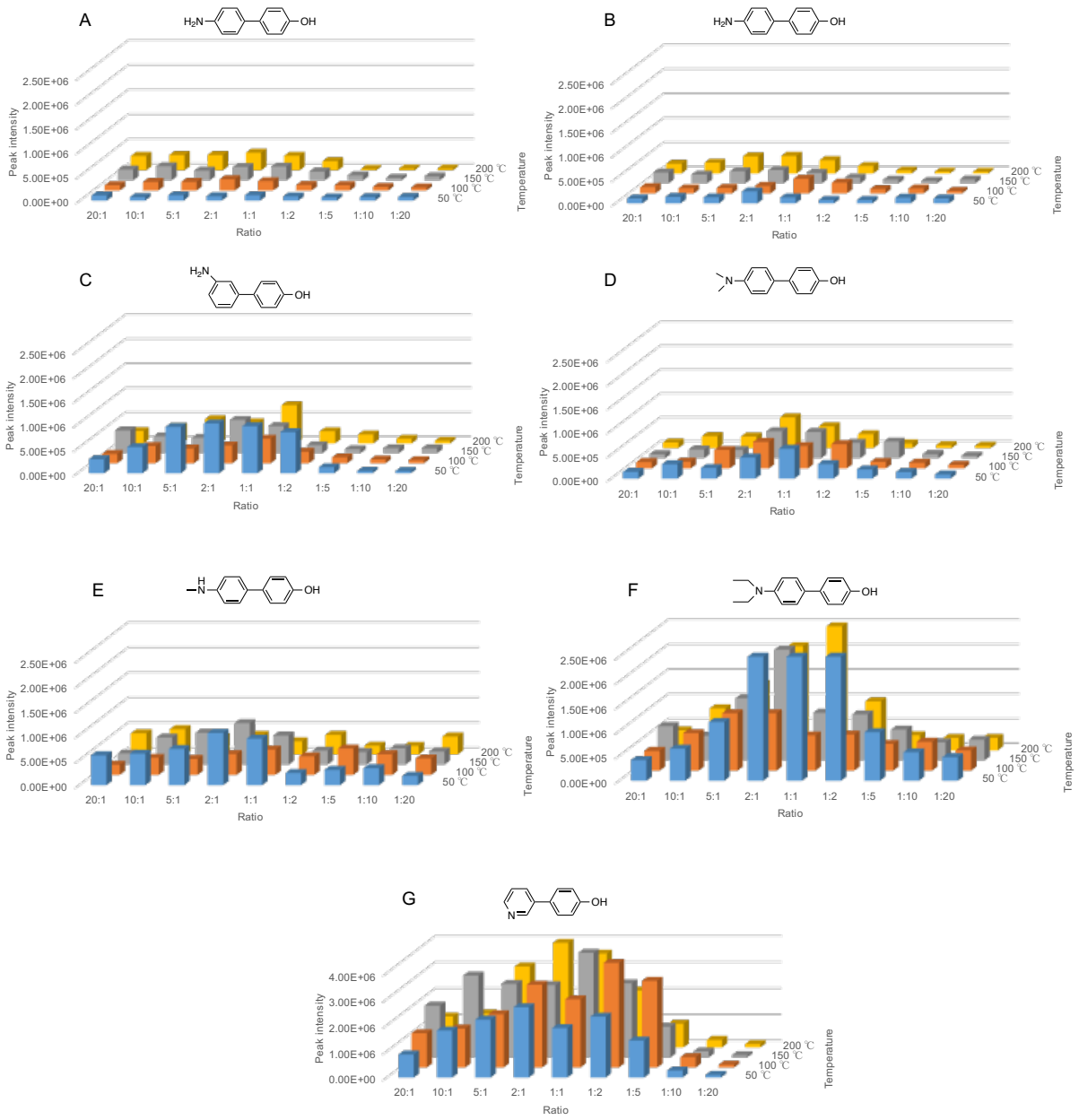

Figure 3.3 Comparative coupling efficiencies for aniline-type biphenyl products formed under different temperature and stoichiometric conditions. Reactant concentrations were 200 mmol, 400 mmol DBU, and 10% XPhosPdG3. A = **1**+**6**; B = **1**+**7**; C = **1**+**8**; D = **1**+**10**, E = **1**+**9**, F = **1**+**11**, G = **1**+**12**.

Electron-rich amino aryl halides (**6-11**) were also transformed to the corresponding biphenyl products, yielding moderate peak intensities for the cross-coupled products (Figure 3.3A-G). As seen in the anisole family of compounds, the meta product, **17** (**1**+**8,** Figure 3.3C) produces

a higher peak intensity than para, **16** (**1+6/7,** Figure 3.2A&B), for the primary amine substrates. When aniline- and anisole-derived products were compared, higher product peak intensities were observed for the anisole family of compounds, **13-15,** than the anilines series, **16-20** (Figures 3.2 and 3.3). We attribute these finding to the greater electron donating property of the amine versus methoxy substituents such that formation of the aminophenyl palladium intermediate is less favorable in the rate limiting oxidative addition step of the catalytic cycle in the aniline series.

Table 3.2 Product peak intensities observed for 504 unique S-M reactions run in bulk mode with the order of addition of base solution after the catalyst. Each quantity is an average of two experimental measurements. Each row indicates reactions of nine ratios of substrates including the control reactions at two different temperatures. Each set of similar substrates and stoichiometries appears as a set of four conditions wherein the top left, top right, bottom left and bottom right entries are reactions run at 200 °C, 150 °C, 100 °C and 50 °C, respectively. The first two columns (St. = **1**:0) and last four columns (St. = (R'X:0 and 0:0) are the negative controls. Sub = substrates; St = stoichiometry.

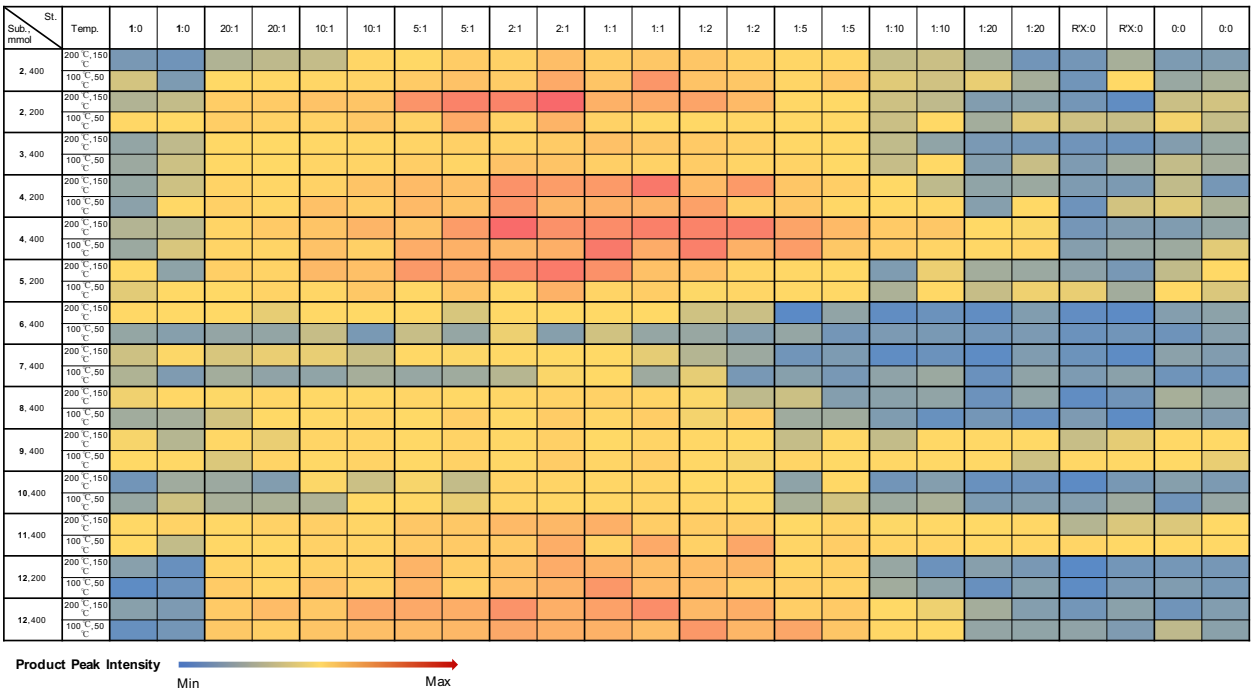

The product peak intensities for secondary and tertiary were higher than those observed for the primary amines (Figure 3.3A-C vs. Figure 3.3D-F), consistent with the observation that primary amines are known to more readily coordinate with palladium catalysts than secondary or tertiary amines due to steric hindrance.[31] In the case of the pyridine derivative, a higher product

peak intensity was observed due to the comparative electron deficiency of the pyridine ring relative to the aniline series (**1**+**12,** Figure 3.3G).

Table 3.2 shows the product peak intensities for 504 unique Suzuki-Miyaura reactions, employing one of 11 different aryl halides and 4-hydroxyphenyl boronic acid in the presence of DBU and 10% XPhosPdG3. Since some low level product peak intensities were observed in the negative control reactions, we used >50% peak intensity as a selection criterion to select reaction hotspots in this map for evaluation in a subsequent set of microfluidic reactions.

3.2.2 Microfluidic Evaluation of HT Experimentation Leads

After identifying reaction hotspots from the high throughput experimentation campaign, we proceeded to test one of the favorable conditions for each reaction to determine the confidence level that could be assumed for the two different reaction formats (i.e., batch 96-well vs. continuous flow). For all microfluidic reactions, the reactions employing a 1:1 ratio of 4-hydroxyphenylboronic acid and aryl halide were evaluated for 0.5, 1, 3 and 6 min residence times at either 100 °C or 150 °C. Reactions using 10% catalyst loadings were complicated by chip clogging problems shortly after initiating the reaction. This problem was obviated by reducing the

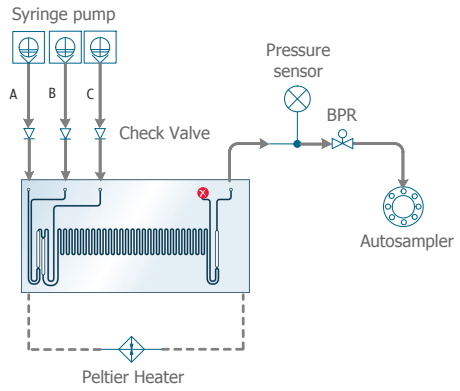

Figure 3.4 Chemtrix reactor and fluid handling for continuous flow synthesis of S-M cross coupling reactions. A = 1:1 mixture of 4-hydroxyphenylboronic acid and aryl halide; B = DBU, C = XPhosPdG3.

catalyst loading to 0.5% since prior work has shown that S-M transformations are more efficient in continuous flow than under traditional bulk reaction conditions due to superior mass and heat transfer and greater mixing efficiency in the narrow reactor channels. The order of addition did

not matter in the microfluidic synthesis since all the reagents come into contact within the same mixing region (Figure 3.4). The formation of the expected products was confirmed by TLC and MS. As the data in Table 3.3 shows, the results from microfluidic continuous reactions were comparable to the findings from bulk screening.

Table 3.3 Comparison of microfluidic and bulk screening outcomes for S-M reactions performed under similar conditions using 200 mmol substrate loading and a 1:1 4-hydroxyphenylboronic acid:aryl halide stoichiometry. In the microfluidic reaction tables, time is reported in min and temperature in °C.

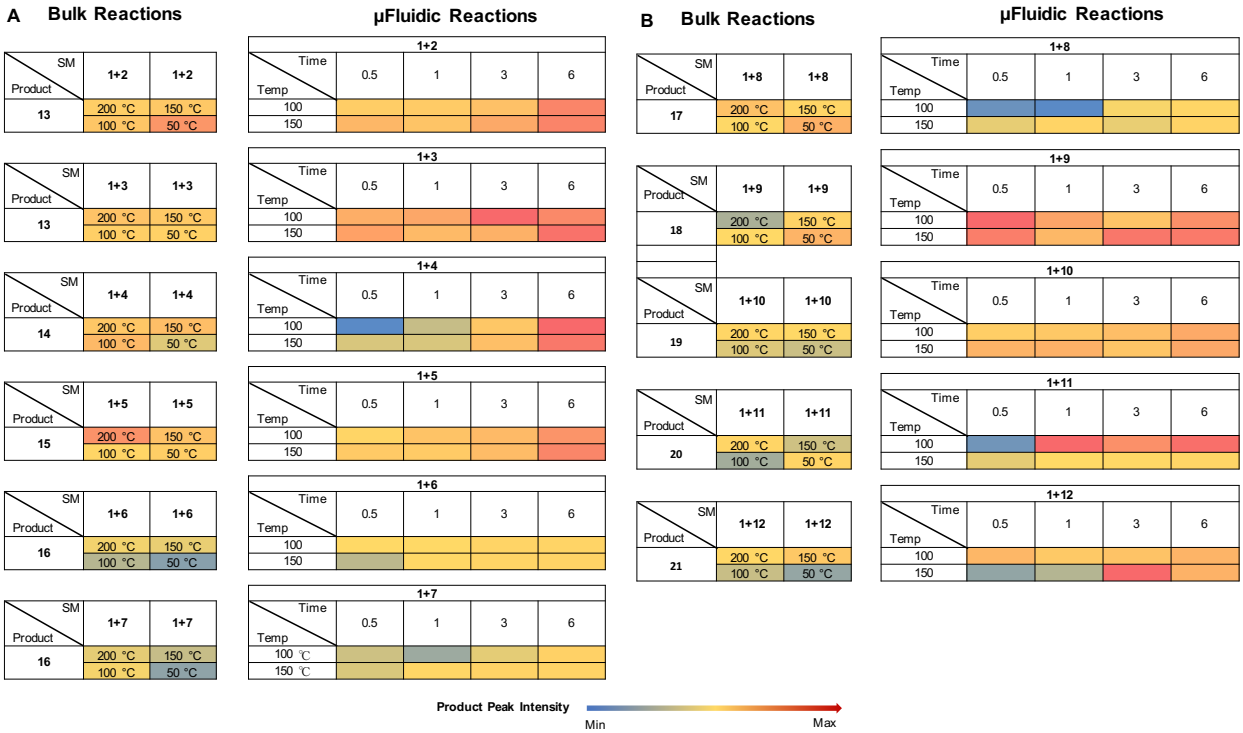

The data in Table 3.3 shows that the S-M reaction tolerates electron donating substitutes in the aryl halide substrate to afford the cross coupled products with varying efficiency. In both bulk and microfluidic experiments, meta (**1**+**4**) directed anisole biphenyl products showed higher product conversion than ortho (**1**+**5**), but in continuous flow processes, para (**1**+**2** & **1**+**3**) also showed higher product peak intensities (Figure 3.3 and Table 3.3). Similarly, bulky tertiary amine (**1**+**9**) and pyridine (**1**+**12**) precursors generated higher product peak intensities in both the bulk screening and flow synthesis formats.

We next investigated the negative results obtained from HTE to evaluate those reaction conditions under continuous flow (Table 3.4). In both cases, almost no product peak was observed even at extended residence times (e.g., 15 min at 150 °C in the case of **1**+**8**).

Table 3.4: Comparison of microfluidic and bulk screening outcomes for S-M reactions that gave negative bulk reaction results. The same reaction conditions were used in each case with 200 mmol substrate loading and 1:20 4-hydroxyphenylboronic acid:aryl halide stoichiometry. In the microfluidic reaction tables, the units are time in min and temperature in °C.

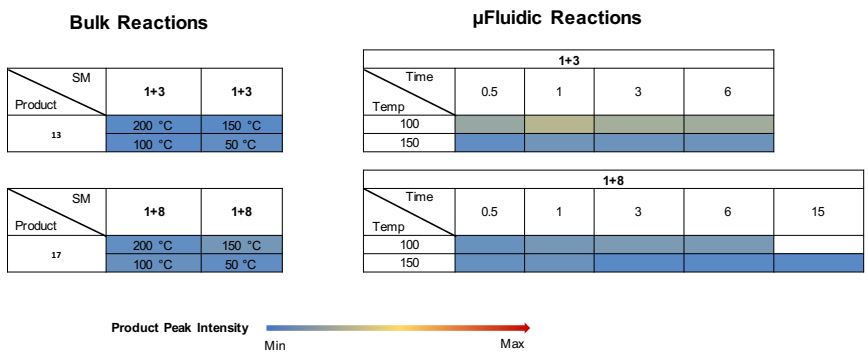

Next, we focused on testing the validity of using product ion intensities as a measure of reaction progress. The anisole and pyridine reaction products were selected for evaluation by HPLC/MS-MS since these products showed high peak intensities in both bulk screening and microfluidic reactions.

Table 3.5 Quantified yields of some S-M microfluidic reactions using HPLC/MS-MS. The same reaction conditions were used in each case (i.e., 200 mmol substrate loading and 1:1 4-hydroxyphenylboronic acid:aryl halide stoichiometry). Peak intensity values are multiples of 1×10^6.

Reaction Condition	13 (1+2)		13 (1+3)		14 (1+4)		15 (1+5)		21 (1+12)	
	Peak intensity	%Yield	Peak intensity	%Yield	Peak intensity	%Yield	Peak intensity	%Yield	Peak intensity	%Yield
100 ℃, 0.5 min	1.1	3.4	3.1	13.8	1.3	46.8	0.6	3.5	6.1	23.2
100 ℃, 1 min	1.1	4.6	3.5	24.5	2.6	54.0	1.6	6.5	4.7	37.7
100 ℃, 3 min	1.8	6.1	7.6	27.8	3.7	70.9	2.1	15.1	5.1	47.7
100 ℃, 6 min	5.2	10.5	5.6	48.1	6.1	95.5	4.3	17.6	6.3	48.1
150 ℃, 0.5 min	2.3	8.0	4.4	48.7	2.8	61.9	1.2	5.6	1.8	45.8
150 ℃, 1 min	1.6	12.5	2.2	71.2	2.8	93.9	1.1	15.1	2.3	68.6
150 ℃, 3 min	3.2	35.4	2.8	71.8	3.9	95.6	2	17.1	12.2	70.5
150 ℃, 6 min	5.3	77.8	7.1	73.1	5.8	97.9	5.2	20.8	6.5	95.6

A general trend of increasing product yield was observed for all anisoles (**2-5**) and pyridine **12** starting materials (Table 3.5). High yields were observed for **14** and **21** as was expected from the screening results. In most of the cases, there was good agreement between peak intensities and quantitative product yield**.** The reason for this outlier remains unclear at this time. Low yield for **15** were observed due to the steric demands of the o-MeO substituent that requires more energy to derive the reaction[27, 30]. The rest of the figures and datasets related to this chapter are in APPENDIX B.

3.3 Experimental

3.3.1 Chemicals

All chemicals and reagents were purchased from Sigma-Aldrich (St. Louis, MO) and used without purification. All standards for quantitation were purchased from Combi-Blocks, Inc. (San Diego, CA).

3.3.2 Liquid Handling Robot

Reaction plate set up and sample preparation for automated mass spectrometry analysis (384-well) was performed using a dual-bridge liquid handling Biomek FX robot (Beckman Coulter, Inc., Indianapolis, IN). A 96-tip head enables the simultaneous transfer of 96 samples under the same conditions (speed of aspiration and dispensing, height of pipetting at source and destination positions, pattern of pipetting, etc.). Although the 8-channel head treated less sample simultaneously, it provided more flexibility in terms of volumes transferred, layout of source and destination plates, pipetting height, and speed. The high capacity deck of this device fits all labware (robotic tips, plates, reservoirs) needed for one operational step. Tips boxes were transferred to the loading station with the Biomek FX gripper, thus minimizing human intervention into the process. All robotic tips were disposable polypropylene to maximize organic solvent and reagent compatibility. Polypropylene multi-well plates and reservoirs, as well as custom made Teflon reservoirs, were used during the experiments to evaluate catalyst and base resistance. Methods were developed and validated using the Biomek software-unique point-and-click programming tool. The standard pipetting techniques of the device were modified to optimize accurate transfer of highly volatile liquids.

3.3.3 Customized Heating Block

An aluminum heating block containing four, 100 W cartridge heaters was fabricated in-house. Temperature control was provided by a CNi series temperature controller (Omega Engineering, Stamford, CT) and a solid state relay was used to modulate the 120 V power to the heaters to provide temperature control over a range from +20 °C to +200 °C.

3.3.4 Mass Spectrometry

The mass spectrometer used was a TSQ Quantum Access MAX connected to a Dionex Ultimate 3000 Series Pump and WPS-3000 Autosampler (Thermo Fisher Scientific, Waltham, MA). Electrospray ionization (ESI) analysis in full scan mode was used to monitor each reaction in both positive and negative ion modes. These data were recorded using parameters optimized for the ESI source and MS as follows: spraying solvent, acetonitrile; spray voltage +3.5 kV (positive mode) & -4.0 kV (negative mode); capillary temperature, 250 °C; sheath gas pressure, 10 psi; scan time, 1 s; Q1 peak width (FWHM), 0.70 Th; micro scans, 3. The autosampler settings were as follows: MS acquire time, 2 min; sample injection volume, 10 µL. Data acquisition and processing were performed using Thermo Fisher Xcalibur software. MS data from Xcalibar software were converted to text files using MS converter. Script was written for Perl terminal command to convert the text file to csv format. (see APPENDIX B to find the script)

3.3.5 Microfluidics

All microfluidic validation reactions were performed using a Labtrix S1 (Chemtrix, Ltd, Netherlands). The system is same as described in chapter 2. Here, the staggered orientated micro-reactor (SOR) chip 3225 (four inlets and one outlet, volume 10 µL) that has channels width 300 µm wide and 120 µm deep was used. Gastight glass syringes mounted on the Chemtrix unit were obtained from Innovative Labor System (ILS, Philadelphia, PA). All operations were controlled via the Chemtrix GUI software.

3.3.6 HPLC/MS-MS Analysis

Chromatographic separations were performed using an Agilent 1100 HPLC system with an Agilent XDB-C18 (2.1 × 50 mm, 3.5 µm) reversed-phase column for all anisole compounds, **13-15,** or an Agilent SB-CN (4.6 × 150 mm, 3.5 µm) reversed-phase column for **21** with a flow

rate of 0.4 mL/min at ambient temperature. The mobile phase consisted of A (0.1% formic acid in water) and B (0.1% formic acid in acetonitrile), starting with 10% B for 0.5 min, with a linear gradient of 10–100% B from 0.5-6 min, and a hold at 100% B from 6-7 min. Column re-equilibration was performed from 100-10% B from 7-7.1 min, with at 10% B hold from 7.1-10 min. Online mass spectrometry detection was performed using an Agilent 6410 triple quadrupole mass spectrometer, utilizing negative electrospray ionization mode. ESI capillary voltage was −4.0 kV, nebulizer gas pressure was set at 40 psig, gas temperature was 325 °C, and the drying gas flow rate was 8.0 L/min. Multiple Reaction Monitoring (MRM) was used and quantitation was accomplished using a multi-level calibration curve constructed with authentic standards ranging from 0.01 – 100 mM. (see APPENDIX B for details table)

3.3.7 High Throughput Bulk Screening

High-throughput screening of palladium catalyzed S-M reactions were performed in 96-well parallel synthesis metal block assemblies (Analytical Sales and Services, Inc., Flanders, NJ). The reaction mixtures in each glass vial insert of the 96-well metal block were prepared using the Beckman Coulter FX liquid handling robot. 4-Hydroxyphenylboronic acid (**1**, 400 mmol) and aryl halide (**2-12**, 400 mmol) in EtOH were pipetted via the Span 8 arm into a master plate and then distributed equally into another set of three 96-well plates using the 96-tip head (Figure 3.5). A master plate was made containing nine different ratios of boronic acid, **1,** and aryl halide **2-12**. Next, DBU (800 mmol) was dispensed separately into each plate followed by XPhosPdG3 (40 mmol) solutions in EtOH using the 96-tip head. The top of the metal block was covered with a sheet of perfluoroalkoxy (PFA) film and two silicone rubber mats that fully covered the reaction vials. The metal blocks were heated at 50 °C, 100 °C, 150 °C or 200 °C using the home made block heater for 1 h (Figure 3.5). Extensive testing revealed that the reactor is sealed well enough to heat above the solvent boiling point with less than 5% solvent loss and no cross talk between wells. After 1 h heating, the plates were cooled to room temperature, centrifuged, and loaded back onto the deck of the liquid handling robot. Samples for MS autosampling were prepared in 384-well plates by robotic pipetting and diluted by 1000-fold in EtOH. The MS analysis method includes pre-wash and post-wash of the needle to avoid contamination between sample analyses.

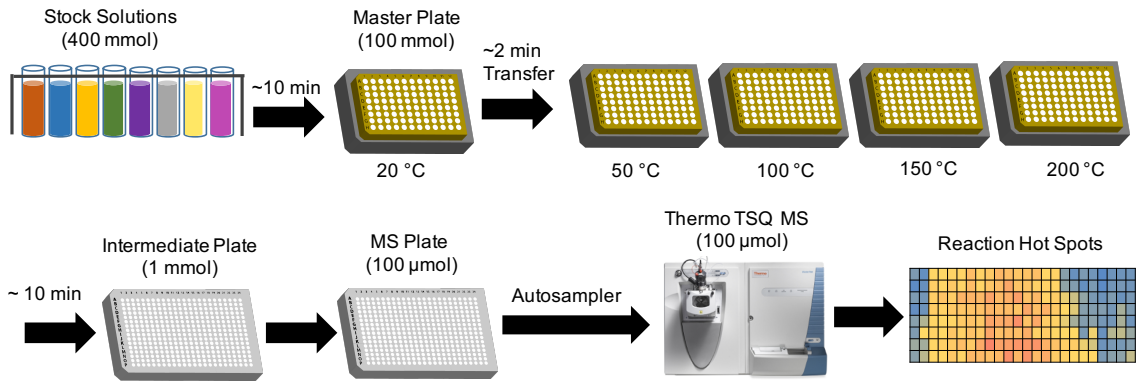

Figure 3.5 Schematic flow of preparation and analysis of microtiter plates for bulk screening of S-M reaction.

3.3.8 MS Data Analysis Procedure

ESI-MS was performed using a TSQ Quantum Access MAX connected with Dionex Ultimate 3000 Series Pump and WPS-3000 Autosampler (Thermo Fisher Scientific, Waltham, MA). Full scan mode was used for ESI analysis. Data from Thermo TSQ Xcalibar software was converted to text files using MS converter (Figure 3.6). The Script that was used in the Perl terminal command to convert text files to the csv format is given in APPENDIX B. All other analysis was done using Microsoft Excel 2016.

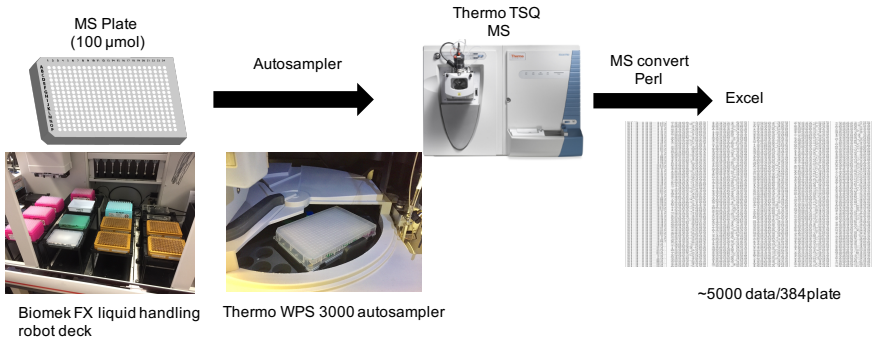

Figure 3.6 Schematic flow of 384-well plate preparation for MS and analysis using an auto-sampler.

3.3.9 Microfluidic Reactions

A 1:1 mixture of 4-hydroxyphenylboronic acid (**1**, 400 mmol, 1 equiv) and aryl halide (**2-12**, 400 mmol, 1 equiv) in EtOH was loaded into a 1 mL ILS gas tight glass syringe. DBU (800

mmol, 2 equiv) and XPhosPdG3 (2 mmol, 0.5%) solutions in EtOH were individually loaded into another two 1 mL ILS gastight glass syringes. Each solution was successively dispensed into the SOR 3225 reactor to engage the reactants. All cross-coupling reactions were run at either 100 °C or 150 °C, with residence times of 0.5, 1, 3, or 6 min. The reaction mixtures were collected after quenching and stored at -80 °C. The subsequent ESI-MS and HPLC/MS-MS analyses were performed without further purification.

3.4 Conclusion

This investigation explored the use of a robotic HTE technique to execute reactions in 96-well arrays that were subsequently coupled with fast MS analysis using an autosampler. Palladium catalyzed S-M cross-coupling reactions were screened in this system to generate a heat map of reactivity to inform conditions for the downstream scale up in continuous flow. A total of 648 unique experiments using 4-hydroxyphenylboronic acid and 11 different aryl halides were explored in duplicate and the results reported as a function of MS peak intensity. The comparison of some successful reactions from HTE were run under microfluidic conditions; these experiments confirmed that the positive conditions identified by HTE were true positives. Furthermore, negatives reaction conditions identified by HTE also produced negative results under microfluidic conditions, even when long residence times at higher temperature were used. Moreover, quantitative analysis by HPLC/MS-MS provided evidence of a good correlation between HTE and microfluidic reactions.

This HTE and microfluidic validation approach may be equally applicable to other catalytic and noncatalytic reactions to rapidly reveal vast reactivity landscapes to guide reaction optimization efforts. This approach might also be applied to the identification of the best conditions for challenging substrates or the discovery of new routes for the production of bioactive molecules. Further investigation along these lines will be needed to strengthen this correlation.

3.5 Acknowledgements

We gratefully acknowledge the financial support from the Department of Defense: Defense Advanced Research Projects Agency (award no. W911NF-16-2-0020). The effort of Ryan Hilger

(Amy Facility at Purdue University, Department of Chemistry, heating block fabrication), Tiago J. P. Sobreira, Michael Wleklinski and Andy Koswara are also noted with great appreciation.

3.6 References

1. Selekman, J. A.; Qiu, J.; Tran, K.; Stevens, J.; Rosso, V.; Simmons, E.; Xiao, Y.; Janey, J., High-throughput automation in chemical process development. *Annual Review of Chemical and Biomolecular Engineering* **2017,** *8*, 525-547.

2. Macarron, R.; Banks, M. N.; Bojanic, D.; Burns, D. J.; Cirovic, D. A.; Garyantes, T.; Green, D. V. S.; Hertzberg, R. P.; Janzen, W. P.; Paslay, J. W.; Schopfer, U.; Sittampalam, G. S., Impact of high-throughput screening in biomedical research. *Nature Reviews Drug Discovery* **2011,** *10*, 188.

3. Liu, M.; Chen, K.; Christian, D.; Fatima, T.; Pissarnitski, N.; Streckfuss, E.; Zhang, C.; Xia, L.; Borges, S.; Shi, Z.; Vachal, P.; Tata, J.; Athanasopoulos, J., High-throughput purification platform in support of drug discovery. *ACS Combinatorial Science* **2012,** *14*, 51-59.

4. Chen, P., Electrospray Ionization Tandem Mass Spectrometry in High-throughput screening of homogeneous catalysts. *Angew. Chem. Int. Ed.* **2003,** *42*, 2832-2847.

5. Buitrago Santanilla, A.; Regalado, E. L.; Pereira, T.; Shevlin, M.; Bateman, K.; Campeau, L.-C.; Schneeweis, J.; Berritt, S.; Shi, Z.-C.; Nantermet, P.; Liu, Y.; Helmy, R.; Welch, C. J.; Vachal, P.; Davies, I. W.; Cernak, T.; Dreher, S. D., Nanomole-scale high-throughput chemistry for the synthesis of complex molecules. *Science* **2015,** *347*, 49-53.

6. Troshin, K.; Hartwig, J. F., Snap deconvolution: An informatics approach to high-throughput discovery of catalytic reactions. *Science* **2017,** *357*, 175-181.

7. Wleklinski, M.; Loren, B. P.; Ferreira, C. R.; Jaman, Z.; Avramova, L.; Sobreira, T. J. P.; Thompson, D. H.; Cooks, R. G., High throughput reaction screening using desorption electrospray ionization mass spectrometry. *Chem. Sci.* **2018**.

8. Kim, H.; Min, K. I.; Inoue, K.; Im, D. J.; Kim, D. P.; Yoshida, J., Submillisecond organic synthesis: Outpacing Fries rearrangement through microfluidic rapid mixing. *Science* **2016,** *352*, 691-694.

9. Snead, D. R.; Jamison, T. F., A three-minute synthesis and purification of ibuprofen: pushing the limits of continuous-flow processing. *Angew. Chem. Int. Ed. Engl.* **2015,** *54*, 983-7.

10. Perera, D.; Tucker, J. W.; Brahmbhatt, S.; Helal, C. J.; Chong, A.; Farrell, W.; Richardson, P.; Sach, N. W., A platform for automated nanomole-scale reaction screening and micromole-scale synthesis in flow. *Science* **2018,** *359*, 429-434.

11. Len, C.; Bruniaux, S.; Delbecq, F.; Parmar, V., Palladium-Catalyzed Suzuki–Miyaura Cross-Coupling in Continuous Flow. *Catalysts* **2017,** *7*, 146.

12. Falcone, C. E.; Jaman, Z.; Wleklinski, M.; Koswara, A.; Thompson, D. H.; Cooks, R. G., Reaction screening and optimization of continuous-flow atropine synthesis by preparative electrospray mass spectrometry. *Analyst* **2017,** *142*, 2836-2845.

13. Loren, B. P.; Wleklinski, M.; Koswara, A.; Yammine, K.; Hu, Y.; Nagy, Z. K.; Thompson, D. H.; Cooks, R. G., Mass spectrometric directed system for the continuous-flow synthesis and purification of diphenhydramine. *Chem. Sci.* **2017,** *8*, 4363-4370.

14. Ewan, H. S.; Iyer, K.; Hyun, S.-H.; Wleklinski, M.; Cooks, R. G.; Thompson, D. H., Multistep flow synthesis of diazepam guided by droplet-accelerated reaction screening with mechanistic insights from rapid mass spectrometry analysis. *Org. Process Res. Dev.* **2017,** *21*, 1566-1570.

15. Wleklinski, M.; Falcone, C. E.; Loren, B. P.; Jaman, Z.; Iyer, K.; Ewan, H. S.; Hyun, S.-H.; Thompson, D. H.; Cooks, R. G., Can accelerated reactions in droplets guide chemistry at scale? *Eur. J. Org. Chem.* **2016,** *2016*, 5480-5484.

16. Roughley, S. D.; Jordan, A. M., The Medicinal Chemist's Toolbox: An analysis of reactions used in the pursuit of drug candidates. *J. Med. Chem.* **2011,** *54*, 3451-3479.

17. Brambilla, M.; Tredwell, M., Palladium-catalyzed Suzuki–Miyaura cross-coupling of secondary α-(trifluoromethyl)benzyl tosylates. *Angew. Chem. Int. Ed.* **2017,** *56*, 11981-11985.

18. Suzuki, A., Cross-Coupling Reactions Of Organoboranes: An easy way to construct c-c bonds (nobel lecture). *Angew. Chem. Int. Ed.* **2011,** *50*, 6722-6737.

19. Chatterjee, A.; Ward, T. R., Recent Advances in the Palladium Catalyzed Suzuki–Miyaura Cross-Coupling Reaction in Water. *Catal. Lett.* **2016,** *146*, 820-840.

20. Reizman, B. J.; Wang, Y.-M.; Buchwald, S. L.; Jensen, K. F., Suzuki–Miyaura cross-coupling optimization enabled by automated feedback. *Reaction Chemistry & Engineering* **2016,** *1*, 658-666.

21. Noël, T.; Musacchio, A. J., Suzuki–Miyaura cross-coupling of heteroaryl halides and arylboronic acids in continuous flow. *Org. Lett.* **2011,** *13*, 5180-5183.

22. Noël, T.; Kuhn, S.; Musacchio, A. J.; Jensen, K. F.; Buchwald, S. L., Suzuki–Miyaura cross-coupling reactions in flow: Multistep Synthesis Enabled by a Microfluidic Extraction. *Angew. Chem. Int. Ed.* **2011,** *123*, 6065-6068.

23. Fukumoto, S.; Ujikawa, O.; Morimoto, S.; Asano, Y.; Mikami, S.; Tokunaga, N.; Kori, M.; Imaeda, T.; Fukuda, K.; Nakamura, S., Sulfonamide derivative and use thereof. Google Patents2012.

24. Fu, S.; Xiang, W.; Chen, J.; Ma, L.; Chen, L., Synthesis and biological evaluation of 1, 2, 4-oxadiazole derivatives as novel GPR119 agonists. *Chemical Biology & Drug Design* **2017,** *89*, 815-819.

25. Sánchez-Peris, M.; Murga, J.; Falomir, E.; Carda, M.; Marco, J. A., Synthesis of honokiol analogues and evaluation of their modulating action on VEGF protein secretion and telomerase-related gene expressions. *Chemical Biology & Drug Design* **2017,** *89*, 577-584.

26. Gregor, V. E., Tricyclic compound derivatives useful in the treatment of neoplastic diseases, inflammatory disorders and immunomodulatory disorders. Google Patents2014.

27. Sánchez-Peris, M.; Falomir, E.; Murga, J.; Carda, M.; Marco, J. A., Synthesis and evaluation of biphenyl derivatives as potential downregulators of VEGF protein secretion and telomerase-related gene expressions. *Biorg. Med. Chem.* **2016,** *24*, 3108-3115.

28. Murray, P. R. D.; Browne, D. L.; Pastre, J. C.; Butters, C.; Guthrie, D.; Ley, S. V., Continuous Flow-Processing of Organometallic Reagents Using an Advanced Peristaltic Pumping System and the Telescoped Flow Synthesis of (E/Z)-Tamoxifen. *Org. Process Res. Dev.* **2013,** *17*, 1192-1208.

29. Jang, K.-S., Biphenyl-based liquid crystal precursors with alkanoate and hydroxyl group. *Molecular Crystals and Liquid Crystals* **2016,** *633*, 123-128.

30. Schmidt, B.; Riemer, M., Suzuki–Miyaura coupling of halophenols and phenol boronic acids: systematic investigation of positional isomer effects and conclusions for the synthesis of phytoalexins from pyrinae. *J. Org. Chem.* **2014,** *79*, 4104-4118.

31. Düfert, M. A.; Billingsley, K. L.; Buchwald, S. L., Suzuki-Miyaura cross-coupling of unprotected, nitrogen-rich heterocycles: substrate scope and mechanistic investigation. *J. Am. Chem. Soc.* **2013,** *135*, 12877-12885.

CHAPTER 4. ON-DEMAND RAPID SYNTHESIS OF LOMUSTINE UNDER CONTINUOUS FLOW CONDITIONS

Reproduced (adapted) from Jaman, Z.; Sobreira, T. J. P.; Mufti, A.; Ferreira, C. R.; Cooks, R. G.; Thompson, D. H., 'On-Demand Rapid Synthesis of Lomustine Under Continuous Flow Conditions' *Org. Process Res. Dev* **2019**, 23, 334–341 with permission provided by American Chemical Society Publications.

4.1 Introduction

Lomustine, a widely used anticancer agent, is a highly lipophilic alkylating agent that produces chloroethyl carbonium ions and carbamylating intermediates *in vivo*.[1, 2] This electrophilic compound attacks the nucleophilic sites on DNA to form alkylated products.[1] Other anticancer agents such as mitomycin C, streptonigrin, bleomycin, and the anthracyclines require bioactivation to react with their cellular targets, whereas lomustine does not require pre-activation.[3] Unlike alkylating agents that form adducts at the most reactive N^7 position of guanine, chloroethylating compounds like lomustine form adducts at O^6, leading to interstrand DNA cross-linking. If DNA repair does not occur, this crosslinking can cause double strand breaks during DNA replication, eventually leading to cell death via apoptosis.[4]

Lomustine, 1-(2-chloroethyl)-3-cyclohexyl-l-nitroso-urea (commercial names: CCNU, CeeNU, Gleostine) is used as an oral antineoplastic agent that is administered every 6 weeks. It was first evaluated in clinical trials in the late 1960s[5] and approved by the US FDA in 1976[6] for primary and metastatic brain tumors as well as Hodgkin's lymphoma.[4] Bristol-Myers Squibb originally held the patent for the agent under the brand name CeeNu. In 2014, Next Source Biotechnology LLC (NSB) was approved by the FDA for the rebranding of lomustine under the trade name Gleostine.[6] The average wholesale price for one dose of rebranded Gleostine is $1,645.68, while the generic formulation costs $203.38.[6] The huge price discrepancy (700%) between Gleostine and the generic formulation has created patient access problems, thus motivating our effort to develop a rapid and low cost lomustine synthesis method by continuous flow.

Continuous flow synthesis has been reported as an efficient methodology and has been explored in both industry and academic labs for the last few decades.[7-18] Compared to traditional batch synthesis processes, flow reactors provide better control over reaction conditions and selectivity owing to rapid mixing and precise control of reaction parameters such as temperature, stoichiometry, pressure, and residence time. The enhanced heat and mass transfer capabilities also provide safer and greener operational conditions.[8, 19-25] Generally, these aspects of continuous flow synthesis contribute to improved chemical reaction efficiency[25, 26] and shorter reaction times, enabling process intensification[19], and more facile scale-up, with improved quality and consistency in production. Motivated by these factors, continuous flow synthesis of active pharmaceutical ingredient has recently become more attractive,[23, 27-39] however efficient execution of multistep reactions in a telescoped manner still remains a challenge due to challenges arising from workup conditions[32, 40, 41], solvent switches,[42, 43] and flow rate differences.[42, 44] Moreover, optimization of continuous flow conditions and analysis require significant investments in time and material.[32, 45-50]

Recently, our group reported a robust high throughput reaction screening method using desorption electrospray ionization mass spectrometry (DESI-MS) to guide scalable synthesis in continuous flow reactors at scale.[49] Herein, we report the continuous flow synthesis of lomustine using an optimization protocol that was guided by DESI-MS. The final method consists of two reactions telescoped without isolation or purification of intermediates. This approach can reduce production costs radically by using a simple reactor set up and inexpensive starting materials (Scheme 4.1). To the best of our knowledge, this is the first synthesis of lomustine telescoped in continuous flow using an approach that does not interrupt the flow sequence due to intermediate workup requirements.

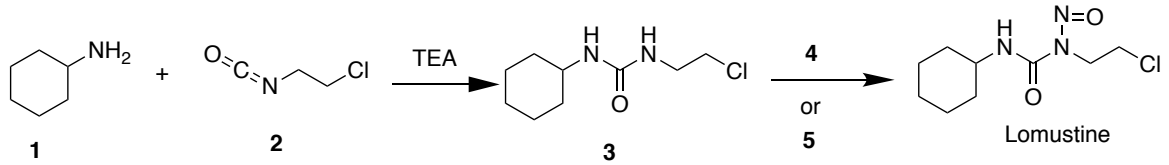

Scheme 4.1 Synthesis plan for lomustine in continuous flow, where **4** = $NaNO_2/HCO_2H$ and **5** = ^tBuONO.

4.1.1 Brief Summary of this Chapter

Lomustine, an important agent for treatment of brain tumors and Hodgkin's lymphoma, has been synthesized using continuous flow methodology. DESI-MS was used to quickly explore a large number of reaction conditions and guide the efficient translation of optimized conditions to continuous lomustine production at a rate of approximately one dose/2h. Using only four inexpensive commercially available starting materials and a total residence time of 9 min, lomustine was prepared via a linear sequence of two chemical reactions performed separately in two telescoped flow reactors. Sequential offline extraction and filtration resulted in 63% overall yield of pure lomustine at a production rate of 110 mg/h. The primary advantage of this approach lies in the rapid manufacture of lomustine with two telescoped steps to avoid isolation and purification of a labile intermediate, thereby decreasing the production cost of this active pharmaceutical ingredient to approximately $5/gram in total material cost.

4.2 Results and Discussion

4.2.1 Continuous Synthesis of 1-(2-Chloroethyl)-3-cyclohexylurea, **3**

The first step in the synthesis of lomustine (Scheme 1) is a fast reaction at room temperature. This transformation was optimized in continuous flow as a function of temperature, solvent, and stoichiometry to discover the conditions for maximum product yield. The reactions were monitored by TLC and MS using a triple quadrupole mass spectrometer operating in positive ion mode to afford rapid investigation of full mass spectra and product ion distribution for each reaction condition.

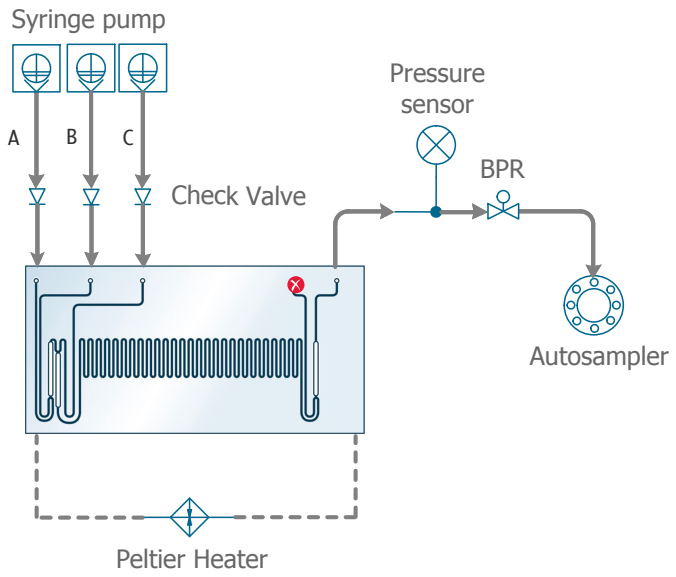

Figure 4.1 Microfluidic synthesis of intermediate **3** in a glass reactor chip (Chemtrix SOR 3225). A = **1** in THF; B = **2** in THF, C = TEA in THF.

A cascade method was designed to reveal the best conditions for the first step. Cyclohexylamine, **1**, 1-chloro-2-isocyanatoethane, **2,** and triethylamine (TEA) solutions were pumped through a Chemtrix 3225 SOR chip with automatic collection of the products in vials via an autosampler (Figure 4.1). The individual reaction mixtures were evaporated and the white solid

Table 4.1: Reaction conditions evaluated for the synthesis of **3** in flow using a Chemtrix S1 glass system fitted with a 3225 SOR reactor chip.

Entry	Solvent	2 equivalent	Temperature, °C	Residence time, sec	Isolated Yield %
1	EtOH	1	50	10	42.8
2	EtOH	1	50	30	0.00
3	EtOH	1	50	60	0.00
4	ACN	1	50	10	56.2
5	ACN	1	50	30	clogged
6	ACN	1	25	30	clogged
7	Toluene	1	50	10	clogged
8	Ether	1	50	10	clogged
9	THF	1	25	10	50.0
10	THF	1	25	30	56.4
11	THF	1	50	10	59.5
12	THF	1	50	30	62.1
13	THF	1	65	10	47.5
14	THF	1	65	30	29.1
15	THF	1.2	50	10	61.2
16	THF	1.2	50	30	64.8
17	THF	1.2	50	60	71.3
18	THF	1.4	50	10	67.1
19	THF	1.4	50	30	82.0
20	THF	1.4	50	60	91.7
21	THF	1.4	50	180	82.8

washed with cold Et_2O before drying under vacuum for overnight prior to analysis by TLC, MS, MS/MS, and NMR (^1H and ^{13}C).

Parameters such as residence time (τ), reaction temperature (T), and 1-chloro-2-isocyanatoethane:cyclohexylamine ratio were investigated systematically under continuous flow conditions. As shown in Table 1, product yield dropped sharply in EtOH at longer residence times (entries 1−3) due to ethanolysis of the 1-chloro-2-isocyanato-ethane starting material. Though the yield of **3** in ACN was significant, its low solubility in this solvent led to significant chip clogging (entries 4−6). Similar clogging problems were found for toluene and Et_2O, even at low concentrations (entries 7−8). The yield increased to 50-62% with longer residence times (entries 9−14) in THF, reaching a maximum when τ = 30 s at 50 °C and decayed rapidly with increased temperature (entries 13, 14) due to increased product decomposition at elevated temperature. The yield of **3** was also found to increase with proportions of **2** ratio (entries 15-21), whereas longer residence times promoted product decomposition (entry 21). Consequently, a maximum yield of intermediate **3** (92%) was achieved under conditions of τ = 60 s, T = 50 °C, and 1.4 equivalents of 1-chloro-2-isocyanatoethane (entry 20).

4.2.2 Synthesis of Lomustine, Guided by DESI-MS High Throughput Experimentation.

We employed DESI-MS to evaluate the impact of solvent, concentration and nitrosation reagent type on the efficiency of lomustine production. DESI-MS was originally applied to the surface analysis of intact samples such as biological tissues for cancer diagnosis or human fingerprints for drug detection,[51, 52] although more recently, the DESI-MS approach has been used for reaction analysis.[49] This approach is based on the phenomena of reaction acceleration that occurs within confined volumes such as microdroplets that originate from spray-based MS ionization processes.[51] MS analysis speeds approaching 10,000 reaction spots/hour can be achieved by this technique.[49]

As shown in Scheme 4.1 (2nd step), two nitrosation methods were investigated. First, the efficiency of sodium nitrite, **4,** in formic acid as the nitrosation reagent toward the conversion of **3** to lomustine was evaluated. This conversion was then compared with tert-butyl nitrite (TBN, **5**) as the nitrosation reagent. DESI-MS was used to evaluate the $NaNO_2/HCO_2H$ transformation under different reactant concentrations and solvents. The expected *m/z* 234 value for lomustine was not observed. Analysis of a commercial lomustine sample yielded a very similar MS, suggesting that fragmentation occurs readily during the ionization process. Triple quadrupole MS

with electrospray ionization, as well as ion trap mass spectrometry coupled with DESI, revealed the presence of a stable lomustine ion at *m/z* 169. This was further confirmed by the fact that the losmustine fragments from this reaction matched with commercially available lomustine (See APPENDIX C for the figures). Reactions for all $NaNO_2$ concentrations in THF:H_2O worked better than for ACN:H_2O (Figure 2, A). Also, the fragments from **3** were most abundant in the ACN:H_2O reactions compared to reactions in THF:H_2O, suggesting that the conversion of starting material was comparatively sluggish in ACN:H_2O. Next, eight different solvents (EtOH, MeOH, DCM, ACN, toluene, DMSO, THF and EtOAc) were compared for guiding the continuous flow synthesis. All eight solvents produced similar outcomes using **4** as the nitrosation reagent (Figure 2, B). When **5** was used, lomustine was detected in all solvents except THF and EtOAc (Figure 2, C).

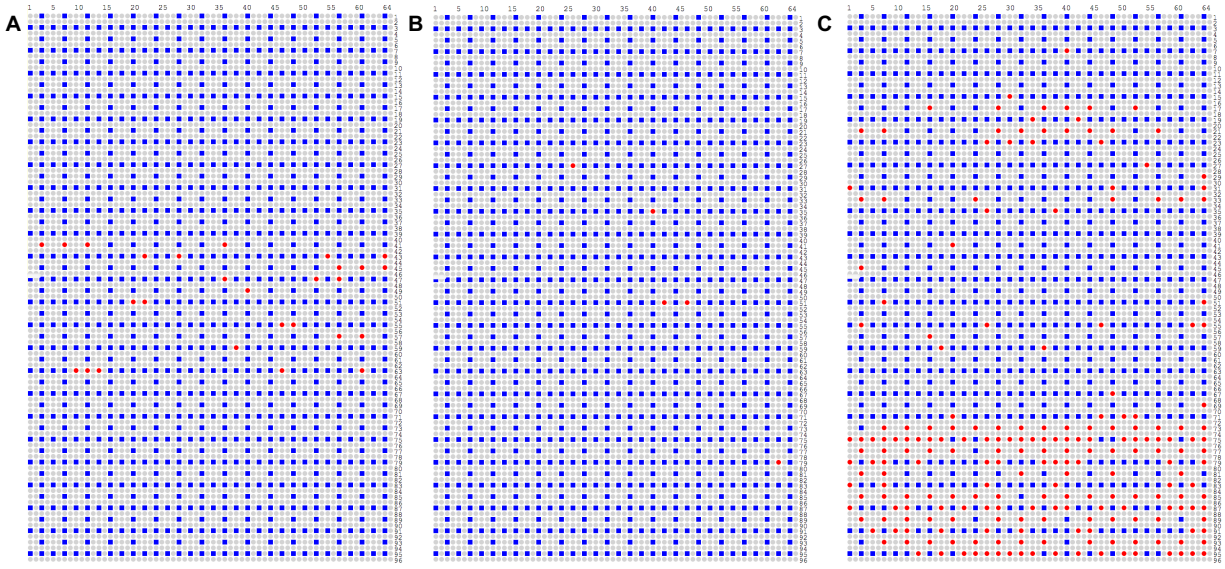

Figure 4.2 DESI-MS plate maps showing the presence or absence of expected ions at each spot where the nitrosation reaction conditions were tested using different stoichiometries and with commercially available standards. Blue dots indicate the presence of the *m/z* 169 expected stable fragment for the reaction product (successful reaction), Red dots indicate that the expected *m/z* for the reaction product was not present at the reaction spot (unsuccessful reaction condition). A: Concentration screening using the lomustine ion (*m/z* 169) intensity and $NaNO_2$ as nitrosation reagent; B: Solvent screening using the lomustine ion (*m/z* 169) intensity and $NaNO_2$ as nitrosation reagent; C: Solvent screening using the lomustine ion (*m/z* 169) intensity and tBuONO as nitrosation reagent.

4.2.3 Nitrosation Reaction Optimization in Continuous Flow

We utilized the reaction conditions emerging from the DESI-MS high throughput

experiments to optimize the flow synthesis and also check whether unsuccessful reactions identified by DESI-MS would also negatively translate under flow conditions. From the DESI-MS experiments, THF was identified as the best solvent for nitrosation using **4**. Excess **4** was also used to maximize conversion of **3** to lomustine since the nitrosation reagents are hygroscopic and readily oxidize to nitrate.[53, 54] Overall, the DESI-MS experiments were in excellent agreement with the outcomes of flow reaction conditions in terms of stoichiometry, reagents and solvents.

A series of reactions (Table 4.2) were performed to maximize the conversion of **3** to lomustine under continuous synthesis conditions (Figure 4.3). Initially, we examined the reaction at 0 °C with a residence time of 30 sec using TLC and MS to monitor the reaction progress. Gratifyingly, lomustine was obtained through this very short reaction time, albeit in low conversion (Table 2, entry 1). A systematic evaluation of residence times led to good lomustine yields and starting material conversions, however, longer residence times appeared enhance the decomposition of lomustine (Table 2, entries 2-6). Consequently, we kept the temperature constant at 0 °C to avoid $NaNO_2$ decomposition of sodium nitrite to the diazonium salt that occurs at higher temperatures.[54]

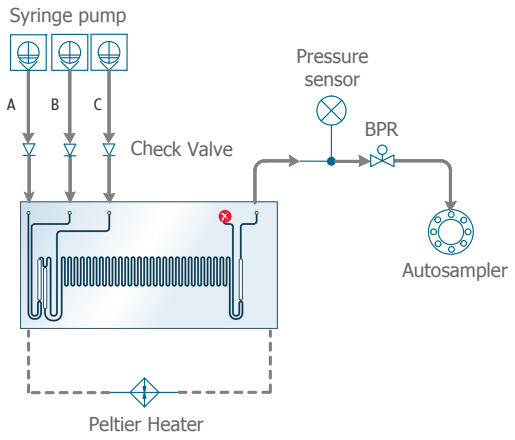

Figure 4.3 Microfluidic synthesis of lomustine using $NaNO_2/HCO_2H$ as nitrosation reagent in a Chemtrix 3225 SOR glass reactor chip. A = **3** in THF; B = HCO_2H (neat), C = $NaNO_2$ in MeOH:H_2O (4:1).

Different purification methods were evaluated to isolate pure lomustine. At first, the product was extracted with Et_2O (3 times) to exploit the low solubility of **3** in this solvent (Method

1). Unfortunately, the TLC analysis revealed the presence of **3** in the organic layer as well as in the aqueous layer. Therefore, the combined organic extracts were dried over anhydrous Na_2SO_4 and concentrated in vacuo to produce a yellowish oil that re-dissolved in Et_2O, heated and cooled in an ice bath to precipitate **3** from the mixture. NMR analysis of the filtrate revealed that 22% of **3** remained in the isolated lomustine product. Next, we purified the product by recrystallization from ACN (Method 2). Although we obtained very pure lomustine as identified by NMR analysis, recovery using this approach was low. Finally, we found that hot filtration from petroleum ether removed the insoluble **3** impurity (Method 3). Concentration of the filtrate after drying gave pure lomustine without detectable amount of **3** by NMR. Using this method, we obtained 74% isolated yield of pure lomustine under the conditions of 0 °C reaction and a residence time of 5 min using 3 equivalents of **4** (see APPENDIX C for NMR).

Table 4.2 Isolated yields of lomustine under different reaction conditions using **4** as the nitrosation reagent. Temperture = 0 °C, solvent = MeOH:H_2O (4:1)

Entry	**Residence time, min**	**Isolated Yield (Method 1) %**	**Isolated Yield (Method 2) %**	**Isolated Yield (Method 3) %**
1	0.5	26.8	---	43.7
2	1	48.8	---	50.6
3	3	51.6	41.2	63.1
4	5	79.0	54.4	74.5
5	8	59.0	---	68.7
6	10	50.2	---	65.3

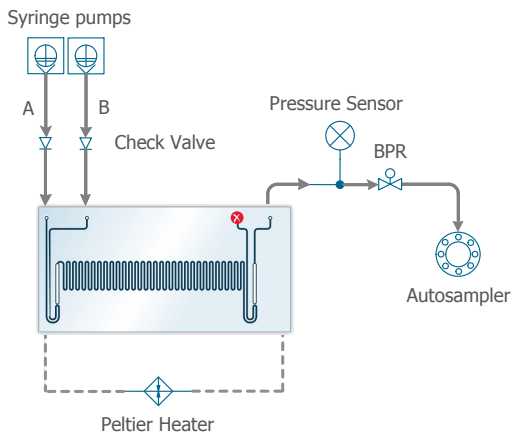

Figure 4.4 Microfluidic synthesis of lomustine using **5** as nitrosation reagent in a Chemtrix 3223 SOR glass reactor chip. A = **3** in ACN:EtOH (3.7:1) ; B = **5** in ACN.

Table 4.3 Synthesis of lomustine under at different reaction conditions using **5** as the nitrosation reagent.

Entry	Solvent (3.7:1)	Temperature, (°C)	Residence time, (min)	Isolated Lomustine Yield (%)
1	ACN:EtOH	50	0.5	68.3
2	ACN:EtOH	50	1	69.8
3	ACN:EtOH	50	3	60.0
4	ACN:EtOH	50	5	58.8
5	ACN:EtOH	50	8	51.9
6	ACN:EtOH	50	10	49.4
7	ACN:EtOH	25	0.5	48.8
8	ACN:EtOH	25	1	54.1
9	ACN:EtOH	25	3	66.5
10	ACN:EtOH	25	5	79.3
11	ACN:EtOH	25	8	91.2
12	ACN:EtOH	25	10	89.8
13	THF	25	3	36.5

The reaction was also optimized with respect to residence time, temperature, and solvent using **5** as nitrosation agent (Figure 4.4 and Table 4.3). This optimization process led to the finding that an elevated residence time (8 min), lower temperature (25 °C) and increased **5** ratio (3 equiv) resulted in the most efficient conversion to lomustine (91% isolated yield) after Method 3 purification (Table 4.3, entry 11).

4.2.4 Telescoped Synthesis of Lomustine

The next step was to adapt the whole two step sequence to a continuous flow setup. We sought to telescope the carbamylation and nitrosation reactions using the Chemtrix reactor chips, however, an extraction needed to be incorporated between the steps to remove the TEA present in the first reaction to avoid competitive consumption of the nitrosation reagent in the second step. We achieved this objective by incorporating a commercially available Zaiput liquid-liquid extractor to remove the base before the nitrosation step and by re-optimizing the synthesis using FEP tubing reactors (Figure 4.5). In the beginning, the best reaction conditions were a 1 min residence time at 50 °C for the first step and a 5 min residence time at 0 °C for the second step, yielding 43 mg (51.8% overall yield) of pure lomustine (Table 4.4, entry 1). Efforts to improve the lomustine yield by changing the residence times of either the first or second steps were unsuccessful in the FEP tubing reactor using **4** as nitrosation reagent (Table 4.4, entry 1-4).

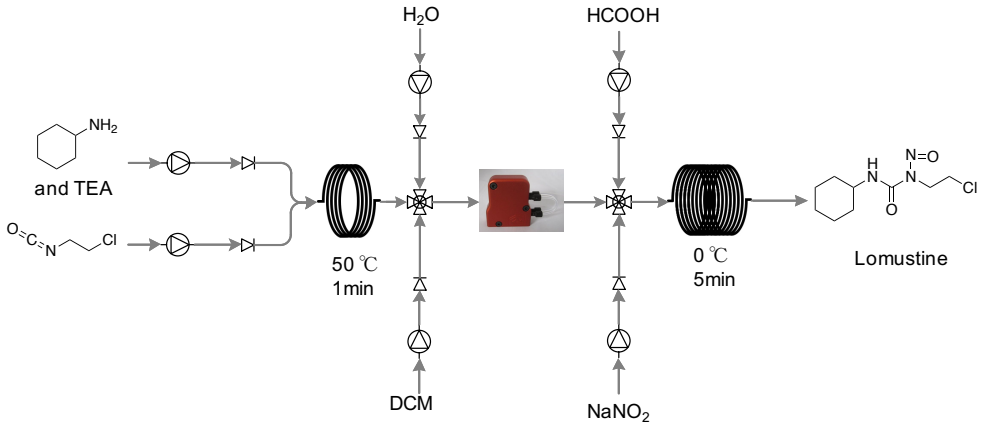

Figure 4.5 Schematic for the telescoped synthesis of lomustine using $NaNO_2/HCO_2H$ (**4**) as nitrosation reagent.

Table 4.4 Lomustine synthesis yields for telescoped reactions under different reagents, residence time, stoichiometry, and temperature conditions.

Entry	Nitrosation reagent	Step 1	Step 2	TEA Stoichiometry	Isolated Lomustine Yield %
1	**4**	1 min, 50 °C	5 min, 0 °C	1	51.8
2	**4**	2 min, 50°C	5 min, 0 °C	1	44.2
3	**4**	10 min, 50 °C	5 min, 0 °C	1	38.6
4	**4**	10 min, 50 °C	3 min, 0 °C	1	24.0
5	**5**	1 min, 50 °C	5 min, 50 °C	1	41.5
6	**5**	1 min, 50 °C	5 min, 25 °C	1	21.8
7	**5**	1 min, 50 °C	8 min, 25 °C	1	24.6
8	**5**	1 min, 50 °C	8 min, 25 °C	0.1	55.5
9	**5**	1 min, 50 °C	8 min, 25 °C	0.01	63.7

Subsequent telescoping experiments indicated that **5** was a better nitrosation reagent than **4** for the efficient synthesis of lomustine in flow. This is also true when the synthesis of lomustine were performed separately in glass reactor chips (Table 4.2 and 4.3). The final optimized conditions were 1 min reaction time at 50 °C for the first step and 8 min reaction time at 25 °C for the second step (Figure 4.6). As the small amount of extracted TEA from the first step minimized the TBN activity, lowering the amount of TEA used led to an increased production of lomustine (Table 4, entries 7-9) such that 1% TEA produced 110 mg (63% overall yield) of pure isolate lomustine via this reaction setup (Table 4.4, entry 9). TLC, NMR (^{1}H and ^{13}C), MS and MS/MS data of lomustine obtained by this telescoped continuous route were a direct match with values measured for commercially available lomustine.

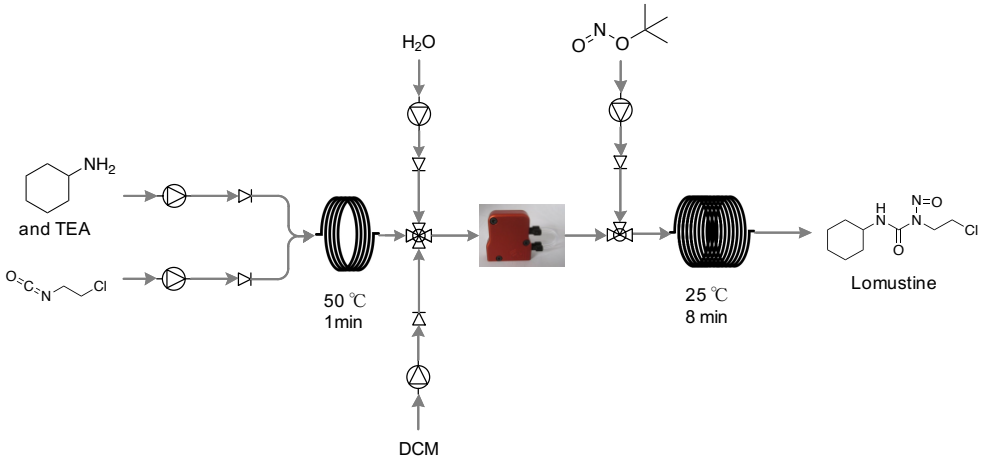

Figure 4.6 Schematic for the final telescoped synthesis of lomustine using **5** as a nitrosation reagent.

HPLC-MS was used to certify the purity of the synthesized lomustine and compare the total ion chromatogram (TIC) values of this material with a commercial lomustine standard. The TIC profile fully overlapped with the commercial standard without the appearance of any new byproducts (Figure 7).

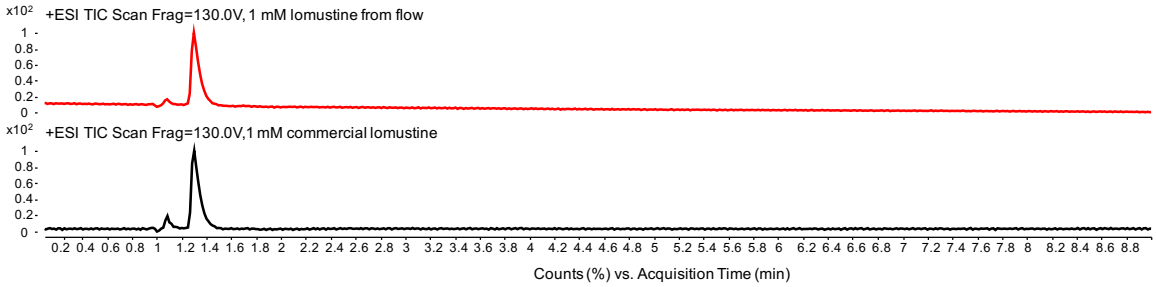

Figure 4.7 Total ion chromatogram (TIC) from HPLC-MS/MS and comparison between synthesized lomustine (top, red) and commercially available lomustine (bottom, black).

4.3 Experimental

4.3.1 Chemicals

All chemicals and reagents were purchased from Sigma-Aldrich (St. Louis, Missouri) and used without any purification. Intermediate **3** standard was purchased from 1Click Chemistry, Inc. (Kendall Park, NJ). Lomustine was purchased from ApexBio (Houston, TX).

4.3.2 Liquid Handling Robot

Assay plate set up and sample preparation steps for DESI-MS were done using a Biomek i7 (Beckman Coulter, Inc., Indianapolis, IN) dual-bridge liquid handling robot. A 384-tip head was employed to enable simultaneous transfer of 384 samples under the same conditions (speed of aspiration and dispensing, height of pipetting at source and destination positions, pattern of pipetting, etc.). An 8-channel head was used to provide more flexibility in terms of volumes transferred, layout of source and destination places, pipetting height, speed, and reaction stoichiometry. The high capacity deck accommodated all labware (robotic tips, plates, reservoirs) needed for assembling one reaction step. All robotic tips were made of chemically resistant polypropylene and disposable. Polypropylene multi-well plates and reservoirs, as well as custom made Teflon reservoirs were used during the experiments for reagent solutions. Methods were developed and validated using the Biomek point-and-click programming tool. Standard pipetting techniques used in this software were modified to optimize accurate transfer of highly volatile liquids.

4.3.3 Mass Spectrometer

Samples were analyzed using a Thermo Fisher TSQ Quantum Access MAX mass spectrometer that was connected with a Dionex Ultimate 3000 Series Pump and WPS-3000 Autosampler (Thermo Fisher Scientific, Waltham, MA). Electrospray ionization (ESI) analysis in full scan mode was used to monitor each reaction in both positive and negative ion modes. These data were recorded using optimized parameters for the ESI source and MS as follows: spraying solvent, ACN; spray voltage +3.5 kV (positive mode) and -4.0 kV (negative mode); capillary temperature, 250 °C; Sheath gas pressure, 10 psi; scan time, 1 s; Q1 peak width (FWHM), 0.70 Th; micro scans, 3. The autosampler settings were as follows: MS acquire time, 2 min; sample injection volume, 10 μL. Thermo Fisher Xcalibur software was used to process the data from the MS spectrometer.

4.3.4 Microfluidics

The first and second steps of the lomustine synthesis were individually optimized using a Labtrix S1 (Chemtrix, Ltd, Netherlands) fitted with glass microreactor containing staggered orientated ridges (SOR): chips 3223 (three inlets and one outlet, volume = 10 μL) and 3225 (four

inlets and one outlet, volume = 10 μL) having channel widths of 300 μm and channel depth 120 μm. The S1 unit is able to independently drive five syringes connected to the micro reactor mounted on a Peltier heating and cooling unit. All the gastight glass syringes were bought separately from Hamilton Company (Hamilton, Reno, Nevada). FEP tubing and fittings were used to connect the syringes with the selected connection port on the microreactor. All operations were controlled using a ChemTrix GUI software installed on a laptop that was connected to the Labtrix S1 via an USB cable.

4.3.5 HPLC-MS Analysis

HPLC/MS analysis was performed using an Agilent 6545 UPLC/quadrupole time-of-flight (Q-TOF) mass spectrometer (Palo Alto, CA), with an Agilent XDB-C18 column (3.5 μm, 150 x 2.1 mm i.d.) and 5 μL injection volume. A binary mobile phase, consisting of solvent systems A and B was used. A was 0.1% formic acid (v/v) in ddH_2O and B was 0.1% formic acid (v/v) in ACN. Isocratic elution of A:B at 95:5 was used, with a column flow rate of 0.3 mL/min. Following the separation, the column effluent was introduced by positive mode electrospray ionization (ESI) into the mass spectrometer. High mass accuracy spectra were collected between 70 – 1000 m/z. Mass accuracy was improved by continuously infusing Agilent Reference Mass Correction Solution (G1969-85001). The MS detection conditions were: ESI capillary voltage, 3.5 kV; nebulizer gas pressure, 30 psig; gas temperature, 325 °C; drying gas flow rate, 8.0 L/min; fragmentor voltage, 130 V; skimmer, 45 V; and OCT RF V, 750 V.

4.3.6 DESI-MS Analysis

The DESI-MS evaluation was done following the previously published method of Wleklinski *et* al[49] except that the density of reaction spots was 1,536 spots/plate instead of 6,144/plate using reagents that were pipetted into standard polypropylene 384-well plates using a liquid handling robot (Biomek i7; Beckman-Coulter, US). DESI-MS slides were fabricated from porous PTFE sheets (EMD, Millipore Fluoropore, Saint-Gobain) glued onto a glass support (Foxx Life Sciences). The PTFE sheet was cut with scissors and bonded to the glass slides using spray adhesive (Scotch Spray mount). No signs of interference from the glue was observed. The reagents were mixed at 1:1 stoichiometry in various solvents (EtOAc, THF, DMSO, Toluene, ACN, DCM, EtOH and MeOH) and rhodamine B dye was added to some wells of the plate as a fiducial marker.

After the reagents were mixed, 50 nL of the reactions were deposited onto a porous PTFE surface at 1,536 spot density using a magnetic pin tool equipped with slotted transfer pins. DESI-MS data was acquired using a linear ion trap mass spectrometer (LTQ XL; Thermo Scientific, San Jose, CA) equipped with a commercial DESI-imaging source (DESI 2D source, Prosolia Inc., Indianapolis, IN). The instrument was controlled using Xcalibur v. 4.0 software to run worklists for DESI-MS data acquisition. The DESI spray angle was 55° using MeOH as spray solvent, and with an applied voltage of 5kV. Mass spectra were acquired at the positive ion mode over the *m/z* range of 50-500. The DESI-MS imaging lateral resolution was 350 µm. This was achieved using stage speed of 4,376 µm/sec and the instrument scan time of 80 ms. For data processing, data were visualized using an in-house software designed[49] to automatically search for the *m/z* values of reactants, intermediates, and lomustine fragments to generate a YES/NO visualization output for each spot in the PTFE plate imaged by DESI-MS. Data files also were combined into .img files using Firefly software (Prosolia Inc., Indianapolis, IN). Ion images were plotted using BioMAP (Novartis, freeware). The expected *m/z* values for the lomustine fragments were plotted and visualized using the BioMAP rainbow false color scale where the minimum and maximum ion intensity values were set to the best contrast for each ion.

4.3.7 NMR Analysis

^{1}H-NMR and ^{13}C-NMR were acquired using a Bruker AV-III-500-HD NMR spectrometer (Billerica, Massachusetts, USA). Samples for NMR were prepared by dissolving ~5 mg of sample in CDCl3. MestReNova 10.0 software was used to analyze the ^{1}H-NMR and ^{13}C-NMR.

4.3.8 Carbamylation of Cyclohexylamine

A solution of cyclohexylamine (**1**, 500 mmol, 1 equiv) in THF was loaded into 1 mL Hamilton gas tight glass syringe. Triethylamine (TEA) (500 mmol, 1 equiv) and 1-chloro-2-isocyanatoethane (**2,** 700 mmol, 1.4 equiv) solutions in THF were individually loaded into another two 1 mL Hamilton gas tight glass syringes. Each solution was simultaneously dispensed into the SOR 3225 reactor to engage the reactants. The syringe containing **2** was protected from light by covering it with aluminum foil. The reactions were run at 25 °C, 50 °C and 65 °C at residence times of 10 sec, 30 sec, 60 sec and 180 sec. The reactions were monitored by TLC and ESI-MS. Product **3** was collected after evaporation and washing with cold Et_2O. The white solid product

was stored in the dark at 4 °C. Any clogged chips or tubing of the setup was cleaned using THF and EtOH. The subsequent TLC, ESI-MS, MS/MS and NMR (^{1}H and ^{13}C) analyses were performed after purification.

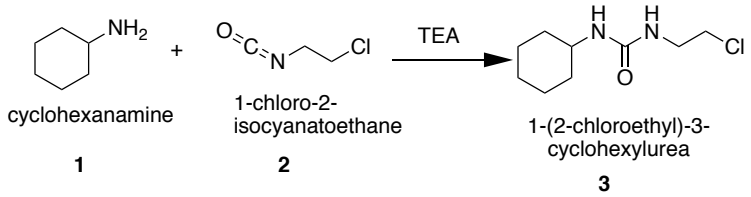

Scheme 4.2 Synthesis of **3** in flow.

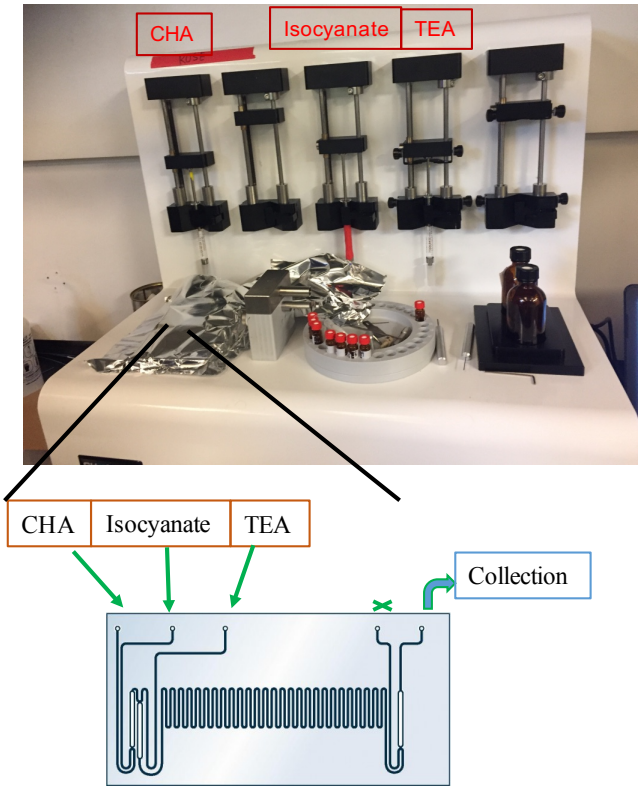

Figure 4.8 Set up of continuous flow synthesis of **3**, using chemtrix S1 system.

NMR

^{1}H NMR (500 MHz, $CDCl_3$, ppm): δ_H = 4.84 (t, J= 5.85, 1 H), 4.42 (d, J = 7.35 Hz, 1 H), 3.62 (t, J=5.60Hz, 2 H), 3.54 (t, J=5.70Hz, 2 H), 3.51-3.45 (m, 1 H), 1.95-1.92 (m, 2 H), 1.72-1.67 (m, 2 H), 1.62-1.58 (m, 1 H), 1.39-1.30 (m, 2 H), 1.19-1.06 (m, 3 H); ^{13}C NMR (500 MHz, $CDCl_3$, ppm):

δ_C= 157.04, 49.29, 45.25, 42.12, 33.88, 25.57, 24.9 (see APPENDIX C for the spectrum).

ESI-MS

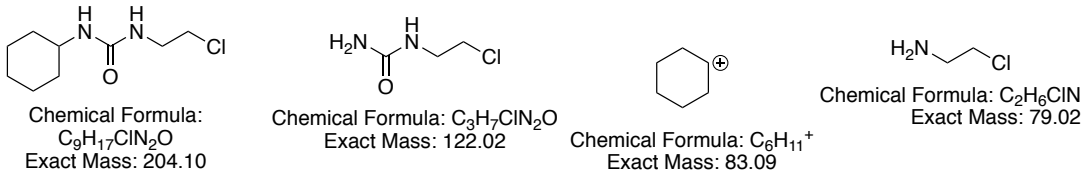

Figure 4.9 Fragments from 1-(2-chloroethyl)-3-cyclohexylurea, **3.**

ESI-MS (*m/z*): 205/207 ($M+H^+$), 227/229 ($M+Na^+$).

ESI-MS/MS of *m/z* 205: 205 ($M+H^+$), 123 ($C_3H_7ClN_2O+H^+$), 83 ($C_6H_{11}^+$) (80 ($C_2H_6ClN^+$)

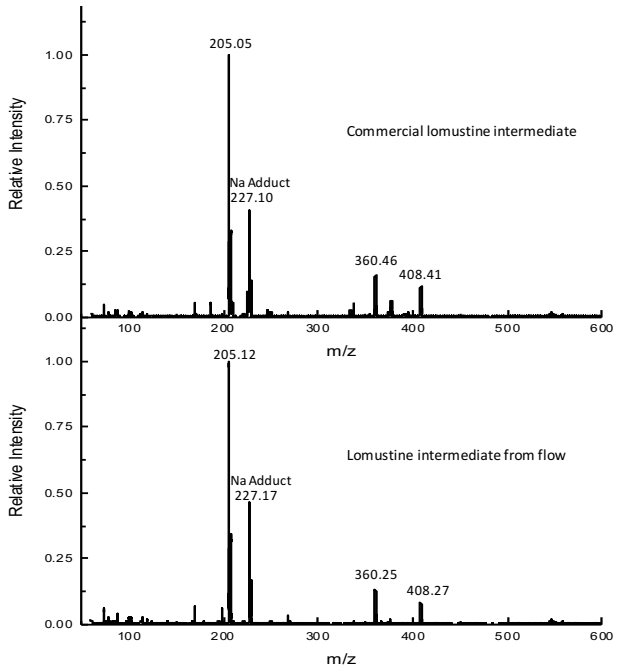

Figure 4.10 Full ESI-MS scan of commercially available **3** and synthesized **3** derived from flow under the reaction conditions of 50 °C, 1 min.

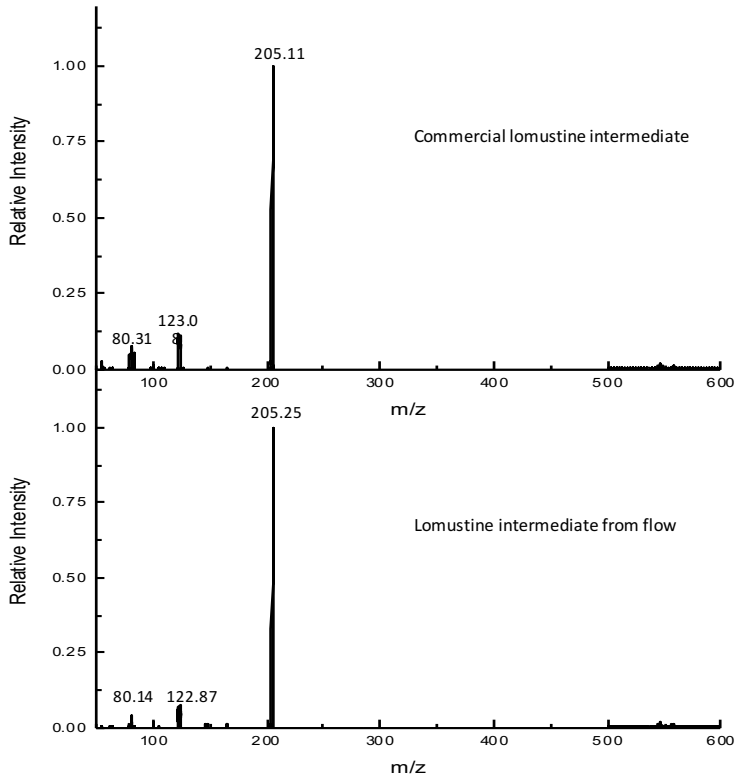

Figure 4.11 MS/MS of m/z=205 from commercially available **3** and synthesized **3** derived from flow under the reaction conditions of 50 °C, 1 min.

4.3.9 Preparation of Reaction (Master) Plates and Stamping on DESI-MS Slides

Stock solutions of **3** and nitrosation reagents were made at 4 different concentrations (50, 100, 150, 200 mmol) in THF and ACN (Figure S2). Each reagent solution was also prepared (0.1 M) in eight different solvents ((EtOAc, THF, DMSO, Toluene, ACN, DCM, EtOH and MeOH) (Figure S3). At first, 20 µL of **3** solution was dispensed into a 384-well master plate and then the corresponding nitrosation reagents added to the plate in a stoichiometry 1:1 using a Beckman i7 liquid handling robot, resulting in a final volume of 40 µL in each well. Moreover, a master plate was made using only commercially available **3** and lomustine to compare the data (Figure S4). Rhodamine was dissolved in acetonitrile (0.25mg/mL) and transferred to a reservoir. A pin tool fitted with 50 nL pins was used to transfer solutions from the master plates as well as from the Rhodamine reservoir onto the DESI-MS substrates. The master plate was pinned three times in separate locations with reaction mixtures and Rhodamine once, resulting in 1,536 density on the microtiter plate used as the DESI-MS substrate.

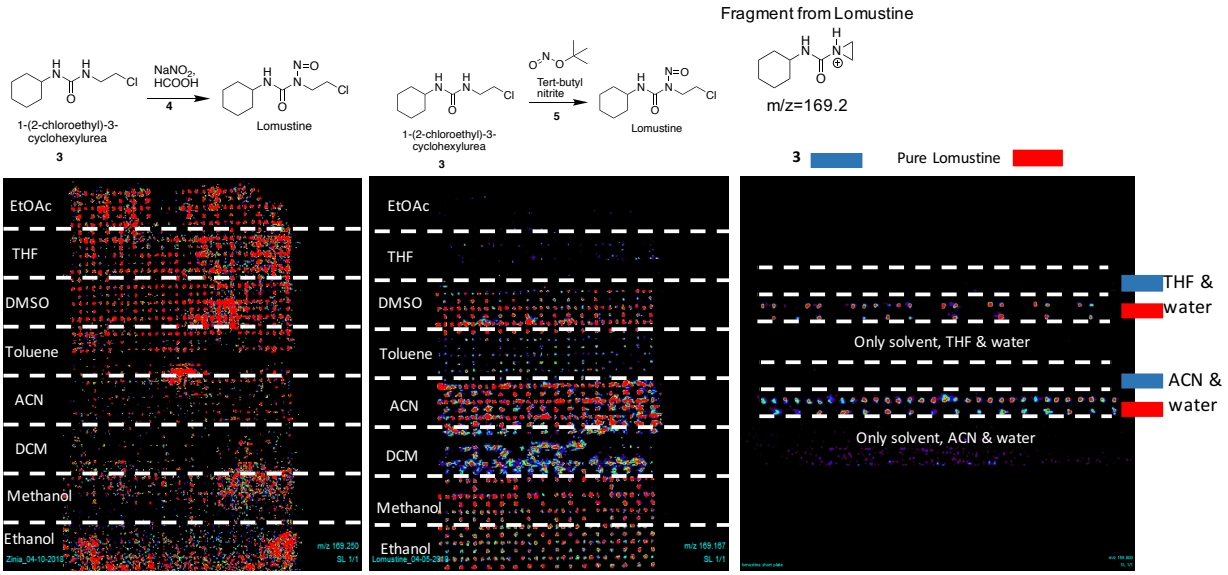

Figure 4.12 (left & center) Direct DESI-MS data comparison between the two nitrosation reactions in different solvents. (right) DESI-MS data of commercially available 3 and lomustine standards. The data was analyzed using BioMAP imaging software.

4.3.10 Nitrosation of 1-(2-chloroethyl)-3-cyclohexylurea, **3**

A solution of **3** (245 mmol, 1 equiv) in 98% formic acid was loaded into a 1 mL Hamilton gas tight glass syringe. $NaNO_2$ (735 mmol, 3 equiv) solution in MeOH:H_2O (4:1) was separately loaded into another 1 mL Hamilton gas tight glass syringe and dispensed into the SOR 3225 reactor to engage the reactants. The reactions were run at 0 °C at residence times of 30 sec, 1 min, 3 min, 5 min, 8 min, and 10 min. For nitrosation with **5**, a solution of **3** in ACN:EtOH (3.7:1) (200 mmol, 1 equiv) and **5** in ACN (600 mmol, 3 equiv, protected from light by covering the syringe with aluminum foil) were loaded into two separate 1 mL Hamilton gas tight glass syringes and dispensed into the SOR 3223 reactor. All the reactions were monitored at two different temperatures (50 °C and 25 °C) at residence times of 30 sec, 1 min, 3 min, 5 min, 8 min, and 10 min. Reaction progress was monitored by TLC and ESI-MS. The reaction mixtures were extracted by Et_2O, evaporated, and dried over anhydrous Na_2SO_4. The crude oily product was purified by dissolving it in hot petroleum ether, hot filtering the solution, and evaporating the filtrate to dryness in vaccuo to give the yellowish solid lomustine that was stored at -20 °C. TLC, ESI-MS, MS/MS, NMR (^{1}H and ^{13}C), and yield analyses were performed after purification. Three purification

methods were examined to purify the compounds as described in the main manuscript. The NMR spectra for the different purification methods are shown here for comparison.

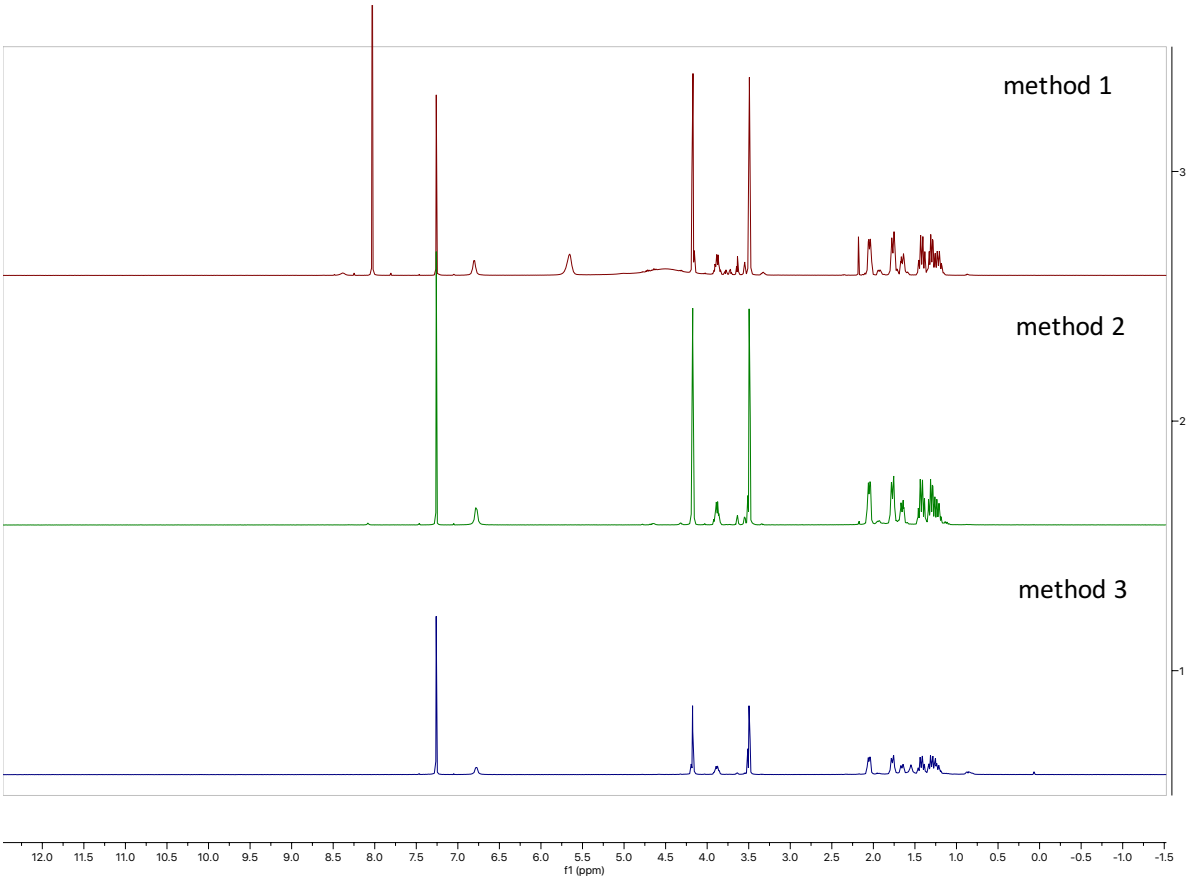

Figure 4.13 Comparison of 1H NMR of lomustine synthesized by continuous flow for different methods of purification. Method 1: extraction with Et_2O; method 2: recrystallization from CAN; method 3: hot filtration and recrystallization from petroleum ether

ESI-MS

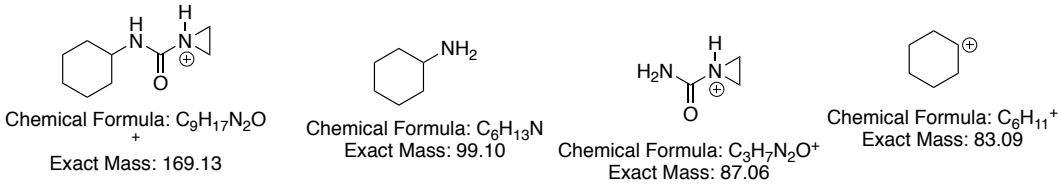

Figure 4.14 Fragments of lomustine in MS

ESI-MS (*m/z*): 169 ($C_9H_{17}N_2O^+$), 100 ($C_6H_{13}N+H^+$), 87($C_3H_7N_2O^+$), 83 ($C_6H_{11}^+$)

ESI-MS/MS of *m/z* 169: 169 ($C_9H_{17}N_2O^+$), 100 ($C_6H_{13}N+H^+$), 87 ($C_3H_7N_2O^+$)

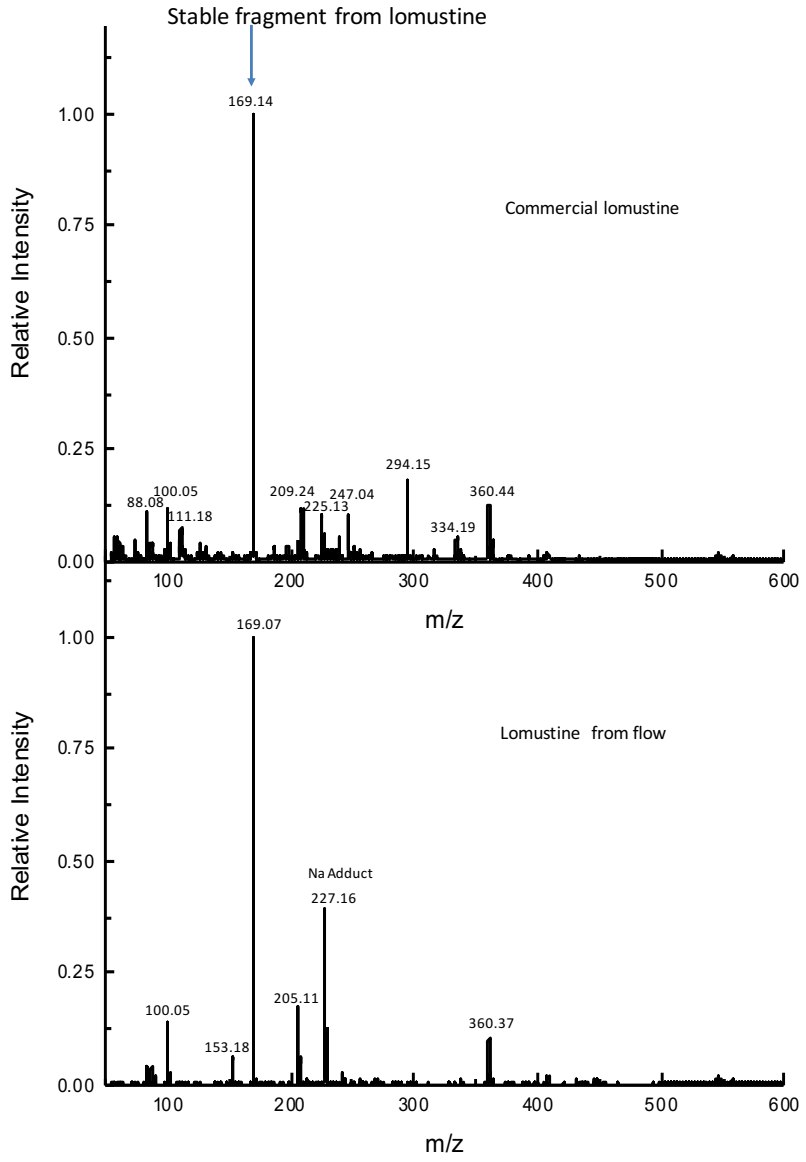

Figure 4.15 Full MS scan of commercially available lomustine and synthesized lomustine from flow. Reaction conditions were 25 °C, 8 min.

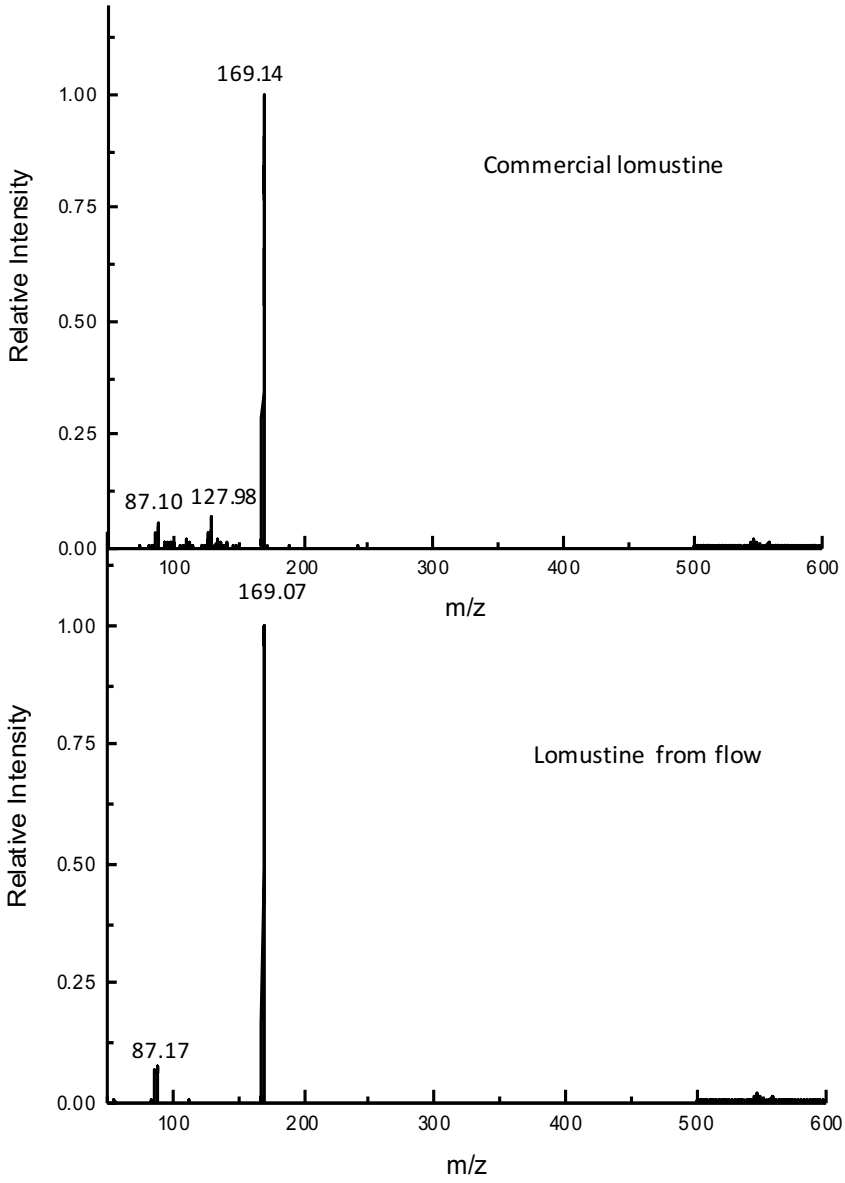

Figure 4.16 MS/MS of m/z=169 from commercially available lomustine and synthesized lomustine from flow. Reaction conditions were 25 °C, 8 min.

4.3.11 Telescoped Synthesis of Lomustine

Reactors: For scale up and telescoping of the two steps, fluorinated ethylene propylene (FEP) tubing was used. The outer diameter of the FEP tube was 1/16 inches and the inner diameter is 0.8mm. The first reactor volume was 5 μL and the second reactor volume was 100 μL.

Experimentation: Cyclohexaneamine, **1** (1 M, 1 equiv) and triethylamine (0.01 M, 0.01 equiv) were prepared in DCM separately. Next, the two separate solutions were mixed in a 1:1 (v:v) ratio and loaded into a 5 mL Hamilton gastight syringe. Then, a solution of 1-chloro-2-isocyanatoethane, **2** (0.7 M) was prepared in THF and loaded into a 5 mL Hamilton gastight syringe that was covered with aluminum-tape for light protection since it is light sensitive. The two syringes were connected to a T-connection and outlet of the T-connector was connected to the first tubing reactor using micro-tubes, check valves and other connectors (Figure S14 & S15). The setup for producing **3** was assembled and placed in a heated H_2O bath that was maintained at 50 °C. The outlet of the tube-reactor was connected to a four-way connector, where two of the outlets of the connectors were connected to a 10 mL Hamilton gastight syringe containing H_2O and a 5 mL Hamilton gastight syringe containing DCM. The four-way connector provide sufficient mixing for the extraction of the triethylamine base in the aqueous phase and leaving **3** in the organic phase. The fourth outlet was connected to the liquid-liquid separator (SEP-10) in which the DCM passes through the membrane carrying with it **3** to the next reaction step. The outlet of the aqueous phase from the separator was connected to a waste vial. For using sodium nitrite as a nitrosation reagent, the outlet of the organic phase was connected to a four-way connector. Sodium nitrite, **4** (1.5 M, 3 equiv) solution in THF and formic acid were loaded into two separate 5 mL Hamilton gastight syringes and connected to the a four-way connector. The outlet of the four-way connector is connected to the second tubing reactor. When using TBN, **5**, as a nitrosation reagent, we doubled the concentration of the starting material. The outlet of the organic phase from liquid-liquid extractor was connected to a T-connector, where one outlet was connected to a 5 mL Hamilton gastight syringe containing tert-butyl nitrite, **5** (5 M) in ACN. The outlet of the T-connector was connected to the second tubing reactor. The second reactor was placed in a H_2O bath with a constant temperature of 25 °C and the outlet of this reactor was connected to a collection vial. The reactions were monitored by TLC and ESI-MS. The purification and analyses were conducted as described above, except that HPLC-MS analysis was performed to evaluate the purity of the product (Figures are in APPENDIX C).

TLC and Purification: Reaction progress was monitored by TLC using 1:1 EtOAc:Hexanes as eluent. Lomustine was visualized under shortwave UV light (230 nm), while **3** was observed after staining with ninhydrin solution and heating. The extraction and purification was conducted by taking 500 µL from the collection vial and washing it with 2 mL of H_2O and 2 mL of Et_2O and

extracted three times. The combined organic layers were dried using anhydrous $NaSO_4$. The Et_2O was evaporated and the yellowish oil/solid was dissolved in hot petroleum ether, hot filtered, and the filtrate was removed under vacuum. The resulting solid was recrystallized from petroleum ether.

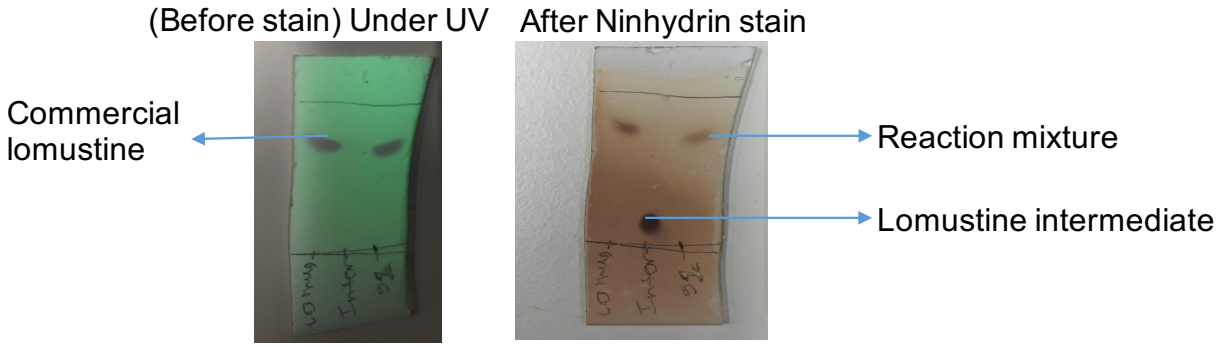

Figure 4.17 TLC monitoring during lomustine synthesis in flow.

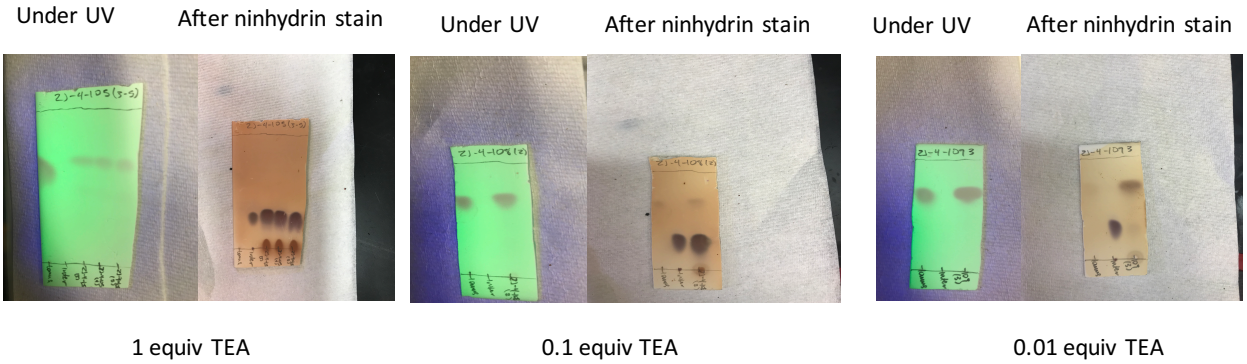

Figure 4.18 Comparison of TLC of telescoped lomustine synthesis using different equivalents of base

NMR

^{1}H NMR (500 MHz, $CDCl_3$, ppm): δ_H = 6.78 (s, 1H), 4.18 (t, J= 7.5, 2 H), 3.92-3.84 (m, 1H), 3.50 (t, J = 7.5 Hz, 2 H), 2.07-2.04 (m, 2 H), 1.79-1.75 (m, 2 H), 1.68-1.63 (m, 1 H), 1.45-1.39 (m, 2 H), 1.32-1.24 (m, 3 H); ^{13}C NMR (500 MHz, $CDCl_3$, ppm): δ_C= 151.78, 49.98, 40.03, 38.89, 33.09, 25.39, 24.76 (NMR spectrum are in APPENDIX C).

4.4 Conclusion

In summary, we have developed a rapid continuous synthesis of lomustine using DESI-MS to guide the selection of reaction conditions in the second step of the two steps overall transformation. The total residence time is 9 minutes to produce pure lomustine in 63% overall isolated yield compared to over 2 hours to generate a lower product yield using batch conditions.[2, 3, 55, 56] The two synthetic steps were optimized separately in glass chips and then translated to FEP tubing for telescoped scaling of the whole process. Only one in-line workup step was required for the two-step reaction sequence. Mixed solvents were used in the telescoped reaction to avoid clogging due to the low solubility of **3**. *t*Butyl nitrite, **5**, was found to be a milder and more efficient nitrosation reagent in this process to enable the isolation of pure lomustine via simple extraction, filtration and washing. This synthesis is a faster and greener process that affords a significant reduction in reaction time, lower waste production, and avoidance of any chromatographic steps. Using this method, 110 mg/hour of lomustine can be produced, equivalent to one dose/2h for an agent that is administered orally every 6 weeks. Scale up and in-line recrystallization of lomustine are in progress.

4.5 References

1. Chakkath, T.; Lavergne, S.; Fan, T. M.; Bunick, D.; Dirikolu, L., Alkylation and carbamylation effects of lomustine and its major metabolites and mgmt expression in canine cells. *Veterinary sciences* **2015,** *2*, 52-68.

2. Dirikolu, L.; Chakkath, T.; Fan, T.; Mente, N. R., Synthesis of trans-and cis-4′-hydroxylomustine and development of validated analytical method for lomustine and trans- and cis-4′-hydroxylomustine in canine plasma. *J. Anal. Toxicol.* **2009,** *33*, 595-603.

3. Lown, J. W.; Chauhan, S. M. S., Synthesis of specifically nitrogen-15- and carbon-13-labeled antitumor (2-haloethyl)nitrosoureas. The study of their conformations in solution by nitrogen-15 and carbon-13 nuclear magnetic resonance electronic control in their aqueous decomposition. *J. Org. Chem.* **1981,** *46*, 5309-5321.

4. Kaina, B.; Christmann, M.; Naumann, S.; Roos, W. P., MGMT: Key node in the battle against genotoxicity, carcinogenicity and apoptosis induced by alkylating agents. *DNA Repair* **2007,** *6*, 1079-1099.

5. Lee, F. Y.; Workman, P.; Roberts, J. T.; Bleehen, N. M., Clinical pharmacokinetics of oral CCNU (lomustine). *Cancer chemotherapy and pharmacology* **1985,** *14*, 125-131.

6. Funaro, J.; Friedman, H.; Weant, M., A costly "rebranding" of an old drug comes with a 700% price increase *Cancer Lett.* **2017**, 13-14.

7. Webb, D.; Jamison, T. F., Continuous flow multi-step organic synthesis. *Chem. Sci.* **2010,** *1*, 675-680.

8. Wegner, J.; Ceylan, S.; Kirschning, A., Ten key issues in modern flow chemistry. *Chem Commun (Camb)* **2011,** *47*, 4583-92.

9. Yoshida, J. I.; Kim, H.; Nagaki, A., Green and sustainable chemical synthesis using flow microreactors. *Chemsuschem* **2011,** *4*, 331-340.

10. Yoshida, J.-i.; Takahashi, Y.; Nagaki, A., Flash chemistry: flow chemistry that cannot be done in batch. *ChemComm* **2013,** *49*, 9896-9904.

11. Hessel, V.; Kralisch, D.; Kockmann, N.; Noël, T.; Wang, Q., Novel process windows for enabling, accelerating, and uplifting flow chemistry. *ChemSusChem* **2013,** *6*, 746-789.

12. Jensen, K. F.; Reizman, B. J.; Newman, S. G., Tools for chemical synthesis in microsystems. *Lab Chip* **2014,** *14*, 3206-12.

13. Gutmann, B.; Cantillo, D.; Kappe, C. O., Continuous-flow technology-a tool for the safe manufacturing of active pharmaceutical ingredients. *Angew. Chem. Int. Ed. Engl.* **2015,** *54*, 6688-728.

14. Cambié, D.; Bottecchia, C.; Straathof, N. J. W.; Hessel, V.; Noël, T., Applications of continuous-flow photochemistry in organic synthesis, material science, and water treatment. *Chem. Rev.* **2016,** *116*, 10276-10341.

15. Poh, J. S.; Makai, S.; von Keutz, T.; Tran, D. N.; Battilocchio, C.; Pasau, P.; Ley, S. V., Rapid asymmetric synthesis of disubstituted allenes by coupling of flow-generated diazo compounds and propargylated amines. *Angew. Chem. Int. Ed.* **2017,** *56*, 1864-1868.

16. Yu, Z.; Ye, X.; Xu, Q.; Xie, X.; Dong, H.; Su, W., A Fully Continuous-Flow Process for the Synthesis of p-Cresol: Impurity analysis and process optimization. *Org. Process Res. Dev.* **2017,** *21*, 1644-1652.

17. Britton, J.; Raston, C. L., Multi-step continuous-flow synthesis. *Chem. Soc. Rev.* **2017,** *46*, 1250-1271.

18. Berton, M.; Huck, L.; Alcázar, J., On-demand synthesis of organozinc halides under continuous flow conditions. *Nature Protocols* **2018,** *13*, 324.

19. V., H., Novel Process Windows – Gate to Maximizing Process Intensification via Flow Chemistry. *Chemical Engineering & Technology* **2009,** *32*, 1655-1681.

20. Zaborenko, N.; Bedore, M. W.; Jamison, T. F.; Jensen, K. F., Kinetic and Scale-Up Investigations of epoxide aminolysis in microreactors at high temperatures and pressures. *Org. Process Res. Dev.* **2011,** *15*, 131-139.

21. Wiles, C.; Watts, P., Recent advances in micro reaction technology. *ChemComm* **2011,** *47*, 6512-6535.

22. Wegner, J.; Ceylan, S.; Kirschning, A., Flow chemistry – a key enabling technology for (multistep) organic synthesis. *Adv. Synth. Catal.* **2012,** *354*, 17-57.

23. Snead, D. R.; Jamison, T. F., End-to-end continuous flow synthesis and purification of diphenhydramine hydrochloride featuring atom economy, in-line separation, and flow of molten ammonium salts. *Chem. Sci.* **2013,** *4*, 2822-2827.

24. Len, C.; Bruniaux, S.; Delbecq, F.; Parmar, V., Palladium-catalyzed Suzuki–Miyaura cross-coupling in continuous flow. *Catalysts* **2017,** *7*, 146.

25. A.M., L. J.; D., M. P.; L., B. R.; F., J. T., Towards more efficient, greener syntheses through flow chemistry. *The Chemical Record* **2017,** *17*, 667-680.

26. Morse, P. D.; Jamison, T. F., Synthesis and utilization of nitroalkyne equivalents in batch and continuous flow. *Angew. Chem. Int. Ed.* **2017,** *56*, 13999-14002.

27. Gustafsson, T.; Ponten, F.; Seeberger, P. H., Trimethylaluminium mediated amide bond formation in a continuous flow microreactor as key to the synthesis of rimonabant and efaproxiral. *ChemComm* **2008**, 1100-1102.

28. Hopkin, M. D.; Baxendale, I. R.; Ley, S. V., An expeditious synthesis of imatinib and analogues utilising flow chemistry methods. *Org Biomol Chem* **2013,** *11*, 1822-39.

29. Deadman, B. J.; Hopkin, M. D.; Baxendale, I. R.; Ley, S. V., The synthesis of Bcr-Abl inhibiting anticancer pharmaceutical agents imatinib, nilotinib and dasatinib. *Org. Biomol. Chem.* **2013,** *11*, 1766-1800.

30. Murray, P. R. D.; Browne, D. L.; Pastre, J. C.; Butters, C.; Guthrie, D.; Ley, S. V., Continuous flow-processing of organometallic reagents using an advanced peristaltic pumping system and the telescoped flow synthesis of (e/z)-tamoxifen. *Org. Process Res. Dev.* **2013,** *17*, 1192-1208.

31. Zhang, P.; Russell, M. G.; Jamison, T. F., Continuous flow total synthesis of rufinamide. *Org. Process Res. Dev.* **2014,** *18*, 1567-1570.

32. Snead, D. R.; Jamison, T. F., A three-minute synthesis and purification of ibuprofen: pushing the limits of continuous-flow processing. *Angew. Chem. Int. Ed. Engl.* **2015,** *54*, 983-7.

33. Adamo, A.; Beingessner, R. L.; Behnam, M.; Chen, J.; Jamison, T. F.; Jensen, K. F.; Monbaliu, J. C.; Myerson, A. S.; Revalor, E. M.; Snead, D. R.; Stelzer, T.; Weeranoppanant, N.; Wong, S. Y.; Zhang, P., On-demand continuous-flow production of pharmaceuticals in a compact, reconfigurable system. *Science* **2016,** *352*, 61-7.

34. Lin, H.; Dai, C.; Jamison, T. F.; Jensen, K. F., A Rapid total synthesis of ciprofloxacin hydrochloride in continuous flow. *Angew. Chem. Int. Ed.* **2017,** *56*, 8870-8873.

35. Zhang, P.; Weeranoppanant, N.; Thomas, D. A.; Tahara, K.; Stelzer, T.; Russell, M. G.; O'Mahony, M.; Myerson, A. S.; Lin, H.; Kelly, L. P.; Jensen, K. F.; Jamison, T. F.; Dai, C.; Cui, Y.; Briggs, N.; Beingessner, R. L.; Adamo, A., Advanced Continuous Flow Platform for On-Demand Pharmaceutical Manufacturing. *Chem. Eur. J.* **2018,** *24*, 2776-2784.

36. Falcone, C. E.; Jaman, Z.; Wleklinski, M.; Koswara, A.; Thompson, D. H.; Cooks, R. G., Reaction screening and optimization of continuous-flow atropine synthesis by preparative electrospray mass spectrometry. *Analyst* **2017,** *142*, 2836-2845.

37. Loren, B. P.; Wleklinski, M.; Koswara, A.; Yammine, K.; Hu, Y.; Nagy, Z. K.; Thompson, D. H.; Cooks, R. G., Mass spectrometric directed system for the continuous-flow synthesis and purification of diphenhydramine. *Chem. Sci.* **2017,** *8*, 4363-4370.

38. Wleklinski, M.; Falcone, C. E.; Loren, B. P.; Jaman, Z.; Iyer, K.; Ewan, H. S.; Hyun, S.-H.; Thompson, D. H.; Cooks, R. G., Can Accelerated Reactions in Droplets Guide Chemistry at Scale? *Eur. J. Org. Chem.* **2016,** *2016*, 5480-5484.

39. Ewan, H. S.; Iyer, K.; Hyun, S.-H.; Wleklinski, M.; Cooks, R. G.; Thompson, D. H., Multistep flow synthesis of diazepam guided by droplet-accelerated reaction screening with mechanistic insights from rapid mass spectrometry analysis. *Org. Process Res. Dev.* **2017,** *21*, 1566-1570.

40. Elena, R.; Anna, R.; Stefania, G.; Daniele, P.; Marisa, M., Synthesis of (+)-dumetorine and congeners by using flow chemistry technologies. *Chem. Eur. J.* **2011,** *17*, 6221-6226.

41. Ahmed-Omer, B.; Sanderson, A. J., Preparation of fluoxetine by multiple flow processing steps. *Org. Biomol. Chem.* **2011,** *9*, 3854-3862.

42. Newton, S.; Carter, C. F.; Pearson, C. M.; Alves, L. D.; Lange, H.; Thansandote, P.; Ley, S. V., Accelerating spirocyclic polyketide synthesis using flow chemistry. *Angewandte Chemie-International Edition* **2014,** *53*, 4915-4920.

43. Ludmila, P.; Joao, D. S. B.; Zsofia, H.; Florine, B.; Florian, C.; Andrew, L., Continuous consecutive reactions with inter-reaction solvent exchange by membrane separation. *Angew. Chem. Int. Ed.* **2016,** *55*, 13576-13579.

44. Malte, B.; M., M. J.; Simon, S.; H., R. J.; B., H. A., A Gram-scale batch and flow total synthesis of perhydrohistrionicotoxin. *Chem. Eur. J.* **2010,** *16*, 11471-11480.

45. Jensen, K. F., Silicon-based microchemical systems: Characteristics and applications. *MRS Bull.* **2006,** *31*, 101-107.

46. Geyer, K.; Gustafsson, T.; Seeberger, P. H., Developing continuous-flow microreactors as tools for synthetic chemists. *Synlett* **2009**, 2382-2391.

47. Kim, H.; Min, K. I.; Inoue, K.; Im, D. J.; Kim, D. P.; Yoshida, J., Submillisecond organic synthesis: Outpacing Fries rearrangement through microfluidic rapid mixing. *Science* **2016,** *352*, 691-694.

48. Troshin, K.; Hartwig, J. F., Snap deconvolution: An informatics approach to high-throughput discovery of catalytic reactions. *Science* **2017,** *357*, 175-181.

49. Wleklinski, M.; Loren, B. P.; Ferreira, C. R.; Jaman, Z.; Avramova, L.; Sobreira, T. J. P.; Thompson, D. H.; Cooks, R. G., High throughput reaction screening using desorption electrospray ionization mass spectrometry. *Chem. Sci.* **2018,** *9*, 1647-1653.

50. Zinia, J.; Ahmed, M.; Samyukta, S.; Larisa, A.; H., T. D., High throughput experimentation and continuous flow validation of suzuki–miyaura cross-coupling reactions. *Chem. Eur. J.* **2018,** *24*, 9546-9554.

51. Xin, Y.; M., B. R.; Graham, C. R., Organic reactions in microdroplets: reaction acceleration revealed by mass spectrometry. *Angew. Chem. Int. Ed.* **2016,** *55*, 12960-12972.

52. Ifa, D. R.; Manicke, N. E.; Dill, A. L.; Cooks, R. G., Latent Fingerprint Chemical Imaging by Mass Spectrometry. *Science* **2008,** *321*, 805-805.

53. Freeman, E. S., The kinetics of the thermal decomposition of sodium nitrate and of the reaction between sodium nitrite and oxygen. *The Journal of Physical Chemistry* **1956,** *60*, 1487-1493.

54. Fox, J. B.; Suhre, F. B., The determination of nitrite: a critical review. **1985**.

55. Johnston, T. P.; McCaleb, G. S.; Montgomery, J. A., Synthesis of chlorozotocin, the 2-chloroethyl analog of the anticancer antibiotic streptozotocin. *J. Med. Chem.* **1975,** *18*, 104-106.

56. Ileana, B.; I., N.-D., Potential anticancer agents. XXVIII. Synthesis of some cyclohexanone derived n-nitrosoureas. *Journal für Praktische Chemie* **1985,** *327*, 675-681.

CHAPTER 5. HIGH THROUGHPUT EXPERIMENTATION AND CONTINUOUS FLOW VALIDATION OF NUCLEOPHILIC AROMATIC SUBSTITUTION REACTIONS

5.1 Introduction

High throughput experimentation (HTE) technique allows the implementation of a large numbers of experiments in parallel, spending minimum amounts of compounds and time, and involving less labor per experiment.[1, 2] The technique can boost the lab productivity by rapid generation of comprehensive data and knowledge for the selected transformation.[1, 3] HTE based experiment focused across a range of settings have spread in biology, drug discovery[4], medicinal chemistry[5, 6] as well as catalysis.[2, 7, 8] Analysis of the resulting large data sets can be a bottleneck. The discovery and optimization of reaction conditions in chemical process development can be accelerated when HTE is coupled with MS analysis.[7, 9, 10] These impacts are particularly evident in the fields of pharmaceutical and biopharmaceutical industries where reduction in the time of experimental cycle is a necessity due to the higher importance of these product classes.[11, 12] HTE described in this chapter is based on two well-established techniques: (i) desorption electrospray ionization (DESI) and (ii) bulk microtiter (small scale batch) reaction. The reaction product analysis for HTE is done using a quick DESI-MS method (usually < 1 s per reaction spot)[13]. DESI can accelerate reactions on a surface in droplets in some cases by reportedly reducing the energy required for desolvation of reagents.[14, 15]

Nucleophilic aromatic substitution (S_NAr) reactions are a versatile transformation in the modern organic chemistry arsenal[16] and one of the important reactions used for making pharmacologically[17, 18] and biologically important molecules.[19-24] The S_NAr reaction mechanism have been extensively investigated.[25, 26] It involves stepwise addition–elimination process[27-29] wherein the first step involves nucleophilic attacks of the substrate to provide a Meisenheimer complex (MC) followed by the loss of the leaving group (LG) through either catalyzed or non-catalyzed pathways.[29-31] The reaction typically involves an amine as the nucleophile.[25] This chapter reports S_NAr reaction in HTE for both DESI and bulk microtiter formats that are coupled with electrospray ionization mass spectrometry (ESI-MS) using amines and aryl halides in presence of bases.

After HTE optimization, quick validation reactions of the hotspots were performed to increase confidence in the HTE findings. Microfluidic reactions versions of these are attractive alternatives for these transformations in organic synthesis, especially in catalysis, since continuous flow methods have shown great potential to achieve faster syntheses in a greener way[32] for more than a decade. Moreover, fast microfluidic synthesis of small drug molecules and analysis using ESI-MS has been reported by our group[33-36]. The S_NAr reaction is already known in flow[37], but we chose new substrates for this study since these derivatives are biologically as well as pharmaceutically important synthons.[10] The preparation of automated S_NAr reactions mixtures for both HTE methods was performed in glass-lined 96-well metal plates using sixteen different amines and thirteen different aryl halides. Additional variables included bases, reaction solvent, DESI analysis spray solvent, and temperature at various time points in the bulk reaction.

5.1.1 Brief Summary of this Chapter

An important class of reactions, nucleophilic aromatic substitution (S_NAr), was explored using HTE techniques. A total of 3,072 unique reactions were evaluated in DESI and bulk techniques using only approximately 3.5 sec/reaction for analysis. Microfluidic reactions were also performed to determine the correlation between bulk, DESI and flow based on heat map finding from HTE.

5.2 Results and Discussion

5.2.1 High throughput experimentation (HTE)

Automated preparation of the HTE of S_NAr reaction plates were done using a Beckman i7 high-precision nanoliter robot in conjunction with high throughput MS analysis. Two high throughput experimentation methods were tested: reaction in droplets using the DESI technique and reactions in bulk microtiter plates. N-Methyl-2-pyrrolidone (NMP) and 1,4 dioxane were chosen as solvents for the reaction because all the reagents dissolved in these solvents and they are polar aprotic reaction media.[38] DESI-MS analysis allowed rapid investigation of reactions that were capable of producing a diverse product profile. The spray solvents were MeOH or MeOH with 1% formic acid (FA). Full mass spectra in positive mode were recorded for each reaction mixture.

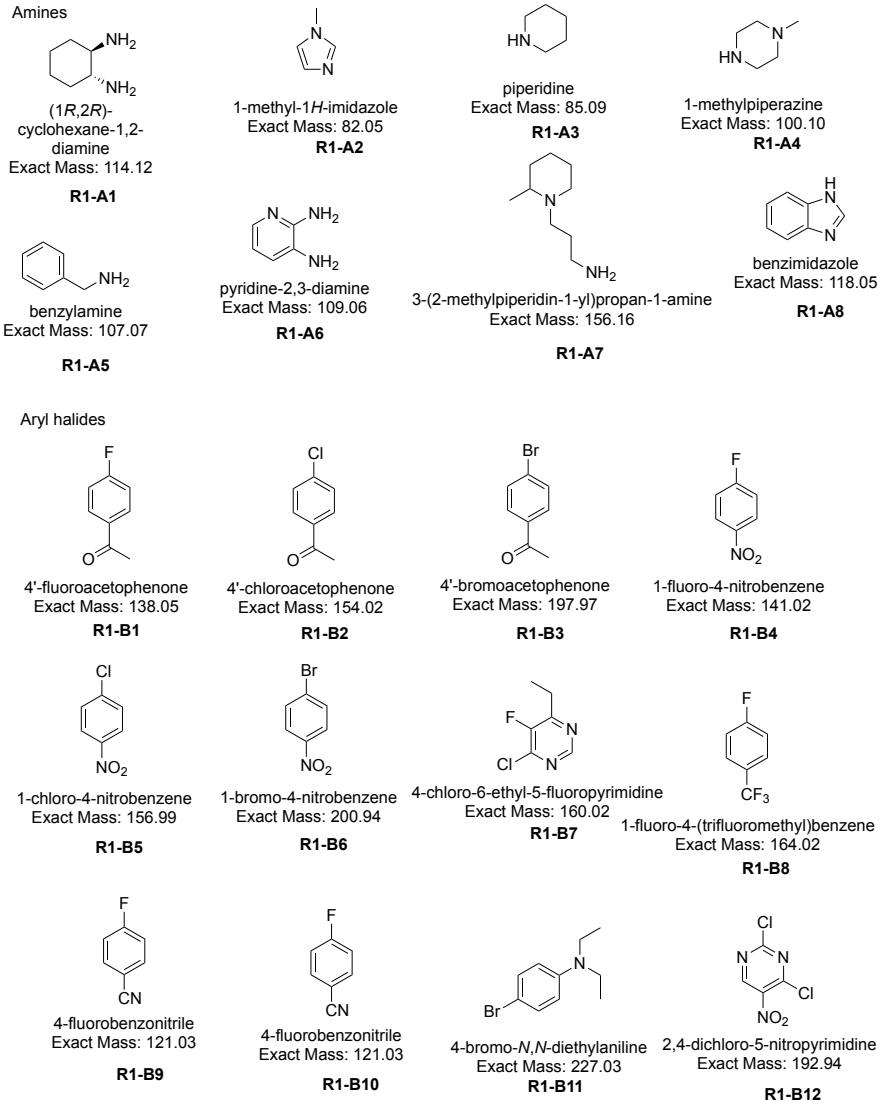

Scheme 5.1. Scope of different substitutes in S_NAr reactions studied using a high throughput experimentation (HTE) protocol (Round 1).

Initially, the S_NAr reactions were screened between eight amines and twelve aryl halides (Scheme 5.1) using different bases in NMP and 1,4-dioxane. The bulk HTE was done at 150 °C for 15 h. The ratio between the amines and aryl halides were 1:1 and 2.5 equivalent of different bases were used. All the amines and aryl halides for this reaction were explored without additional protection/deprotection steps. A Beckman-Coulter Biomek i7 liquid handling robot was used to prepare the reaction mixtures in either 96 well metal blocks or 384 well plates. A total of 400 μL

Table 5.1: A) The DESI and B) bulk HTE result of the same set of reaction condition. The conditions are, spray solvent: methanol; reaction solvent: NMP; base: DIPEA. C) Same B condition but the spray solvent is methanol with 1% formic acid, FA D) Same condition as C, but the solvent is 1,4 dioxane.

A)

	R1-B1	R1-B2	R1-B3	R1-B4	R1-B5	R1-B6	R1-B7	R1-B8	R1-B9	R1-B10	R1-B11	R1-B12 (S)	B12 (D)
R1-A1	5.3	3.3	6.6	281.3	12.4	6.3	3564.2	50.0	7.0	9.7	8.0	241.3	139.8
R1-A2	8.6	18.0	11.9	5.0	0.0	0.0	35.3	3.0	0.0	0.0	2.5	135.0	495.2
R1-A3	1.6	0.0	0.0	5.7	1.7	3.0	12.8	3.6	0.5	1.6	2.0	6.2	131.5
R1-A4	90.3	21.0	36.5	1213.7	30.0	15.4	38.9	7.5	511.1	117.4	5.1	286.8	3939.0
R1-A5	3.7	1.1	2.9	17.5	18.1	22.6	15.5	0.6	0.0	1.4	8.0	14.0	35.3
R1-A6	4.3	5.0	9.7	27.4	13.1	6.0	6.5	1.8	2.3	7.0	24.6	159.7	22.7
R1-A7	23.4	21.5	8.8	1080.1	8.3	8.7	5302.0	79.4	69.2	11.2	13.9	2787.1	91.9
R1-A8	19.8	7.6	5.8	4.0	9.2	4.7	11.5	4.7	7.5	2.6	3.4	2.5	33.6

B)

	R1-B1	R1-B2	R1-B3	R1-B4	R1-B5	R1-B6	R1-B7	R1-B8	R1-B9	R1-B10	R1-B11	R1-B12 (S)	B12 (D)
R1-A1	1094.1	25.5	24.1	1194.2	656.6	585.0	2243.6	197.7	1392.9	374.1	10.4	16.0	181.9
R1-A2	185.4	18.6	30.0	1058.7	68.8	76.5	49.6	64.6	508.6	56.1	6.0	256.4	431.4
R1-A3	113.6	6.4	10.2	69.2	324.5	154.8	6.3	6.2	5.9	14.0	24.0	7.7	548.2
R1-A4	999.1	312.1	1226.1	1367.7	4597.2	4515.4	2765.5	18.4	1112.3	4002.5	13.4	20.3	1296.5
R1-A5	32.8	18.6	13.4	25.1	14.2	16.9	1794.2	2.6	6.6	9.8	9.6	10.3	129.3
R1-A6	13.6	10.2	7.9	97.6	20.5	27.4	380.3	7.6	42.3	3.9	31.9	98.4	26.7
R1-A7	3534.2	166.5	200.2	5661.2	2939.8	2234.9	12713.1	203.8	1446.7	1292.6	11.9	18.5	2074.6
R1-A8	117.7	51.2	28.9	144.9	18.3	10.1	744.7	3.9	66.3	6.6	4.5	1.2	24.3

C)

	R1-B1	R1-B2	R1-B3	R1-B4	R1-B5	R1-B6	R1-B7	R1-B8	R1-B9	R1-B10	R1-B11	R1-B12 (S)	B12 (D)
R1-A1	3190.2	96.7	184.1	5502.0	1555.6	1730.2	4618.4	1363.4	7221.4	1584.5	31.3	27.0	243.1
R1-A2	277.5	56.9	56.2	1978.4	93.7	120.0	123.8	226.0	759.2	63.5	24.2	357.7	605.4
R1-A3	826.1	11.7	24.6	667.0	522.0	219.5	8.0	34.2	17.4	16.8	44.6	8.9	1069.7
R1-A4	3499.9	641.3	3345.7	4973.7	7199.4	10005.9	1267.5	63.9	2467.0	5317.5	25.8	27.5	893.9
R1-A5	1226.0	26.4	79.7	347.5	113.6	137.4	5435.5	17.2	488.3	54.4	44.4	67.8	431.9
R1-A6	61.7	31.2	37.1	209.2	53.4	93.1	684.4	35.6	110.5	29.3	31.5	757.1	62.0
R1-A7	6125.1	342.7	826.9	9886.8	4780.8	5175.7	15343.0	229.0	11798.2	2489.6	37.4	34.3	2467.7
R1-A8	703.4	145.3	113.3	5357.4	69.5	72.8	360.8	68.8	1975.1	40.1	14.8	17.0	110.5

D)

	R1-B1	R1-B2	R1-B3	R1-B4	R1-B5	R1-B6	R1-B7	R1-B8	R1-B9	R1-B10	R1-B11	R1-B12 (S)	B12 (D)
R1-A1	192.9	22.2	34.4	1434.0	34.6	149.1	3245.3	78.6	76.2	24.4	56.2	49.4	201.0
R1-A2	31.5	43.9	37.6	115.7	25.1	32.4	43.8	104.5	42.9	46.5	43.7	97.1	379.0
R1-A3	129.8	85.2	70.0	1271.0	270.3	474.3	51.2	30.6	26.4	13.4	538.0	26.4	159.6
R1-A4	804.0	506.7	481.4	6017.3	2571.8	5834.3	9662.2	92.0	50.5	51.1	50.6	140.4	171.2
R1-A5	248.3	67.4	40.3	272.1	30.1	37.8	7219.7	22.1	24.8	18.1	21.9	59.7	152.0
R1-A6	50.8	77.0	92.8	443.1	195.7	181.1	565.0	43.6	51.9	25.8	181.9	94.8	109.6
R1-A7	1217.9	456.7	426.0	4228.0	1030.4	1271.5	8747.6	89.7	37.8	43.5	61.2	56.1	208.3
R1-A8	1640.6	1819.0	860.8	4791.9	19.3	11.6	530.2	36.6	20.7	26.4	27.7	75.8	92.2

Green cells represent "yes" reactions (product ion intensity > 150 counts)

Red cells represent "no" reactions (product ion intensity < 150 counts)

Each cell is an average of two data points

B12 can form both single and double addition products, and the double addition product can form multiple ions

B12 (S) is the singly charged ion of the single addition product

B12 (D) is the sum of the average intensities of all the double addition ions

of the reaction solution was used per well in the 96 well metal plates. Four identical metal blocks were prepared each utilizing one of the four different bases. The bases used were: i) N,N-Diisopropylethylamine (DIPEA), (ii) Sodium tert-butoxide (NaO^tBu), (iii) Triethylamine (TEA) and (iv) no base, only added same amount of solvent. The reaction solution (40 μL) were then transferred to a 384 well plate and a DESI slide was prepared (porous Polytetrafluoroethylene, PTFE sheet glued on a glass support) using the 384 pin-tool by spotting the reaction solutions onto the PTFE surface of the DESI slide. The work flow for the automated high throughput reaction screening experiment by DESI-MS was described by Wleklinski et.[13] The liquid handling robot transferred 50 nL volumes of each reaction mixture to the DESI plate for the droplet reactions. The remaining reaction solutions in the metal blocks were heated for 15 h at 150 °C to effect the bulk reaction. After heating, the well plates were cooled, and transferred to 384 well plates for DESI-MS analysis. This set of experiments were spotted on the same DESI plate using the same pin-tool to enable direct comparison. Rhodamine in solution was used as a reference spot and the DESI plate was analyzed after spotting both reactions (droplet and bulk). An in-house software was used to analyze the data and produce heat map capable of guiding MS/MS experiments for structural conformation of both products and byproducts.

We analyzed the S_NAr reactions using both the DESI and bulk HTE techniques. Though the ionization varies for different compounds, a uniform analysis tool was used to plot peak intensities of the product m/z values for simple comparison of reaction efficiencies. Each square in Table 5.1 represents a unique reaction condition and is an average of two data points. Twelve successful reactions were found for the droplet reactions where as for the same conditions in bulk, 41 successful reactions were found (Table 5.1, A &B). There was no doubt that some of the reactions were favorable under droplet conditions, however S_NAr reaction are typically accelerated with heating,[39] so it was not surprising that more 'yes' reaction were observed in the bulk reaction conditions. Moreover, MeOH with 1% FA was found to be a better spray solvent than MeOH alone due to the better product ionization in presence of acid[40, 41] (Table 5.1, C). This change increased the number of successful reactions by 30% (54 count). It is also worth noting that the reaction worked better in NMP than 1,4 dioxane (54 'yes' reactions vs 40 'yes' reactions) (Table 5.1, C &D) since NMP is much more polar and basic [38], we attribute these finding to the stabilization of sigma complex transition state found after the addition step.

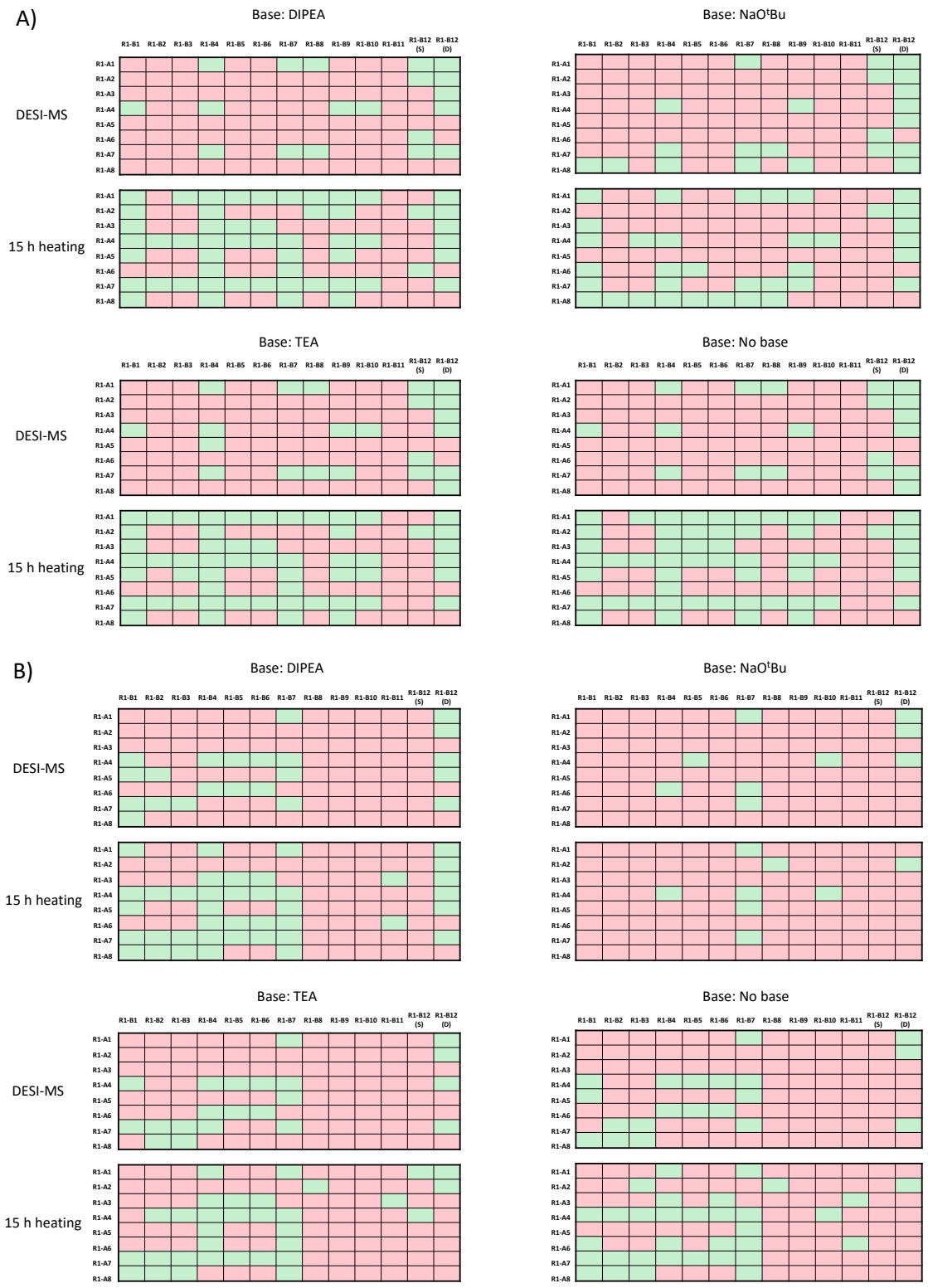

Figure 5.1. Heat map of 1,536 reactions of R-1 S_NAr HTE using MeOH with 1% FA as spray solvent under DESI-MS or bulk microtiter plate conditions at 150°C with four different basic condition. A) reaction solvent: NMP; B) reaction solvent: 1,4-dioxane.

Figure 5.1 shows the heat map of S_NAr HTE reactions (R-1) using eight amines and twelve aryl halides in both DESI and bulk using MeOH with 1% FA as spray solvent. In general, electron donating groups (EDG) in the aromatic moiety of the amines and electron withdrawing groups (EWG) in the aryl halides favored product formation.[25, 26] For this experiments, the most reactive amines were 1-methylpiperazine, **R1-A4** and 3-(2-methylpiperidin-1-yl) propan-1-amine, **R1-A7**, both of which possess electron donating groups. Similarly, a strong electron withdrawing nitro group in 1-fluoro-4-nitrobenzene, **R1-B4**, 1-chloro-4-nitrobenzene, **R1-B5**, 1-bromo-4-nitrobenzene, **R1-B6**, and 2,4-dichloro-5-nitropyrimidine, **R1-B12** makes these aryl halides very reactive. 4-Bromo-N,N-diethylaniline, **R1-B11** did not work at all (except for 2 reactions) due to the electron donating amine group. All other aryl halides reacted to the same extent. Also, ortho substituents in both amines or aryl halides retarded the reaction due to steric hindrances.[42] Thus, pyridine-2,3-diamine, **R1-A6** or 2,4-dichloro-5-nitropyrimidine, **R1-B12** did not react well, although (1R,2R)-cyclohexane-1,2-diamine, **R1-A1** reactions were facile since the two adjacent amino groups are on different faces of the cyclohexane ring. 1-Methyl-1H-imidazole, **R1-A2**, a tertiary amine, do not react. Also, **R1-A2** is less reactive because of dearomatization meaning that the loan pair of nitrogen are less available due to participation in the aromatic resonance. APPENDIX D represents all the data tables in detail.

Table 5.2: Summary of Round 1 S_NAr reaction. FA=formic acid

No. of successful reactions in DESI-MS HTE								
Base →	DIPEA		NaO^tBu		TEA		No Base	
Spray solvent ↓/reaction solvent →	NMP	Dioaxne	NMP	Dioxane	NMP	Dioxane	NMP	Dioxane
MeOH	12	--	10	--	21	--	13	--
MeOH with 1% FA	18	22	22	09	22	21	19	20
No. of successful reactions in Bulk HTE								
MeOH	41	--	18	--	40	--	41	--
MeOH with 1% FA	54	40	35	08	55	32	54	33

The structure of piperidine, **R1-A3**, and 1-methylpiperazine, **R1-A4** are similar, but **R1-A4** always worked better than **R1-A3** due to the presence of an electron donating group (EDG) in **R1-A4** that enhances its reactivity. Moreover, benzylamine, **R1-A5**, pyridine-2,3-diamine, **R1-A6**, and benzimidazole, **R1-A8** showed lower reactivity due to the oresence of an electron withdrawing aromatic moiety in these molecules that makes them less nucleophilic toward the addition reaction step in the sequence.

The summary of successful S_NAr reactions of 1,536 unique reactions both in DESI and bulk is shown in Table 5.2. Among all the reactions, 311 'yes' reactions were observed in bulk HTE while less than half that number were observed (153) in DESI-MS HTE. All the results are normalized and reported with the average peak intensity for each reaction.

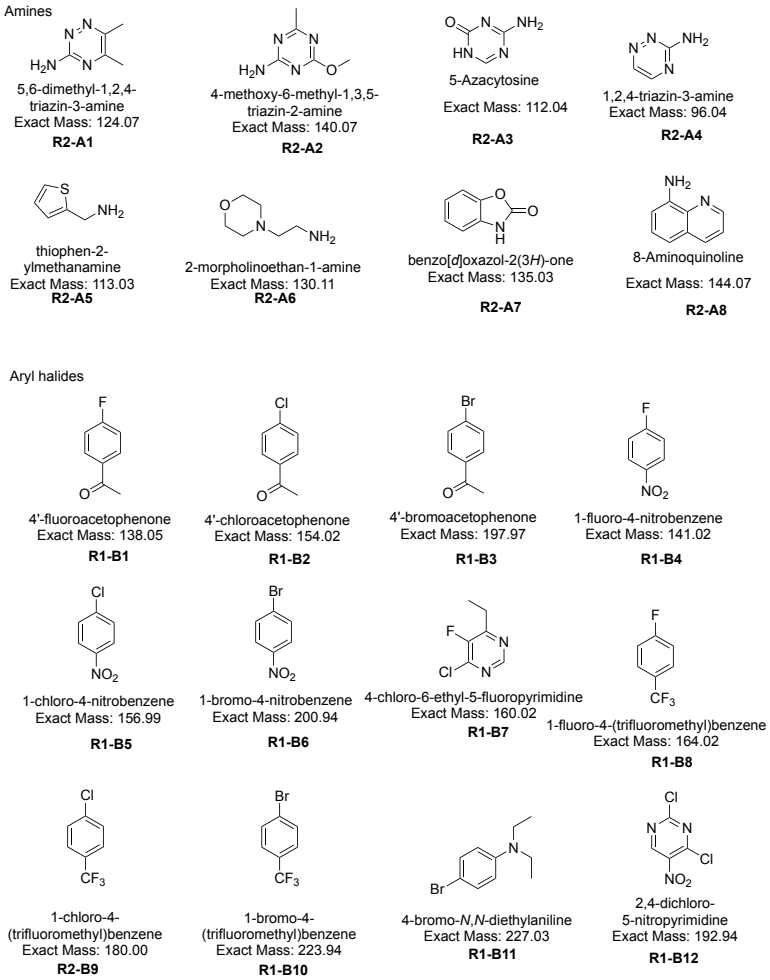

Scheme 5.2. Scope of different substitutes in S_NAr reactions in HTE protocol (Round 2).

After observing a set of successful HTE S_NAr reactions, a second family of biologically active amines was evaluated. For this, a new set of eight different amines were chosen, however the aryl halides were same except for **R1-B9**. The new **R1-B9** was 1-chloro-4-(trifluoromethyl) benzene (Scheme 5.2).

The reaction conditions for this set of S_NAr reaction was also almost same as R-1for the HTE. The only difference was the bulk reaction analyses were performed in only NMP solvent at three different time points. The analyses of the bulk reactions were performed after 1 h, 4 h and 15 h heating at 150 °C. Furthermore, methanol with 1% FA was the only spray solvent used. Figure 5.2 shows the heat map of the R-2 THE study. These results are normalized to show the average peak intensity for each reaction (Figure 5.2 A).

Unfortunately, this set of reactions did not work very well because most of the amines used have electron withdrawing groups in the aromatic moiety, thus making them much very less nucleophilic toward the addition step (Figure 5.2 B). Only thiophen-2-ylmethanamine, **R2-A5**, and 2-morpholinoethan-1-amine, **R2-A6**, worked comparatively better than the other amines due to their electron donating moiety. Again, **R1-B4**, **R1-B5**, **R1-B6**, **R1-B7**, and **R1-B12** worked better due to the presence of their strong electron withdrawing nitro and chloro groups. The result after 1 h and 4 h were almost the same indicating that long time reaction times did not push the reaction, rather the product seemed to be decomposed after 15 h heating (Table 5.3).

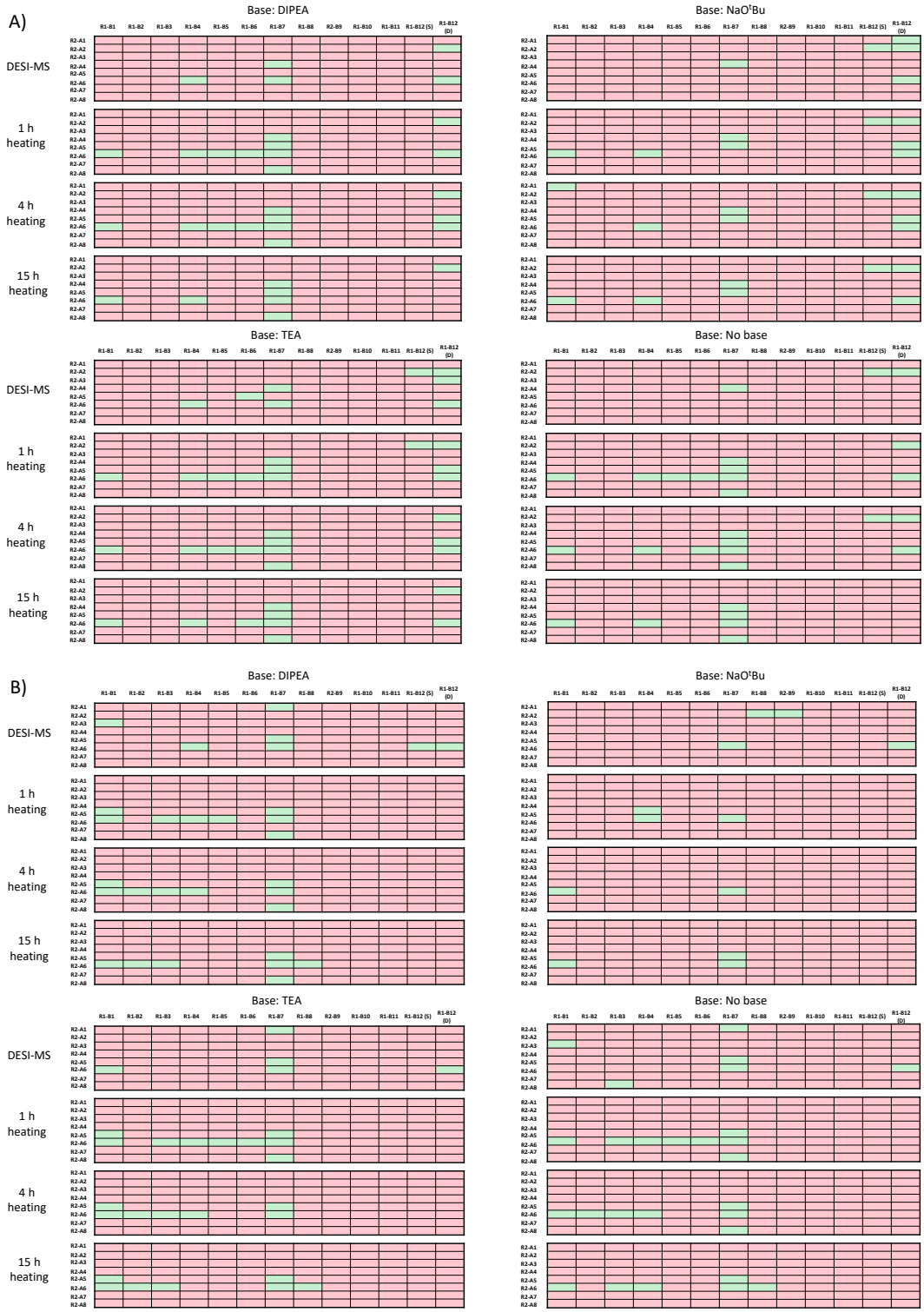

Figure 5.2. Heat map of 1,536 reactions (768 in DESI and 768 in bulk at three time points) of R-2 S_NAr HTE using MeOH with 1% FA as spray solvent in NMP at A) 150 °C; B) 200 °C.

Table 5.3. Summary of Round 2 S_NAr HTE reactions. The bulk reaction results are reported for three different the time points.

	DIPEA				NaO^tBu				TEA				No Base			
°C	DESI	Bulk (h)			DESI	Bulk (h)			DESI	Bulk (h)			DESI	Bulk (h)		
		1	4	15		1	4	15		1	4	15		1	4	15
150	4	8	9	6	4	8	7	7	7	11	11	9	3	11	9	6
200	7	8	9	6	4	3	2	3	5	9	7	7	6	8	7	6

Table 5.3 shows the summary of the R-2 S_NAr HTE reactions both in DESI and bulk at different time points. Only 18 reactions worked in DESI where as 38 reactions worked in bulk after 1 h heating. Efforts to push the reaction at higher temperatures and times (200 °C for 15 h), did not improve the outcome (Figure 5.2 B). Heating helped to promote reactions with the most reactive aryl halides (**R1-B1-R1B7**) with the most reactive amine being 2-morpholinoethan-1-amine, **R2-A6**, however, very high heating appeared to promote product degradation. Actually, most of the amines were much less nucleophilic, therefore higher reaction temperatures did not help the reaction even after longer times reaction at higher temperature. See APPENDIX D for detailed peak intensity values.

5.2.2 Microfluidic Evaluation.

After identifying reaction hotspots from HTE, we sought to validate some of the good reaction conditions to build the confidence between three different sets of reactions. For all microfluidic reactions, the reactions were explored for 30 sec, 1 min, 3 min, and 5 min residence times at 100 °C and/or 150 °C using 1:1 ratio of amines and aryl halides in NMP (Figure 5.3). DIPEA (2.5 equiv.) was used as it showed the most successful results for both sets of HTE. Reactions in 1,4-dioxane were confounded by the low solubility of the base that ultimately clogged the chip when using this solvent.

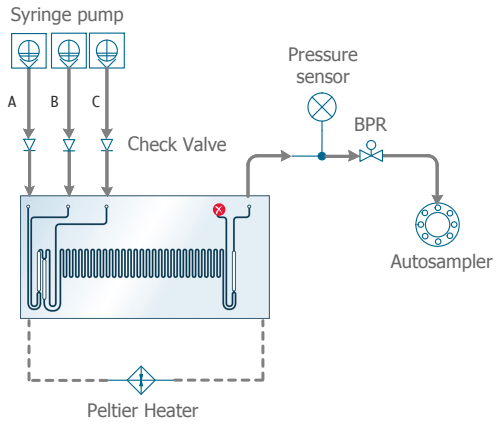

Figure 5.3. Continuous flow synthesis of S_NAr reactions in a glass chip reactor, SOR 3225. A = amine; B=aryl halide; C = DIPEA

The reaction evaluation were begun from 30 sec because the transformation has been already proven to be more efficient in continuous flow than in traditional bulk reaction due to superior mass to heat transfer capability and greater mixing in narrow reactor channel. The formation of expected product was confirmed by TLC and TSQ ESI-MS and the results from the microfluidic reactions were comparable to bulk and DESI screening experiments. Scheme 5.3 showed the 'yes' reactions that were conducted in flow. Here, it was also observed that amines with EWG reacted successfully. The reaction of 4-chloro-6-ethyl-5-fluoropyrimidine, **R1-B7**, with 3-(2-methylpiperidin-1-yl) propan-1-amine, **R1-A7**, and 1-methylpiperazine, **R1-A4**, always produced the chloride eliminated products. 1-Methyl-1H-imidazole, **R1-A2,** does not have a reactive amine site and did not participate in S_NAr reaction. The possibility of obtaining a false positive result in MS for the reaction between 1-methyl-1H-imidazole, **R1-A2**, and 4-bromo-N,N-diethylaniline, **R1-B11**, because the m/z of the aryl halide starting material and the product are same. 2-Morpholinoethan-1-amine, **R2-A6**, was the only reactive amine in the round 2 reaction set and the continuous flow synthesis using this amine that was explored. A negative result was observed for this reaction, however, both under HTE and in continuous flow conditions. We also examined some other negative results obtained from HTE and evaluated those reaction conditions under continuous flow. In both cases, almost no product peak was observed (Scheme 5.4) (see Appendix D for spectrum).

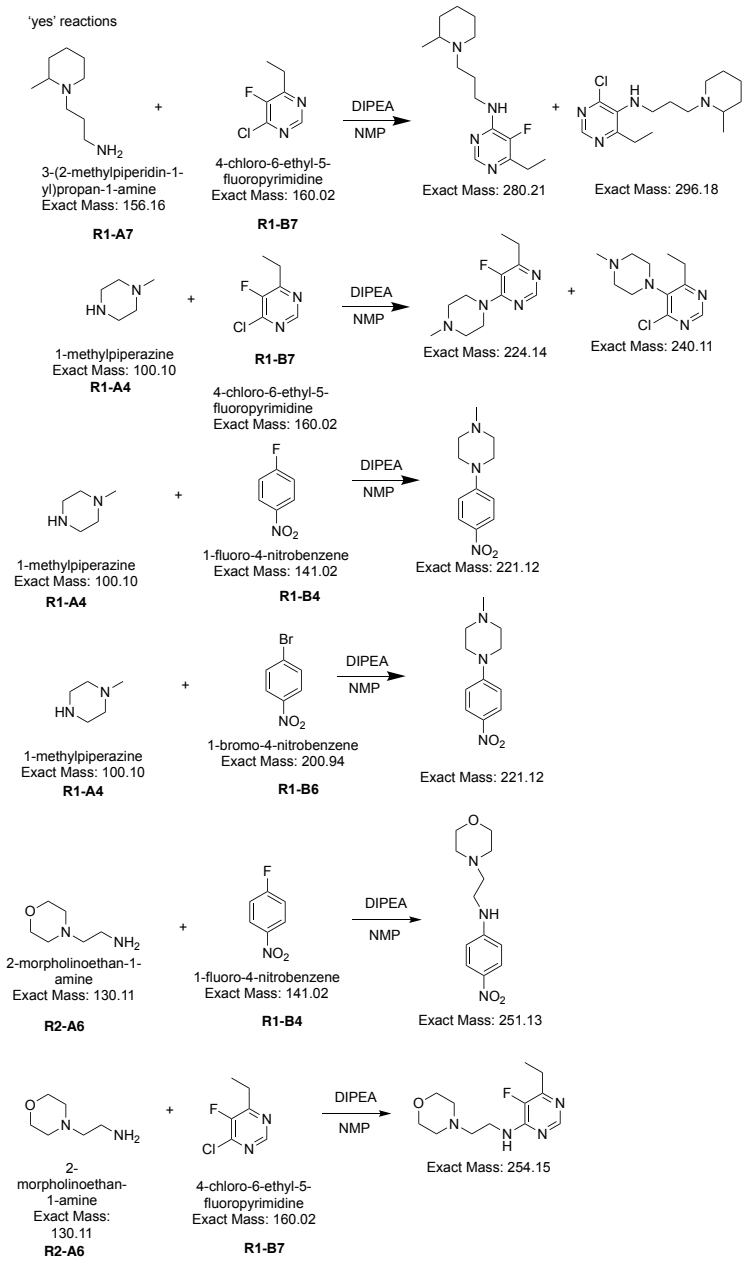

Scheme 5.3. Microfluidic evaluation of select 'yes' reactions from the HTE study.

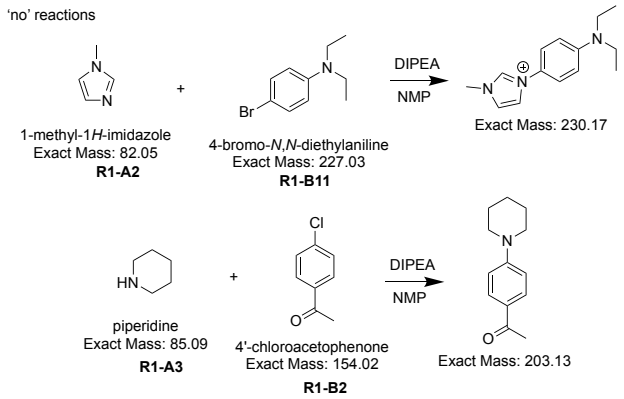

Scheme 5.4. Microfluidic evaluation of some 'no' reactions from the HTE.

5.3 Experimental

5.3.1 Chemicals

All chemicals and reagents were purchased from Sigma-Aldrich (St Louis, Missouri) and used without any purification.

5.3.2 Liquid Handling Robot

Samples in 96 well aluminum blocks fitted with glass vial liners (Analytical Sales and Services, Inc., NJ, USA) or 384 well polypropylene plates (Analytical Sales and Services, Inc., NJ, USA) were prepared both for DESI-MS and bulk HTE using a Biomek i7 (Beckman Coulter, Inc., Indianapolis, IN) dual-bridge liquid handling robot. A 384-tip head was used to transfer a single volume of 384 samples under the same speed of aspiration and dispensing conditions. Also, the heights of pipetting at the source and destination positions, pattern of pipetting, etc. remained constant for each transfer. An 8-channel head provided more flexibility in the amount of liquid transferred. Moreover, the 8-channel tip head provided better flexibility in terms of the layout of source and destination platforms, speed, pipetting height, and reaction stoichiometry. The i7 deck is also capable of accommodating all necessary labware including robotic tips, plates, reservoirs, etc. for assembling one reaction step. Chemically resistant polypropylene and disposables tips (Beckman Coulter, Inc., Indianapolis, IN) were used to make the reaction mixtures. The reservoirs of reagents solutions were the polypropylene multi-well plates and reservoirs, as well as custom

made Teflon reservoirs. Development of new transfer methods and validation were done using the Biomek point-and-click programming tool. Standard pipetting techniques that used this software were adjusted and optimized for highly volatile liquids.

5.3.3 Customized Heating Block

The heating device made of an aluminum heater block containing four, 100 W cartridge heaters was fabricated to accommodate standard size 96 well plates. A CNi series temperature controller (Omega Engineering) enabled precise temperature control and a solid-state relay was used to modulate the 120 Vac power to the heaters.[2] The heating blocks tolerates temperatures ranging from -20 °C to 200 °C.

5.3.4 DESI-MS Analysis

DESI-MS analysis was performed following the previously published method of Wleklinski et al[13]. However, in this work, the density of reaction spots was 3,072 spots/plate instead of 6144/plate. The Biomek i7 robot was used to prepare the DESI slide using reagents that were pipetted into standard polypropylene 384-well plates. Porous polytetrafluoroethylene (PTEF) sheets (EMD, Millipore Fluoropore, Saint-Gobain) were glued (Scotch Spray mount) onto glass slides (Foxx Life Sciences) to make the DESI-MS slides. No signs of interference from the glue were observed. The reagents were mixed, and rhodamine B dye in a separate reservoir was added to the robotic deck as a fiducial marker. The liquids (50 nL) were deposited onto a porous PTFE surface using the magnetic pin tool at 3,072 spot densities. A linear ion trap mass spectrometer (LTQ XL; Thermo Scientific, San Jose, CA) equipped with a commercial DESI-imaging source (DESI 2D source, Prosolia Inc., Indianapolis, IN) was used to collect the DESI-MS data. Xcalibur v. 4.0 software is used to control the instrument and run the worklists for DESI-MS data acquisition. The DESI spray angle was 56° using MeOH or MeOH with 1% formic acid (FA) as spray solvent, and with an applied voltage of 5 kV. Mass spectra were collected in positive ion mode over the m/z range of 50-500. The DESI-MS imaging lateral resolution was 350 µm. This was achieved using a stage speed of 4,376 µm/sec and an instrument scan time of 80 ms. For data processing, data were visualized using an in-house software designed[13] to automatically search for the m/z values of reactants, intermediates, and byproducts. The analysis using the in-house software

generates a heat map indicating 'yes/no' output for each spot on the PTFE surface of the DESI slide.

5.3.5 DESI-MS Analysis Software (CHRIS)

The Chemical Reaction Integrated Screening (CHRIS) is an In-house software suite developed to automatically control the DESI system (mass spectrometer, solvents system, and Prosolia DESI 2D stage) and search the captured data for m/z values that correspond to the starting materials, intermediates, by-products, and products. CHRIS generates a yes/no report, through a web interface and displays the mass spectrum of any spot as well as spreadsheets with the intensity for the selected molecules, the possible contaminants, or unknown by-products as guided by the user.

5.3.6 Mass Spectrometer

A Thermo Fisher TSQ Quantum Access MAX mass spectrometer connected to a Dionex Ultimate 3000 Series Pump and WPS-3000 Autosampler (Thermo Fisher Scientific, Waltham, MA), was used to acquire electrospray ionization mass spectra (ESI-MS) of the samples. The analysis was performed in full scan mode, monitoring each analysis in both positive and negative ion modes. The optimized parameters for the ESI source and MS are as follows: spraying solvent, MeOH; spray voltage +5 kV (positive mode) and -5.0 kV (negative mode); capillary temperature, 250 °C; Sheath gas pressure, 20; scan time, 0.5 s; Q1 peak width (FWHM), 0.70 Th; micro scans, 1. The autosampler settings were as follows: MS acquire time, 2 min; sample injection volume, 1 μL. The data from MS spectrometer was processed using Thermo Fisher Xcalibur software.

5.3.7 Microfluidics

All microfluidic validation reactions were performed using the Labtrix S1 (Chemtrix, Ltd, Netherlands). The system was described in chapter 2 & 3.[2,33] All the gastight glass syringes were bought separately from Hamilton Company (Hamilton, Reno, Nevada). All operations are controlled via a ChemTrix GUI software, connected to the Labtrix S1 casing using a USB cable.

5.3.8 High Throughput Experimentation

High throughput S_NAr experimentation in bulk was performed in 96-well metal block assemblies (Analytical Sales and Services, Inc., NJ, USA). The reaction mixtures were prepared

in 1 mL glass inserts of the 96-well metal block. All the reagent transfers and mixing were performed by the Beckman Coulter i7 liquid handling robot. The stock solutions were 111 mM for amines and aryl halides, and the base stock solution concentration was 1.25 M in NMP or 1,4-dioxane. The final reaction concentrations were 50 mM (1 equiv.) both for the amines and aryl halides, and 125 mM (2.5 equiv.) for the bases. All solutions were prepared in appropriate solvent, and they were added to the 96-well plate in a ratio of 9:9:2 (amine:aryl halide:base). Solvent was used instead of base for the 'no base' condition. For DESI-MS HTE, 384 well plates were prepared from the 96 well plates using the robot; a 384 pintool was used to transfer the final reagent mixtures (50 nL) onto the PTFE slides. For bulk HTE, the plates were heated in the customized heating block at 150 °C or 200 °C for varying times. The cover on top of the glass inserts (top of the metal block) is made by chemically resistant perfluoroalkoxy (PFA) film. Double silicone rubber mats were used on top of the PFA film, providing a tight seal that is enough to heat the solution above the boiling point with less than 5% solvent loss and no cross talk between wells. After heating, the plates were cooled to room temperature, and loaded back on the deck of the liquid handling robot to prepare 384-well plates. The reactions mixtures were pinned onto the same DESI slide as described above before and after heating using the same transfer method.

5.3.9 Microfluidic Reaction Evaluation

Solutions of amines (100 mM, 1 equiv) and aryl halides (100 mM, 1equiv) in NMP were loaded individually into two separate 1 mL Hamilton gastight glass syringes (Hamilton Company, Reno, NV). DIPEA (150 mM, 1.5 equiv) solution in NMP was loaded into another 1 mL Hamilton gastight glass syringe. Each solution was continuously dispensed into the SOR 3225 reactor to engage the reactants. All the S_NAr reactions were run at 100 °C and/or 150 °C using residence times of 30 sec, 1 min, 3 min, and 5 min. The products were collected without quenching and stored at -80 °C. TLC analyses were performed at the end of the reactions. Also, the subsequent ESI-MS analysis was performed after extraction in ether and dilution into methanol. (see Appendix D for details).

5.4 Conclusion

The power of HTE both in DESI and bulk reaction modes enables chemists to rapidly

perform large arrays of rationally designed experiments. Moreover, it makes it possible to derive multidimensional hypotheses that can be explained from easily collected huge data sets. This investigation led to a robotic HT technique to execute S_NAr reactions in 96-well arrays which was coupled with a fast DESI-MS analysis that boosts the reaction screening process. A total sixteen amines and thirteen aryl halides were used for the HTE. A total 1,536 unique reactions in droplet mode and 1,536 reactions in bulk were performed using four different bases in two different solvents. A total of 170 reactions were worked in DESI and 351 reactions worked were worked in bulk screening. The general expectations for the impact donating and withdrawing substituents on S_NAr reactions were observed in the HTE. The comparison of a few successful reactions identified by HTE were evaluated in continuous flow conditions. These finding showed that the positive conditions identified by HTE were true positives. Furthermore, the same was true for negative reaction conditions. Though we found a lot of unsuccessful reactions in HTE, these negative results are valuable in that they are very important for machine learning.[43, 44] The next step in this project is to use these results for machine learning.

An easy, simple and efficient technique for identifying S_NAr reaction conditions with different functional groups tolerance is described. Biologically important synthons were synthesized without protecting the functional groups. The HT screening was used as a faster way of finding the best reaction parameters that can lead to faster optimization of microfluidic reactions by eliminating failed reaction conditions. Decreasing the number of unsuccessful opportunities will result in libraries with more compounds for evaluating various physicochemical properties. Further, by applying this process to other common important class of reactions, it may have a significant impact on library synthesis and identifying of the right conditions for challenging substrates. The data could also be used to find new opportunities and patterns of the chemical reactivity, and reaction design that may facilitate new routes for organic synthesis.

5.5 References

1. Shevlin, M., Practical High-throughput experimentation for chemists. *ACS Med. Chem. Lett.* **2017,** *8*, 601-607.

2. Zinia, J.; Ahmed, M.; Samyukta, S.; Larisa, A.; H., T. D., High throughput experimentation and continuous flow validation of Suzuki–Miyaura cross-coupling reactions. *Chem. Eur. J.* **2018,** *24*, 9546-9554.

3. Selekman, J. A.; Qiu, J.; Tran, K.; Stevens, J.; Rosso, V.; Simmons, E.; Xiao, Y.; Janey, J., High-throughput automation in chemical process development. *Annu. Rev. Chem. Biomol. Eng.* **2017,** *8*, 525-547.

4. Ichiishi, N.; Caldwell, J. P.; Lin, M.; Zhong, W.; Zhu, X.; Streckfuss, E.; Kim, H.-Y.; Parish, C. A.; Krska, S. W., Protecting group free radical C–H trifluoromethylation of peptides. *Chem. Sci.* **2018,** *9*, 4168-4175.

5. Macarron, R.; Banks, M. N.; Bojanic, D.; Burns, D. J.; Cirovic, D. A.; Garyantes, T.; Green, D. V. S.; Hertzberg, R. P.; Janzen, W. P.; Paslay, J. W.; Schopfer, U.; Sittampalam, G. S., Impact of high-throughput screening in biomedical research. *Nature Reviews Drug Discovery* **2011,** *10*, 188.

6. Liu, M.; Chen, K.; Christian, D.; Fatima, T.; Pissarnitski, N.; Streckfuss, E.; Zhang, C.; Xia, L.; Borges, S.; Shi, Z.; Vachal, P.; Tata, J.; Athanasopoulos, J., High-throughput purification platform in support of drug discovery. *ACS Combinatorial Science* **2012,** *14*, 51-59.

7. Chen, P., Electrospray ionization tandem mass spectrometry in high-throughput screening of homogeneous catalysts. *Angew. Chem. Int. Ed.* **2003,** *42*, 2832-2847.

8. Buitrago Santanilla, A.; Regalado, E. L.; Pereira, T.; Shevlin, M.; Bateman, K.; Campeau, L.-C.; Schneeweis, J.; Berritt, S.; Shi, Z.-C.; Nantermet, P.; Liu, Y.; Helmy, R.; Welch, C. J.; Vachal, P.; Davies, I. W.; Cernak, T.; Dreher, S. D., Nanomole-scale high-throughput chemistry for the synthesis of complex molecules. *Science* **2015,** *347*, 49-53.

9. Troshin, K.; Hartwig, J. F., Snap deconvolution: An informatics approach to high-throughput discovery of catalytic reactions. *Science* **2017,** *357*, 175-181.

10. Wleklinski, M.; Loren, B. P.; Ferreira, C. R.; Jaman, Z.; Avramova, L.; Sobreira, T. J. P.; Thompson, D. H.; Cooks, R. G., High throughput reaction screening using desorption electrospray ionization mass spectrometry. *Chem. Sci.* **2018**.

11. Kim, H.; Min, K. I.; Inoue, K.; Im, D. J.; Kim, D. P.; Yoshida, J., Submillisecond organic synthesis: Outpacing Fries rearrangement through microfluidic rapid mixing. *Science* **2016,** *352*, 691-694.

12. Snead, D. R.; Jamison, T. F., A three-minute synthesis and purification of ibuprofen: pushing the limits of continuous-flow processing. *Angew. Chem. Int. Ed. Engl.* **2015,** *54*, 983-7.

13. Wleklinski, M.; Loren, B. P.; Ferreira, C. R.; Jaman, Z.; Avramova, L.; Sobreira, T. J. P.; Thompson, D. H.; Cooks, R. G., High throughput reaction screening using desorption electrospray ionization mass spectrometry. *Chem. Sci.* **2018,** *9*, 1647-1653.

14. Pirro, V.; Alfaro, C. M.; Jarmusch, A. K.; Hattab, E. M.; Cohen-Gadol, A. A.; Cooks, R. G., Intraoperative assessment of tumor margins during glioma resection by desorption electrospray ionization-mass spectrometry. *Proceedings of the National Academy of Sciences* **2017,** *114*, 6700-6705.

15. Chen, X.; Cooks, R. G., Accelerated reactions in field desorption mass spectrometry. *J. Mass Spectrom.* **2018,** *53*, 942-946.

16. Goldstein, S. W.; Bill, A.; Dhuguru, J.; Ghoneim, O., Nucleophilic aromatic substitution—addition and identification of an amine. *J. Chem. Educ.* **2017,** *94*, 1388-1390.

17. Scales, S.; Johnson, S.; Hu, Q.; Do, Q.-Q.; Richardson, P.; Wang, F.; Braganza, J.; Ren, S.; Wan, Y.; Zheng, B.; Faizi, D.; McAlpine, I., Studies on the regioselective nucleophilic aromatic substitution (S_NAr) reaction of 2-substituted 3,5-dichloropyrazines. *Org. Lett.* **2013,** *15*, 2156-2159.

18. Roughley, S. D.; Jordan, A. M., The Medicinal Chemist's Toolbox: An Analysis of Reactions Used in the Pursuit of Drug Candidates. *J. Med. Chem.* **2011,** *54*, 3451-3479.

19. Cvijetić, I. N.; Verbić, T. Ž.; Ernesto de Resende, P.; Stapleton, P.; Gibbons, S.; Juranić, I. O.; Drakulić, B. J.; Zloh, M., Design, synthesis and biological evaluation of novel aryldiketo acids with enhanced antibacterial activity against multidrug resistant bacterial strains. *European Journal of Medicinal Chemistry* **2018,** *143*, 1474-1488.

20. Trump, R. P.; Blanc, J.-B. E.; Stewart, E. L.; Brown, P. J.; Caivano, M.; Gray, D. W.; Hoekstra, W. J.; Willson, T. M.; Han, B.; Turnbull, P., Design and Synthesis of an Array of Selective Androgen Receptor Modulators. *J. Comb. Chem.* **2007,** *9*, 107-114.

21. Chen, L.; Fu, W.; Feng, C.; Qu, R.; Tong, L.; Zheng, L.; Fang, B.; Qiu, Y.; Hu, J.; Cai, Y.; Feng, J.; Xie, H.; Ding, J.; Liu, Z.; Liang, G., Structure-based design and synthesis of 2,4-diaminopyrimidines as EGFR L858R/T790M selective inhibitors for NSCLC. *European Journal of Medicinal Chemistry* **2017,** *140*, 510-527.

22. Phuangsawai, O.; Beswick, P.; Ratanabunyong, S.; Tabtimmai, L.; Suphakun, P.; Obounchoey, P.; Srisook, P.; Horata, N.; Chuckowree, I.; Hannongbua, S.; Ward, S. E.; Choowongkomon, K.; Gleeson, M. P., Evaluation of the anti-malarial activity and cytotoxicity of 2,4-diamino-pyrimidine-based kinase inhibitors. *European Journal of Medicinal Chemistry* **2016,** *124*, 896-905.

23. La Pietra, V.; Sartini, S.; Botta, L.; Antonelli, A.; Ferrari, S. M.; Fallahi, P.; Moriconi, A.; Coviello, V.; Quattrini, L.; Ke, Y.-Y.; Hsing-Pang, H.; Da Settimo, F.; Novellino, E.; La Motta, C.; Marinelli, L., Challenging clinically unresponsive medullary thyroid cancer: Discovery and pharmacological activity of novel RET inhibitors. *European Journal of Medicinal Chemistry* **2018,** *150*, 491-505.

24. Li, L.; Lv, K.; Yang, Y.; Sun, J.; Tao, Z.; Wang, A.; Wang, B.; Wang, H.; Geng, Y.; Liu, M.; Guo, H.; Lu, Y., Identification of n-benzyl 3,5-dinitrobenzamides derived from pbtz169 as antitubercular agents. *ACS Med. Chem. Lett.* **2018,** *9*, 741-745.

25. Gazitúa, M.; Tapia, R. A.; Contreras, R.; Campodónico, P. R., Effect of the nature of the nucleophile and solvent on an S_NAr reaction. *New J. Chem.* **2018,** *42*, 260-264.

26. Kwan, E. E.; Zeng, Y.; Besser, H. A.; Jacobsen, E. N., Concerted nucleophilic aromatic substitutions. *Nat. Chem.* **2018,** *10*, 917-923.

27. Bunnett, J. F.; Zahler, R. E., Aromatic nucleophilic substitution reactions. *Chem. Rev.* **1951,** *49*, 273-412.

28. Um, I.-H.; Hong, J.-Y.; Kim, J.-J.; Chae, O.-M.; Bae, S.-K., Regioselectivity and the nature of the reaction mechanism in nucleophilic substitution reactions of 2,4-dinitrophenyl x-substituted benzenesulfonates with primary amines. *J. Org. Chem.* **2003,** *68*, 5180-5185.

29. Ormazabal-Toledo, R.; Santos, J. G.; Ríos, P.; Castro, E. A.; Campodónico, P. R.; Contreras, R., Hydrogen bond contribution to preferential solvation in S_NAr reactions. *J. Phys. Chem. B* **2013,** *117*, 5908-5915.

30. Ormazábal-Toledo, R.; Contreras, R.; Tapia, R. A.; Campodónico, P. R., Specific nucleophile–electrophile interactions in nucleophilic aromatic substitutions. *Org. Biomol. Chem.* **2013,** *11*, 2302-2309.

31. Gazitúa, M.; Tapia, R. A.; Contreras, R.; Campodónico, P. R., Mechanistic pathways of aromatic nucleophilic substitution in conventional solvents and ionic liquids. *New J. Chem.* **2014,** *38*, 2611-2618.

32. Len, C.; Bruniaux, S.; Delbecq, F.; Parmar, V., Palladium-catalyzed Suzuki–Miyaura cross-coupling in continuous flow. *Catalysts* **2017,** *7*, 146.

33. Falcone, C. E.; Jaman, Z.; Wleklinski, M.; Koswara, A.; Thompson, D. H.; Cooks, R. G., Reaction screening and optimization of continuous-flow atropine synthesis by preparative electrospray mass spectrometry. *Analyst* **2017,** *142*, 2836-2845.

34. Loren, B. P.; Wleklinski, M.; Koswara, A.; Yammine, K.; Hu, Y.; Nagy, Z. K.; Thompson, D. H.; Cooks, R. G., Mass spectrometric directed system for the continuous-flow synthesis and purification of diphenhydramine. *Chem. Sci.* **2017,** *8*, 4363-4370.

35. Ewan, H. S.; Iyer, K.; Hyun, S.-H.; Wleklinski, M.; Cooks, R. G.; Thompson, D. H., Multistep flow synthesis of diazepam guided by droplet-accelerated reaction screening with mechanistic insights from rapid mass spectrometry analysis. *Org. Process Res. Dev.* **2017,** *21*, 1566-1570.

36. Wleklinski, M.; Falcone, C. E.; Loren, B. P.; Jaman, Z.; Iyer, K.; Ewan, H. S.; Hyun, S.-H.; Thompson, D. H.; Cooks, R. G., Can accelerated reactions in droplets guide chemistry at scale? *Eur. J. Org. Chem.* **2016,** *2016*, 5480-5484.

37. Örkényi, R.; Éles, J.; Faigl, F.; Vincze, P.; Prechl, A.; Szakács, Z.; Kóti, J.; Greiner, I., Continuous synthesis and purification by coupling a multistep flow reaction with centrifugal partition chromatography. *Angew. Chem. Int. Ed.* **2017,** *56*, 8742-8745.

38. Jessop, P. G.; Jessop, D. A.; Fu, D.; Phan, L., Solvatochromic parameters for solvents of interest in green chemistry. *Green Chemistry* **2012,** *14*, 1245-1259.

39. Forlani, L., Are weak interactions responsible for kinetic catalytic behaviour in S_NAr reactions? *J. Phys. Org. Chem.* **1999,** *12*, 417-424.

40. Miao, Z.; Chen, H., Direct Analysis of Liquid Samples by Desorption Electrospray Ionization-Mass Spectrometry (DESI-MS). *J. Am. Soc. Mass. Spectrom.* **2009,** *20*, 10-19.

41. Badu-Tawiah, A.; Bland, C.; Campbell, D. I.; Cooks, R. G., Non-aqueous spray solvents and solubility effects in desorption electrospray ionization. *J. Am. Soc. Mass. Spectrom.* **2010,** *21*, 572-579.

42. Crampton, M. R.; Emokpae, T. A.; Howard, J. A. K.; Isanbor, C.; Mondal, R., Leaving group effects on the mechanism of aromatic nucleophilic substitution (S_NAr) reactions of some phenyl 2,4,6-trinitrophenyl ethers with aniline in acetonitrile. *J. Phys. Org. Chem.* **2004,** *17*, 65-70.

43. Fong, R. C.; Scheirer, W. J.; Cox, D. D., Using human brain activity to guide machine learning. *Scientific Reports* **2018,** *8*, 5397.

44. Borji, A., Negative results in computer vision: A perspective. *image and vision computing* **2018,** *69*, 1-8.

APPENDIX A

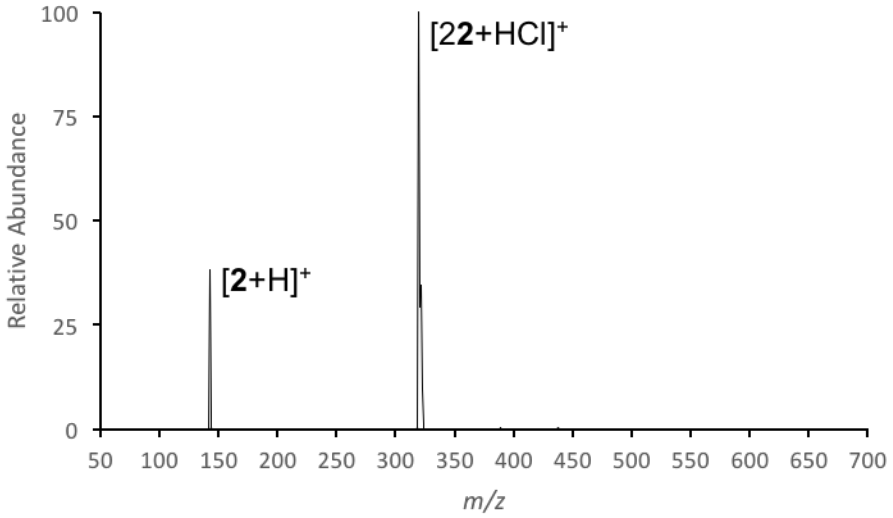

Figure A1: Full scan MS of the preparative ES product of scheme 1a with HCl in water

Full scan positive ion mode mass spectrum of the preparative ES product from the first step of the atropine synthesis with tropine, phenyl acetic acid and hydrochloric acid in water. In this sample m/z 142 $[\text{tropine}+H]^+$ and m/z 319 $[2\text{tropine} + HCl]^+$ are the most abundant ions.

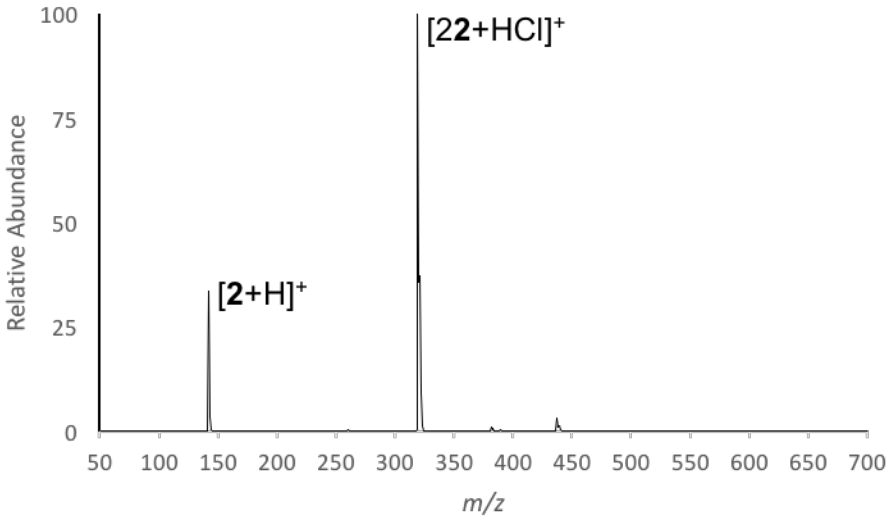

Figure A2: Full scan MS of the preparative ES product of scheme 1a with HCl in dioxane

Full scan positive ion mode mass spectrum of the preparative ES product from the first step of the atropine synthesis with tropine, phenylacetic acid and hydrochloric acid in dioxane. In this sample m/z 142 $[\text{tropine} +H]^+$ and m/z 319 $[2\text{tropine} + HCl]^+$ are the most abundant ions.

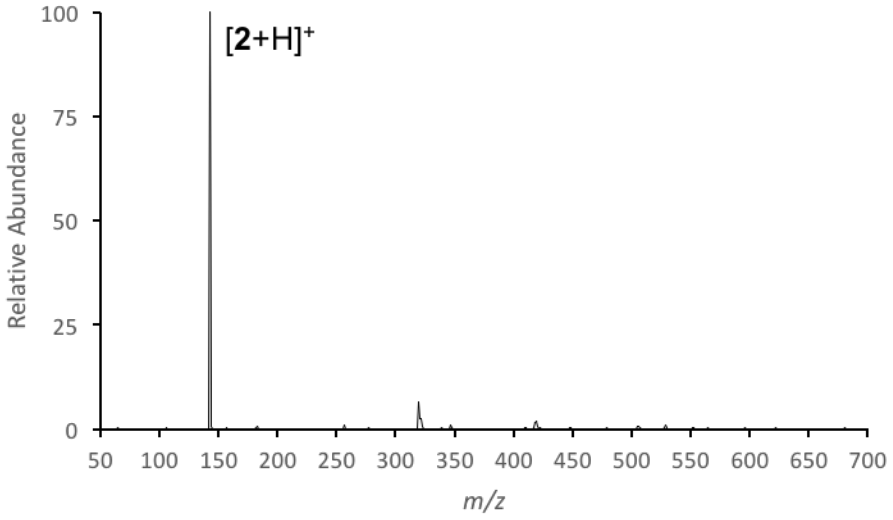

Figure A3: Full scan MS of the preparative ES product of scheme 1b with DMA

Full scan positive ion mode mass spectrum of the preparative ES product from the first step of the atropine synthesis with tropine and phenylacetic acid in DMA. In this sample m/z 142 [tropine +H]$^+$ is the most abundant ion.

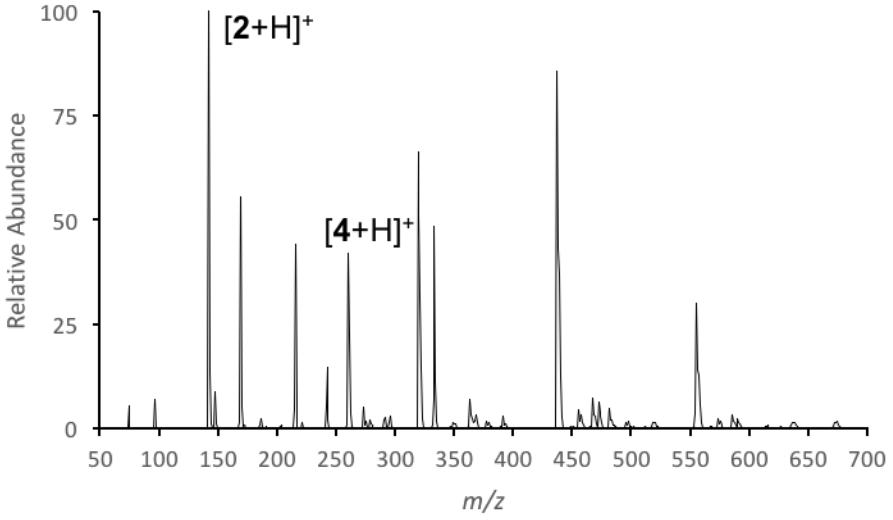

FigureA4: Full scan MS of the preparative ES product of scheme 1c with HCl in dioxane

Full scan positive ion mode mass spectrum of the preparative ES product from the first step of the atropine synthesis with tropine, phenylacetyl chloride acid and hydrochloric acid in dioxane. In this sample m/z 142 [tropine +H]$^+$, m/z 260 [intermediate +H]+, and m/z 319 [2tropine + HCl]$^+$ are present.

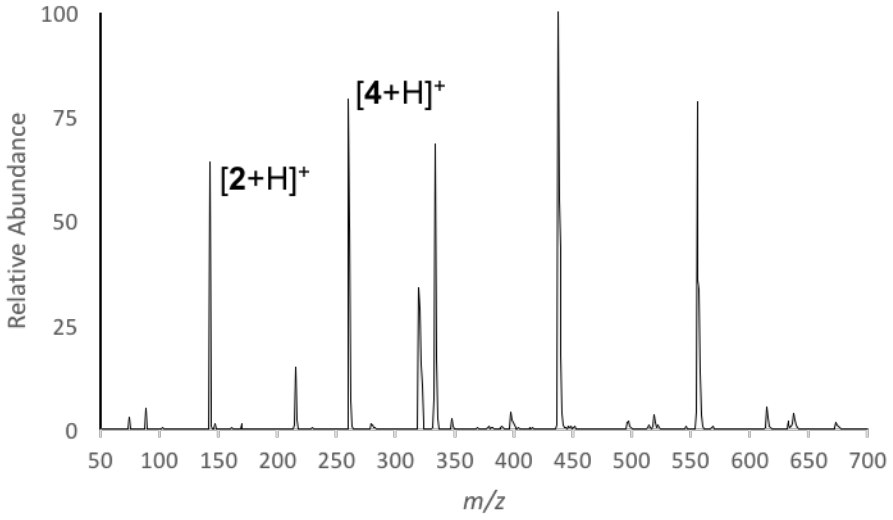

Figure A5: Full scan MS of the preparative ES product of scheme 1d with DMA

Full scan positive ion mode mass spectrum of the preparative ES product from the first step of the atropine synthesis with tropine, phenylacetyl chloride acid and hydrochloric acid in dioxane. In this sample m/z 142 [tropine +H]$^+$ and m/z 260 [intermediate +H]$^+$ are present.

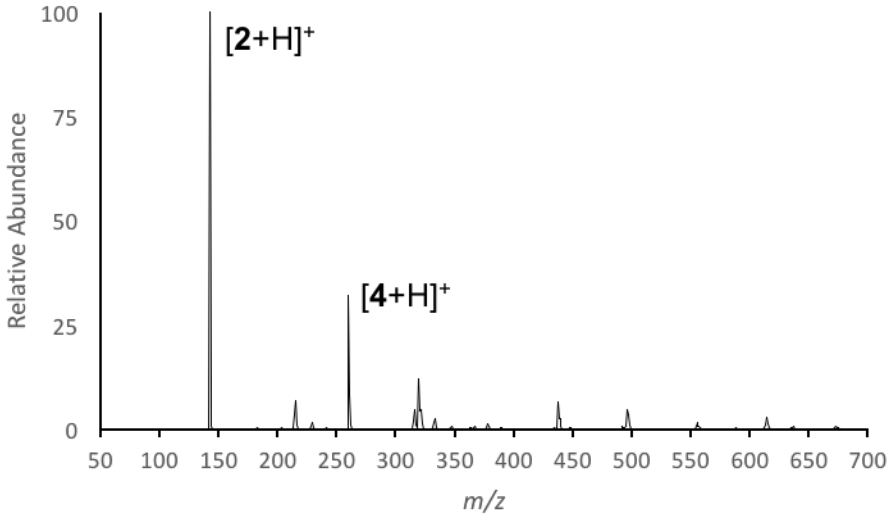

Figure A6: Full scan MS of the preparative ES product of scheme 1d with DMF

Full scan positive ion mode mass spectrum of the preparative ES product from the first step of the atropine synthesis with tropine and phenylacetyl chloride acid in DMF. In this sample m/z 142 [tropine +H]$^+$ and m/z 260 [intermediate +H]+ are the most abundant ions.

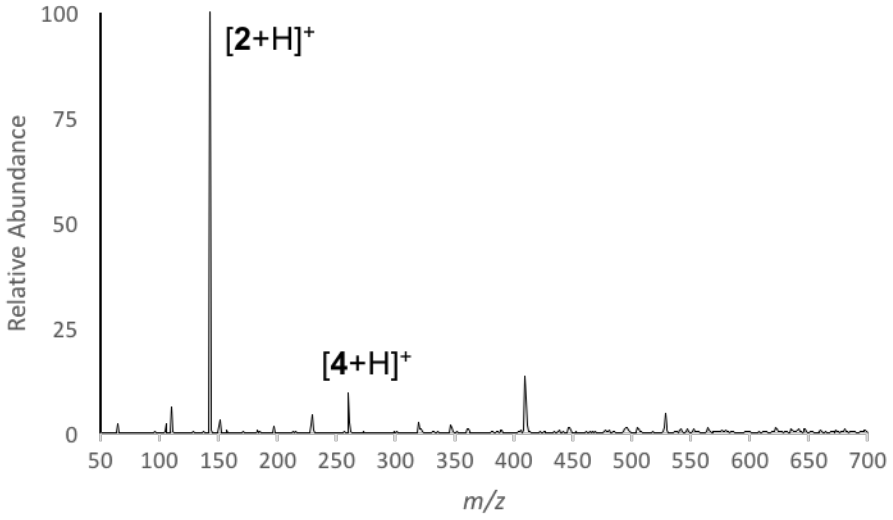

Figure A7: Full scan MS of the preparative ES product of scheme 1d with ethanol

Full scan positive ion mode mass spectrum of the preparative ES product from the first step of the atropine synthesis with tropine and phenylacetyl chloride acid in ethanol. In this sample m/z 142 [tropine +H]$^+$ and m/z 260 [intermediate +H]$^+$ are present.

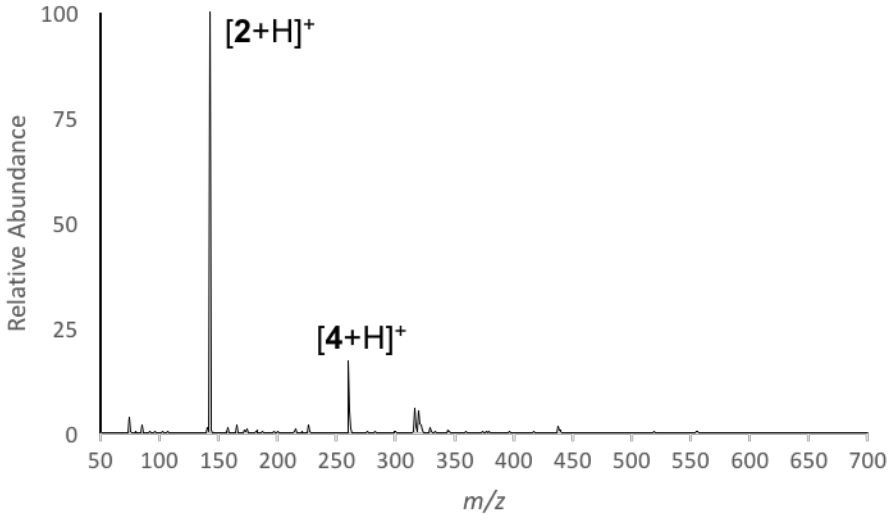

Figure A8: Full scan MS of the preparative ES product of scheme 1d with methanol

Full scan positive ion mode mass spectrum of the preparative ES product from the first step of the atropine synthesis with tropine and phenylacetyl chloride acid in methanol. In this sample m/z 142 [tropine +H]$^+$ and m/z 260 [intermediate +H]$^+$ are the most abundant ions.

Table A1: Microfluidic synthesis of intermediate **4** using hydrochloric acid in dioxane

R1 Tropine (0.4M) µl/min	R2 HCl in dioxane (0.4M) µl/min	R3 Phenylacetyl chloride (0.4M) µl/min	R4 DMF µl/min	1st Residence time Tr_1min	2nd Residence time Tr_2 min	Temperature °C	Conversion of Intermediate (%) (by nESI-MS)
2.5	2.5	2.75	2.5	1	1.29	200	19.44
1.25	1.25	1.37	1.25	2	2.78	200	6.29
0.625	0.625	0.687	0.625	4	5.16	200	4.34
2.5	2.5	2.75	2.5	1	1.29	150	61.45
1.25	1.25	1.37	1.25	2	2.78	150	89.67
0.625	0.625	0.687	0.625	4	5.16	150	85.63
2.5	2.5	2.75	2.5	1	1.29	100	75.37
1.25	1.25	1.37	1.25	2	2.78	100	80.34
0.625	0.625	0.687	0.625	4	5.16	100	90.62

All reactions used the SOR 3224 chip (5+10 µl) and a pressure of 7 bar

Table A2: Microfluidic synthesis of intermediate **4** without hydrochloric acid

R1 Tropine (1M) µl/min	R2 Phenylacetyl chloride (1M) µl/min	Residence time Tr min	Ratio	Temperature °C	Conversion of intermediate (%) (by nESI-MS)
9.286	10.214	1	1:1.1	200	67.76
4.643	5.107	2	1:1.1	200	87.22
2.321	2.554	4	1:1.1	200	93.19
9.286	10.214	1	1:1.1	150	93.45
4.643	5.107	2	1:1.1	150	93.27
2.321	2.554	4	1:1.1	150	94.45
9.286	10.214	1	1:1.1	100	90.41
4.643	5.107	2	1:1.1	100	88.94
2.321	2.554	4	1:1.1	100	88.39
4.643	5.107	2	1:1	100	89.33

All reactions used the SOR 3227 chips (19.5 µl), pressure of 6 bar and DMA

Table A3: Percent conversion of the second step base screen in preparative ES

Base	**4** *m/z* 260	**6** *m/z* 272	**1** *m/z* 290	**7** *m/z* 304	**8** *m/z* 320
ammonia	98.8%	<1%	<1%	<1%	<1%
dabco	99.2%	<1%	<1%	<1%	<1%
1,5-diazabicyclo[4.3.0]non-5-ene	38.9%	11.4%	47.4%	<1%	2.2%
1,8-diazabicyclo[5.4.0]undec-7-ene	40.7%	16.0%	15.0%	13.7%	14.6%
diethylamine	99.8%	<1%	<1%	<1%	<1%
N,N-diisopropylethylamine	99.8%	<1%	<1%	<1%	<1%
diisopropylmethylamine	Not Soluble				
4-(dimethylamino)pyridine	79.8%	11.1%	2.1%	3.1%	3.9%
2,6-lutidine	95.6%	1.6%	1.2%	<1%	<1%
pH 10 buffer	96.6%	1.3%	1.6%	<1%	<1%
piperidine	87.4%	4.2%	<1%	2.1%	5.6%
potassium ethoxide	10.7%	64.7%	15.7%	1.1%	7.8%
potassium methoxide	15.3%	45.1%	7.6%	<1%	31.1%
potassium tert-butoxide	Not Soluble				
sodium ethoxide	12.1%	66.1%	16.4%	<1%	5.2%
sodium hydroxide	42.8%	40.3%	15.4%	<1%	1.4%
sodium methoxide	20.6%	66.3%	9.9%	1.8%	1.4%
sodium tert-butoxide	Not Soluble				
tetrabutylammonium hydroxide	5.1%	19.0%	16.6%	48.6%	10.7%
tetramethylammonium hydroxide	4.2%	9.5%	1.1%	1.8%	83.4%
1,5,7-triazabicyclo[4.4.0]dec-5-ene	Not Soluble				
triethylamine	99.8%	<1%	<1%	<1%	<1%

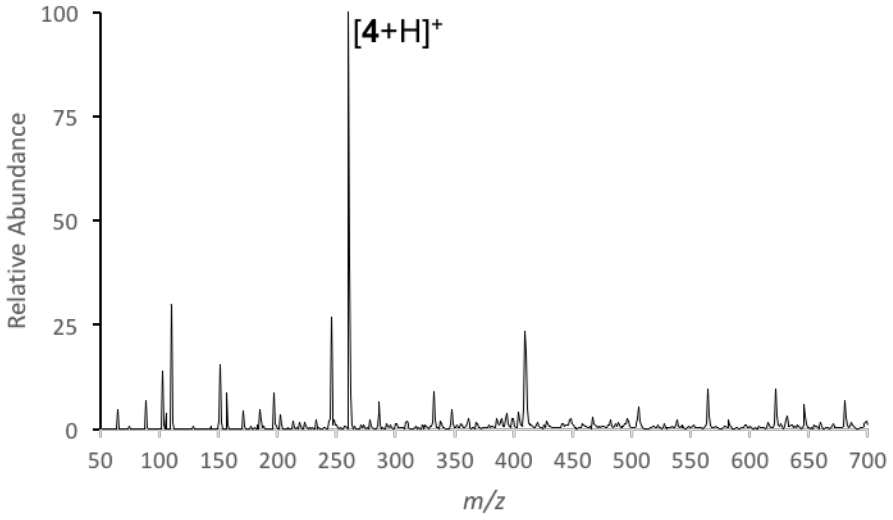

Figure A9: Full scan MS of the second step of the atropine synthesis by preparative ES using ammonia.

Full scan positive ion mode mass spectrum of the preparative ES product from the second step of the atropine synthesis with step 1 product, aqueous formaldehyde and ammonia. In this sample m/z 260 [intermediate +H]$^+$ is the most abundant ion.

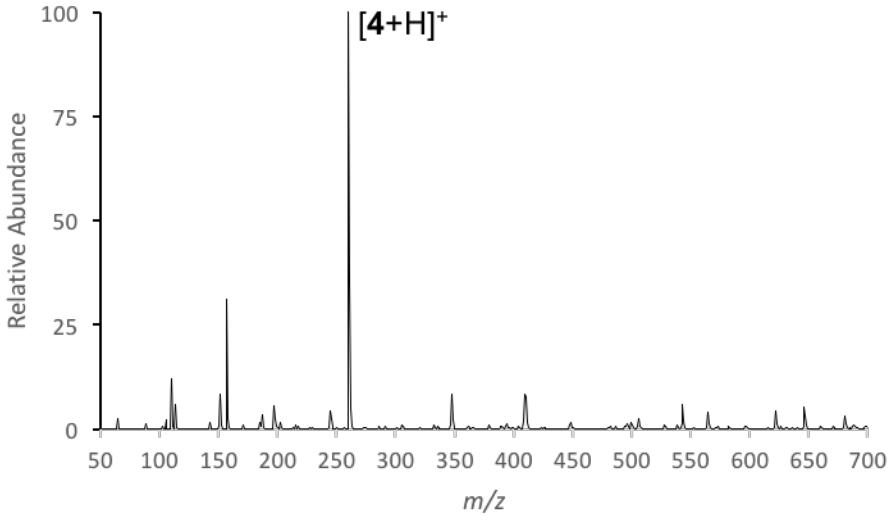

Figure A10: Full scan MS of the second step of the atropine synthesis by preparative ES using dabco

Full scan positive ion mode mass spectrum of the preparative ES product from the second step of the atropine synthesis with step 1 product, aqueous formaldehyde and dabco. In this sample m/z 260 [intermediate +H]$^+$ is the most abundant ion.

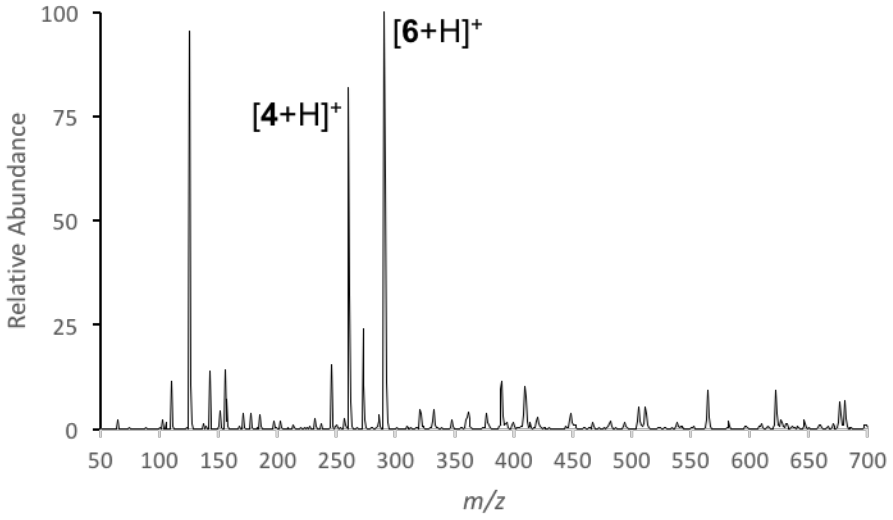

Figure A11: Full scan MS of the second step of the atropine synthesis by preparative ES using 1,5-diazabicyclo[4.3.0]non-5-ene

Full scan positive ion mode mass spectrum of the preparative ES product from the second step of the atropine synthesis with step 1 product, aqueous formaldehyde and 1,5-diazabicyclo[4.3.0]non-5-ene. In this sample m/z 260 [intermediate +H]$^+$ and m/z 290 [atropine+H]$^+$ are the most abundant ions.

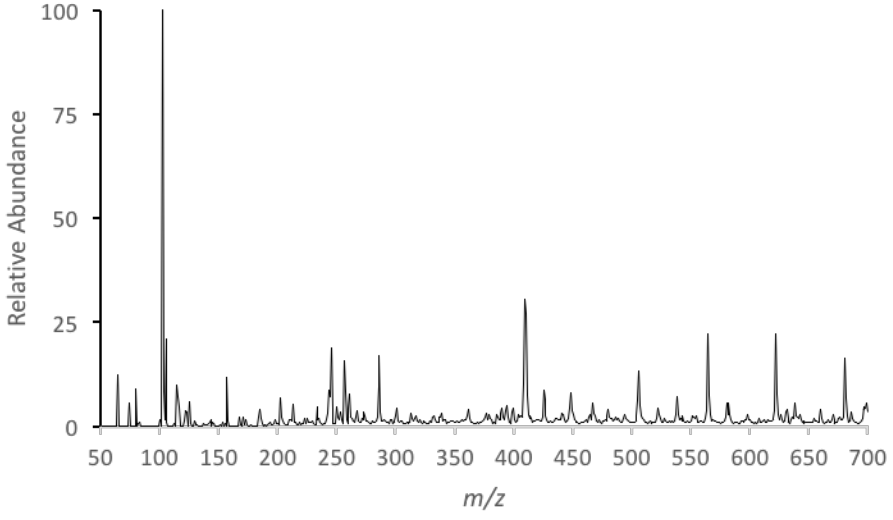

Figure A12: Full scan MS of the second step of the atropine synthesis by preparative ES using 1,8-diazabicyclo[5.4.0]undec-7-ene

Full scan positive ion mode mass spectrum of the preparative ES product from the second step of the atropine synthesis with step 1 product, aqueous formaldehyde and 1,8-diazabicyclo[5.4.0]undec-7-ene.

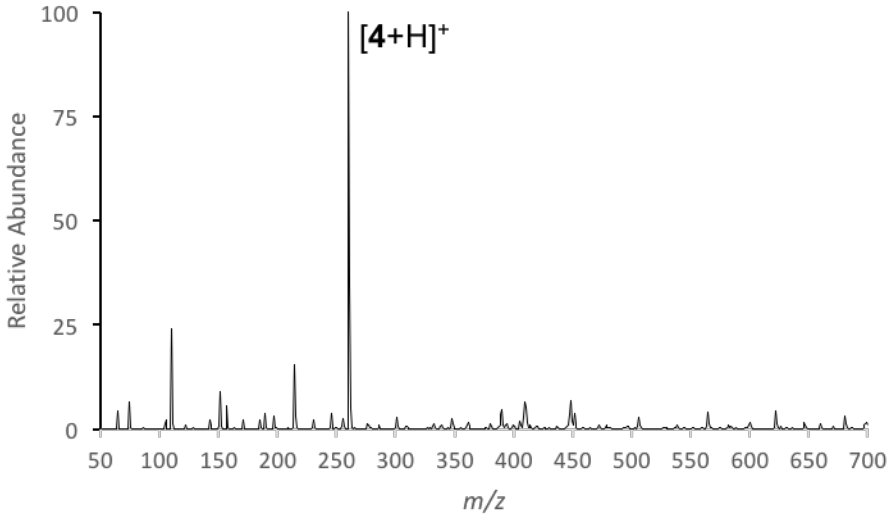

Figure A13: Full scan MS of the second step of the atropine synthesis by preparative ES using diethylamine.

Full scan positive ion mode mass spectrum of the preparative ES product from the second step of the atropine synthesis with step 1 product, aqueous formaldehyde and diethylamine. In this sample m/z 260 [intermediate +H]$^+$ is the most abundant ion.

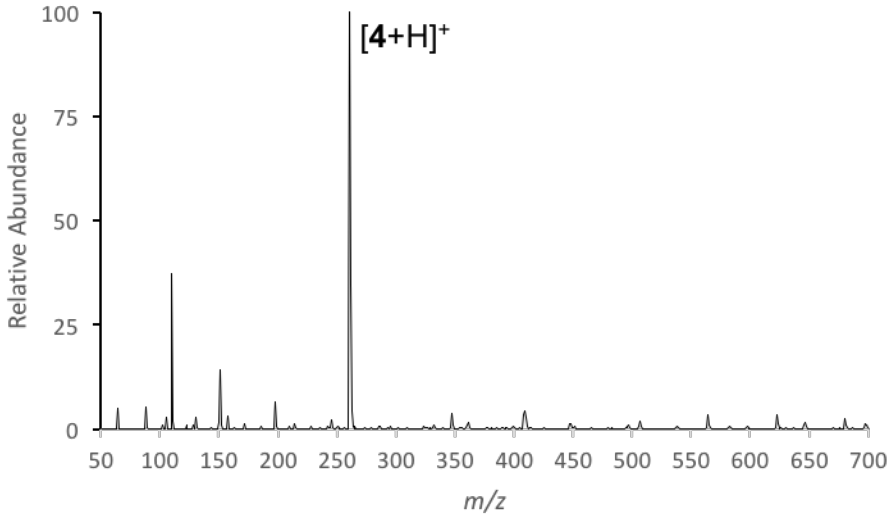

Figure A14: Full scan MS of the second step of the atropine synthesis by preparative ES using N,N-diisopropylethylamine

Full scan positive ion mode mass spectrum of the preparative ES product from the second step of the atropine synthesis with step 1 product, aqueous formaldehyde and N,N-diisopropylethylamine. In this sample m/z 260 [intermediate +H]$^+$ is the most abundant ion.

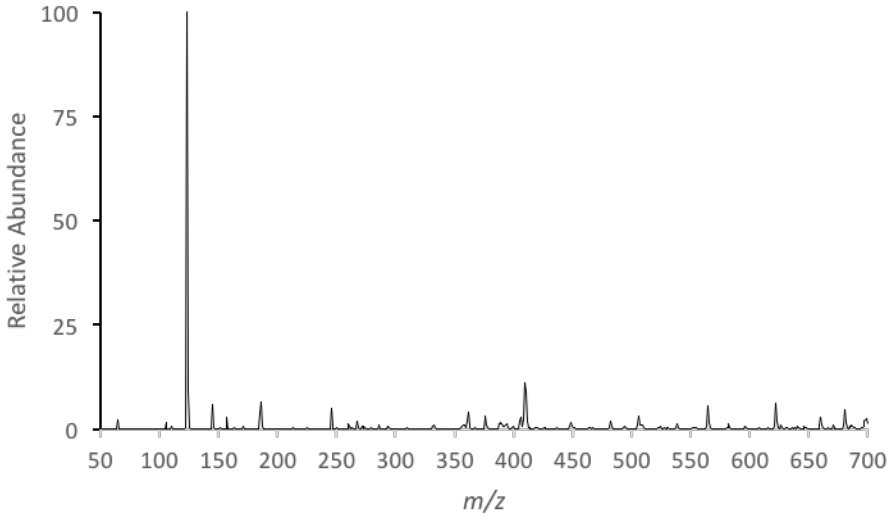

Figure A15: Full scan MS of the second step of the atropine synthesis by preparative ES using 4-(dimethylamino)pyridine

Full scan positive ion mode mass spectrum of the preparative ES product from the second step of the atropine synthesis with step 1 product, aqueous formaldehyde and 4-(dimethylamino)pyridine.

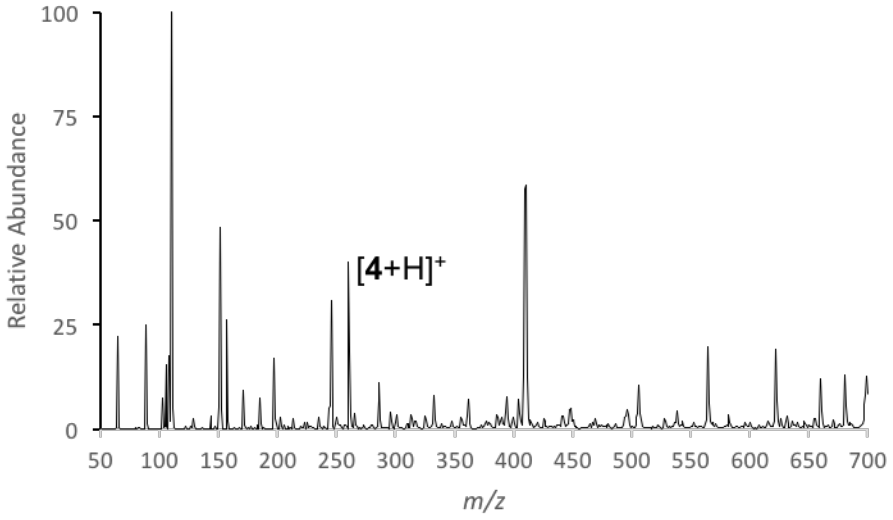

Figure A16: Full scan MS of the second step of the atropine synthesis by preparative ES using 2,6-lutidine

Full scan positive ion mode mass spectrum of the preparative ES product from the second step of the atropine synthesis with step 1 product, aqueous formaldehyde and 2,6-lutidine. In this sample m/z 260 [intermediate +H]$^+$ is the most abundant ion.

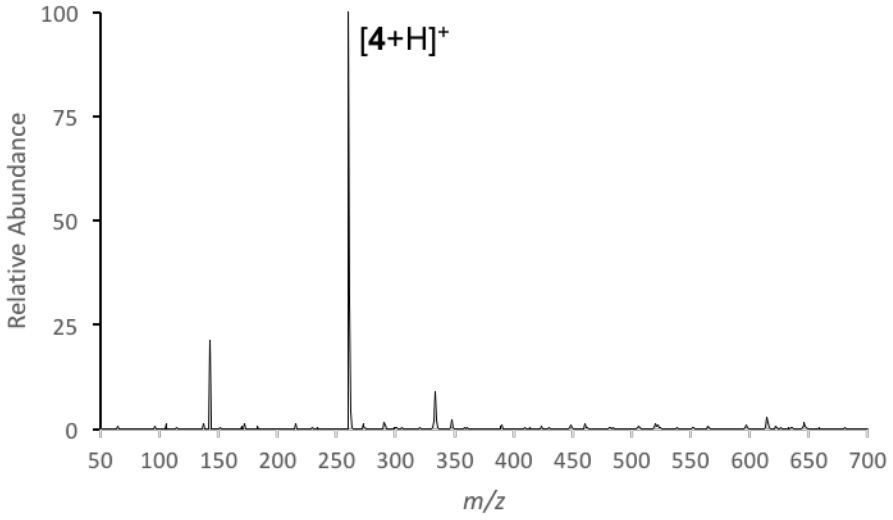

Figure A17: Full scan MS of the second step of the atropine synthesis by preparative ES using pH 10 buffer

Full scan positive ion mode mass spectrum of the preparative ES product from the second step of the atropine synthesis with step 1 product, aqueous formaldehyde and pH 10 buffer. In this sample m/z 260 [intermediate +H]$^+$ is the most abundant ion.

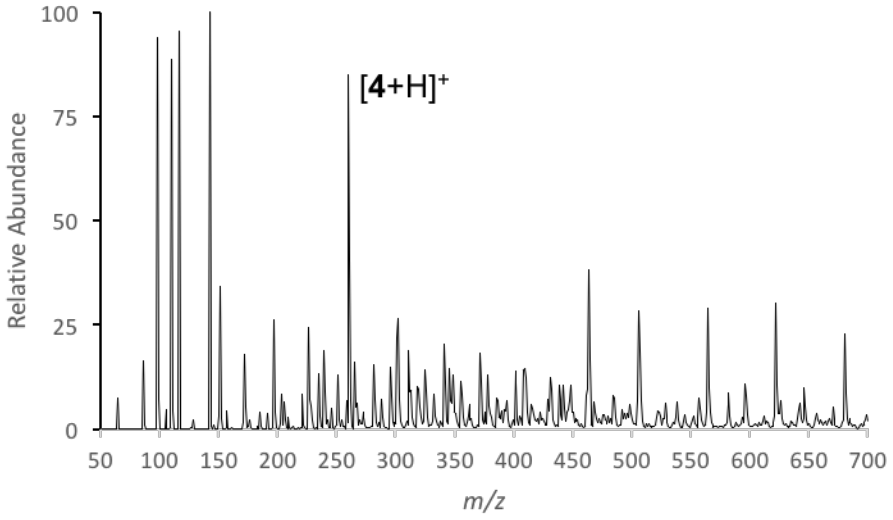

Figure A18: Full scan MS of the second step of the atropine synthesis by preparative ES using piperidine

Full scan positive ion mode mass spectrum of the preparative ES product from the second step of the atropine synthesis with step 1 product, aqueous formaldehyde and piperidine. In this sample m/z 260 [intermediate +H]$^+$ is one of the most abundant ions.

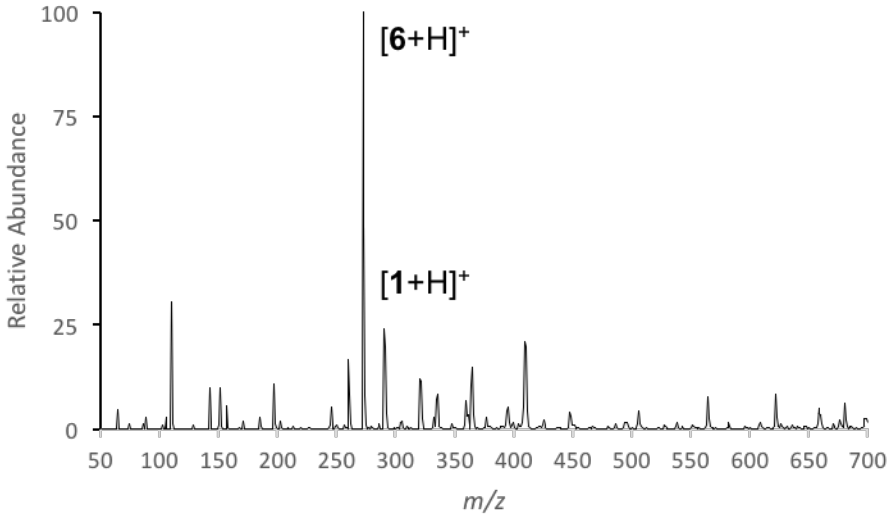

Figure A19: Full scan MS of the second step of the atropine synthesis by preparative ES using potassium ethoxide

Full scan positive ion mode mass spectrum of the preparative ES product from the second step of the atropine synthesis with step 1 product, aqueous formaldehyde and potassium ethoxide. In this sample the byproduct m/z 272 $[6 +H]^+$ is the most abundant ion and the product m/z 290 [atropine+H]+ is also present.

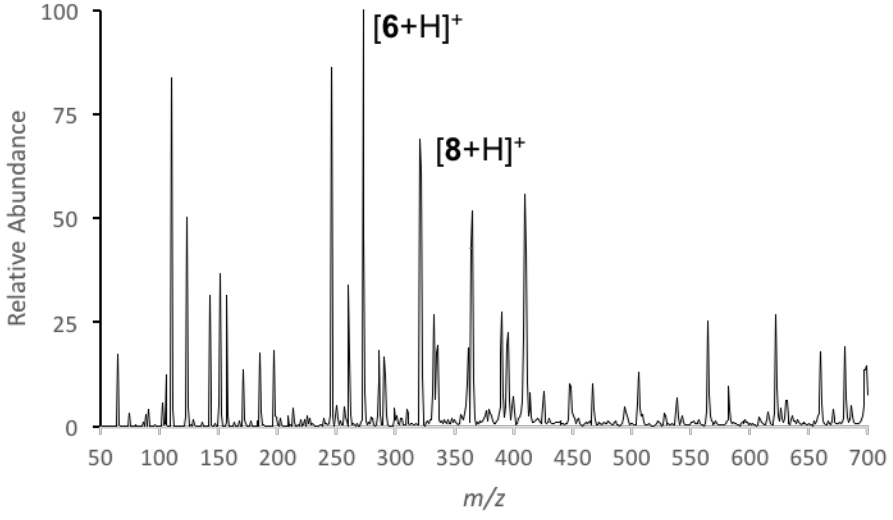

Figure A20: Full scan MS of the second step of the atropine synthesis by preparative ES using potassium methoxide

Full scan positive ion mode mass spectrum of the preparative ES product from the second step of the atropine synthesis with step 1 product, aqueous formaldehyde and potassium methoxide. In this sample the byproduct m/z 272 $[6 +H]^+$ is the most abundant ion and the byproduct m/z 320 [8+H]+ is also present in high abundance.

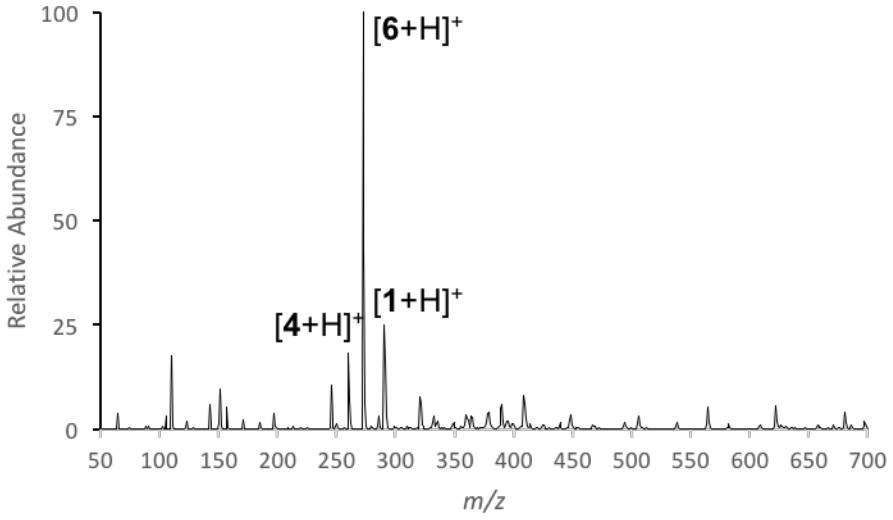

Figure A21: Full scan MS of the second step of the atropine synthesis by preparative ES using sodium ethoxide

Full scan positive ion mode mass spectrum of the preparative ES product from the second step of the atropine synthesis with step 1 product, aqueous formaldehyde and sodium ethoxide. In this sample the byproduct m/z 272 $[6 +H]^+$ is the most abundant ion and both m/z 260 [intermediate +H]+ and m/z 290 [atropine +H]+ are present.

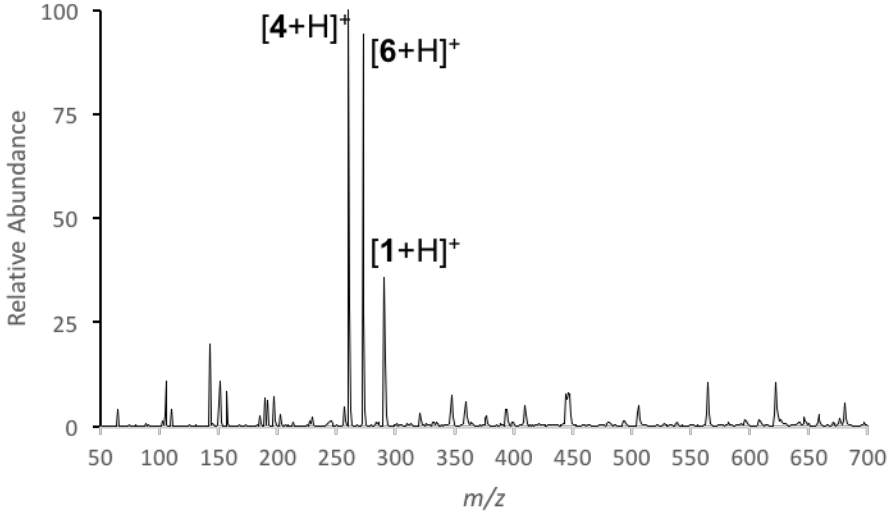

Figure A22: Full scan MS of the second step of the atropine synthesis by preparative ES using sodium hydroxide.

Full scan positive ion mode mass spectrum of the preparative ES product from the second step of the atropine synthesis with step 1 product, aqueous formaldehyde and sodium hydroxide. In this sample the m/z 260 $[\text{intermediate} +H]^+$ and byproduct m/z 272 $[6 +H]^+$ are the most abundant ions and the product m/z 290 $[\text{atropine} +H]^+$ is present.

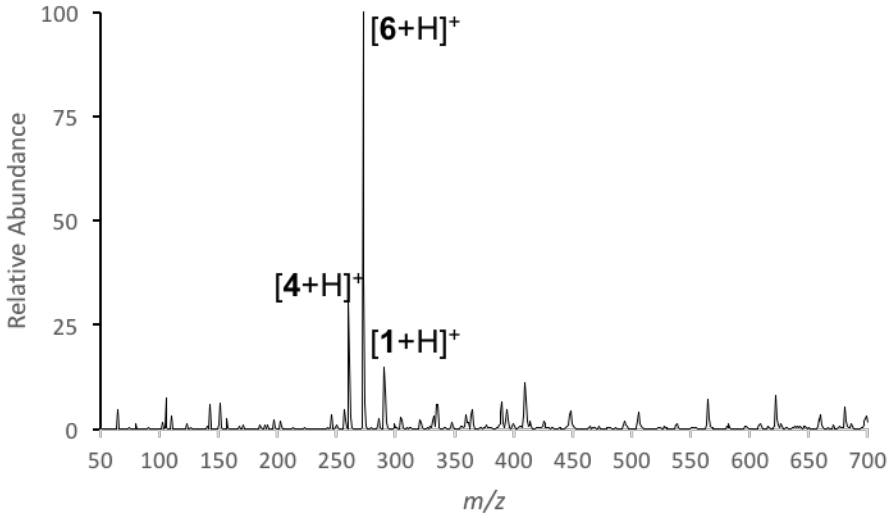

Figure A23: Full scan MS of the second step of the atropine synthesis by preparative ES using sodium methoxide

Full scan positive ion mode mass spectrum of the preparative ES product from the second step of the atropine synthesis with step 1 product, aqueous formaldehyde and sodium methoxide. In this sample the byproduct m/z 272 $[6 +H]^+$ is the most abundant ion and both m/z 260 [intermediate +H]+ and m/z 290 [atropine +H]+ are present.

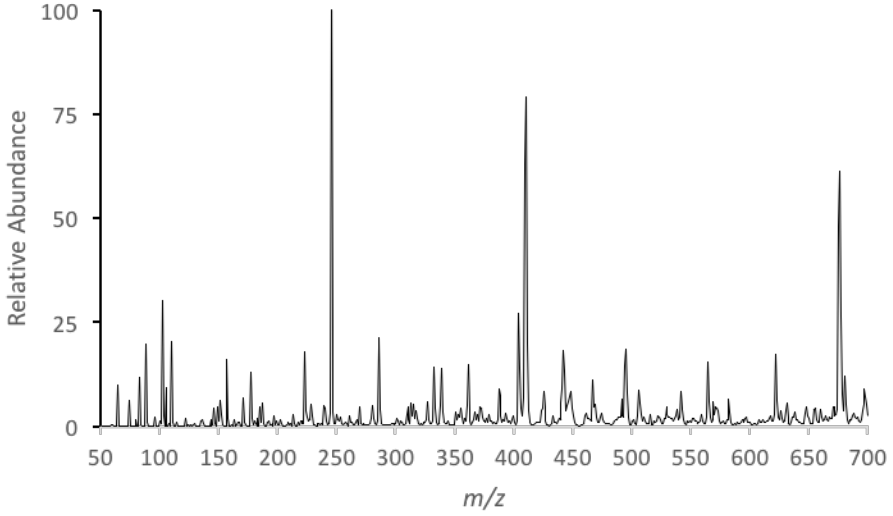

Figure A24: Full scan MS of the second step of the atropine synthesis by preparative ES using tetrabutyl ammonium hydroxide.

Full scan positive ion mode mass spectrum of the preparative ES product from the second step of the atropine synthesis with step 1 product, aqueous formaldehyde and tetrabutyl ammonium hydroxide.

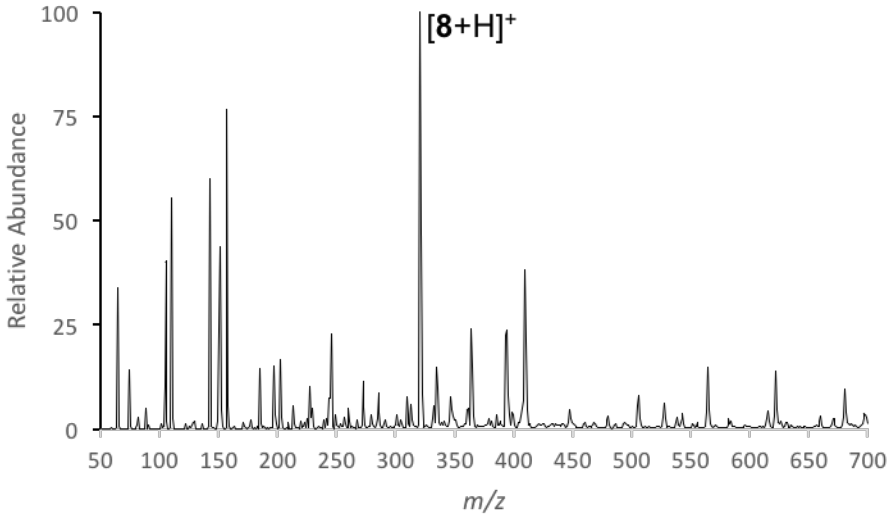

Figure A25: Full scan MS of the second step of the atropine synthesis by preparative ES using tetramethyl ammonium hydroxide.

Full scan positive ion mode mass spectrum of the preparative ES product from the second step of the atropine synthesis with step 1 product, aqueous formaldehyde and tetramethyl ammonium hydroxide. In this sample byproduct m/z 320 $[8+H]^+$ is the most abundant ion.

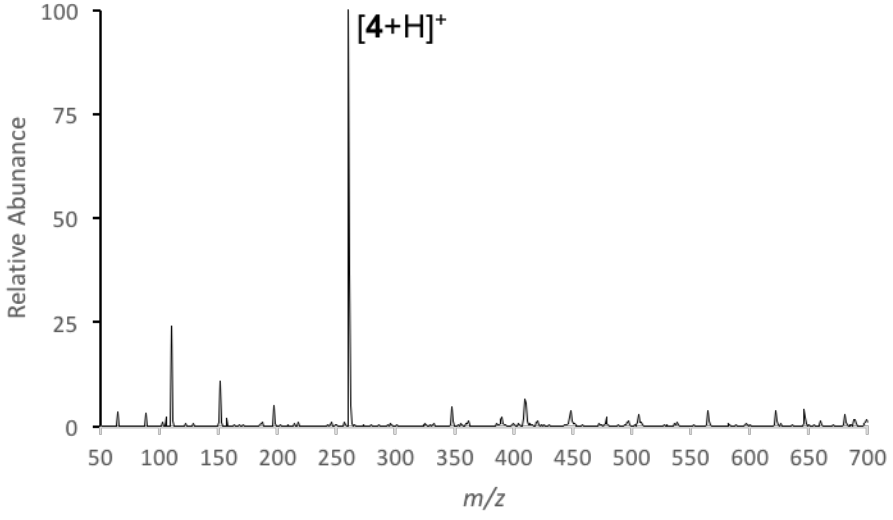

Figure A26: Full scan MS of the second step of the atropine synthesis by preparative ES using triethylamine

Full scan positive ion mode mass spectrum of the preparative ES product from the second step of the atropine synthesis with step 1 product, aqueous formaldehyde and triethylamine. In this sample m/z 260 $[\text{intermediate} +H]^+$ is the most abundant ion.

Table A4: Microfluidic synthesis of atropine with pH 10 buffer

R1 Intermediate and formaldehyde (0.117M) µl/min	R2 pH10 (10.18M) µl/min	Residence time Tr min	Temperature °C	Conversion to atropine (%) (by nESI-MS)
9.286	10.214	1	200	13.67
4.643	5.107	2	200	12.49
2.321	2.554	4	200	15.59
9.286	10.214	1	150	17.61
4.643	5.107	2	150	30.00
2.321	2.554	4	150	25.25
9.286	10.214	1	100	15.89
4.643	5.107	2	100	6.61
2.321	2.554	4	100	3.78

All reactions used chip 3227 (19.5 µl), with 87 equivalents of formaldehyde and a pressure of 6 bar.

Table A5: Microfluidic synthesis of atropine with sodium methoxide

R1 Intermediate (0.5M) µl/min	R2 Formaldehyde (13.3M) µl/min	R3 Sodium methoxide (0.5M) µl/min	Base equivalent	Residence time Tr min	Conversion to atropine (%) (by nESI-MS)
0.4	1.504	2.37	5.9	2.34	18.98
0.4	1.504	1.8	4.5	2.7	16.91
0.3	1.128	2.5	8.3	2.55	18.22
0.3	1.128	1.5	5.0	3.42	18.33
0.2	0.752	2.5	12.5	2.9	23.57
0.2	0.752	1.5	7.5	4.08	19.62
0.1	0.372	2.5	25	3.36	21.15

All reactions used chip 3225 (10 µl) at 50°C and pressure of 9 bar.

Table A6: Microfluidic synthesis of atropine with tetramethyl ammonium hydroxide

R Intermediate (0.5M) µl/min	R2 Formaldehyde (1M) µl/min	R3 Tetramethyl ammonium hydroxide (0.6M) µl/min	Residence time Tr sec	Conversion to atropine (%) (by nESI-MS)	Conversion to atropine (%) (by LC-MS)
5	30	35	8.6	22.8	32.3
2	10	12	21.4	30.2	36.4
1	6	7	42.9	16.3	--
0.5	3	3.5	85.8	7.3	--

All reactions used chip 3222 (5 µl) at 100°C and pressure of 8 bar.

Table A7: Base comparison of microfluidic synthesis of atropine

R1 Intermediate µl/min	R2 Base & formaldehyde (1M) µl/min	R3 water µl/min	Residence time Tr min	Conversion to atropine (%)					
				1,5-Diazabicyclo[4.3.0]non-5-ene		CH_3OK		NaOH	
				LC-MS	nESI-MS	LC-MS	nESI-MS	LC-MS	nESI-MS
3.25	6.5	8.12	2	41.62	32.1	24.38	18.1	11.35	22.6
1.62	3.25	4.06	4	44.58	34.1	20.9	13.7	7.15	13.4
1.08	2.17	2.71	6	44.4	37.2	16.89	6.9	6.07	10.4
0.812	1.62	2.03	8	39.76	28.3	19.3	6.8	5.35	11.4

All reactions used chip 3227 (19.5 µl) at 70°C and pressure of 9 bar.

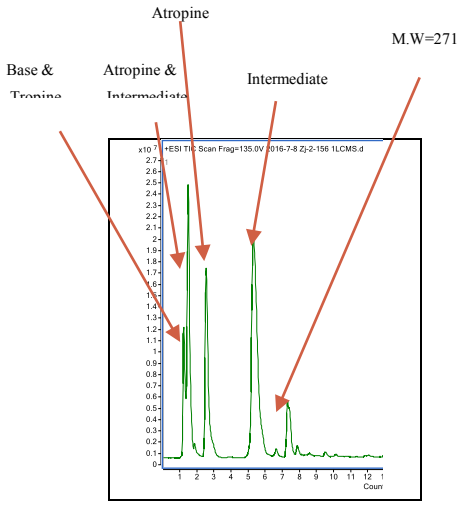

Figure A27: LC-MS analysis of microfluidic synthesis of atropine using1,5-diazabicyclo[4.3.0]non-5-ene

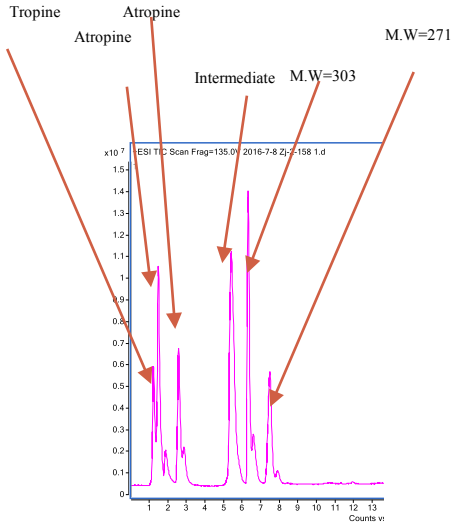

Figure A28: LC-MS analysis of microfluidic synthesis of atropine using CH_3OK

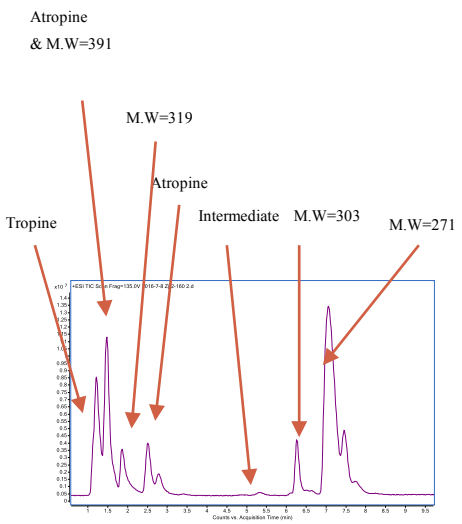

Figure A29: LC-MS analysis of microfluidic synthesis of atropine using NaOH

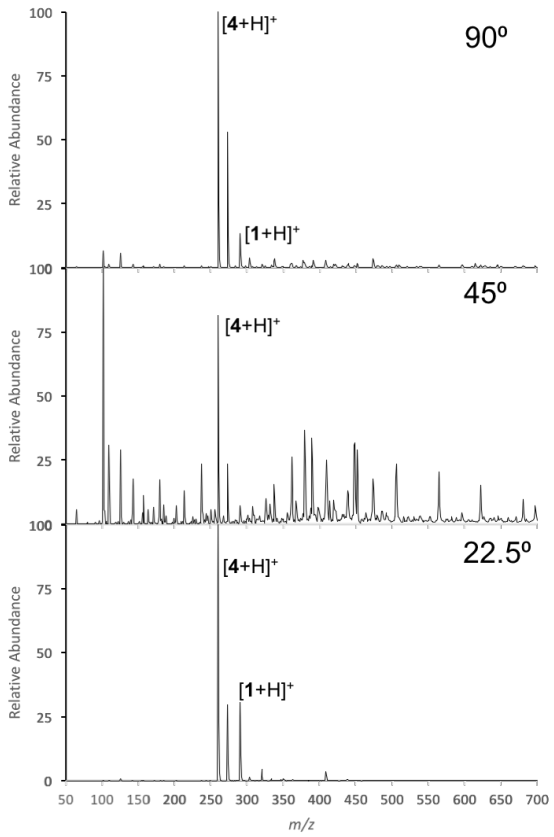

Figure A30: Angle dependence of the continuous synthesis of atropine by preparative reactive extractive electrospray

Full scan positive ion mode mass spectrum of the preparative reactive EES product from the continuous synthesis of atropine varying only the angle of intersection of the ES emitters. The percent conversion to atropine at 90°, 45° and 22.5° were 7.9%, 6.3% and 19.2% respectively.

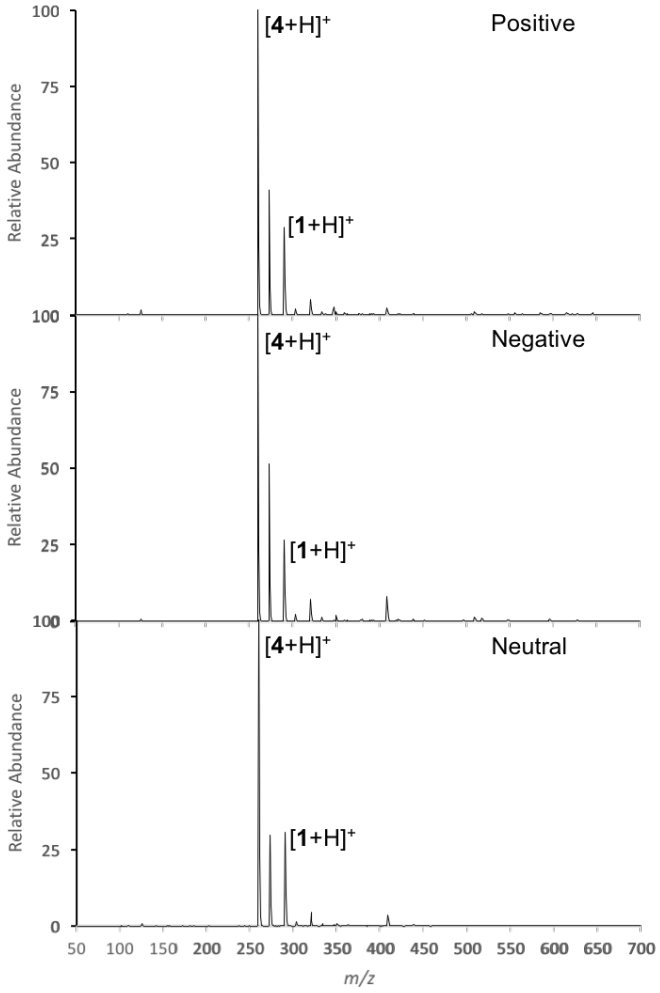

Figure A31: Voltage dependence of the continuous synthesis of atropine by preparative reactive extractive electrospray

Full scan positive ion mode mass spectrum of the preparative reactive EES product from the continuous synthesis of atropine varying only the polarity of the voltage of the ES emitter spraying the second step reagents. The percent conversion to atropine at positive, negative and neutral polarities were 15%, 17% and 19.2% respectively.

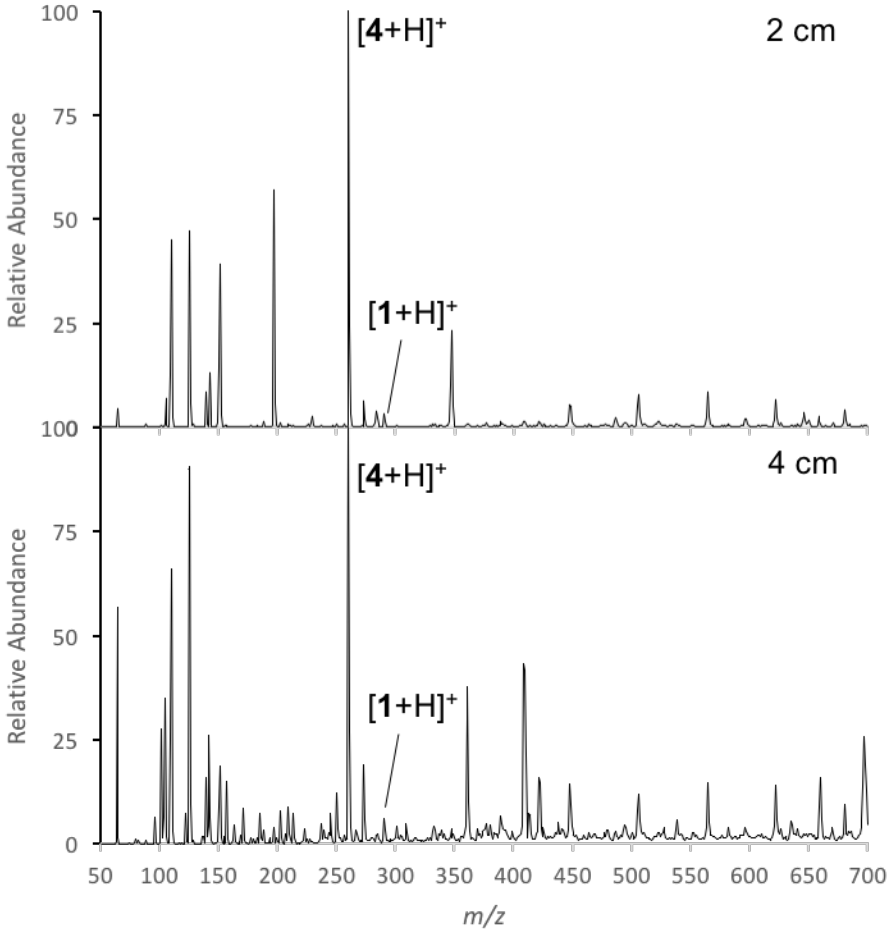

Figure A32: Distance dependence of point of intersection in the continuous synthesis of atropine by preparative reactive extractive electrospray

Full scan positive ion mode mass spectrum of the preparative reactive EES product from the continuous synthesis of atropine varying only the distance of intersection of the two ES emitters. The percent conversion to atropine at 2cm and 4cm were 3.1% and 5.8% respectively. The was not a significant difference in percent conversion because the first step of the reaction occurs rapidly.

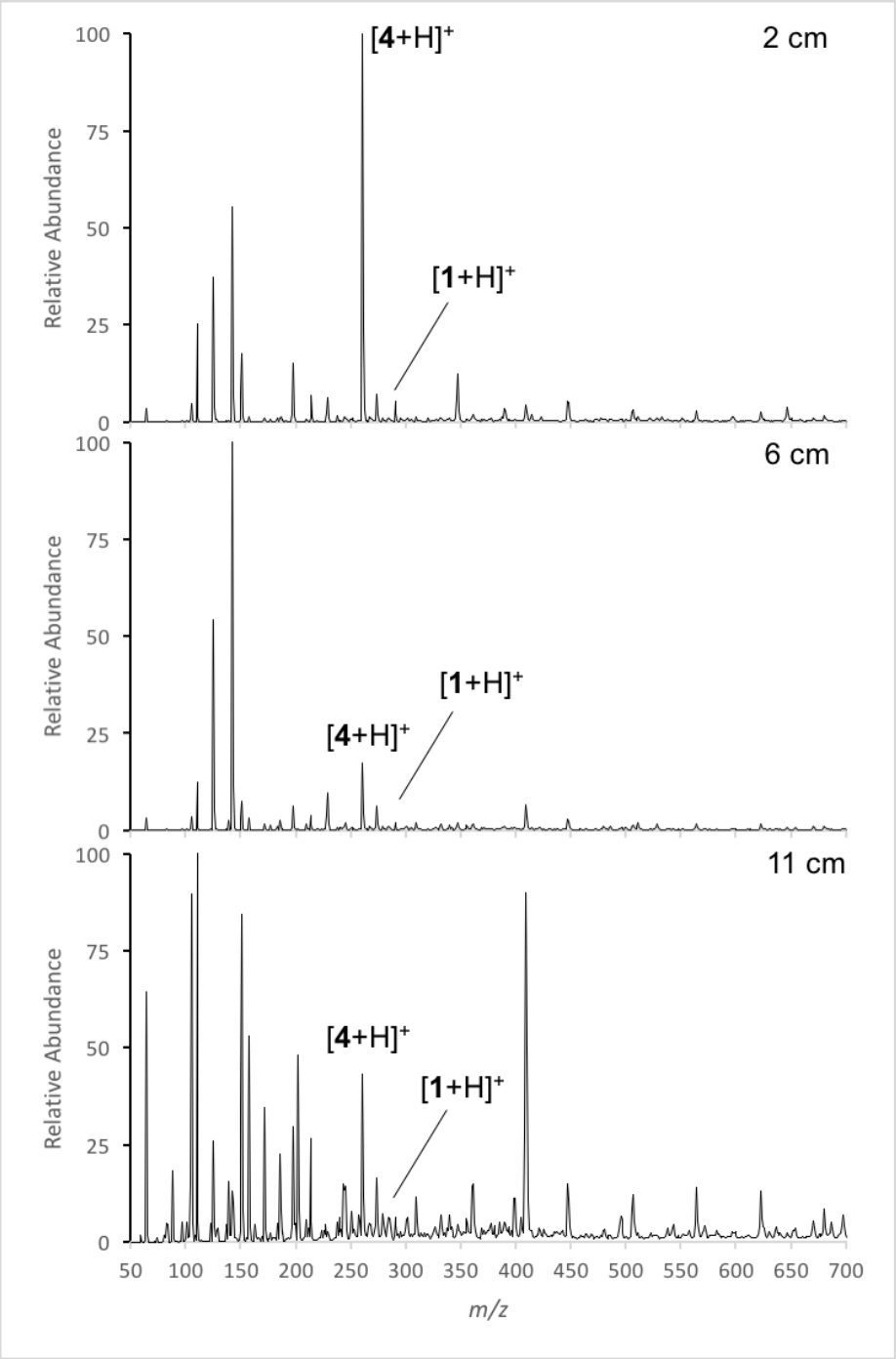

Figure A33: Distance dependence of deposition distance in the continuous synthesis of atropine by preparative reactive extractive electrospray

Full scan positive ion mode mass spectrum of the preparative reactive EES product from the continuous synthesis of atropine varying only the distance of the deposition surface. The percent conversion to atropine at 2cm, 6cm and 11cm were 4.7%, 7.9%, and 9.4% respectively. The percent conversion to product increased with the deposition distance, however there is a decrease in collection efficiency.

Table A8: Continuous synthesis of atropine in one chip in microfluidics

R1, µl/min (2+3)	R2, µl/min (Formaldehyde)	R3, µl/min (base)	R4, µl/min (water)	1st Residence time, Tr_1 min	2nd Residence time, Tr_2 min	Conversion of atropine by ESI-MS	Yield of Atropine (by UPLC)
1.25	1.25	1.25	1.25	2.00	2.69	27.5	--
1.00	1.00	1.00	1.00	2.50	3.33	21.0	6.67
0.75	0.75	0.75	0.75	3.33	4.44	24.5	6.88
0.5	0.5	0.5	0.5	5.00	6.67	7.0	7.10

All reactions used 1,5-diazabicyclo[4.3.0]non-5-ene chip 3224 (5+10 µl) at 100°C and pressure of 7 bar.

Table A9: Continuous synthesis of atropine in two chips in microfluidics

R1, tropine (1 M) µl/min	R2, Phenylacetyl chloride (1M) µl/min	R3, (R1+R2) µl/min	R4, formaldehyde +base (0.85M) µl/min	R5, Water µl/min	1st Residence time, Tr1 min	2nd Residence time, Tr2 min	Conversion of atropine by ESI-MS	Yield of Atropine (by UPLC)
0.25	0.25	0.5	1.17	1.67	2	6	32.14	33.45

The first step used chip 3221 (1 µl) at 100°C and pressure of 7 bar and the second step used 1,5-diazabicyclo[4.3.0]non-5-ene, chip 3223 (10 µl) at 70°C and pressure of 7 bar.

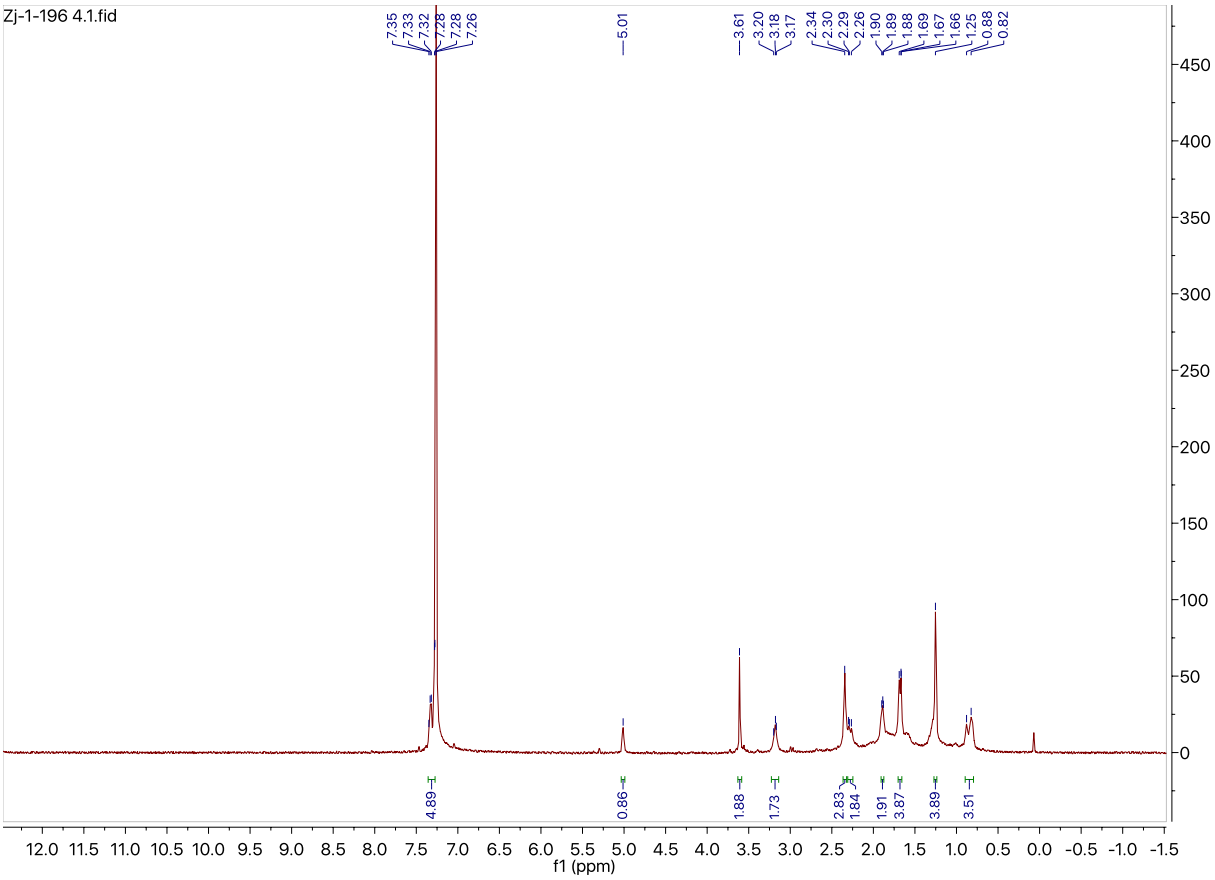

Figure A34: ^{1}H NMR of crude intermediate **4**

NMR analysis was performed after neutralization and extraction of the reaction mixture.

^{1}H NMR (500 MHz, $CDCl_3$): δ = 7.35-7.28 (m, 5 H), 5.01 (t, J = 5 Hz, 1 H), 3.61 (s, 2 H), 3.20-3.17 (m,2 H), 2.34 (s, 3 H), 2.30-2.26 (m, 2 H), 1.90-1.88 (m, 2 H), 1.69-1.66 (m, 4 H)

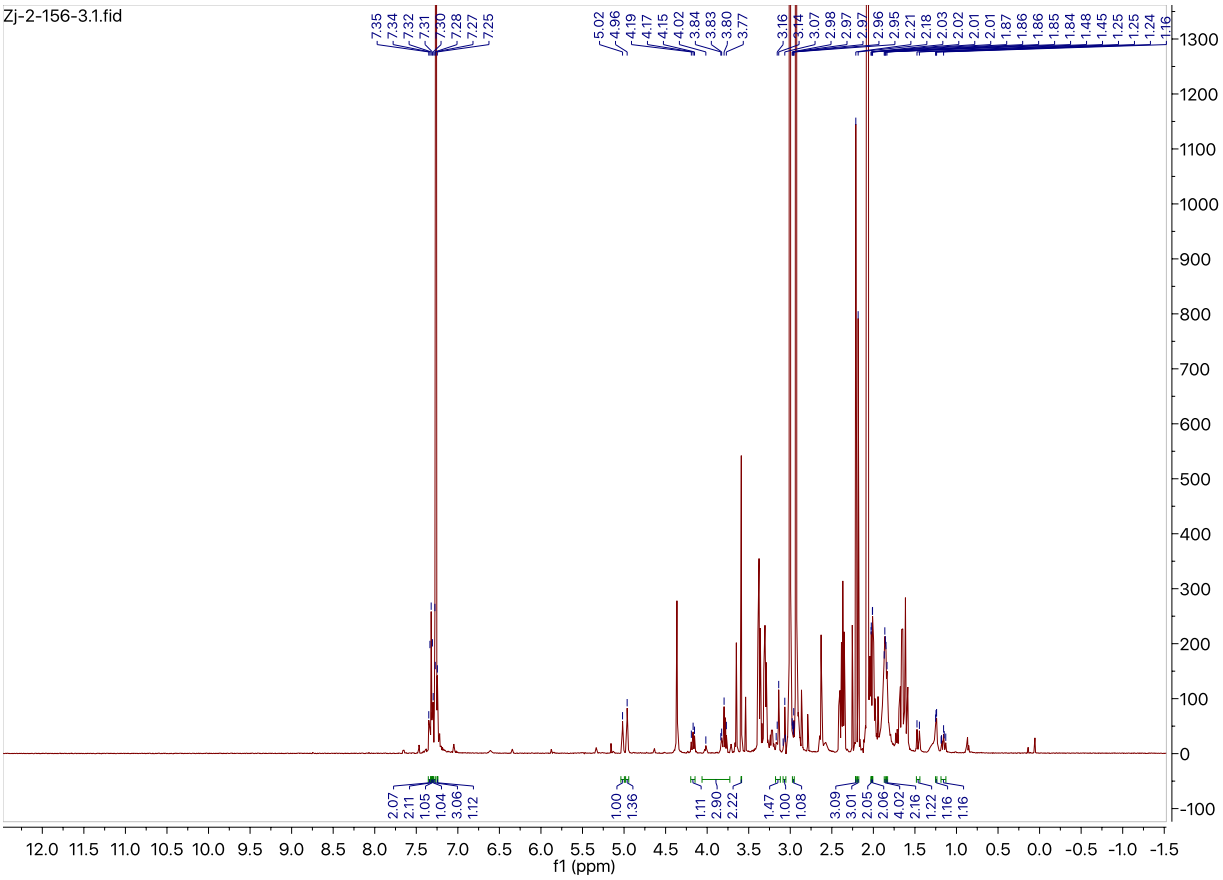

Figure A35: ^{1}H NMR of crude atropine.

^{1}H NMR (500 MHz, $CDCl_3$): δ = 7.35-7.31 (m, 5 H), 5.02 (t, J = 5.0 Hz, 1 H), 4.19-4.15 (m, 1 H), 4.02-3.77 (m, 3 H), 3.09-3.06(m, 1 H), 2.97-2.95 (m, 1 H), 2.18 (s, 3 H), 2.03-2.02 (m, 2 H), 1.87-1.86 (m, 4 H), 1.48-1.43 (m, 1 H), 1.18-1.13 (m, 1 H).

APPENDIX B

The Script that was used in Chapter three in the Perl terminal command to convert text files to the csv format is given below. All other analysis was done using Microsoft Excel 2016.

```
#!/usr/bin/perl

@ms_list = qw"m/z values";

$mz_error = 0.5;

open (OUT, ">$ARGV[0]");
print OUT "File";

for my $ms (@ms_list){
   print OUT ",$ms";
}
print OUT "\n";
@ls = `ls -1 *.txt`;
#@ls = `dir /b *.txt`;
chomp @ls;
#print "@ls\n";

for $file (@ls){
#print "$file\n" ;
#next;
   open (DATA,"$file");

   %data = ();
   %tic_data = ();
   while(<DATA>){
```

```
#print;
if ($_ =~ m/cvParam: scan start time,\s+([\d\.]+), minute/){
   $time = $1
}
$mz = 1 if ($_=~ m/cvParam: m\/z array, m\/z/);
$int = 1 if ($_=~ m/cvParam: intensity array/);

$tic_time = 1 if ($_=~ m/cvParam: time array, minute/);
$tic = 1 if ($_=~ m/cvParam: intensity array, number of detector counts/);



if (($mz == 1) && ($_ =~  m/binary: \[\d+\] (.*)/)){
   @mz = split (/\s+/,$1);
   $mz = 0;
}
if (($int == 1) && ($_ =~  m/binary: \[\d+\] (.*)/)){
   @int = split (/\s+/,$1);
   $int = 0;

   $cont = 0;
   for $mz (@mz){
         for $mz_value (@ms_list){
            if (($mz >= $mz_value - $mz_error) && ($mz <= $mz_value + $mz_error )){
                  $data{$time}{$mz_value} += $int[$cont];
            }
         }
         $cont++
   }
}

if (($tic_time == 1) && ($_ =~  m/binary: \[\d+\] (.*)/)){
```

```
        @tic_time = split (/\s+/,$1);
        $tic_time = 0;
    }
    if (($tic == 1) && ($_ =~  m/binary: \[\d+\] (.*)/)){
        @tic = split (/\s+/,$1);
        $tic = 0;

        $cont = 0;
        for $tic_time (@tic_time){
            $tic_data{$tic_time} = $tic[$cont];
            $cont++
        }
    }
}
close(DATA);

$average_time = 4;
@last3 = ();
$sum_max = 0;
@sum_max = ();

for $tic_time(sort {$a<=>$b} keys %tic_data){
    if (@last3+0 >= $average_time){
        shift(@last3);
        push (@last3,$tic_time);

        $sum = 0;
        for my $aux (@last3){
            $sum += $tic_data{$aux};
        }
```

```
            if ($sum > $sum_max){
                $sum_max = $sum;
                @sum_max = @last3;
            }
        }
        else{
            push (@last3,$tic_time);
        }
    }
    %average = ();
    for $time(sort {$a<=>$b} keys %data){
        for $time1(@sum_max){
            if (($time >= $time1 - 0.03) && ($time <= $time1 + $0.03 )){
                for $mz(sort {$a<=>$b} keys %{$data{$time}}){
                    $average{$mz} += $data{$time}{$mz};
                }
            }
        }
    }

    print OUT "\"$file\"";
    for $mz(@ms_list){
        print OUT ",",$average{$mz}/$average_time;
    }
    print OUT "\n";

}
close(OUT);
```

Order of addition

a)

Addition Sequence: 1+ R'X → Base → XPhos Pd G3

Product Peak Intensity: Min – Max

St. / Sub., mmol	Temp.	1:0	1:0	20:1	20:1	10:1	10:1	5:1	5:1	2:1	2:1	1:1	1:1	1:2	1:2	1:5	1:5	1:10	1:10	1:20	1:20	R'X:0	R'X:0	0:0	0:0
1+3, 100	200°C, 150°C	200 °C	150 °C	200 °C	150 °C	200 °C	150 °C	200 °C	150 °C	200 °C	150 °C	200 °C	150 °C	200 °C	150 °C	200 °C	150 °C	200 °C	150 °C	200 °C	150 °C	200 °C	150 °C	200 °C	150 °C
	100°C, 50°C	100 °C	50 °C	100 °C	50 °C	100 °C	50 °C	100 °C	50 °C	100 °C	50 °C	100 °C	50 °C	100 °C	50 °C	100 °C	50 °C	100 °C	50 °C	100 °C	50 °C	100 °C	50 °C	100 °C	50 °C
1+3, 200	200°C, 150°C	200 °C	150 °C	200 °C	150 °C	200 °C	150 °C	200 °C	150 °C	200 °C	150 °C	200 °C	150 °C	200 °C	150 °C	200 °C	150 °C	200 °C	150 °C	200 °C	150 °C	200 °C	150 °C	200 °C	150 °C
	100°C, 50°C	100 °C	50 °C	100 °C	50 °C	100 °C	50 °C	100 °C	50 °C	100 °C	50 °C	100 °C	50 °C	100 °C	50 °C	100 °C	50 °C	100 °C	50 °C	100 °C	50 °C	100 °C	50 °C	100 °C	50 °C
1+4, 100	200°C, 150°C	200 °C	150 °C	200 °C	150 °C	200 °C	150 °C	200 °C	150 °C	200 °C	150 °C	200 °C	150 °C	200 °C	150 °C	200 °C	150 °C	200 °C	150 °C	200 °C	150 °C	200 °C	150 °C	200 °C	150 °C
	100°C, 50°C	100 °C	50 °C	100 °C	50 °C	100 °C	50 °C	100 °C	50 °C	100 °C	50 °C	100 °C	50 °C	100 °C	50 °C	100 °C	50 °C	100 °C	50 °C	100 °C	50 °C	100 °C	50 °C	100 °C	50 °C
1+4, 200	200°C, 150°C	200 °C	150 °C	200 °C	150 °C	200 °C	150 °C	200 °C	150 °C	200 °C	150 °C	200 °C	150 °C	200 °C	150 °C	200 °C	150 °C	200 °C	150 °C	200 °C	150 °C	200 °C	150 °C	200 °C	150 °C
	100°C, 50°C	100 °C	50 °C	100 °C	50 °C	100 °C	50 °C	100 °C	50 °C	100 °C	50 °C	100 °C	50 °C	100 °C	50 °C	100 °C	50 °C	100 °C	50 °C	100 °C	50 °C	100 °C	50 °C	100 °C	50 °C

Addition Sequence: 1+ R'X → XPhos Pd G3 → Base

Product Peak Intensity: Min – Max

St. / Sub., mmol	Temp.	1:0	1:0	20:1	20:1	10:1	10:1	5:1	5:1	2:1	2:1	1:1	1:1	1:2	1:2	1:5	1:5	1:10	1:10	1:20	1:20	R'X:0	R'X:0	0:0	0:0
1+3, 100	200°C, 150°C	200 °C	150 °C	200 °C	150 °C	200 °C	150 °C	200 °C	150 °C	200 °C	150 °C	200 °C	150 °C	200 °C	150 °C	200 °C	150 °C	200 °C	150 °C	200 °C	150 °C	200 °C	150 °C	200 °C	150 °C
	100°C, 50°C	100 °C	50 °C	100 °C	50 °C	100 °C	50 °C	100 °C	50 °C	100 °C	50 °C	100 °C	50 °C	100 °C	50 °C	100 °C	50 °C	100 °C	50 °C	100 °C	50 °C	100 °C	50 °C	100 °C	50 °C
1+3, 200	200°C, 150°C	200 °C	150 °C	200 °C	150 °C	200 °C	150 °C	200 °C	150 °C	200 °C	150 °C	200 °C	150 °C	200 °C	150 °C	200 °C	150 °C	200 °C	150 °C	200 °C	150 °C	200 °C	150 °C	200 °C	150 °C
	100°C, 50°C	100 °C	50 °C	100 °C	50 °C	100 °C	50 °C	100 °C	50 °C	100 °C	50 °C	100 °C	50 °C	100 °C	50 °C	100 °C	50 °C	100 °C	50 °C	100 °C	50 °C	100 °C	50 °C	100 °C	50 °C
1+4, 100	200°C, 150°C	200 °C	150 °C	200 °C	150 °C	200 °C	150 °C	200 °C	150 °C	200 °C	150 °C	200 °C	150 °C	200 °C	150 °C	200 °C	150 °C	200 °C	150 °C	200 °C	150 °C	200 °C	150 °C	200 °C	150 °C
	100°C, 50°C	100 °C	50 °C	100 °C	50 °C	100 °C	50 °C	100 °C	50 °C	100 °C	50 °C	100 °C	50 °C	100 °C	50 °C	100 °C	50 °C	100 °C	50 °C	100 °C	50 °C	100 °C	50 °C	100 °C	50 °C
1+4, 200	200°C, 150°C	200 °C	150 °C	200 °C	150 °C	200 °C	150 °C	200 °C	150 °C	200 °C	150 °C	200 °C	150 °C	200 °C	150 °C	200 °C	150 °C	200 °C	150 °C	200 °C	150 °C	200 °C	150 °C	200 °C	150 °C
	100°C, 50°C	100 °C	50 °C	100 °C	50 °C	100 °C	50 °C	100 °C	50 °C	100 °C	50 °C	100 °C	50 °C	100 °C	50 °C	100 °C	50 °C	100 °C	50 °C	100 °C	50 °C	100 °C	50 °C	100 °C	50 °C

b)

Addition Sequence: 1+ R'X → Base → XPhos Pd G3

Product Peak Intensity: Min – Max

St. / Sub., mmol	Temp.	1:0	1:0	20:1	20:1	10:1	10:1	5:1	5:1	2:1	2:1	1:1	1:1	1:2	1:2	1:5	1:5	1:10	1:10	1:20	1:20	R'X:0	R'X:0	0:0	0:0
1+3, 100	200°C, 150°C	7.55E+04	7.94E+04	2.10E+06	1.18E+06	1.79E+06	2.98E+06	5.37E+06	8.92E+05	3.18E+06	8.12E+05	4.17E+05	1.57E+05	6.50E+04	1.15E+05	7.77E+04	9.27E+04	7.73E+04	1.15E+05	4.70E+04	1.34E+05	5.20E+04	9.21E+04	8.73E+04	7.35E+04
	100°C, 50°C	9.51E+04	6.69E+04	1.33E+05	3.18E+05	2.08E+05	4.95E+05	1.24E+05	8.41E+05	1.33E+05	4.51E+05	1.09E+05	2.61E+05	1.12E+05	2.68E+05	8.93E+04	1.12E+05	7.93E+04	8.36E+04	2.75E+04	4.73E+04	2.40E+04	2.60E+04	6.46E+04	1.93E+04
1+3, 200	200°C, 150°C	8.31E+04	4.66E+04	2.00E+06	1.74E+06	1.67E+06	3.45E+06	5.28E+06	1.56E+06	2.47E+06	7.03E+05	4.35E+05	1.12E+05	2.05E+05	8.52E+04	5.98E+04	1.23E+05	3.71E+04	1.48E+05	3.42E+04	8.94E+04	3.79E+04	9.09E+04	8.63E+04	5.55E+04
	100°C, 50°C	3.97E+04	6.93E+04	1.28E+05	1.76E+05	1.69E+05	4.47E+05	1.59E+05	7.57E+05	1.00E+05	1.08E+06	8.01E+04	2.98E+05	3.00E+04	2.03E+05	4.78E+04	1.31E+05	6.23E+04	9.66E+04	4.79E+04	3.13E+04	3.63E+04	2.57E+04	4.91E+04	3.41E+04
1+4, 100	200°C, 150°C	1.65E+05	2.15E+05	8.94E+05	6.59E+05	1.80E+06	1.52E+06	4.02E+06	9.66E+05	5.44E+06	2.55E+05	1.90E+05	1.41E+05	1.30E+05	1.18E+05	7.09E+04	1.37E+05	1.10E+05	1.47E+05	1.12E+05	9.75E+04	1.05E+05	1.02E+05	1.64E+05	1.94E+05
	100°C, 50°C	2.84E+05	2.27E+05	1.65E+05	2.58E+05	2.89E+05	6.07E+05	2.51E+05	5.04E+05	1.94E+05	8.49E+05	3.47E+05	5.54E+05	2.16E+05	4.11E+05	1.34E+05	2.33E+05	1.27E+05	2.93E+05	1.92E+05	1.74E+05	1.73E+05	2.46E+05	2.25E+05	2.56E+05
1+4, 200	200°C, 150°C	2.16E+05	1.74E+05	6.95E+05	1.01E+06	2.45E+06	1.28E+06	4.32E+06	1.82E+06	2.84E+06	1.18E+06	1.05E+06	1.46E+05	1.06E+05	5.86E+04	1.39E+05	1.15E+05	1.21E+05	1.17E+05	1.07E+05	9.95E+04	1.03E+05	7.53E+04	1.97E+05	2.06E+05
	100°C, 50°C	4.15E+05	2.93E+05	2.08E+05	5.47E+05	5.78E+05	7.96E+05	4.93E+05	4.21E+05	4.39E+05	5.44E+05	3.92E+05	3.01E+05	1.63E+05	2.96E+05	2.93E+05	2.83E+05	2.27E+05	2.23E+05	1.68E+05	2.52E+05	1.80E+05	1.95E+05	2.05E+05	1.71E+05

Addition Sequence: 1+ R'X → XPhos Pd G3 → Base

Product Peak Intensity: Min – Max

St. / Sub., mmol	Temp.	1:0	1:0	20:1	20:1	10:1	10:1	5:1	5:1	2:1	2:1	1:1	1:1	1:2	1:2	1:5	1:5	1:10	1:10	1:20	1:20	R'X:0	R'X:0	0:0	0:0
1+3, 100	200°C, 150°C	8.92E+04	4.56E+04	6.07E+05	4.33E+05	7.30E+05	7.73E+05	2.48E+06	9.82E+05	1.66E+06	2.96E+06	2.45E+06	1.81E+06	1.96E+06	2.29E+06	5.97E+05	7.90E+05	1.11E+05	5.19E+04	8.80E+04	6.88E+04	2.66E+04	6.10E+04	6.37E+04	6.48E+04
	100°C, 50°C	3.32E+04	5.13E+04	1.13E+06	5.53E+05	1.62E+06	8.20E+05	2.48E+06	7.18E+05	1.90E+06	2.50E+06	4.18E+06	2.03E+06	1.92E+06	9.96E+05	8.96E+05	6.85E+05	1.24E+05	9.84E+04	4.61E+04	8.63E+04	3.24E+04	7.05E+04	7.87E+04	6.68E+04
1+3, 200	200°C, 150°C	9.04E+04	7.44E+04	1.18E+06	1.98E+06	1.30E+06	3.13E+06	3.10E+06	2.81E+06	4.44E+06	2.77E+06	3.59E+06	4.78E+06	2.17E+06	2.83E+06	9.07E+05	1.17E+06	2.85E+05	2.29E+05	1.28E+05	8.39E+04	6.14E+04	9.21E+04	5.76E+04	8.14E+04
	100°C, 50°C	4.49E+04	6.21E+04	1.31E+06	8.80E+05	1.49E+06	1.80E+06	2.04E+06	2.21E+06	3.17E+06	2.69E+06	2.61E+06	1.89E+06	4.09E+06	2.33E+06	3.31E+06	1.41E+06	3.95E+05	2.69E+05	1.05E+05	1.01E+05	1.00E+05	7.74E+04	1.63E+05	9.22E+04
1+4, 100	200°C, 150°C	1.09E+05	1.84E+05	6.55E+05	4.44E+05	8.92E+05	1.52E+06	2.06E+06	1.68E+06	4.44E+06	3.82E+06	4.01E+06	5.98E+06	2.07E+06	3.99E+06	1.39E+06	9.13E+05	2.81E+05	1.63E+05	1.00E+05	1.16E+05	7.64E+04	7.37E+04	1.68E+05	6.55E+04
	100°C, 50°C	9.37E+04	3.29E+05	8.39E+05	4.35E+05	1.72E+06	9.70E+05	2.09E+06	1.53E+06	4.27E+06	2.28E+06	2.61E+06	2.38E+06	3.58E+06	8.60E+05	1.34E+06	4.07E+05	3.34E+05	3.86E+05	8.67E+04	2.93E+05	5.42E+04	1.91E+05	2.09E+05	1.38E+05
1+4, 200	200°C, 150°C	1.48E+05	1.58E+05	5.79E+05	1.14E+06	1.53E+06	2.43E+06	1.59E+06	3.91E+06	6.77E+06	4.53E+06	4.81E+06	5.53E+06	5.33E+06	5.54E+06	3.42E+06	2.11E+06	1.16E+06	1.36E+06	2.90E+05	2.45E+05	8.33E+04	8.03E+04	7.95E+04	1.05E+05
	100°C, 50°C	1.16E+05	1.99E+05	5.72E+05	5.72E+05	1.66E+06	8.33E+05	2.91E+06	2.63E+06	2.25E+06	2.73E+06	5.95E+06	2.93E+06	5.55E+06	2.63E+06	3.84E+06	1.29E+06	9.52E+05	6.02E+05	3.75E+05	5.99E+05	8.60E+04	1.10E+05	1.19E+05	2.13E+05

Figure B1. HT experimentation of bulk reaction results using the same set of reactants, but different orders of addition of catalyst and base. a) Temperature details b) peak intensity values

Peak intensities data from HT screening

a)

Product Peak Intensity — Min → Max

Sub., mmol \ St.	Temp.	1:0	1:0	20:1	20:1	10:1	10:1	5:1	5:1	2:1	2:1	1:1	1:1	1:2	1:2	1:5	1:5	1:10	1:10	1:20	1:20	R'X:0	R'X:0	0:0	0:0
2, 400	200 °C, 150 °C	200 °C	150 °C	200 °C	150 °C	200 °C	150 °C	200 °C	150 °C	200 °C	150 °C	200 °C	150 °C	200 °C	150 °C	200 °C	150 °C	200 °C	150 °C	200 °C	150 °C	200 °C	150 °C	200 °C	150 °C
	100 °C, 50 °C	100 °C	50 °C	100 °C	50 °C	100 °C	50 °C	100 °C	50 °C	100 °C	50 °C	100 °C	50 °C	100 °C	50 °C	100 °C	50 °C	100 °C	50 °C	100 °C	50 °C	100 °C	50 °C	100 °C	50 °C
2, 200	200 °C, 150 °C	200 °C	150 °C	200 °C	150 °C	200 °C	150 °C	200 °C	150 °C	200 °C	150 °C	200 °C	150 °C	200 °C	150 °C	200 °C	150 °C	200 °C	150 °C	200 °C	150 °C	200 °C	150 °C	200 °C	150 °C
	100 °C, 50 °C	100 °C	50 °C	100 °C	50 °C	100 °C	50 °C	100 °C	50 °C	100 °C	50 °C	100 °C	50 °C	100 °C	50 °C	100 °C	50 °C	100 °C	50 °C	100 °C	50 °C	100 °C	50 °C	100 °C	50 °C
3, 400	200 °C, 150 °C	200 °C	150 °C	200 °C	150 °C	200 °C	150 °C	200 °C	150 °C	200 °C	150 °C	200 °C	150 °C	200 °C	150 °C	200 °C	150 °C	200 °C	150 °C	200 °C	150 °C	200 °C	150 °C	200 °C	150 °C
	100 °C, 50 °C	100 °C	50 °C	100 °C	50 °C	100 °C	50 °C	100 °C	50 °C	100 °C	50 °C	100 °C	50 °C	100 °C	50 °C	100 °C	50 °C	100 °C	50 °C	100 °C	50 °C	100 °C	50 °C	100 °C	50 °C
4, 200	200 °C, 150 °C	200 °C	150 °C	200 °C	150 °C	200 °C	150 °C	200 °C	150 °C	200 °C	150 °C	200 °C	150 °C	200 °C	150 °C	200 °C	150 °C	200 °C	150 °C	200 °C	150 °C	200 °C	150 °C	200 °C	150 °C
	100 °C, 50 °C	100 °C	50 °C	100 °C	50 °C	100 °C	50 °C	100 °C	50 °C	100 °C	50 °C	100 °C	50 °C	100 °C	50 °C	100 °C	50 °C	100 °C	50 °C	100 °C	50 °C	100 °C	50 °C	100 °C	50 °C
4, 400	200 °C, 150 °C	200 °C	150 °C	200 °C	150 °C	200 °C	150 °C	200 °C	150 °C	200 °C	150 °C	200 °C	150 °C	200 °C	150 °C	200 °C	150 °C	200 °C	150 °C	200 °C	150 °C	200 °C	150 °C	200 °C	150 °C
	100 °C, 50 °C	100 °C	50 °C	100 °C	50 °C	100 °C	50 °C	100 °C	50 °C	100 °C	50 °C	100 °C	50 °C	100 °C	50 °C	100 °C	50 °C	100 °C	50 °C	100 °C	50 °C	100 °C	50 °C	100 °C	50 °C
5, 200	200 °C, 150 °C	200 °C	150 °C	200 °C	150 °C	200 °C	150 °C	200 °C	150 °C	200 °C	150 °C	200 °C	150 °C	200 °C	150 °C	200 °C	150 °C	200 °C	150 °C	200 °C	150 °C	200 °C	150 °C	200 °C	150 °C
	100 °C, 50 °C	100 °C	50 °C	100 °C	50 °C	100 °C	50 °C	100 °C	50 °C	100 °C	50 °C	100 °C	50 °C	100 °C	50 °C	100 °C	50 °C	100 °C	50 °C	100 °C	50 °C	100 °C	50 °C	100 °C	50 °C
6, 400	200 °C, 150 °C	200 °C	150 °C	200 °C	150 °C	200 °C	150 °C	200 °C	150 °C	200 °C	150 °C	200 °C	150 °C	200 °C	150 °C	200 °C	150 °C	200 °C	150 °C	200 °C	150 °C	200 °C	150 °C	200 °C	150 °C
	100 °C, 50 °C	100 °C	50 °C	100 °C	50 °C	100 °C	50 °C	100 °C	50 °C	100 °C	50 °C	100 °C	50 °C	100 °C	50 °C	100 °C	50 °C	100 °C	50 °C	100 °C	50 °C	100 °C	50 °C	100 °C	50 °C
7, 400	200 °C, 150 °C	200 °C	150 °C	200 °C	150 °C	200 °C	150 °C	200 °C	150 °C	200 °C	150 °C	200 °C	150 °C	200 °C	150 °C	200 °C	150 °C	200 °C	150 °C	200 °C	150 °C	200 °C	150 °C	200 °C	150 °C
	100 °C, 50 °C	100 °C	50 °C	100 °C	50 °C	100 °C	50 °C	100 °C	50 °C	100 °C	50 °C	100 °C	50 °C	100 °C	50 °C	100 °C	50 °C	100 °C	50 °C	100 °C	50 °C	100 °C	50 °C	100 °C	50 °C
8, 400	200 °C, 150 °C	200 °C	150 °C	200 °C	150 °C	200 °C	150 °C	200 °C	150 °C	200 °C	150 °C	200 °C	150 °C	200 °C	150 °C	200 °C	150 °C	200 °C	150 °C	200 °C	150 °C	200 °C	150 °C	200 °C	150 °C
	100 °C, 50 °C	100 °C	50 °C	100 °C	50 °C	100 °C	50 °C	100 °C	50 °C	100 °C	50 °C	100 °C	50 °C	100 °C	50 °C	100 °C	50 °C	100 °C	50 °C	100 °C	50 °C	100 °C	50 °C	100 °C	50 °C
9, 400	200 °C, 150 °C	200 °C	150 °C	200 °C	150 °C	200 °C	150 °C	200 °C	150 °C	200 °C	150 °C	200 °C	150 °C	200 °C	150 °C	200 °C	150 °C	200 °C	150 °C	200 °C	150 °C	200 °C	150 °C	200 °C	150 °C
	100 °C, 50 °C	100 °C	50 °C	100 °C	50 °C	100 °C	50 °C	100 °C	50 °C	100 °C	50 °C	100 °C	50 °C	100 °C	50 °C	100 °C	50 °C	100 °C	50 °C	100 °C	50 °C	100 °C	50 °C	100 °C	50 °C
10, 400	200 °C, 150 °C	200 °C	150 °C	200 °C	150 °C	200 °C	150 °C	200 °C	150 °C	200 °C	150 °C	200 °C	150 °C	200 °C	150 °C	200 °C	150 °C	200 °C	150 °C	200 °C	150 °C	200 °C	150 °C	200 °C	150 °C
	100 °C, 50 °C	100 °C	50 °C	100 °C	50 °C	100 °C	50 °C	100 °C	50 °C	100 °C	50 °C	100 °C	50 °C	100 °C	50 °C	100 °C	50 °C	100 °C	50 °C	100 °C	50 °C	100 °C	50 °C	100 °C	50 °C
11, 400	200 °C, 150 °C	200 °C	150 °C	200 °C	150 °C	200 °C	150 °C	200 °C	150 °C	200 °C	150 °C	200 °C	150 °C	200 °C	150 °C	200 °C	150 °C	200 °C	150 °C	200 °C	150 °C	200 °C	150 °C	200 °C	150 °C
	100 °C, 50 °C	100 °C	50 °C	100 °C	50 °C	100 °C	50 °C	100 °C	50 °C	100 °C	50 °C	100 °C	50 °C	100 °C	50 °C	100 °C	50 °C	100 °C	50 °C	100 °C	50 °C	100 °C	50 °C	100 °C	50 °C
12, 200	200 °C, 150 °C	200 °C	150 °C	200 °C	150 °C	200 °C	150 °C	200 °C	150 °C	200 °C	150 °C	200 °C	150 °C	200 °C	150 °C	200 °C	150 °C	200 °C	150 °C	200 °C	150 °C	200 °C	150 °C	200 °C	150 °C
	100 °C, 50 °C	100 °C	50 °C	100 °C	50 °C	100 °C	50 °C	100 °C	50 °C	100 °C	50 °C	100 °C	50 °C	100 °C	50 °C	100 °C	50 °C	100 °C	50 °C	100 °C	50 °C	100 °C	50 °C	100 °C	50 °C
12, 400	200 °C, 150 °C	200 °C	150 °C	200 °C	150 °C	200 °C	150 °C	200 °C	150 °C	200 °C	150 °C	200 °C	150 °C	200 °C	150 °C	200 °C	150 °C	200 °C	150 °C	200 °C	150 °C	200 °C	150 °C	200 °C	150 °C
	100 °C, 50 °C	100 °C	50 °C	100 °C	50 °C	100 °C	50 °C	100 °C	50 °C	100 °C	50 °C	100 °C	50 °C	100 °C	50 °C	100 °C	50 °C	100 °C	50 °C	100 °C	50 °C	100 °C	50 °C	100 °C	50 °C

b)

Sub., mmol \ St.	Temp.	1:0	1:0	20:1	20:1	10:1	10:1	5:1	5:1	2:1	2:1	1:1	1:1	1:2	1:2	1:5	1:5	1:10	1:10	1:20	1:20	R'X:0	R'X:0	0:0	0:0
2, 400	200 °C, 150 °C	6.88E+04	5.70E+04	1.44E+05	1.63E+05	1.71E+05	4.49E+05	3.46E+05	1.03E+06	7.43E+05	1.90E+06	9.90E+05	1.36E+06	1.42E+06	7.92E+05	4.83E+05	4.48E+05	1.72E+05	1.80E+05	1.27E+05	5.99E+04	6.33E+04	1.32E+05	7.50E+04	7.94E+04
	100 °C, 50 °C	1.92E+05	7.48E+04	2.84E+05	4.26E+05	4.56E+05	6.47E+05	1.12E+06	1.66E+06	1.02E+06	3.02E+06	1.45E+06	4.23E+06	1.56E+06	1.32E+06	5.29E+05	1.28E+06	2.10E+05	1.87E+05	2.22E+05	1.31E+05	5.81E+04	2.53E+05	1.12E+05	1.35E+05
2, 200	200 °C, 150 °C	1.45E+05	1.70E+05	9.92E+05	1.08E+06	1.59E+06	1.49E+06	4.35E+06	5.38E+06	5.29E+06	6.86E+06	2.66E+06	3.03E+06	3.39E+06	2.08E+06	3.94E+05	2.90E+05	1.84E+05	1.64E+05	8.21E+04	9.25E+04	6.30E+04	3.71E+04	1.79E+05	1.90E+05
	100 °C, 50 °C	3.94E+05	3.05E+05	9.43E+05	6.98E+05	7.11E+05	1.26E+06	7.16E+05	3.07E+06	6.64E+05	2.46E+06	6.85E+05	4.27E+05	3.51E+05	4.37E+05	3.16E+05	3.55E+05	1.79E+05	3.00E+05	1.26E+05	2.11E+05	1.85E+05	1.76E+05	2.37E+05	1.73E+05
3, 400	200 °C, 150 °C	1.05E+05	1.64E+05	3.16E+05	3.02E+05	3.78E+05	4.35E+05	5.91E+05	7.95E+05	6.94E+05	1.14E+06	1.67E+06	1.26E+06	1.14E+06	8.39E+05	3.87E+05	3.39E+05	1.66E+05	1.01E+05	7.05E+04	6.35E+04	5.69E+04	5.30E+04	8.30E+04	1.12E+05
	100 °C, 50 °C	1.17E+05	1.83E+05	3.39E+05	2.66E+05	5.33E+05	5.86E+05	9.02E+05	5.11E+05	1.58E+06	1.52E+06	8.97E+05	7.12E+05	1.07E+06	5.96E+05	6.05E+05	2.74E+05	1.73E+05	2.75E+05	8.39E+04	1.76E+05	7.56E+04	1.24E+05	1.70E+05	1.29E+05
4, 200	200 °C, 150 °C	1.09E+05	1.84E+05	6.55E+05	4.44E+05	6.92E+05	1.52E+06	2.06E+06	1.88E+06	4.44E+06	3.82E+06	4.01E+06	5.98E+06	2.07E+06	3.99E+06	1.39E+06	9.13E+05	2.81E+05	1.83E+05	1.00E+05	1.16E+05	7.64E+04	7.37E+04	1.68E+05	6.55E+04
	100 °C, 50 °C	9.37E+04	3.29E+05	8.39E+05	4.35E+05	1.72E+06	9.70E+05	2.09E+06	1.53E+06	4.27E+06	2.28E+06	2.61E+06	2.38E+06	3.58E+06	8.60E+05	1.34E+06	4.07E+05	3.34E+05	3.86E+05	8.67E+04	2.93E+05	5.42E+04	1.91E+05	2.09E+05	1.38E+05
4, 400	200 °C, 150 °C	1.48E+05	1.58E+05	5.79E+05	1.14E+06	1.53E+06	2.43E+06	1.59E+06	3.91E+06	6.77E+06	4.53E+06	4.81E+06	5.53E+06	5.33E+06	5.54E+06	3.42E+06	2.11E+06	1.16E+06	1.36E+06	2.90E+05	2.45E+05	8.33E+04	8.03E+04	7.95E+04	1.05E+05
	100 °C, 50 °C	1.16E+05	1.99E+05	5.72E+05	5.72E+05	1.66E+06	8.33E+05	2.91E+06	2.63E+06	2.25E+06	2.73E+06	5.95E+06	2.93E+06	5.55E+06	2.63E+06	3.84E+06	1.29E+06	9.52E+05	6.02E+05	3.75E+05	5.99E+05	8.60E+04	1.10E+05	1.19E+05	2.13E+05
5, 200	200 °C, 150 °C	2.52E+05	9.85E+04	8.48E+05	6.24E+05	2.17E+06	1.77E+06	4.07E+06	3.30E+06	4.92E+06	5.85E+06	4.50E+06	1.70E+06	1.71E+06	5.22E+05	4.18E+05	2.91E+05	7.79E+04	2.25E+05	1.27E+05	1.15E+05	9.46E+04	6.74E+04	1.88E+05	2.59E+05
	100 °C, 50 °C	2.12E+05	2.55E+05	2.89E+05	6.36E+05	4.72E+05	1.30E+06	4.00E+05	1.54E+06	3.85E+05	2.56E+06	5.70E+05	9.79E+05	2.50E+05	4.64E+05	3.18E+05	3.18E+05	1.38E+05	3.21E+05	1.74E+05	2.29E+05	2.21E+05	1.25E+05	2.91E+05	2.01E+05
6, 400	200 °C, 150 °C	3.57E+05	2.75E+05	2.92E+05	2.20E+05	3.10E+05	2.87E+05	3.10E+05	1.98E+05	3.56E+05	2.72E+05	2.94E+05	2.78E+05	1.86E+05	1.79E+05	2.88E+04	1.03E+05	3.73E+04	5.00E+04	3.64E+04	8.09E+04	3.76E+04	3.10E+04	8.46E+04	9.52E+04
	100 °C, 50 °C	1.06E+05	8.75E+04	1.06E+05	1.05E+05	1.74E+05	6.98E+04	1.75E+05	1.08E+05	2.27E+05	8.77E+04	1.88E+05	1.08E+05	1.11E+05	8.45E+04	1.07E+05	6.24E+04	7.32E+04	7.00E+04	6.09E+04	7.30E+04	5.09E+04	5.79E+04	5.46E+04	8.80E+04
7, 400	200 °C, 150 °C	1.84E+05	2.48E+05	1.99E+05	2.22E+05	2.20E+05	1.79E+05	3.50E+05	2.47E+05	3.59E+05	2.71E+05	2.70E+05	2.16E+05	1.50E+05	1.17E+05	5.91E+04	7.50E+04	3.51E+04	5.02E+04	3.24E+04	7.87E+04	5.24E+04	3.24E+04	9.42E+04	8.05E+04
	100 °C, 50 °C	1.43E+05	7.76E+04	1.27E+05	1.00E+05	1.01E+05	1.31E+05	1.10E+05	1.21E+05	1.52E+05	2.44E+05	2.99E+05	1.19E+05	2.18E+05	6.74E+04	8.91E+04	6.81E+04	9.87E+04	1.16E+05	4.88E+04	9.99E+04	7.52E+04	9.29E+04	5.54E+04	5.82E+04
8, 400	200 °C, 150 °C	2.31E+05	4.03E+05	2.49E+05	4.66E+05	3.41E+05	3.46E+05	4.93E+05	3.16E+05	4.29E+05	6.84E+05	7.80E+05	5.53E+05	2.46E+05	1.64E+05	1.81E+05	8.43E+04	9.28E+04	1.02E+05	5.19E+04	1.01E+05	3.67E+04	5.77E+04	1.33E+05	1.11E+05
	100 °C, 50 °C	1.23E+05	1.31E+05	1.91E+05	2.88E+05	3.53E+05	5.33E+05	3.02E+05	9.49E+05	3.64E+05	1.02E+06	5.01E+05	9.82E+05	2.37E+05	8.41E+05	1.21E+05	1.22E+05	7.81E+04	4.85E+04	6.27E+04	4.50E+04	7.48E+04	3.30E+04	9.24E+04	7.96E+04
9, 400	200 °C, 150 °C	2.41E+05	1.52E+05	4.21E+05	2.22E+05	5.04E+05	5.39E+05	3.39E+05	6.34E+05	3.87E+05	8.27E+05	2.61E+05	5.79E+05	3.90E+05	2.79E+05	1.73E+05	2.51E+05	1.70E+05	3.24E+05	3.56E+05	2.63E+05	1.75E+05	2.16E+05	3.15E+05	2.86E+05
	100 °C, 50 °C	2.93E+05	3.42E+05	2.03E+05	5.95E+05	3.39E+05	6.26E+05	3.17E+05	7.22E+05	4.14E+05	1.04E+06	5.06E+05	9.26E+05	3.70E+05	2.41E+05	5.25E+05	3.03E+05	4.12E+05	3.36E+05	3.28E+05	1.84E+05	4.26E+05	3.32E+05	2.63E+05	2.22E+05
10, 400	200 °C, 150 °C	6.00E+04	1.22E+05	1.17E+05	8.18E+04	2.48E+05	1.81E+05	2.40E+05	1.70E+05	6.42E+05	5.63E+05	4.56E+05	5.48E+05	2.90E+05	3.22E+05	9.85E+04	3.47E+05	5.97E+04	8.42E+04	4.73E+04	5.15E+04	3.18E+04	6.87E+04	8.77E+04	7.38E+04
	100 °C, 50 °C	1.10E+05	1.87E+05	1.33E+05	1.38E+05	1.43E+05	2.99E+05	3.84E+05	2.19E+05	5.52E+05	4.38E+05	4.66E+05	6.23E+05	5.08E+05	3.02E+05	1.35E+05	1.90E+05	1.18E+05	1.36E+05	7.54E+04	8.42E+04	8.48E+04	1.19E+05	5.76E+04	1.08E+05
11, 400	200 °C, 150 °C	3.69E+05	6.45E+05	4.03E+05	6.94E+05	8.47E+05	4.95E+05	1.34E+06	1.26E+06	2.10E+06	2.23E+06	2.71E+06	9.61E+05	9.90E+05	9.29E+05	3.04E+05	6.22E+05	2.49E+05	3.64E+05	2.51E+05	4.17E+05	1.50E+05	2.01E+05	2.04E+05	2.54E+05
	100 °C, 50 °C	3.10E+05	1.69E+05	3.97E+05	4.17E+05	7.55E+05	6.45E+05	1.16E+06	1.18E+06	1.16E+06	2.79E+06	7.09E+05	3.05E+06	7.27E+05	3.23E+06	5.36E+05	9.77E+05	5.79E+05	5.72E+05	4.07E+05	4.73E+05	5.05E+05	3.31E+05	3.13E+05	3.35E+05
12, 200	200 °C, 150 °C	8.92E+04	4.56E+04	6.07E+05	4.33E+05	7.30E+05	7.73E+05	2.48E+06	9.82E+05	1.66E+06	2.96E+06	2.45E+06	1.81E+06	1.96E+06	2.29E+06	5.97E+05	7.90E+05	1.11E+05	5.19E+04	8.80E+04	6.88E+04	2.66E+04	6.10E+04	6.37E+04	6.48E+04
	100 °C, 50 °C	3.32E+04	5.13E+04	1.13E+06	5.53E+05	1.62E+06	8.20E+05	2.48E+06	7.18E+05	1.90E+06	2.50E+06	4.18E+06	2.03E+06	1.92E+06	9.96E+05	8.96E+05	6.85E+05	1.24E+05	9.84E+04	4.61E+04	8.63E+04	3.24E+04	7.05E+04	7.87E+04	6.68E+04
12, 400	200 °C, 150 °C	9.04E+04	7.44E+04	1.18E+06	1.98E+06	1.30E+06	3.13E+06	3.10E+06	2.81E+06	4.44E+06	2.77E+06	3.59E+06	4.78E+06	2.17E+06	2.83E+06	9.07E+05	1.17E+06	2.85E+05	2.29E+05	1.28E+05	8.39E+04	6.14E+04	9.21E+04	5.76E+04	8.14E+04
	100 °C, 50 °C	4.49E+04	6.21E+04	1.31E+06	8.80E+05	1.49E+06	1.80E+06	2.04E+06	2.21E+06	3.17E+06	2.69E+06	2.61E+06	1.89E+06	4.09E+06	2.33E+06	3.31E+06	1.41E+06	3.95E+05	2.69E+05	1.05E+05	1.01E+05	1.00E+05	7.74E+04	1.63E+05	9.22E+04

Figure B2. Product peak intensities for 504 unique S-M reactions run in bulk mode. a) Temperature details, b) Peak intensity values.

A

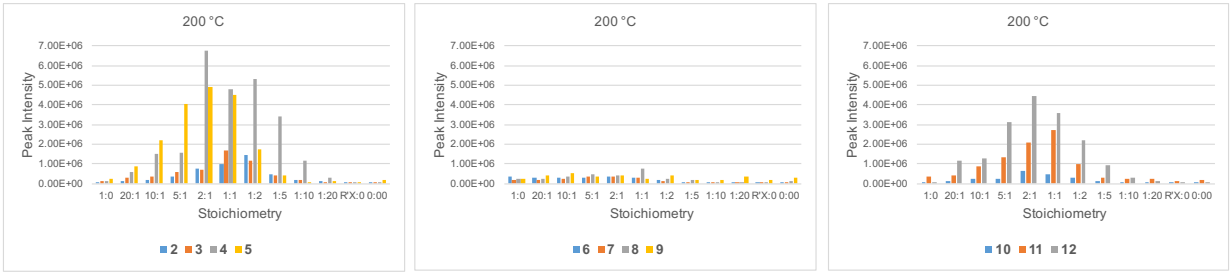

B

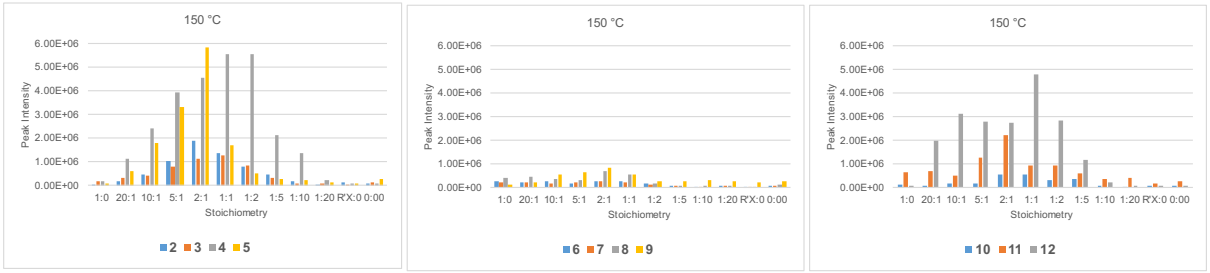

C

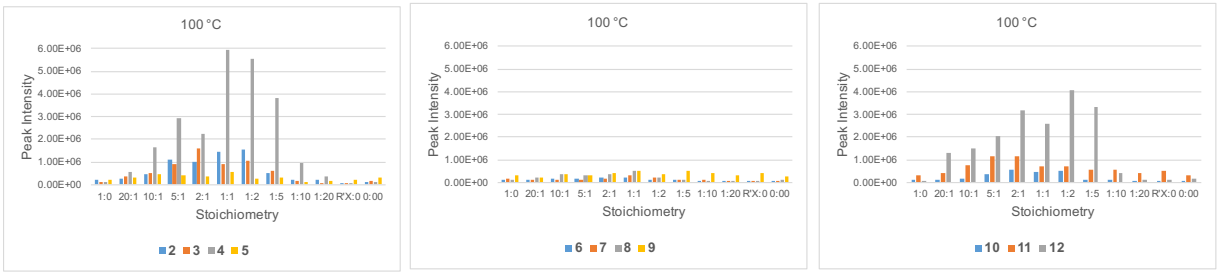

D

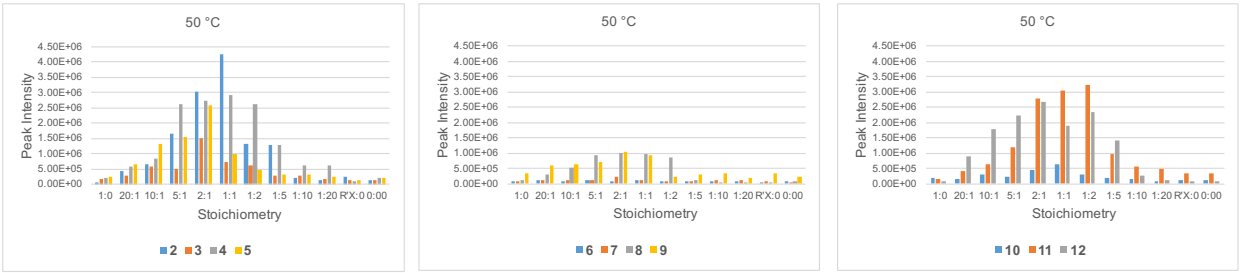

Figure B3. Comparative coupling efficiencies at different temperatures for anisole-type biphenyl products formed under different temperature and stoichiometric conditions. Reactant concentrations were 200 mmol except for **5** that was run at 100 mmol, 400 mmol DBU, and 10% XPhosPdG3. A = 200 °C; B = 150 °C; C = 100 °C; D = 50 °C.

Byproduct analysis

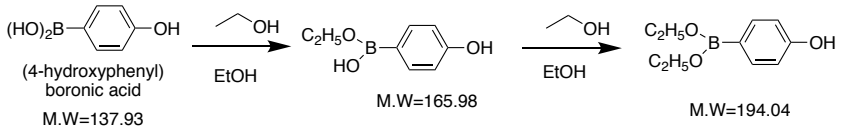

Scheme B1. Ethoxy-modified byproducts generated from 4-hydroxyphenylboronic acid solvolysis.

a)

Product peak intensity

Sub., mmol \ St.	20:1	20:1	10:1	10:1	5:1	5:1	2:1	2:1	1:1	1:1	1:2	1:2	1:5	1:5	1:10	1:10	1:20	1:20
1+3, 100	200°C	150°C	200°C	150°C	200°C	150°C	200°C	150°C	200°C	150°C	200°C	150°C	200°C	150°C	200°C	150°C	200°C	150°C
	100°C	50°C	100°C	50°C	100°C	50°C	100°C	50°C	100°C	50°C	100°C	50°C	100°C	50°C	100°C	50°C	100°C	50°C
1+3, 200	200°C	150°C	200°C	150°C	200°C	150°C	200°C	150°C	200°C	150°C	200°C	150°C	200°C	150°C	200°C	150°C	200°C	150°C
	100°C	50°C	100°C	50°C	100°C	50°C	100°C	50°C	100°C	50°C	100°C	50°C	100°C	50°C	100°C	50°C	100°C	50°C
1+4, 100	200°C	150°C	200°C	150°C	200°C	150°C	200°C	150°C	200°C	150°C	200°C	150°C	200°C	150°C	200°C	150°C	200°C	150°C
	100°C	50°C	100°C	50°C	100°C	50°C	100°C	50°C	100°C	50°C	100°C	50°C	100°C	50°C	100°C	50°C	100°C	50°C
1+4, 200	200°C	150°C	200°C	150°C	200°C	150°C	200°C	150°C	200°C	150°C	200°C	150°C	200°C	150°C	200°C	150°C	200°C	150°C
	100°C	50°C	100°C	50°C	100°C	50°C	100°C	50°C	100°C	50°C	100°C	50°C	100°C	50°C	100°C	50°C	100°C	50°C

b)

Sub., mmol \ St.	20:1	20:1	10:1	10:1	5:1	5:1	2:1	2:1	1:1	1:1	1:2	1:2	1:5	1:5	1:10	1:10	1:20	1:20
1+3, 100	5.34E+05	2.78E+05	3.22E+05	2.15E+05	3.23E+05	1.30E+05	1.40E+05	2.26E+05	1.93E+05	1.46E+05	2.26E+05	2.59E+05	2.64E+05	3.34E+05	2.55E+05	2.29E+05	4.67E+05	3.06E+05
	3.75E+05	2.64E+05	2.46E+05	1.95E+05	2.71E+05	1.39E+05	1.96E+05	3.71E+05	4.85E+05	4.22E+05	3.59E+05	4.93E+05	3.23E+05	3.30E+05	2.58E+05	5.31E+05	2.32E+05	5.59E+05
1+3, 200	2.66E+05	3.92E+05	1.25E+05	3.52E+05	2.28E+05	2.19E+05	1.93E+05	1.11E+05	1.66E+05	2.15E+05	1.65E+05	1.48E+05	2.52E+05	1.22E+05	2.86E+05	2.32E+05	2.48E+05	2.41E+05
	3.18E+05	3.04E+05	1.96E+05	2.94E+05	1.51E+05	2.72E+05	2.38E+05	2.71E+05	1.62E+05	3.41E+05	3.05E+05	3.32E+05	3.06E+05	4.21E+05	2.92E+05	5.57E+05	3.13E+05	3.76E+05
1+4, 100	4.11E+05	3.05E+05	2.87E+05	3.98E+05	3.94E+05	2.34E+05	5.83E+05	3.50E+05	3.26E+05	4.06E+05	1.94E+05	3.66E+05	3.64E+05	2.73E+05	3.72E+05	3.69E+05	3.03E+05	3.28E+05
	4.05E+05	2.67E+05	5.32E+05	3.98E+05	4.30E+05	4.26E+05	4.88E+05	3.28E+05	2.19E+05	6.52E+05	4.94E+05	3.87E+05	3.83E+05	4.22E+05	3.44E+05	8.92E+05	1.94E+05	8.77E+05
1+4, 200	2.15E+05	3.90E+05	4.38E+05	3.12E+05	1.45E+05	3.01E+05	2.72E+05	2.87E+05	1.22E+05	1.63E+05	1.72E+05	1.59E+05	1.84E+05	1.02E+05	1.77E+05	2.10E+05	1.91E+05	2.19E+05
	2.46E+05	3.18E+05	4.00E+05	2.69E+05	3.90E+05	5.55E+05	1.29E+05	5.25E+05	2.51E+05	4.10E+05	2.41E+05	4.21E+05	3.50E+05	4.88E+05	3.01E+05	5.65E+05	3.04E+05	7.81E+05

Figure B4. Product peak intensities of solvolyzed 4-hydroxyphenylboronic acid. a) Temperature details b) peak intensity values.

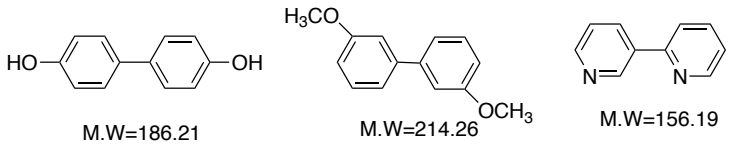

Scheme B2: Self-coupled byproducts from S-M reactions.

Product peak intensity

a)

St. / Sub., mmol	20:1	20:1	10:1	10:1	5:1	5:1	2:1	2:1	1:1	1:1	1:2	1:2	1:5	1:5	1:10	1:10	1:20	1:20
1+3, 100	200°C	150°C	200°C	150°C	200°C	150°C	200°C	150°C	200°C	150°C	200°C	150°C	200°C	150°C	200°C	150°C	200°C	150°C
	100°C	50°C	100°C	50°C	100°C	50°C	100°C	50°C	100°C	50°C	100°C	50°C	100°C	50°C	100°C	50°C	100°C	50°C
1+3, 200	200°C	150°C	200°C	150°C	200°C	150°C	200°C	150°C	200°C	150°C	200°C	150°C	200°C	150°C	200°C	150°C	200°C	150°C
	100°C	50°C	100°C	50°C	100°C	50°C	100°C	50°C	100°C	50°C	100°C	50°C	100°C	50°C	100°C	50°C	100°C	50°C
1+4, 100	200°C	150°C	200°C	150°C	200°C	150°C	200°C	150°C	200°C	150°C	200°C	150°C	200°C	150°C	200°C	150°C	200°C	150°C
	100°C	50°C	100°C	50°C	100°C	50°C	100°C	50°C	100°C	50°C	100°C	50°C	100°C	50°C	100°C	50°C	100°C	50°C
1+4, 200	200°C	150°C	200°C	150°C	200°C	150°C	200°C	150°C	200°C	150°C	200°C	150°C	200°C	150°C	200°C	150°C	200°C	150°C
	100°C	50°C	100°C	50°C	100°C	50°C	100°C	50°C	100°C	50°C	100°C	50°C	100°C	50°C	100°C	50°C	100°C	50°C

b)

St. / Sub., mmol	20:1	20:1	10:1	10:1	5:1	5:1	2:1	2:1	1:1	1:1	1:2	1:2	1:5	1:5	1:10	1:10	1:20	1:20
1+3, 100	8.99E+05	7.13E+05	7.31E+05	4.64E+05	5.90E+05	2.68E+05	2.20E+05	3.82E+05	3.49E+05	2.47E+05	3.03E+05	3.65E+05	2.41E+05	2.72E+05	1.53E+05	1.31E+05	2.01E+05	1.71E+05
	1.22E+06	4.15E+05	9.14E+05	3.26E+05	7.65E+05	2.10E+05	4.19E+05	5.31E+05	7.83E+05	5.05E+05	4.35E+05	4.33E+05	2.78E+05	3.08E+05	1.33E+05	1.61E+05	8.80E+04	1.52E+05
1+3, 200	1.37E+06	2.09E+06	6.83E+05	1.86E+06	7.71E+05	7.13E+05	3.43E+05	2.19E+05	3.11E+05	3.63E+05	3.23E+05	2.43E+05	2.96E+05	1.34E+05	1.36E+05	1.33E+05	1.13E+05	1.18E+05
	8.76E+05	4.81E+05	4.37E+05	4.73E+05	3.65E+05	4.49E+05	4.33E+05	3.27E+05	3.14E+05	3.25E+05	4.30E+05	3.19E+05	3.04E+05	2.88E+05	1.49E+05	1.96E+05	1.25E+05	1.13E+05
1+4, 100	1.39E+06	9.79E+05	7.51E+05	1.96E+06	1.16E+06	9.54E+05	1.08E+06	7.41E+05	4.84E+05	6.74E+05	2.84E+05	5.08E+05	3.81E+05	2.98E+05	2.69E+05	2.35E+05	1.65E+05	2.06E+05
	1.23E+06	4.09E+05	1.41E+06	5.65E+05	1.09E+06	5.37E+05	1.10E+06	3.78E+05	3.92E+05	7.22E+05	6.34E+05	3.69E+05	4.17E+05	2.49E+05	2.49E+05	3.33E+05	9.89E+04	2.75E+05
1+4, 200	9.50E+05	2.36E+06	1.30E+06	1.67E+06	6.54E+05	1.64E+06	9.89E+05	8.84E+05	2.85E+05	2.81E+05	3.55E+05	2.55E+05	2.97E+05	1.24E+05	2.00E+05	2.03E+05	1.33E+05	1.47E+05
	6.18E+05	3.42E+05	8.82E+05	2.67E+05	7.77E+05	4.87E+05	2.96E+05	3.81E+05	5.12E+05	3.34E+05	3.27E+05	3.45E+05	3.55E+05	3.16E+05	2.26E+05	2.77E+05	1.75E+05	3.17E+05

Figure B5. Product peak intensity of self-coupled byproducts from 4-hydroxyphenylboronic acid. a) Temperature details b) peak intensity values.

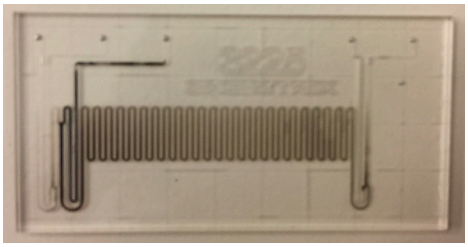

Before cleaning

After cleaning

Figure B6. Cleaning of Chemtrix 3223 reactor chip with aqua regia while using 10% XPhosPdG3.

Table B1. Microfluidic evaluation of Suzuki-Miyaura cross-coupling reactions, Chemtrix reactor chip: 3223, pressure: 6-7 bar

R1 **1** + aryl halide (0.2 M, 1:1) µL/min	R2 DBU (0.4 M) µL/min	R3 XPhosPdG3 (0.5%) µL/min	Residence Time T_r in Minutes	Temperature ^oC
10	5	5	0.5	150
5	2.5	2.5	1	150
1.67	0.833	0.833	3	150
0.833	0.417	0.417	6	150
10	5	5	0.5	100
5	2.5	2.5	1	100
1.67	0.833	0.833	3	100
0.833	0.417	0.417	6	100

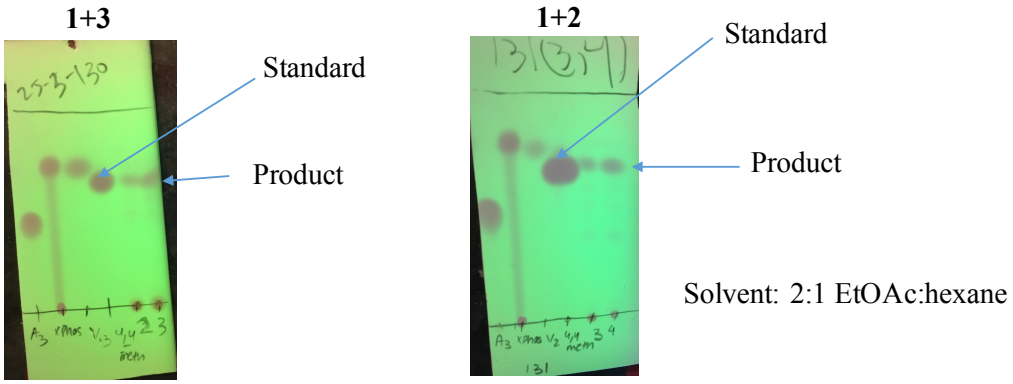

Figure B7: TLC monitoring during the progress of the flow reaction.

Bulk Reactions

Product \ SM	Temp	1+2	1+2
13	200℃, 150℃	990246.12	1364590.17
	100℃, 50℃	1447834.135	4234642.83

Product \ SM	Temp	1+3	1+3
13	200℃, 150℃	1671363.275	1263088.78
	100℃, 50℃	897254.22	711657.23

Product \ SM	Temp	1+4	1+4
14	200℃, 150℃	4811618.73	5528966.635
	100℃, 50℃	5954450.4	2929524.935

Product \ SM	Temp	1+5	1+5
15	200 ℃, 150 ℃	4500215.895	1698903.125
	200 ℃, 150 ℃	569719.71	978615.77

Product \ SM	Temp	1+6	1+6
16	200℃, 150℃	293745.62	278377.375
	100℃, 50℃	188032.525	107663.28

Product \ SM	Temp	1+7	1+7
16	200℃, 150℃	270446.575	215888.81
	100℃, 50℃	298605.635	119435.615

μFluidic Reactions

1+2				
Temp \ Time	30 s	1 min	3 min	6 min
100℃	1045254.566	1135715.833	1749526.509	5241698.855
150℃	2344396.665	1595250.57	3150090.873	5287176.159

1+3				
Temp \ Time	30 s	1 min	3 min	6 min
100℃	3089934.179	3535674.716	7614919.338	5548250.27
150℃	4439708.007	2239429.791	2844453.825	7076129.833

1+4				
Temp \ Time	30 s	1 min	3 min	6 min
100℃	1280039.923	2592778.782	3742014.741	6123280.568
150℃	2817896.446	2816431.707	3945609.983	5751260.16

1+5				
Temp \ Time	30 s	1 min	3 min	6 min
100℃	594787.436	1601403.135	2147694.521	4355349.784
150℃	1248567.952	1140598.862	2037811.558	5181386.451

1+6				
Temp \ Time	30 s	1 min	3 min	6 min
100℃	321320.2423	337953.6909	610049.04	608252.7333
150℃	198264.0848	394147.3008	624356.6029	697738.9077

1+7				
Temp \ Time	30 s	1 min	3 min	6 min
100℃	201553.4201	128198.5386	237022.4222	924855.6602
150℃	220337.8284	582275.727	809019.5278	764825.1542

Bulk Reactions

Product \ SM	Temp	1+8	1+8
17	200℃, 150℃	780387.74	553476.255
	100℃, 50℃	501344.465	962445.065

Product \ SM	Temp	1+9	1+9
18	200℃, 150℃	260528.315	578588.995
	100℃, 50℃	505663.26	925916.11

Product \ SM	Temp	1+10	1+10
19	200℃, 150℃	398943.0025	311925.4
	100℃, 50℃	148754.91	131855.41

Product \ SM	Temp	1+11	1+11
20	200℃, 150℃	2714662.965	960938.575
	100℃, 50℃	708718.535	3054006.93

Product \ SM	Temp	1+12	1+12
21	200℃, 150℃	3587581.115	4780830.23
	100℃, 50℃	2607411.48	1888739.885

μFluidic Reactions

1+8				
Temp \ Time	30 s	1 min	3 min	6 min
100℃	373831.1177	273042.6655	1209101.085	2294966.174
150℃	1109274.763	2965197.248	1115704.543	3291140.394

1+9				
Temp \ Time	30 s	1 min	3 min	6 min
100℃	1759562.89	1101173.843	755932.6836	1343209.712
150℃	1526390.366	878218.2089	1603145.893	1571427.815

1+10				
Temp \ Time	30 s	1 min	3 min	6 min
100℃	1166449.721	1636873.909	2413295.807	3976212.72
150℃	3182389.932	3401777.939	1834187.229	4102829.884

1+11				
Temp \ Time	30 s	1 min	3 min	6 min
100℃	410255.9062	37652381.37	25203829.57	35747590.31
150℃	1093509.365	1280512.677	1619761.193	2652425.337

1+12				
Temp \ Time	30 s	1 min	3 min	6 min
100℃	6129622.177	4668048.409	5139161.758	6344865.739
150℃	1846473.815	2315900.033	12241328.96	6542905.209

Product Peak Intensity Min → Max

Figure B8. Comparison of microfluidic and bulk screening outcomes for S-M reactions performed under similar conditions using 200 mmol substrate loading and 1:1 4-hydroxyphenylboronic acid:aryl halide stoichiometry. The table entries are the relative abundance of the product peak intensities.

Bulk Reactions

Product \ SM	Temp	1+3	1+3
13	200℃, 150℃	70504.85	63536.4
	100℃, 50℃	83851.73	176350.61

Product \ SM	Temp	1+8	1+8
17	200℃, 150℃	51899.775	100566.31
	100℃, 50℃	62714.645	44972.82

μFluidic Reactions

1+3				
Temp \ Time	30 s	1 min	3 min	6 min
100℃	1045905.824	1550626.338	1271433.25	1207885.711
150℃	185445.2739	431687.7856	396757.6716	373794.5328

1+8					
Temp \ Time	30 s	1 min	3 min	6 min	15min
100℃	67844.45041	108250.1439	123654.9512	118368.5928	
150℃	61088.63064	73806.90468	26239.21126	24368.99383	17392.48713

Product Peak Intensity Min → Max

Figure B9. Comparison of microfluidic and bulk screening outcomes for S-M reactions that gave negative bulk reaction results. The same reaction conditions were used in each case with 200 mmol substrate loading and 1:20 4-hydroxyphenylboronic acid:aryl halide stoichiometry. The values are the relative abundance of the product peak intensities.

Full MS spectra

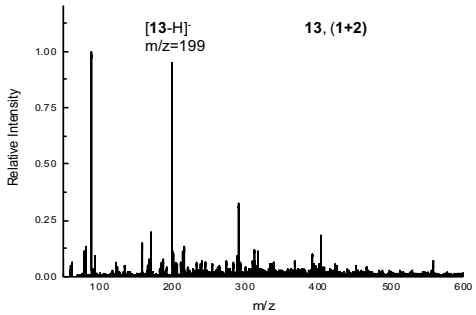

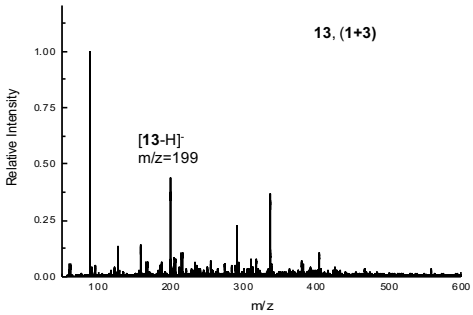

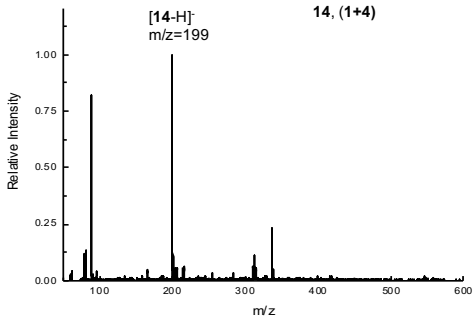

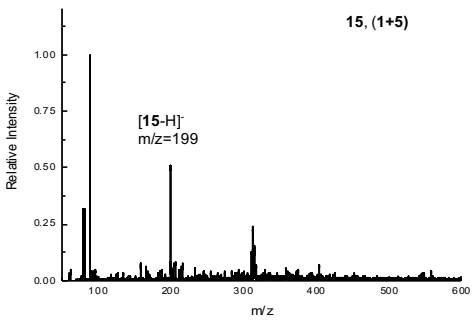

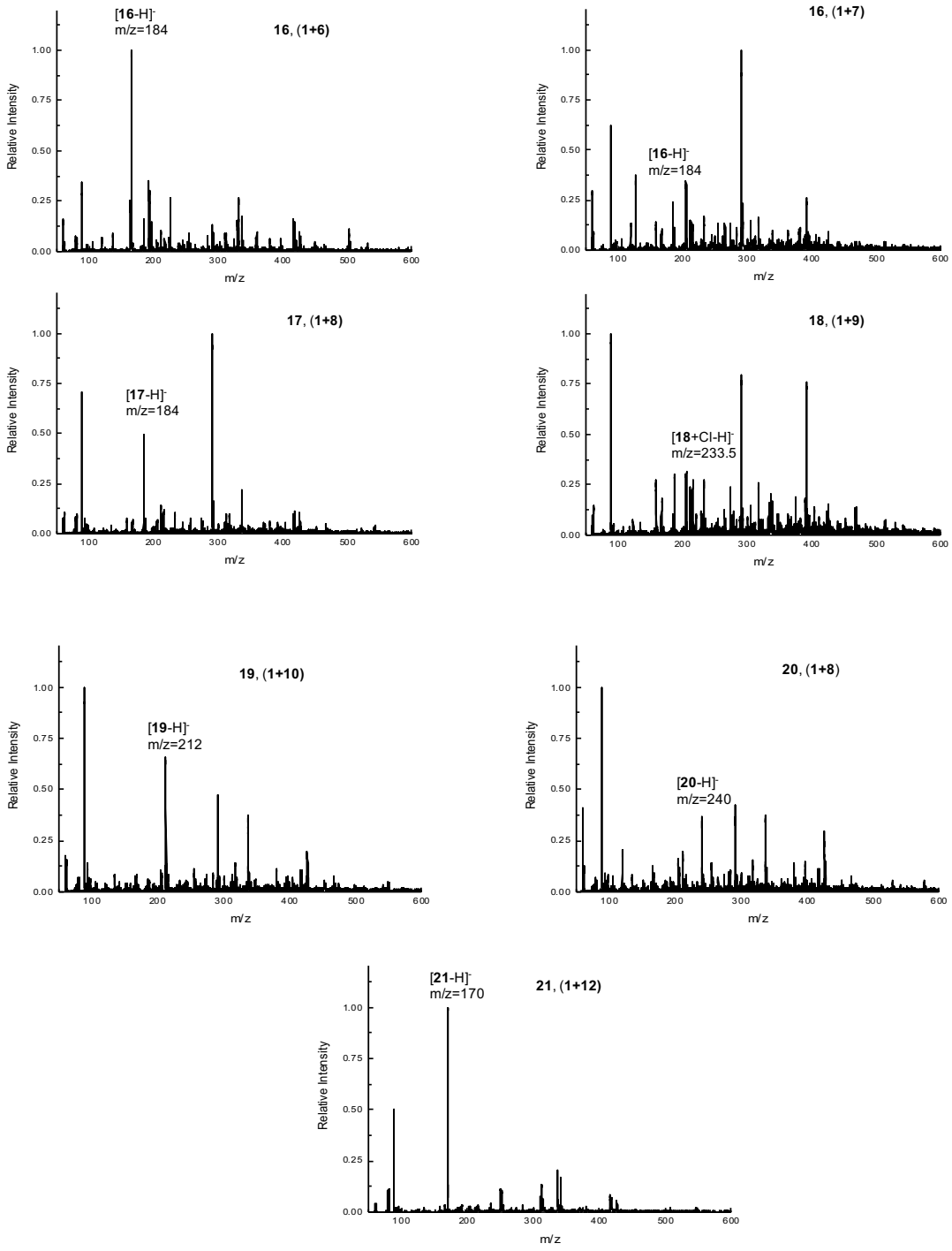

Figure B10: Full MS scan from microfluidic evaluation of S-M reactions identified by HT experimentation. Reaction conditions for each reaction are 150 °C, 6 min.

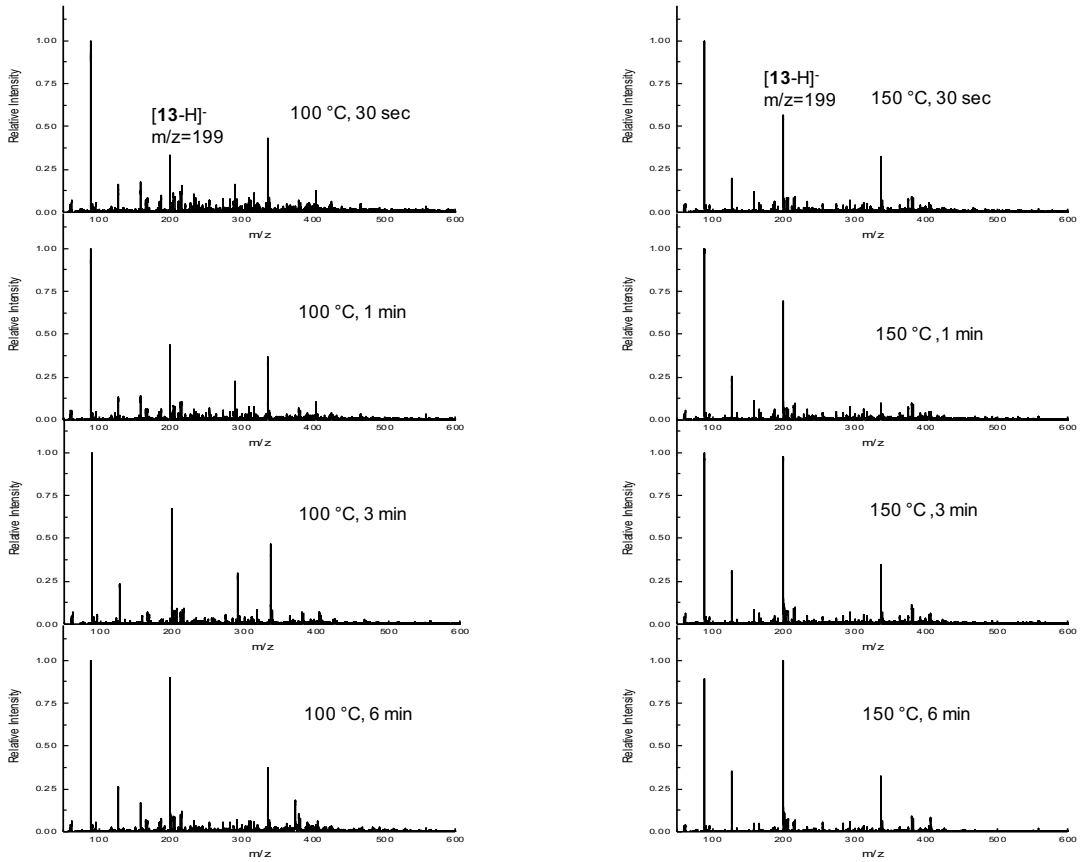

Figure B11. Full MS scan from microfluidic evaluation of S-M reactions between **1** and **3** (product **13**). Reaction conditions for each reaction are labeled on each spectrum.

HPLC/MS-MS analysis

Table B2: Parameters used for Multiple Reaction Monitoring (MRM) via HPLC/MS-MS analysis.

Compound Name	Precursor Ion	MS1 Res	Product Ion	MS2 Res	Dwell (ms)	Fragmentor (V)	Collision Energy (V)	Cell Accelerator Voltage (V)
4,2 methoxy,**13**	199	Unit	184	Unit	80	80	10	1
4,2 methoxy, **13**	199	Unit	183	Unit	80	80	25	1
4,3 methoxy, **14**	199	Unit	184	Unit	80	80	15	1
4,3 methoxy, **14**	199	Unit	156	Unit	80	80	20	1
4,4 methoxy, **15**	199	Unit	184	Unit	80	80	10	1
4,4 methoxy, **15**	199	Unit	156	Unit	80	80	20	1
Pyridine, **21**	170.1	Unit	142.1	Unit	80	80	40	1
Pyridine, **21**	170.1	Unit	93	Unit	80	80	40	1

APPENDIX C

NMR

^{1}H NMR (500 MHz, $CDCl_3$, ppm): δ_H = 4.84 (t, J= 5.85, 1 H), 4.42 (d, J = 7.35 Hz, 1 H), 3.62 (t, J=5.60Hz, 2 H), 3.54 (t, J=5.70Hz, 2 H), 3.51-3.45 (m, 1 H), 1.95-1.92 (m, 2 H), 1.72-1.67 (m, 2 H), 1.62-1.58 (m, 1 H), 1.39-1.30 (m, 2 H), 1.19-1.06 (m, 3 H); ^{13}C NMR (500 MHz, $CDCl_3$, ppm): δ_C= 157.04, 49.29, 45.25, 42.12, 33.88, 25.57, 24.9

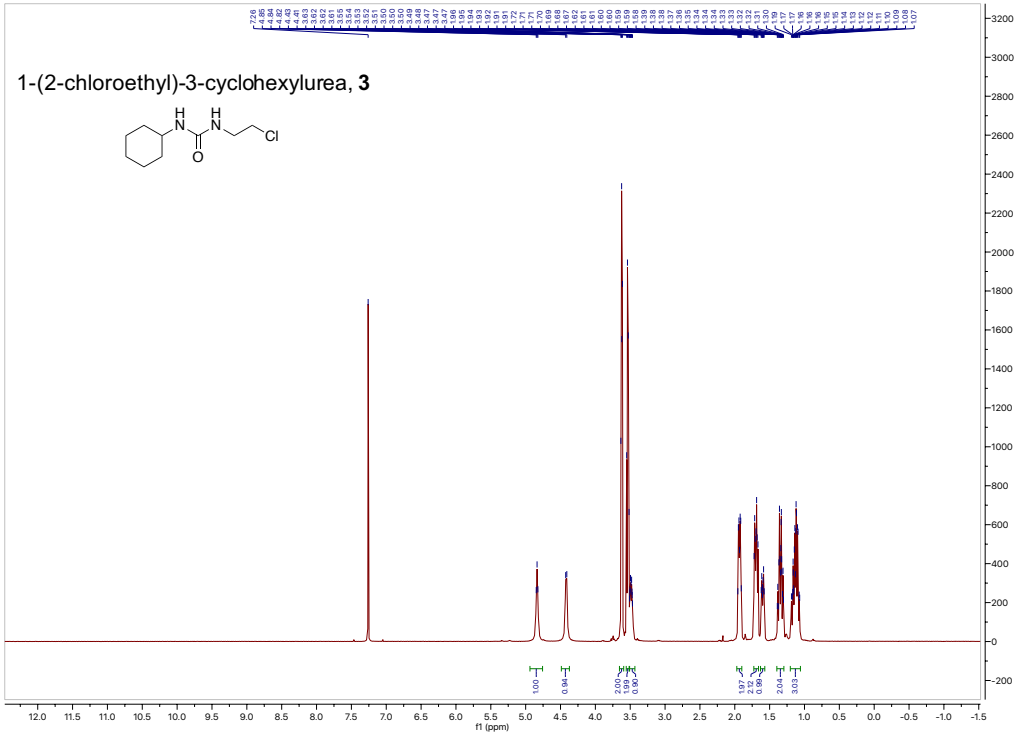

Figure C1: ^{1}H NMR of 1-(2-chloroethyl)-3-cyclohexylurea, **3,** from flow synthesis

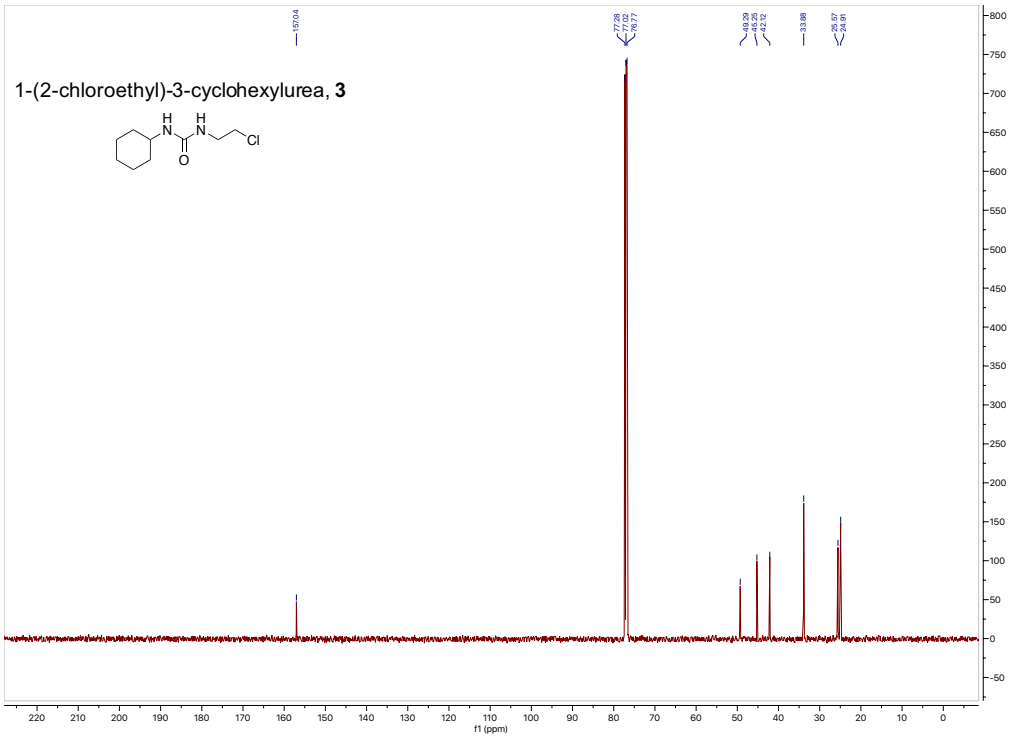

Figure C2: ^{13}C NMR of 1-(2-chloroethyl)-3-cyclohexylurea, **3,** from flow synthesis

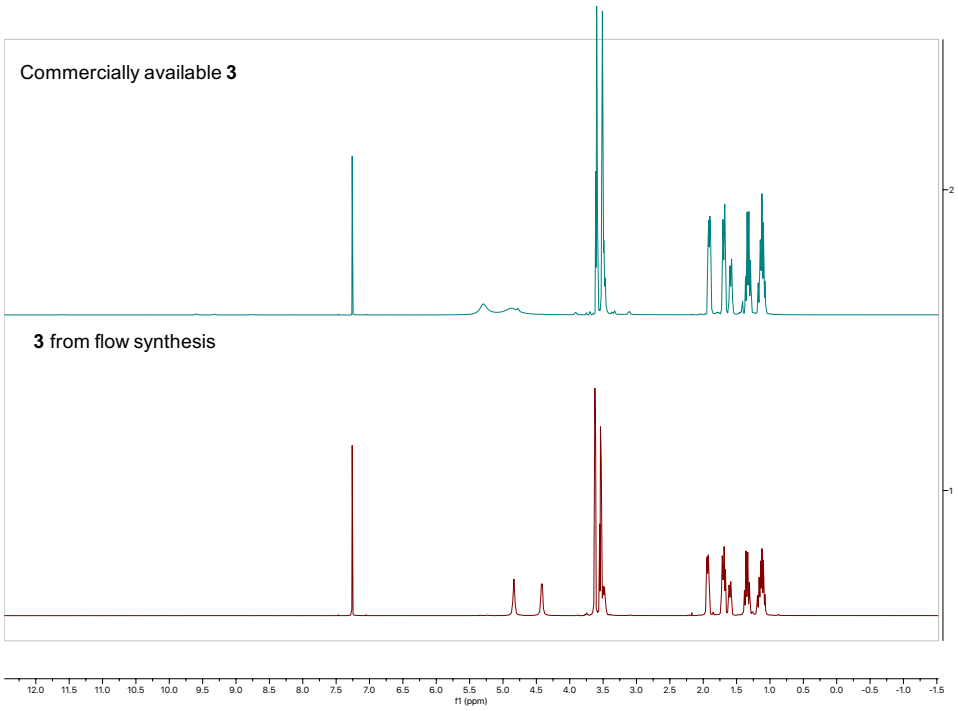

Figure C3: Comparison of ^{1}H NMR of 1-(2-chloroethyl)-3-cyclohexylurea, **3**, derived from flow synthesis with commercially available **3.**

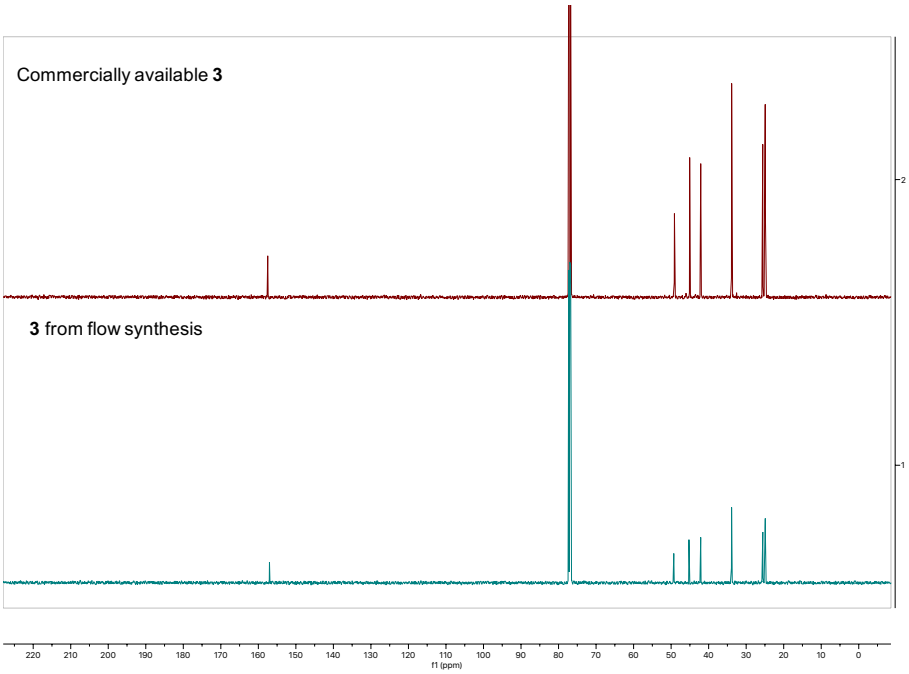

Figure C4: Comparison of ^{13}C NMR of 1-(2-chloroethyl)-3-cyclohexylurea, **3**, derived from flow synthesis with commercially available **3.**

DESI-MS Outline.

1. 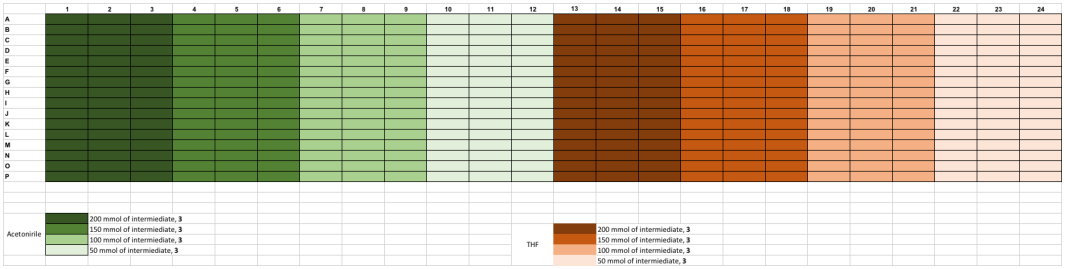

Figure C5: DESI master plate layout using four different concentrations in two solvents.

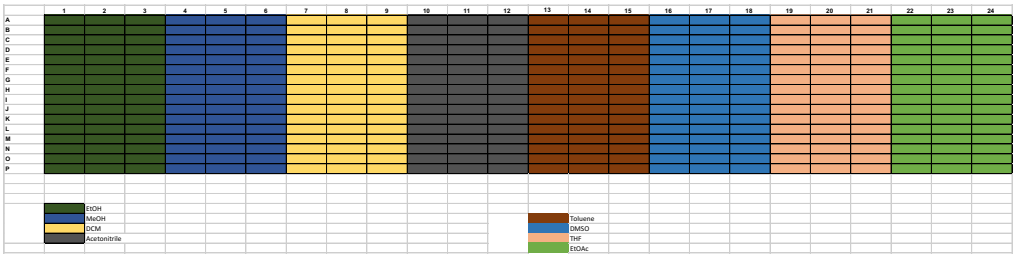

Figure C6: DESI master plate layout using eight different solvents.

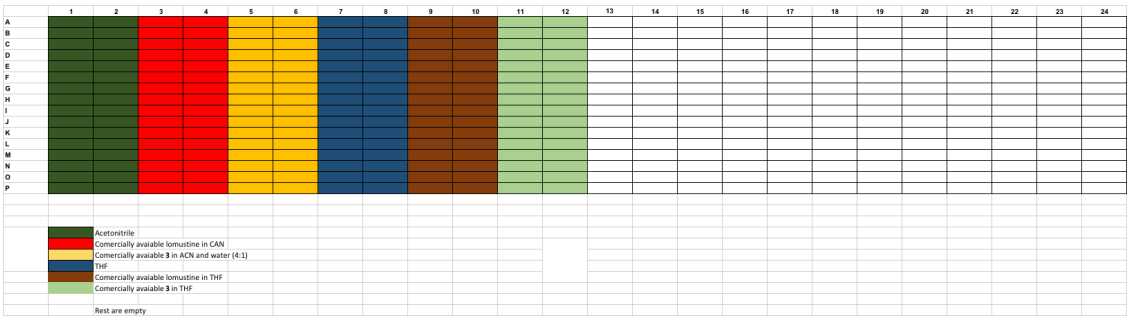

Figure C7: DESI master plate layout using only commercially available **3** and lomustine

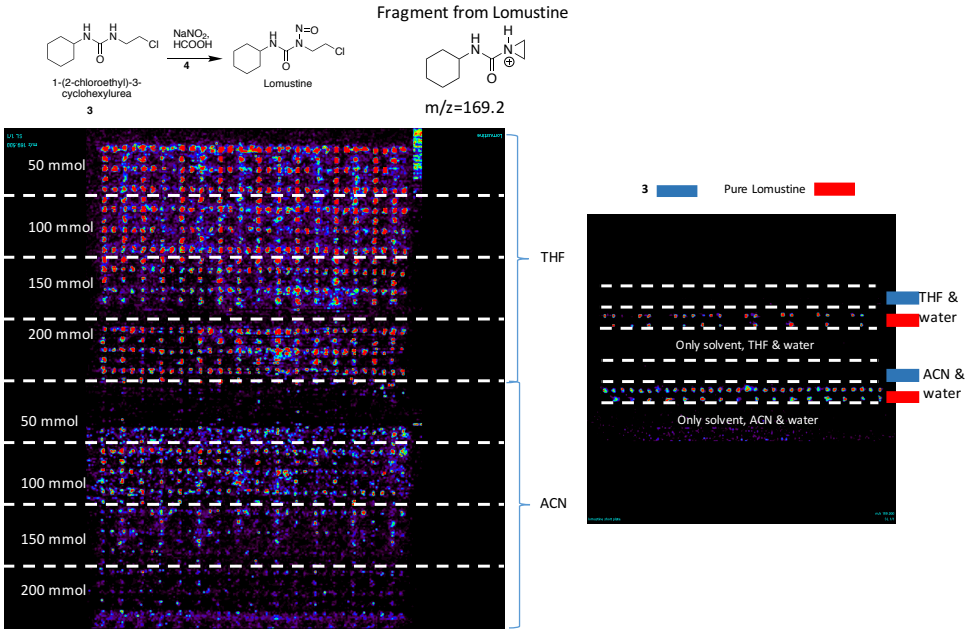

Figure C8: (left) Direct DESI-MS data comparison between the two nitrosation reactions in THF and ACN in different concentration. (right) DESI-MS data of commercially available **3** and lomustine standards. The data was analyzed using BioMAP imaging software.

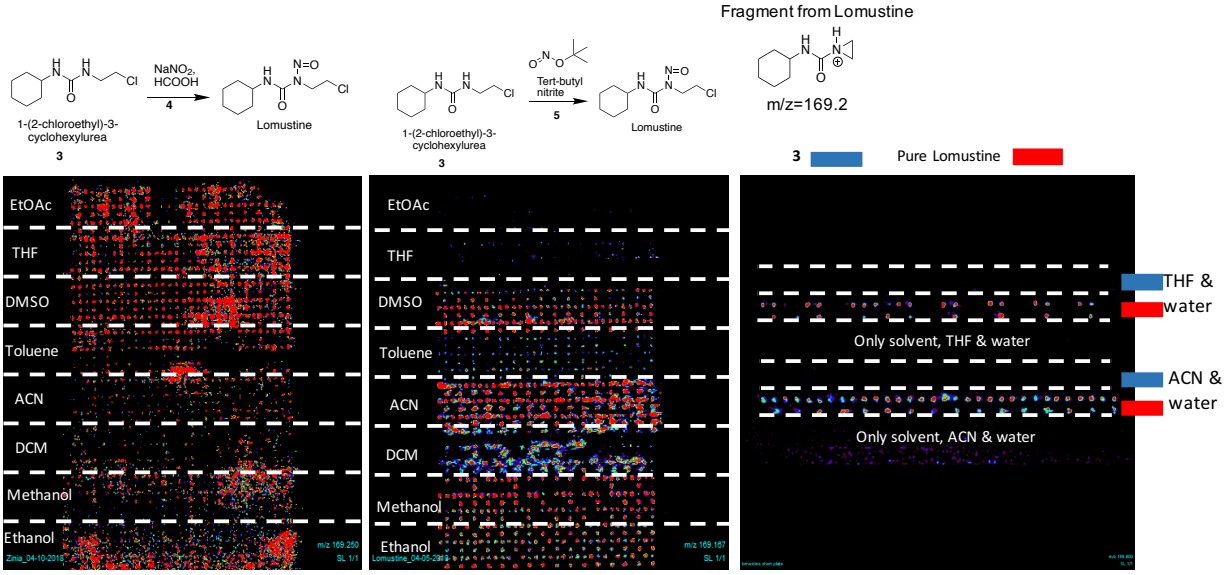

Figure C9: (left & center) Direct DESI-MS data comparison between the two nitrosation reactions in different solvents. (right) DESI-MS data of commercially available **3** and lomustine standards. The data was analyzed using BioMAP imaging software.

A

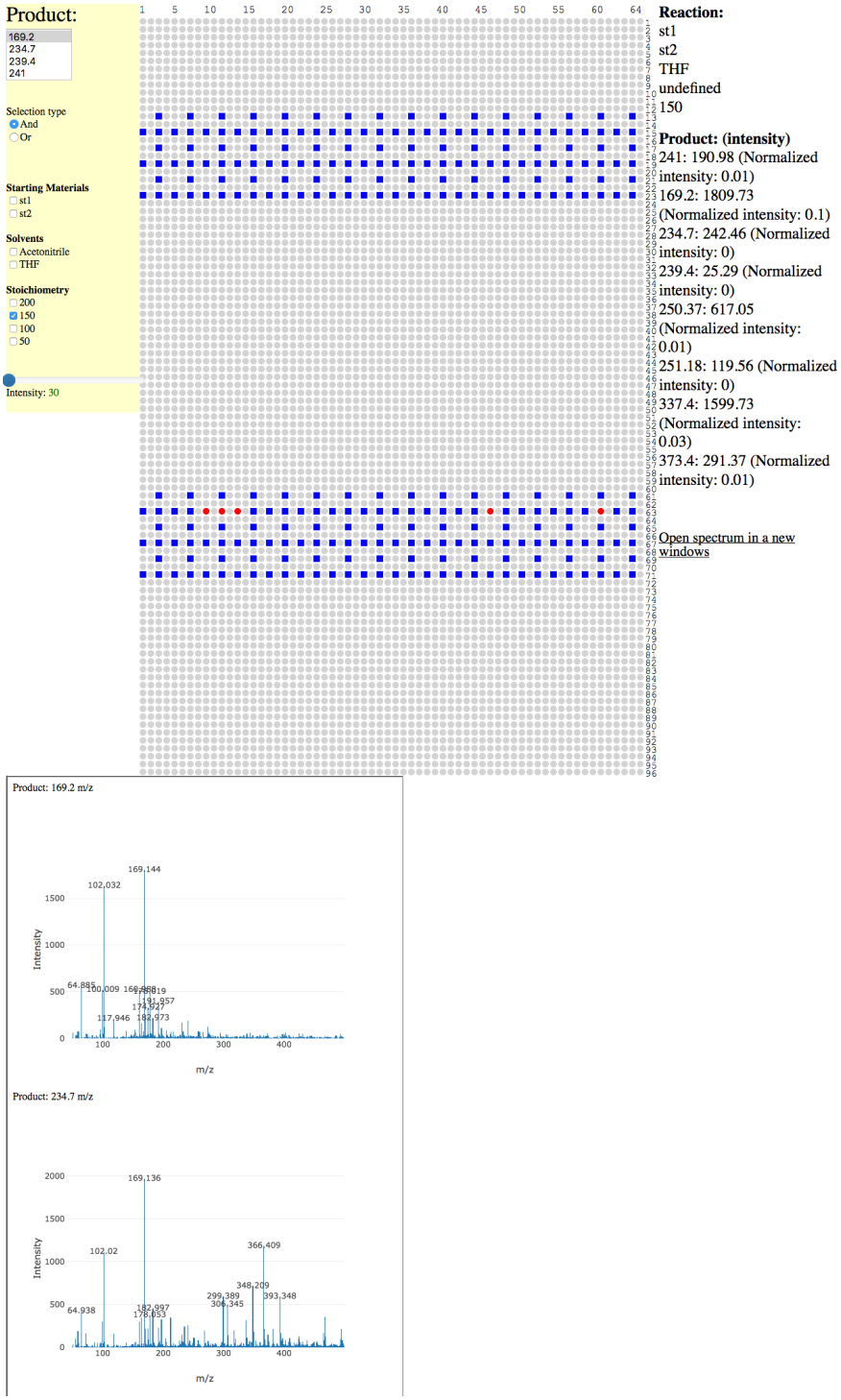
Product:
169.2
234.7
239.4
241
Selection type
And
Or
Starting Materials
st1
st2
Solvents
Acetonitrile
THF
Stoichiometry
200
150
100
50
Intensity: 30
Reaction:
st1
st2
THF
undefined
150
Product: (intensity)
241: 190.98 (Normalized intensity: 0.01)
169.2: 1809.73 (Normalized intensity: 0.1)
234.7: 242.46 (Normalized intensity: 0)
239.4: 25.29 (Normalized intensity: 0)
250.37: 617.05 (Normalized intensity: 0.01)
251.18: 119.56 (Normalized intensity: 0)
337.4: 1599.73 (Normalized intensity: 0.03)
373.4: 291.37 (Normalized intensity: 0.01)
Open spectrum in a new windows
Product: 169.2 m/z
169,144
102,032
Intensity
m/z
Product: 234.7 m/z
169,136
102,02
366,409
348,209
299,389
306,345
393,348
64,938
182,997
178,053
Intensity
m/z

B

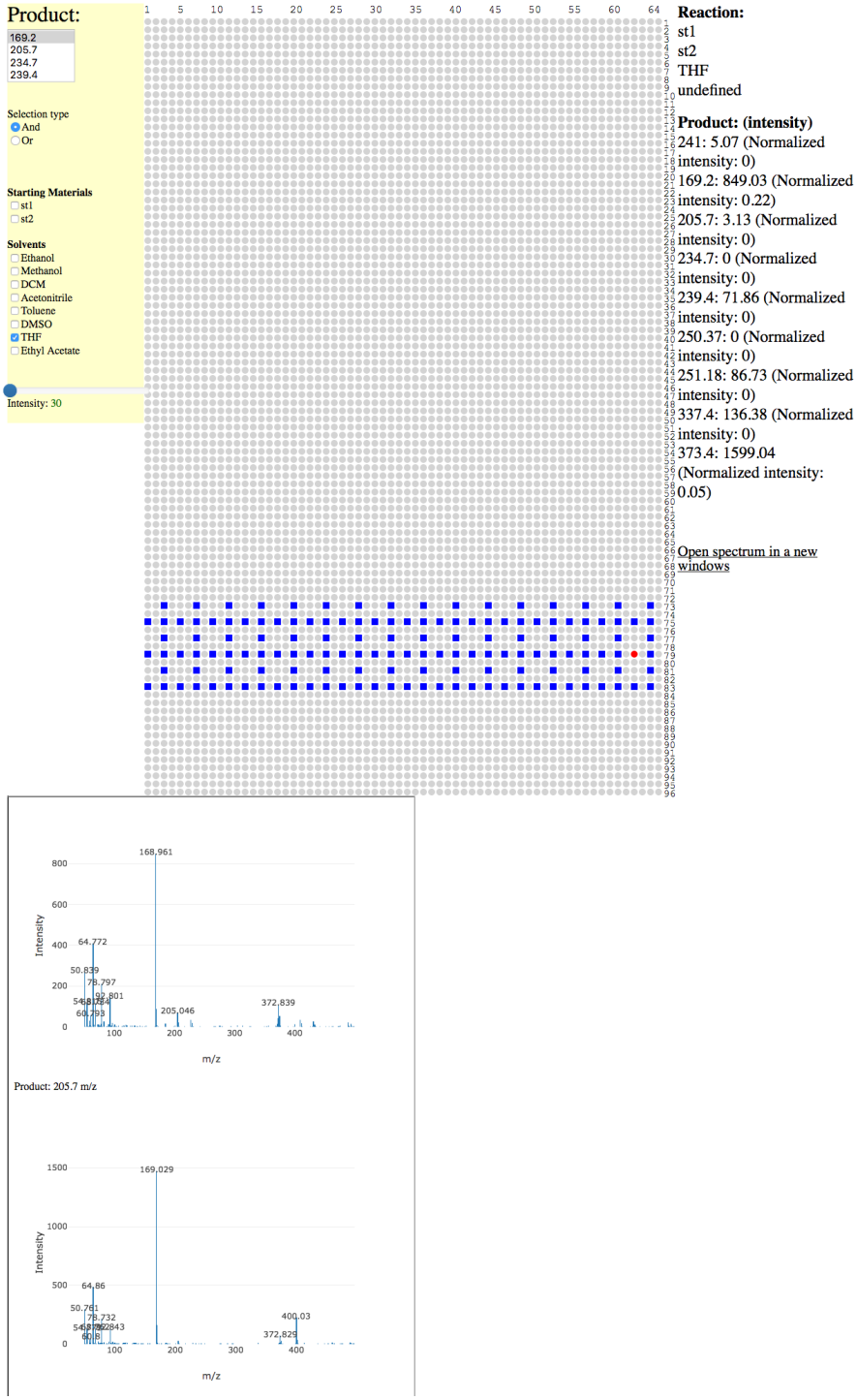
Product:
169.2
205.7
234.7
239.4
Selection type
And
Or
Starting Materials
st1
st2
Solvents
Ethanol
Methanol
DCM
Acetonitrile
Toluene
DMSO
THF
Ethyl Acetate
Intensity: 30
Reaction:
st1
st2
THF
undefined
Product: (intensity)
241: 5.07 (Normalized intensity: 0)
169.2: 849.03 (Normalized intensity: 0.22)
205.7: 3.13 (Normalized intensity: 0)
234.7: 0 (Normalized intensity: 0)
239.4: 71.86 (Normalized intensity: 0)
250.37: 0 (Normalized intensity: 0)
251.18: 86.73 (Normalized intensity: 0)
337.4: 136.38 (Normalized intensity: 0)
373.4: 1599.04 (Normalized intensity: 0.05)
Open spectrum in a new windows
Intensity
m/z
Product: 205.7 m/z

C

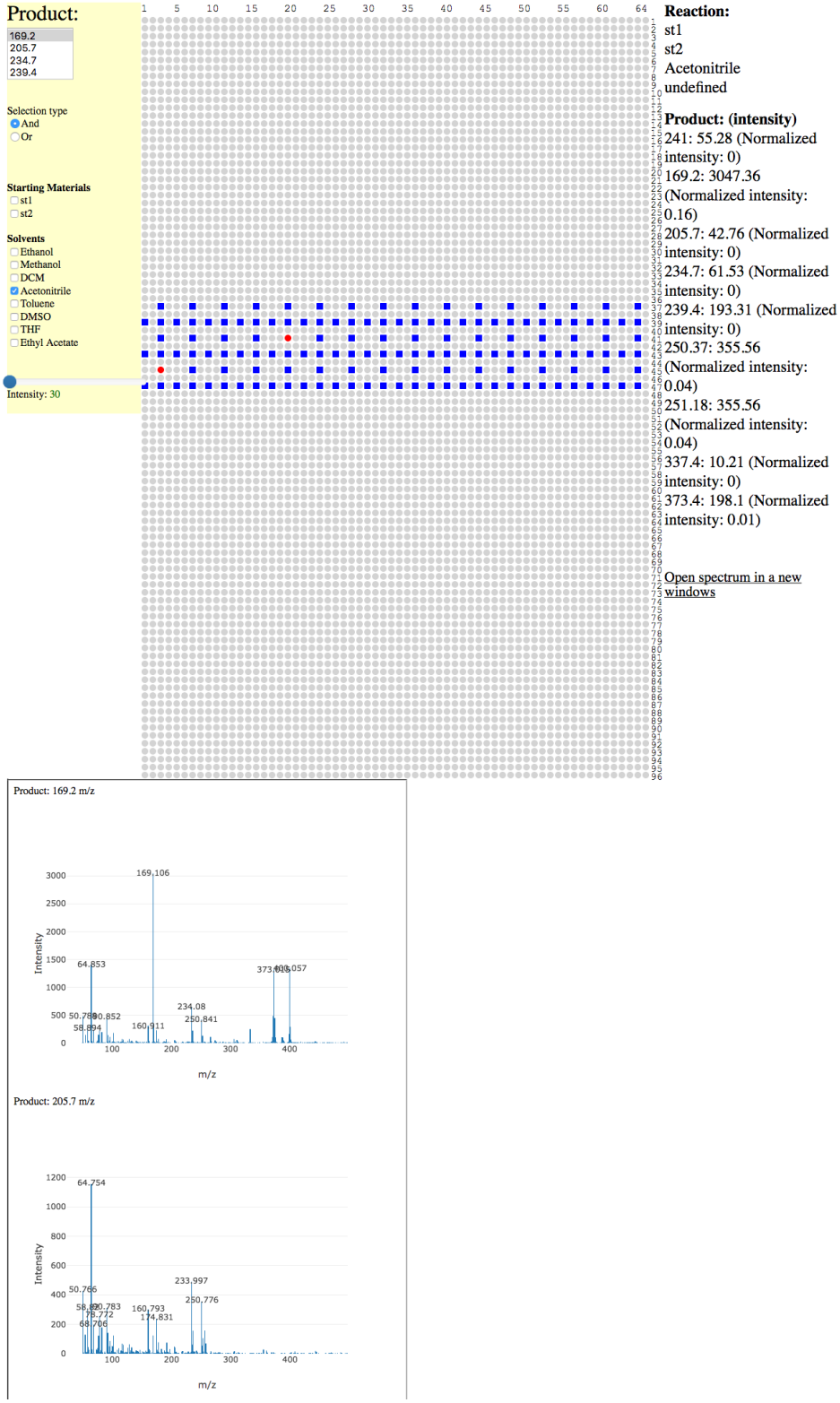

Figure C10: Map of the DESI-MS plates showing some of the expected ions where the nitrosation reaction using was screened using different stoichiometries as well as commercially available

standards. Green dots indicate the presence of the *m/z* expected for the reaction product (successful reaction), Red dots indicate that the expected *m/z* for the reaction product was not present at the reaction spot (unsuccessful reaction condition). A: $NaNO_2$, concentration screening using the lomustine ion (*m/z* 169) intensity; B: $NaNO_2$, solvent screening using the lomustine ion (*m/z* 169) intensity; C: TBN, solvent screening using the lomustine ion (*m/z* 169) intensity

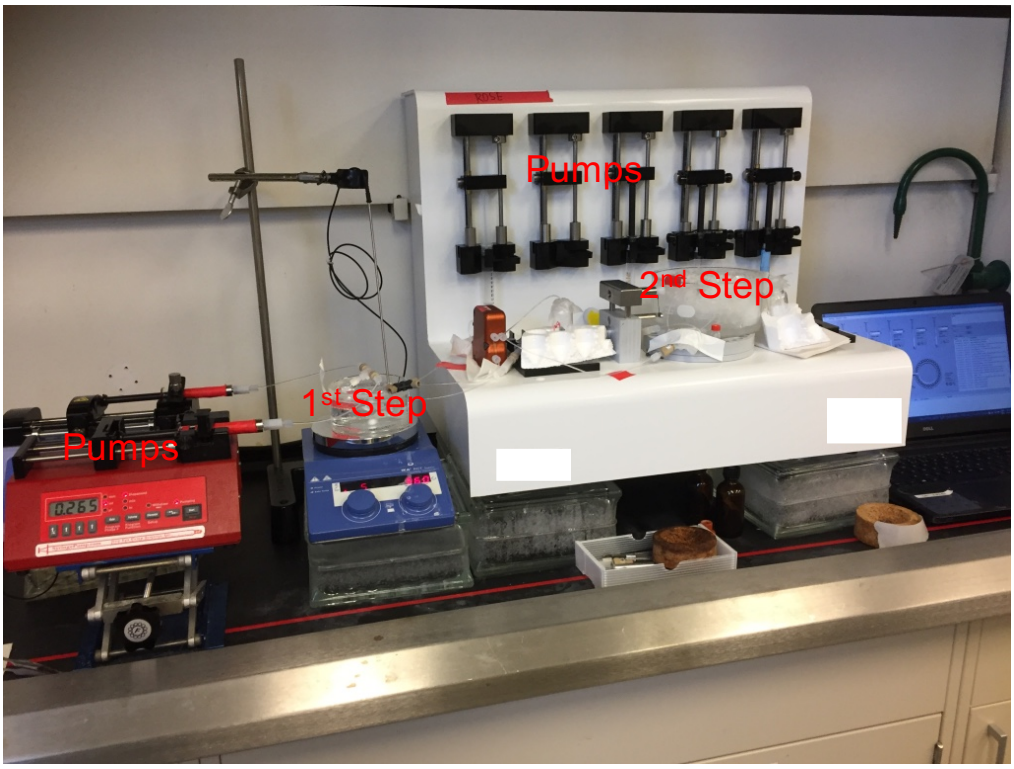

Figure C11: Telescoped two step syntheses of lomustine using sodium nitrite in the second step.

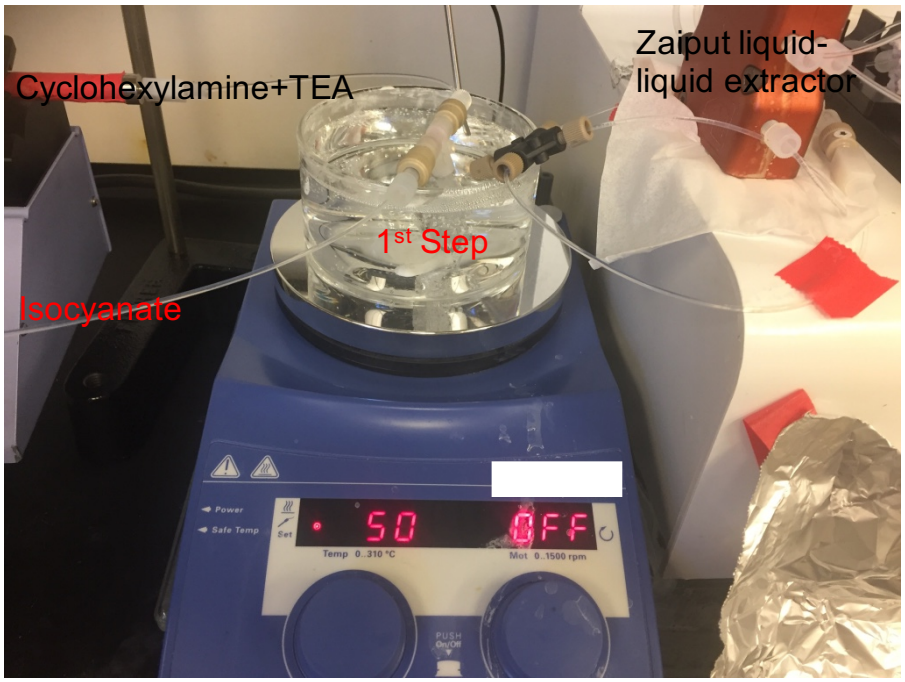

Figure C12: First step of the telescoped synthesis of lomustine.

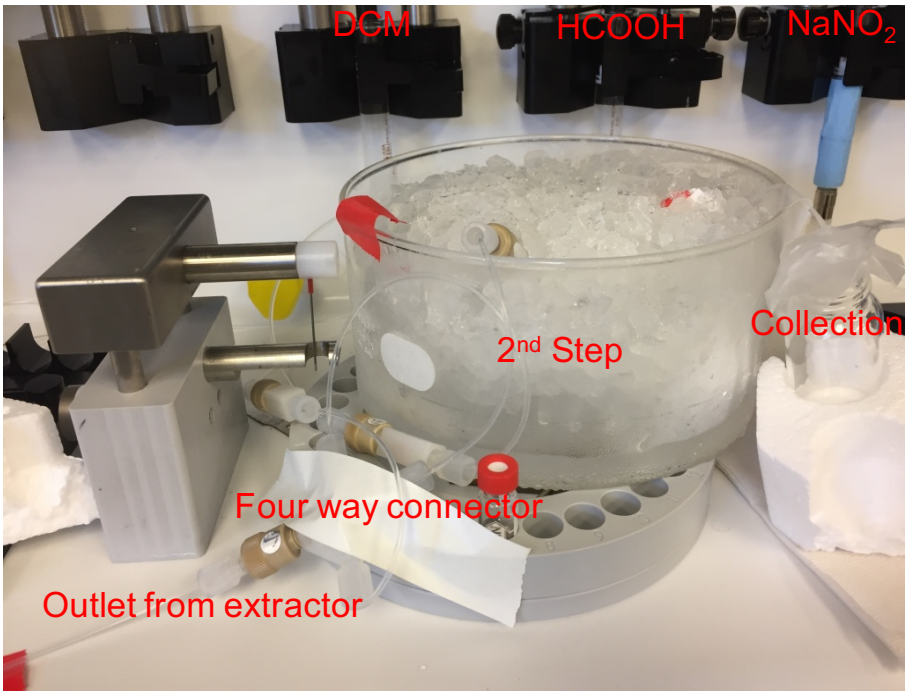

Figure C13: Second step of the telescoped synthesis of lomustine using $NaNO_2$ as a nitrosation reagent.

Figure C14: Telescoped lomustine synthesis using TBN as a nitrosation reagent, before reaction initiation.

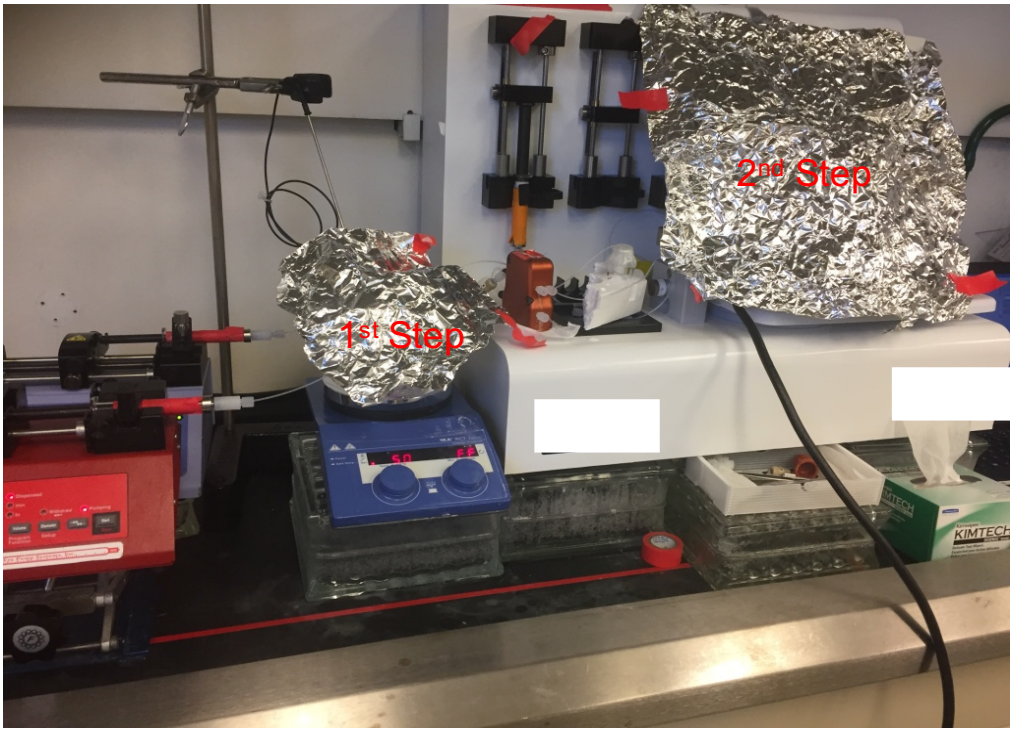

Figure C15: Telescoped lomustine synthesis using TBN (protected from light).

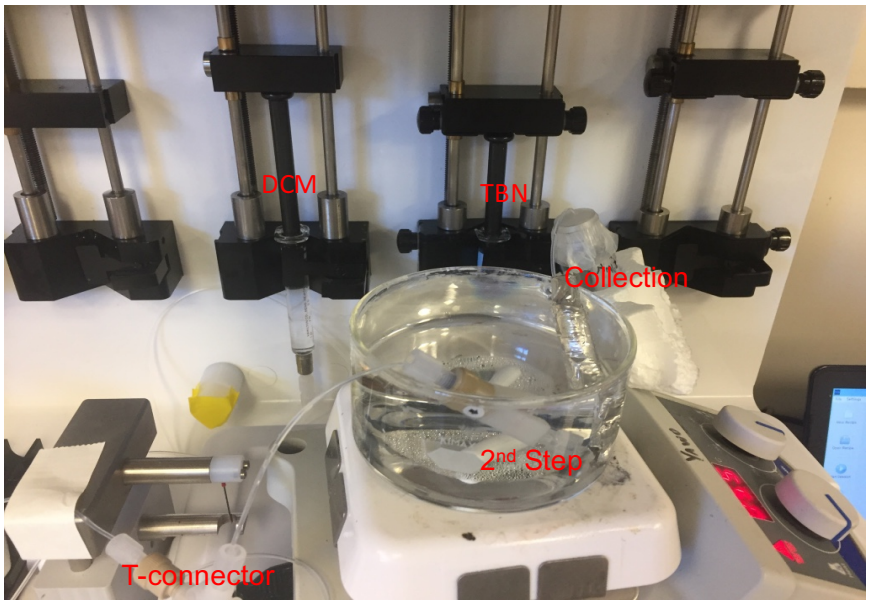

Figure C16: Second step of the telescoped synthesis of lomustine using TBN.

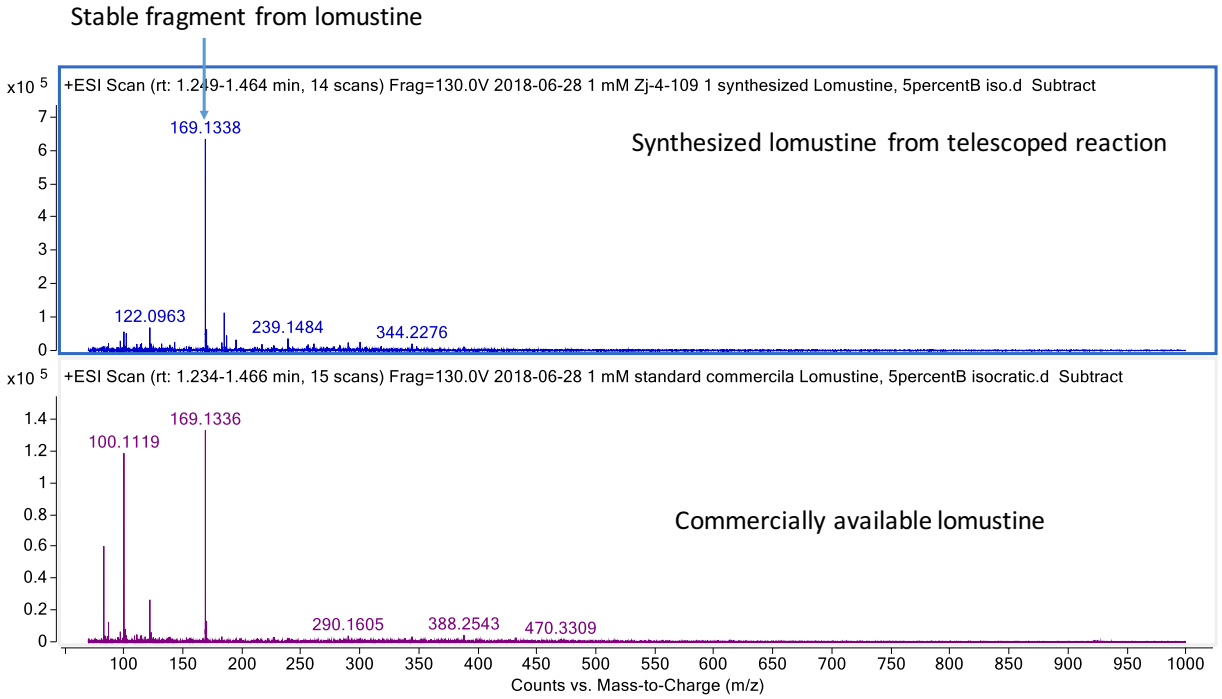

Figure C17: Full MS from HPLC-MS/MS and comparison between synthesized lomustine and commercially available lomustine.

Flow Rates

Table C1: Flow Rates for 1st step Reaction in Labtrix S1 system

Chemtrix reactor chip: 3225, 10 μL, pressure: ambient pressure

R1 Cyclohexane amine, **1** μL/min	R2 Triethylamine μL/min	R3 2-Chloroethyl isocyanate, **2** μL/min	Residence Time in min	Temperature °C
20	20	20	0.167	50
6.67	6.67	6.67	0.5	50
3.33	3.33	3.33	1	50
1.11	1.11	1.11	3	50
0.67	0.67	0.67	5	50
0.417	0.417	0.417	8	50
0.333	0.333	0.333	10	50

Table C2: Flow Rates for 2nd step Reaction using $NaNO_2/HCO_2H$, **4** in Labtrix S1 system

Chemtrix reactor chip: 3225, 10 μL, pressure: ambient pressure

R1 **3** μL/min	R2 Sodium Nitrite μL/min	R3 Formic Acid μL/min	Residence Time in min	Temperature °C
6.67	6.67	6.67	0.5	0
3.33	3.33	3.33	1	0
1.11	1.11	1.11	3	0
0.67	0.67	0.67	5	0
0.417	0.417	0.417	8	0
0.333	0.333	0.333	10	0

Table C3: Flow Rates for 2nd step Reaction using TBN, 5 in Labtrix S1 system.

Chemtrix reactor chip: 3223, 10 µL, pressure: ambient pressure

R1 **3** µL/min	R2 tert-Butyl nitrite µL/min	Residence Time in min	Temperature ^{o}C
10	10	0.5	50
5	5	1	50
1.67	1.67	3	50
1	1	5	50
0.625	0.625	8	50
0.5	0.5	10	50
10	10	0.5	25
5	5	1	25
1.67	1.67	3	25
1	1	5	25
0.625	0.625	8	25
0.5	0.5	10	25

Table C4: Telescoped reaction in Tube

Nitrosation Reagent: $NaNO_2/HCO_2H$ **4**

R1 **1** + Triethyl amine µL/min	R2 **2** µL/min	Reactor volume, cm	Step 1	Extraction step, H_2O µL/min	Extraction step, DCM µL/min	R3 $NaNO_2$ µL/min	R3 HCO_2H µL/min	Step 2
12.56	12.56	Step 1: 5 Step 2: 100	1 min, 50 ℃	50.24	25.12	25.12	25.12	5 min, 0 ℃
12.56	12.56	Step 1: 10 Step 2: 100	2 min, 50 ℃	50.24	25.12	25.12	25.12	5 min, 0 ℃
12.56	12.56	Step 1: 50 Step 2: 100	10 min, 50 ℃	50.24	25.12	25.12	25.12	5 min, 0 ℃
12.56	12.56	Step 1: 50 Step 2: 100	10 min, 50 ℃	50.24	25.12	50.24	67.02	3 min, 0 ℃

Table C5: Nitrosation Reagent: TBN , **5**

Reactor volume: Step 1=5 cm; Step 2= 100 cm

R1 **1** + Triethyl amine µL/min	R2 **2** µL/min	Step 1	Extraction step, H_2O µL/min	Extraction step, DCM µL/min	R3 TBN µL/min	Step 2
12.56	12.56	1 min, 50 ℃	50.24	25.12	50.2	5 min, 25/50 ℃
12.56	12.56	1 min, 50 ℃	50.24	25.12	12.56	8 min, 25 ℃

Table C6: DESI-MS data of the nitrosation reaction using 4 in different stoichiometries

Starting Material	Starting Material	Solvent	Stoichiometry	Product *m/z*	Intensity (Average)	Stdev	Intensity (max)	Normalized Intensity (Average)	Normalized Stdev	Normalized Intensity (max)	no of spots, n
3	**4**	Acetonitrile	150	169.2	213.3	191.6	934.1	0.025	0.030	0.166	144
3	**4**	Acetonitrile	150	234.7	8.0	6.7	45.1	0.001	0.001	0.007	144
3	**4**	Acetonitrile	150	239.4	1206.9	1349.7	6575.7	0.069	0.066	0.284	144
3	**4**	Acetonitrile	150	241.0	390.4	412.9	1980.9	0.022	0.020	0.088	144
3	**4**	Acetonitrile	150	250.4	143.7	184.3	923.0	0.008	0.005	0.024	144
3	**4**	Acetonitrile	150	251.2	34.7	40.6	205.3	0.002	0.001	0.006	144
3	**4**	Acetonitrile	150	337.4	831.0	707.6	4214.5	0.043	0.016	0.100	144
3	**4**	Acetonitrile	150	373.4	195.1	203.4	1017.1	0.010	0.006	0.026	144
3	**4**	Acetonitrile	100	169.2	428.3	487.1	3538.6	0.021	0.019	0.124	144
3	**4**	Acetonitrile	100	234.7	19.3	15.1	80.5	0.002	0.002	0.008	144
3	**4**	Acetonitrile	100	239.4	2066.8	2519.0	12435.6	0.061	0.049	0.220	144
3	**4**	Acetonitrile	100	241.0	664.8	776.1	3676.1	0.020	0.015	0.070	144
3	**4**	Acetonitrile	100	250.4	179.0	200.3	1072.1	0.006	0.003	0.016	144
3	**4**	Acetonitrile	100	251.2	50.4	57.4	348.6	0.002	0.001	0.005	144
3	**4**	Acetonitrile	100	337.4	1541.9	1537.4	9588.3	0.050	0.018	0.105	144
3	**4**	Acetonitrile	100	373.4	261.3	307.9	1751.0	0.008	0.004	0.022	144
3	**4**	Acetonitrile	50	169.2	53.9	58.1	322.0	0.018	0.019	0.105	144
3	**4**	Acetonitrile	50	234.7	11.7	16.2	177.5	0.004	0.002	0.015	144
3	**4**	Acetonitrile	50	239.4	382.9	825.0	5452.0	0.045	0.062	0.326	144
3	**4**	Acetonitrile	50	241.0	124.8	257.2	1692.1	0.016	0.019	0.101	144
3	**4**	Acetonitrile	50	250.4	21.3	24.1	145.3	0.005	0.002	0.012	144
3	**4**	Acetonitrile	50	251.2	6.3	6.7	37.3	0.001	0.001	0.004	144
3	**4**	Acetonitrile	50	337.4	116.2	130.7	681.0	0.020	0.015	0.075	144
3	**4**	Acetonitrile	50	373.4	21.0	24.5	133.5	0.004	0.003	0.014	144
3	**4**	Acetonitrile	200	169.2	134.4	122.3	642.8	0.007	0.002	0.012	144
3	**4**	Acetonitrile	200	234.7	7.7	8.7	57.9	0.001	0.001	0.003	144
3	**4**	Acetonitrile	200	239.4	2162.9	2123.7	15812.4	0.119	0.056	0.297	144
3	**4**	Acetonitrile	200	241.0	608.6	518.4	4106.0	0.035	0.017	0.090	144
3	**4**	Acetonitrile	200	250.4	39.5	26.3	138.1	0.003	0.001	0.006	144
3	**4**	Acetonitrile	200	251.2	20.5	49.7	382.9	0.001	0.000	0.002	144
3	**4**	Acetonitrile	200	337.4	485.0	296.1	1620.7	0.028	0.007	0.042	144
3	**4**	Acetonitrile	200	373.4	73.1	51.3	324.3	0.004	0.001	0.007	144
3	**4**	THF	200	169.2	1024.5	744.7	6746.3	0.041	0.059	0.443	144
3	**4**	THF	200	234.7	30.8	36.3	222.7	0.002	0.001	0.006	144
3	**4**	THF	200	239.4	1067.2	1527.8	7808.4	0.022	0.034	0.174	144
3	**4**	THF	200	241.0	333.9	480.7	2373.1	0.007	0.010	0.057	144
3	**4**	THF	200	250.4	749.2	367.0	2331.3	0.011	0.004	0.022	144
3	**4**	THF	200	251.2	237.1	227.8	1263.0	0.003	0.002	0.009	144
3	**4**	THF	200	337.4	13765.9	7680.8	50455.2	0.186	0.054	0.343	144
3	**4**	THF	200	373.4	1096.5	568.4	3314.2	0.016	0.005	0.038	144
3	**4**	THF	150	169.2	680.3	705.5	3251.7	0.036	0.033	0.202	144
3	**4**	THF	150	234.7	43.2	44.1	295.0	0.003	0.001	0.009	144
3	**4**	THF	150	239.4	1106.3	2107.4	12553.7	0.021	0.031	0.143	144
3	**4**	THF	150	241.0	366.5	601.2	2985.4	0.008	0.009	0.044	144
3	**4**	THF	150	250.4	349.0	338.2	1672.1	0.007	0.004	0.020	144
3	**4**	THF	150	251.2	92.1	92.6	353.0	0.002	0.001	0.008	144
3	**4**	THF	150	337.4	2590.0	3621.7	15618.2	0.044	0.051	0.185	144
3	**4**	THF	150	373.4	291.1	374.6	1736.1	0.006	0.006	0.024	144
3	**4**	THF	100	169.2	1152.9	849.2	4316.7	0.053	0.038	0.236	144
3	**4**	THF	100	234.7	40.4	42.7	243.0	0.002	0.001	0.014	144
3	**4**	THF	100	239.4	486.4	1259.8	8600.9	0.008	0.019	0.149	144
3	**4**	THF	100	241.0	166.2	407.2	2879.3	0.003	0.006	0.044	144
3	**4**	THF	100	250.4	1070.5	451.4	2449.5	0.013	0.004	0.020	144
3	**4**	THF	100	251.2	260.9	172.7	1492.2	0.003	0.001	0.011	144
3	**4**	THF	100	337.4	14213.4	9456.4	39713.7	0.157	0.076	0.339	144
3	**4**	THF	100	373.4	1262.2	675.0	3233.6	0.016	0.006	0.030	144
3	**4**	THF	50	169.2	708.7	560.9	3726.2	0.060	0.034	0.211	144
3	**4**	THF	50	234.7	46.1	56.3	341.8	0.003	0.002	0.020	144
3	**4**	THF	50	239.4	91.6	164.1	938.4	0.003	0.003	0.023	144
3	**4**	THF	50	241.0	54.0	70.6	369.5	0.003	0.003	0.015	144
3	**4**	THF	50	250.4	783.5	422.1	2172.0	0.012	0.003	0.018	144
3	**4**	THF	50	251.2	227.3	310.1	2172.0	0.003	0.002	0.014	144
3	**4**	THF	50	337.4	10050.7	9141.9	52775.8	0.125	0.074	0.268	144
3	**4**	THF	50	373.4	911.9	744.6	4270.9	0.012	0.006	0.022	144
Rhodamine				443.3	12213.1	8739.2	70545.6	0.491	0.101	0.690	384

Table C7: DESI-MS data of the nitrosation reaction using 4 as a nitrosation reagent

Starting Material	Starting Material	Solvent	Product *m/z*	Intensity (Average)	Stdev	Intensity (max)	Normalized Intensity (Average)	Normalized Stdev	Normalized Intensity (max)	No of spots, n
3	**4**	Toluene	169.2	2554.4	5564.3	36332.5	0.406	0.173	0.719	144
3	**4**	Toluene	205.7	7.2	10.4	63.4	0.003	0.003	0.015	144
3	**4**	Toluene	234.7	2.8	4.5	24.2	0.001	0.001	0.004	144
3	**4**	Toluene	239.4	2.7	5.8	38.3	0.000	0.001	0.007	144
3	**4**	Toluene	241.0	2.5	5.8	38.1	0.000	0.001	0.004	144
3	**4**	Toluene	250.4	1.4	4.4	43.3	0.000	0.001	0.004	144
3	**4**	Toluene	251.2	30.9	134.5	1279.6	0.002	0.006	0.039	144
3	**4**	Toluene	337.4	100.7	267.5	1413.6	0.007	0.018	0.146	144
3	**4**	Toluene	373.4	440.4	1209.9	8746.2	0.026	0.043	0.215	144
3	**4**	Acetonitrile	169.2	861.8	2266.6	24796.5	0.471	0.136	0.774	144
3	**4**	Acetonitrile	205.7	6.4	12.7	84.5	0.003	0.004	0.026	144
3	**4**	Acetonitrile	234.7	0.8	2.0	15.5	0.000	0.001	0.007	144
3	**4**	Acetonitrile	239.4	1.1	2.4	17.8	0.000	0.000	0.002	144
3	**4**	Acetonitrile	241.0	6.9	18.6	151.1	0.001	0.002	0.008	144
3	**4**	Acetonitrile	250.4	5.3	13.5	106.8	0.001	0.002	0.012	144
3	**4**	Acetonitrile	251.2	330.2	517.7	2676.7	0.039	0.035	0.213	144
3	**4**	Acetonitrile	337.4	46.4	73.3	493.7	0.005	0.006	0.033	144
3	**4**	Acetonitrile	373.4	651.5	1237.0	9488.0	0.065	0.035	0.190	144
3	**4**	DMSO	169.2	4904.5	8789.6	53558.7	0.355	0.137	0.642	144
3	**4**	DMSO	205.7	25.7	26.7	151.4	0.002	0.002	0.012	144
3	**4**	DMSO	234.7	1.8	2.3	13.1	0.000	0.001	0.002	144
3	**4**	DMSO	239.4	17.1	26.6	228.2	0.001	0.000	0.002	144
3	**4**	DMSO	241.0	5.2	6.1	26.9	0.000	0.000	0.002	144
3	**4**	DMSO	250.4	1.6	9.6	110.6	0.000	0.000	0.001	144
3	**4**	DMSO	251.2	101.2	179.2	1054.9	0.002	0.003	0.021	144
3	**4**	DMSO	337.4	443.8	791.7	4937.7	0.009	0.011	0.053	144
3	**4**	DMSO	373.4	2602.8	3506.2	30323.8	0.049	0.033	0.232	144
3	**4**	THF	169.2	1604.6	1828.4	9837.0	0.343	0.165	0.671	144
3	**4**	THF	205.7	14.3	16.2	107.3	0.002	0.003	0.014	144
3	**4**	THF	234.7	9.2	20.8	141.7	0.000	0.001	0.003	144
3	**4**	THF	239.4	68.5	72.4	381.6	0.002	0.002	0.007	144
3	**4**	THF	241.0	22.7	22.2	99.5	0.001	0.000	0.004	144
3	**4**	THF	250.4	4.1	7.3	32.2	0.000	0.000	0.001	144
3	**4**	THF	251.2	254.1	351.0	1963.4	0.008	0.008	0.040	144
3	**4**	THF	337.4	122.6	116.9	840.1	0.003	0.002	0.019	144
3	**4**	THF	373.4	3643.6	3629.0	24476.2	0.079	0.036	0.222	144
3	**4**	Ethanol	169.2	1939.9	2663.0	23988.5	0.315	0.159	0.644	144
3	**4**	Ethanol	205.7	18.0	22.0	108.9	0.003	0.003	0.017	144
3	**4**	Ethanol	234.7	9.7	28.9	313.9	0.001	0.001	0.003	144
3	**4**	Ethanol	239.4	3.1	3.4	20.9	0.000	0.000	0.002	144
3	**4**	Ethanol	241.0	4.1	3.4	17.3	0.000	0.000	0.003	144
3	**4**	Ethanol	250.4	3.5	3.4	17.0	0.000	0.000	0.002	144
3	**4**	Ethanol	251.2	53.0	37.6	152.7	0.002	0.001	0.006	144
3	**4**	Ethanol	337.4	263.7	193.3	1112.6	0.009	0.005	0.049	144
3	**4**	Ethanol	373.4	553.9	508.5	2842.8	0.024	0.010	0.074	144
3	**4**	DCM	169.2	463.4	643.7	3574.7	0.429	0.135	0.733	144
3	**4**	DCM	205.7	6.8	10.5	72.0	0.005	0.008	0.056	144
3	**4**	DCM	234.7	1.8	9.0	77.5	0.000	0.001	0.006	144
3	**4**	DCM	239.4	1.6	3.8	22.9	0.000	0.001	0.005	144
3	**4**	DCM	241.0	6.9	17.3	111.6	0.001	0.003	0.027	144
3	**4**	DCM	250.4	4.4	11.7	91.1	0.001	0.002	0.009	144
3	**4**	DCM	251.2	68.1	211.5	1683.3	0.009	0.014	0.103	144
3	**4**	DCM	337.4	32.4	77.4	572.0	0.007	0.013	0.060	144
3	**4**	DCM	373.4	381.0	586.2	3159.2	0.072	0.062	0.206	144
3	**4**	Ethyl Acetate	169.2	2710.5	3037.9	15437.7	0.325	0.124	0.586	144
3	**4**	Ethyl Acetate	205.7	23.4	33.0	173.7	0.005	0.006	0.042	144
3	**4**	Ethyl Acetate	234.7	7.6	29.1	260.3	0.001	0.002	0.017	144
3	**4**	Ethyl Acetate	239.4	2.0	3.6	16.7	0.000	0.000	0.002	144
3	**4**	Ethyl Acetate	241.0	4.7	9.6	73.9	0.000	0.000	0.002	144
3	**4**	Ethyl Acetate	250.4	3.5	7.4	58.3	0.000	0.000	0.002	144
3	**4**	Ethyl Acetate	251.2	115.4	304.2	2298.6	0.005	0.009	0.058	144
3	**4**	Ethyl Acetate	337.4	34.3	65.0	512.9	0.002	0.002	0.012	144
3	**4**	Ethyl Acetate	373.4	2627.7	3123.4	13965.7	0.104	0.081	0.247	144
3	**4**	Methanol	169.2	1516.5	3046.6	34891.7	0.369	0.172	0.780	144
3	**4**	Methanol	205.7	15.8	21.8	167.1	0.003	0.004	0.028	144
3	**4**	Methanol	234.7	1.3	1.6	7.2	0.000	0.001	0.002	144
3	**4**	Methanol	239.4	1.6	2.1	15.3	0.000	0.000	0.002	144
3	**4**	Methanol	241.0	2.7	4.0	22.3	0.000	0.000	0.002	144
3	**4**	Methanol	250.4	1.3	2.3	14.7	0.000	0.000	0.002	144
3	**4**	Methanol	251.2	19.6	25.3	173.7	0.001	0.001	0.006	144
3	**4**	Methanol	337.4	288.8	315.4	1590.6	0.013	0.010	0.052	144
3	**4**	Methanol	373.4	510.8	507.8	2698.7	0.027	0.014	0.072	144
3			443.3	12333.9	13328.7	384.0	0.354	0.083	0.646	384

Table C8: DESI-MS data of the nitrosation reaction using 5 as a nitrosation reagent

Starting Material	Starting Material	Solvent	Product*m/z*	Intensity (Average)	Stdev	Intensity (max)	Normalized Intensity (Average)	Normalized Stdev	Normalized Intensity (max)	No of spots, n
3	**5**	Ethyl Acetate	169.2	41.1	47.5	326.1	0.006	0.005	0.028	144
3	**5**	Ethyl Acetate	205.7	26.2	10.1	59.8	0.004	0.001	0.011	144
3	**5**	Ethyl Acetate	234.7	46.6	22.4	225.0	0.007	0.002	0.026	144
3	**5**	Ethyl Acetate	239.4	54.1	121.6	768.5	0.005	0.006	0.027	144
3	**5**	Ethyl Acetate	241.0	18.6	34.1	215.5	0.002	0.002	0.010	144
3	**5**	Ethyl Acetate	250.4	243.1	89.4	605.5	0.038	0.008	0.076	144
3	**5**	Ethyl Acetate	251.2	239.7	89.6	605.5	0.039	0.010	0.112	144
3	**5**	Ethyl Acetate	337.4	6.5	4.5	38.0	0.001	0.001	0.004	144
3	**5**	Ethyl Acetate	373.4	19.5	23.7	107.1	0.003	0.004	0.022	144
3	**5**	Ethanol	169.2	1059.5	1113.0	5710.9	0.047	0.027	0.128	144
3	**5**	Ethanol	205.7	44.2	47.6	224.7	0.002	0.001	0.006	144
3	**5**	Ethanol	234.7	22.5	14.2	73.3	0.001	0.000	0.002	144
3	**5**	Ethanol	239.4	437.1	485.3	2453.7	0.016	0.012	0.091	144
3	**5**	Ethanol	241.0	155.0	199.6	1496.5	0.005	0.004	0.027	144
3	**5**	Ethanol	250.4	75.4	57.5	339.3	0.003	0.002	0.009	144
3	**5**	Ethanol	251.2	33.5	21.6	123.8	0.001	0.000	0.003	144
3	**5**	Ethanol	337.4	28.4	16.3	85.8	0.001	0.000	0.003	144
3	**5**	Ethanol	373.4	547.1	727.2	4628.6	0.021	0.014	0.065	144
3	**5**	THF	169.2	77.4	147.1	824.4	0.008	0.009	0.066	144
3	**5**	THF	205.7	23.6	18.8	81.5	0.004	0.002	0.009	144
3	**5**	THF	234.7	55.6	74.9	771.9	0.008	0.004	0.020	144
3	**5**	THF	239.4	98.5	215.8	1279.6	0.008	0.010	0.046	144
3	**5**	THF	241.0	31.2	63.7	401.6	0.002	0.003	0.013	144
3	**5**	THF	250.4	278.7	221.3	1061.8	0.046	0.021	0.088	144
3	**5**	THF	251.2	285.5	222.9	1061.8	0.048	0.020	0.088	144
3	**5**	THF	337.4	5.7	5.9	46.3	0.001	0.001	0.007	144
3	**5**	THF	373.4	23.1	41.3	258.5	0.003	0.004	0.021	144
3	**5**	DCM	169.2	357.7	408.6	2428.0	0.028	0.018	0.076	144
3	**5**	DCM	205.7	56.1	22.9	159.1	0.005	0.002	0.011	144
3	**5**	DCM	234.7	111.7	69.4	561.9	0.010	0.003	0.017	144
3	**5**	DCM	239.4	255.9	372.5	1692.9	0.019	0.016	0.055	144
3	**5**	DCM	241.0	76.3	115.2	670.7	0.006	0.005	0.018	144
3	**5**	DCM	250.4	538.9	212.4	1632.1	0.057	0.017	0.086	144
3	**5**	DCM	251.2	551.4	202.1	1632.1	0.058	0.015	0.086	144
3	**5**	DCM	337.4	3.3	3.5	28.0	0.000	0.000	0.002	144
3	**5**	DCM	373.4	102.8	212.9	2118.2	0.007	0.007	0.038	144
3	**5**	Toluene	169.2	292.1	271.9	1570.8	0.025	0.016	0.098	144
3	**5**	Toluene	205.7	25.0	15.0	107.4	0.003	0.001	0.011	144
3	**5**	Toluene	234.7	37.9	32.5	268.9	0.005	0.001	0.012	144
3	**5**	Toluene	239.4	179.6	173.3	1095.6	0.012	0.007	0.034	144
3	**5**	Toluene	241.0	57.9	59.1	394.2	0.004	0.002	0.011	144
3	**5**	Toluene	250.4	257.8	80.3	515.9	0.040	0.006	0.054	144
3	**5**	Toluene	251.2	257.5	78.3	463.2	0.040	0.006	0.054	144
3	**5**	Toluene	337.4	5.5	4.5	24.3	0.001	0.000	0.002	144
3	**5**	Toluene	373.4	136.8	119.1	632.3	0.012	0.008	0.045	144
3	**5**	DMSO	169.2	3063.0	4126.1	20263.6	0.192	0.113	0.754	144
3	**5**	DMSO	205.7	28.5	52.8	347.2	0.003	0.002	0.014	144
3	**5**	DMSO	234.7	19.5	14.6	117.7	0.004	0.003	0.033	144
3	**5**	DMSO	239.4	30.2	77.6	745.0	0.002	0.003	0.016	144
3	**5**	DMSO	241.0	10.1	24.1	233.9	0.001	0.001	0.005	144
3	**5**	DMSO	250.4	108.8	94.5	872.6	0.020	0.008	0.039	144
3	**5**	DMSO	251.2	105.8	71.3	325.7	0.022	0.007	0.040	144
3	**5**	DMSO	337.4	5.5	8.9	57.0	0.001	0.001	0.007	144
3	**5**	DMSO	373.4	2038.4	3628.2	27327.2	0.095	0.060	0.239	144
3	**5**	Methanol	169.2	1526.0	1662.0	6465.5	0.070	0.055	0.179	144
3	**5**	Methanol	205.7	46.2	46.0	249.9	0.002	0.001	0.006	144
3	**5**	Methanol	234.7	24.3	25.1	113.3	0.001	0.000	0.003	144
3	**5**	Methanol	239.4	483.9	642.3	3403.1	0.019	0.017	0.090	144
3	**5**	Methanol	241.0	194.0	382.7	3346.8	0.006	0.006	0.029	144
3	**5**	Methanol	250.4	71.5	104.6	744.7	0.003	0.002	0.010	144
3	**5**	Methanol	251.2	43.1	65.4	548.5	0.002	0.001	0.006	144
3	**5**	Methanol	337.4	26.3	29.5	167.7	0.001	0.001	0.004	144
3	**5**	Methanol	373.4	1043.9	1687.0	11607.0	0.039	0.035	0.128	144
3	**5**	Acetonitrile	169.2	3290.0	3100.9	15073.0	0.150	0.056	0.313	144
3	**5**	Acetonitrile	205.7	33.4	12.5	102.0	0.004	0.001	0.008	144
3	**5**	Acetonitrile	234.7	57.2	44.7	317.8	0.006	0.002	0.012	144
3	**5**	Acetonitrile	239.4	187.1	221.0	1440.7	0.008	0.004	0.025	144
3	**5**	Acetonitrile	241.0	64.9	87.3	669.7	0.003	0.001	0.008	144
3	**5**	Acetonitrile	250.4	299.6	100.6	629.8	0.038	0.010	0.063	144
3	**5**	Acetonitrile	251.2	311.5	96.9	629.8	0.040	0.009	0.063	144
3	**5**	Acetonitrile	337.4	8.2	9.1	50.7	0.000	0.000	0.005	144
3	**5**	Acetonitrile	373.4	1274.8	1544.7	12113.3	0.049	0.025	0.120	144
3			443.3	40997.0	24891.7	384.0	0.654	0.118	0.807	384

APPENDIX D

A)

Base: DIPEA

		R1-B1	R1-B2	R1-B3	R1-B4	R1-B5	R1-B6	R1-B7	R1-B8	R1-B9	R1-B10	R1-B11	R1-B12 (S)	R1-B12 (D)
DESI-MS	R1-A1	31.7	28.0	24.5	868.6	17.8	23.0	3866.6	165.5	61.9	45.0	28.7	171.0	244.1
	R1-A2	52.3	29.5	32.6	21.2	5.5	5.8	59.3	40.8	14.4	6.5	17.3	258.0	669.6
	R1-A3	12.2	3.9	9.9	31.4	37.3	30.0	13.2	26.9	12.6	13.5	20.3	22.4	463.9
	R1-A4	410.3	56.8	136.5	1041.5	58.5	55.7	40.7	28.7	1412.2	206.0	9.2	87.7	2215.1
	R1-A5	24.3	6.6	5.3	135.1	32.6	30.6	44.0	9.5	31.2	30.9	28.3	51.0	116.8
	R1-A6	47.2	32.1	28.9	38.1	42.2	18.1	18.0	26.5	14.4	25.6	36.8	382.4	84.2
	R1-A7	38.5	30.0	20.0	4690.9	29.1	26.7	3444.5	183.3	135.2	38.1	31.8	2299.4	418.7
	R1-A8	124.2	14.8	14.4	19.4	26.7	30.4	29.1	20.8	25.1	21.4	16.6	16.6	117.4
15 h heating	R1-A1	3190.2	96.7	184.1	5502.0	1555.6	1730.2	4618.4	1363.4	7221.4	1584.5	31.3	27.0	243.1
	R1-A2	277.5	56.9	56.2	1978.4	93.7	120.0	123.8	226.0	759.2	63.5	24.2	357.7	605.4
	R1-A3	826.1	11.7	24.6	667.0	522.0	219.5	8.0	34.2	17.4	16.8	44.6	8.9	1069.7
	R1-A4	3499.9	641.3	3345.7	4973.7	7199.4	10005.9	1267.5	63.9	2467.0	5317.5	25.8	27.5	893.9
	R1-A5	1226.0	26.4	79.7	347.5	113.6	137.4	5435.5	17.2	488.3	54.4	44.4	67.8	431.9
	R1-A6	61.7	31.2	37.1	209.2	53.4	93.1	684.4	35.6	110.5	29.3	31.5	757.1	62.0
	R1-A7	6125.1	342.7	826.9	9886.8	4780.8	5175.7	15343.0	229.0	11798.2	2489.6	37.4	34.3	2467.7
	R1-A8	703.4	145.3	113.3	5357.4	69.5	72.8	360.8	68.8	1975.1	40.1	14.8	17.0	110.5

Base: NaO^tBu

		R1-B1	R1-B2	R1-B3	R1-B4	R1-B5	R1-B6	R1-B7	R1-B8	R1-B9	R1-B10	R1-B11	R1-B12 (S)	R1-B12 (D)
DESI-MS	R1-A1	47.4	42.1	36.5	36.3	15.8	16.5	757.3	74.0	49.0	31.9	29.0	167.6	167.8
	R1-A2	38.1	31.7	35.7	5.3	4.5	8.4	27.3	119.2	8.7	12.7	26.2	299.3	657.4
	R1-A3	6.9	6.3	7.0	31.7	22.8	26.6	11.0	20.1	5.9	25.2	39.2	9.8	347.9
	R1-A4	46.7	25.1	23.7	1256.3	16.8	16.6	36.1	76.6	266.1	29.4	11.8	52.7	1579.4
	R1-A5	11.1	10.8	8.0	28.7	22.2	25.7	47.7	11.2	15.2	22.0	23.3	41.0	192.5
	R1-A6	38.8	36.2	42.9	69.3	67.6	16.7	34.0	35.0	85.3	17.7	25.9	392.4	82.7
	R1-A7	54.0	38.5	17.7	295.2	35.6	24.0	669.9	211.1	35.2	25.5	62.9	3230.9	378.7
	R1-A8	207.6	542.7	55.8	2714.9	39.4	51.8	698.4	32.3	633.1	30.2	18.7	8.9	152.3
15 h heating	R1-A1	515.8	69.9	60.0	170.3	109.0	31.4	181.3	822.8	209.2	86.0	30.4	26.8	162.9
	R1-A2	28.5	40.4	38.0	10.7	7.8	8.0	44.1	34.3	6.0	13.8	18.2	281.6	451.3
	R1-A3	209.4	14.9	8.3	112.3	41.2	32.3	21.1	19.3	11.1	12.7	62.8	10.9	1220.1
	R1-A4	1170.9	137.5	167.3	1502.7	35.6	27.9	31.5	17.8	1235.4	262.7	22.7	30.6	551.2
	R1-A5	90.6	15.2	14.0	36.8	45.1	55.5	86.3	11.2	37.9	22.9	25.1	53.0	321.1
	R1-A6	566.7	38.5	43.6	212.3	221.5	28.5	16.0	17.7	250.6	54.1	30.1	40.0	61.4
	R1-A7	10173.7	96.6	133.7	1417.9	76.1	64.4	159.4	994.0	576.2	110.1	38.8	37.1	1598.8
	R1-A8	12616.3	2644.3	4162.5	1908.6	798.0	755.3	297.3	1552.9	144.8	126.9	129.6	18.2	101.1

Base: TEA

		R1-B1	R1-B2	R1-B3	R1-B4	R1-B5	R1-B6	R1-B7	R1-B8	R1-B9	R1-B10	R1-B11	R1-B12 (S)	R1-B12 (D)
DESI-MS	R1-A1	31.4	25.9	25.9	668.2	26.9	16.0	1744.8	410.6	43.2	53.9	15.1	205.9	287.8
	R1-A2	42.9	29.3	34.3	6.7	6.7	2.2	55.9	30.2	19.0	11.0	17.1	495.8	981.8
	R1-A3	22.9	5.6	7.5	27.4	42.6	29.7	10.8	23.4	13.3	16.7	15.9	13.7	339.6
	R1-A4	256.2	52.7	133.8	816.7	68.1	49.8	112.8	71.0	1664.2	347.5	13.8	93.2	1968.0
	R1-A5	26.7	9.8	8.5	152.8	27.4	37.6	73.6	13.6	30.9	34.2	44.0	32.2	126.9
	R1-A6	59.6	28.9	36.0	61.0	56.8	72.5	16.3	31.5	18.2	14.0	33.3	494.6	125.7
	R1-A7	70.0	27.2	18.8	2975.9	25.5	31.1	2116.1	323.6	203.9	41.0	37.8	1476.6	844.8
	R1-A8	31.5	69.0	29.1	35.5	19.0	18.8	27.0	21.0	31.9	24.3	15.5	25.3	206.6
15 h heating	R1-A1	4415.0	355.7	453.5	3898.7	1419.4	930.9	2006.8	4209.2	4961.7	2439.3	31.6	23.6	316.0
	R1-A2	906.0	36.7	74.6	203.1	60.0	50.2	21.8	119.0	1585.2	68.6	20.8	330.7	631.4
	R1-A3	458.9	11.7	11.4	674.5	364.5	194.2	19.3	26.3	13.2	13.1	64.8	13.6	1876.8
	R1-A4	2947.3	1736.2	4490.4	4408.3	5651.0	8079.0	1990.6	88.3	3114.8	7248.9	20.5	14.9	576.4
	R1-A5	1807.1	53.5	161.3	407.2	119.9	130.8	1726.1	100.2	784.9	344.6	31.4	81.7	589.7
	R1-A6	81.8	29.7	30.5	236.9	75.9	88.2	210.1	57.4	50.3	25.2	45.0	78.0	107.6
	R1-A7	4214.8	579.6	427.5	6296.3	3314.8	2428.3	13119.6	745.7	8081.4	2200.2	53.7	117.8	686.0
	R1-A8	2620.4	56.2	85.3	3787.6	82.5	89.2	997.8	73.1	2200.6	18.7	15.5	16.4	109.0

Base: No base

		R1-B1	R1-B2	R1-B3	R1-B4	R1-B5	R1-B6	R1-B7	R1-B8	R1-B9	R1-B10	R1-B11	R1-B12 (S)	R1-B12 (D)
DESI-MS	R1-A1	20.3	25.0	25.2	230.2	11.6	12.1	961.5	216.0	61.4	38.9	19.0	381.6	311.1
	R1-A2	31.2	39.2	36.0	4.2	7.4	3.2	41.3	22.9	7.0	8.3	19.9	497.3	764.0
	R1-A3	18.2	4.8	9.6	24.3	26.1	23.8	17.7	19.2	10.0	11.3	14.2	14.4	316.8
	R1-A4	195.8	50.7	79.7	429.5	57.3	44.4	99.1	34.0	1249.7	135.9	10.5	67.8	1051.8
	R1-A5	19.9	13.0	11.8	73.4	28.7	27.6	34.2	7.2	25.1	23.8	53.6	18.5	144.2
	R1-A6	44.6	49.9	71.2	75.7	63.9	57.0	25.0	22.9	25.3	16.9	35.2	248.4	122.1
	R1-A7	61.7	18.6	26.8	2092.5	31.7	26.5	2431.8	251.9	61.7	28.9	34.4	5218.1	1930.3
	R1-A8	139.9	42.5	33.9	37.7	17.5	14.8	52.4	14.4	30.9	12.2	13.3	29.3	175.4
15 h heating	R1-A1	2227.5	128.2	264.1	6332.4	936.7	1176.3	3019.4	1228.2	5713.0	811.7	24.3	15.4	1598.0
	R1-A2	705.9	108.9	81.4	3748.9	466.8	1010.0	236.3	121.9	699.4	94.5	16.1	349.6	530.2
	R1-A3	1151.9	16.7	15.6	806.2	552.9	203.9	11.6	22.0	19.0	34.4	26.2	12.7	2050.1
	R1-A4	1763.0	1480.0	1688.8	7254.4	2988.2	8730.5	2784.0	72.4	2232.3	7262.8	10.3	83.8	558.3
	R1-A5	952.0	70.7	27.1	536.2	95.0	141.2	2197.2	13.7	356.2	37.8	33.7	20.2	561.1
	R1-A6	53.5	40.1	34.8	2411.4	58.7	87.4	112.6	36.8	41.2	34.1	28.8	28.0	80.0
	R1-A7	3759.6	345.3	177.2	9100.4	2474.4	2045.4	14913.2	224.9	5458.0	1381.9	45.6	26.5	12413.1
	R1-A8	352.7	45.5	27.4	7312.9	53.4	48.2	1181.3	14.1	597.6	38.2	11.6	13.5	114.9

B)

Base: DIPEA

		R1-B1	R1-B2	R1-B3	R1-B4	R1-B5	R1-B6	R1-B7	R1-B8	R1-B9	R1-B10	R1-B11	R1-B12 (S)	R1-B12 (D)
DESI-MS	R1-A1	34.1	43.4	39.6	64.1	53.1	56.1	1146.4	45.2	72.3	32.1	37.4	73.5	1511.9
	R1-A2	29.8	52.7	52.7	20.0	5.8	7.2	27.8	56.2	12.3	36.9	54.3	47.8	937.9
	R1-A3	74.5	52.3	76.0	27.5	74.9	55.0	55.5	41.2	18.4	17.3	19.2	28.3	111.3
	R1-A4	332.8	82.0	88.6	511.5	203.4	497.8	504.4	35.4	17.3	46.4	14.9	30.0	242.6
	R1-A5	326.8	155.4	97.1	45.1	33.7	25.8	325.1	21.3	17.3	23.9	47.3	22.4	200.1
	R1-A6	59.1	76.0	69.1	355.6	258.0	281.5	97.3	51.0	81.8	55.5	41.0	47.4	91.0
	R1-A7	233.8	388.0	398.4	63.3	40.9	41.5	3349.6	77.6	32.7	48.1	40.6	46.7	223.3
	R1-A8	316.5	62.0	40.2	44.0	41.9	34.4	72.4	29.6	28.9	41.7	28.4	35.7	114.7
15 h heating	R1-A1	192.9	22.2	34.4	1434.0	34.6	149.1	3245.3	78.6	76.2	24.4	56.2	49.4	201.0
	R1-A2	31.5	43.9	37.6	115.7	25.1	32.4	43.8	104.5	42.9	46.5	43.7	97.1	379.0
	R1-A3	129.8	85.2	70.0	1271.0	270.3	474.3	51.2	30.6	26.4	13.4	538.0	26.4	159.6
	R1-A4	804.0	506.7	481.4	6017.3	2571.8	5834.3	9662.2	92.0	50.5	51.1	50.6	140.4	171.2
	R1-A5	248.3	67.4	40.3	272.1	30.1	37.8	7219.7	22.1	24.8	18.1	21.9	59.7	152.0
	R1-A6	50.8	77.0	92.8	443.1	195.7	181.1	565.0	43.6	51.9	25.8	181.9	94.8	109.6
	R1-A7	1217.9	456.7	426.0	4228.0	1030.4	1271.5	8747.6	89.7	37.8	43.5	61.2	56.1	208.3
	R1-A8	1640.6	1819.0	860.8	4791.9	19.3	11.6	530.2	36.6	20.7	26.4	27.7	75.8	92.2

Base: NaO^tBu

		R1-B1	R1-B2	R1-B3	R1-B4	R1-B5	R1-B6	R1-B7	R1-B8	R1-B9	R1-B10	R1-B11	R1-B12 (S)	R1-B12 (D)
DESI-MS	R1-A1	86.5	37.9	53.0	69.0	27.9	38.9	392.8	62.4	50.2	41.4	21.6	80.4	610.3
	R1-A2	37.0	37.2	32.4	6.9	4.7	7.2	36.6	138.1	9.1	14.1	12.1	28.2	549.9
	R1-A3	15.6	19.9	17.1	38.2	31.6	29.0	121.2	17.2	15.0	14.1	73.7	43.2	53.6
	R1-A4	69.4	46.9	39.2	138.0	200.7	69.2	52.3	31.8	20.5	292.7	8.6	10.8	224.6
	R1-A5	21.0	20.6	24.7	54.7	29.2	30.4	92.9	11.5	14.0	14.8	27.6	8.9	49.4
	R1-A6	61.2	49.0	70.1	164.6	76.9	62.4	8749.3	46.5	42.5	27.9	19.4	40.2	68.5
	R1-A7	46.7	42.2	37.5	36.5	34.2	18.5	649.1	39.9	27.1	30.2	12.2	15.0	74.7
	R1-A8	58.0	38.3	43.3	32.4	23.8	13.9	85.3	129.7	19.2	35.7	29.5	14.4	52.8
15 h heating	R1-A1	34.2	26.8	27.9	36.3	19.2	21.1	537.4	38.6	43.7	51.6	27.9	31.4	119.5
	R1-A2	37.9	38.5	46.4	22.0	7.5	12.4	26.3	469.1	10.7	10.5	14.4	42.0	386.5
	R1-A3	26.1	83.4	26.1	53.0	43.3	21.4	59.3	20.2	21.2	16.4	14.7	13.9	61.8
	R1-A4	46.6	90.7	62.5	269.1	145.6	98.7	2558.7	22.0	26.6	322.8	24.9	15.5	95.1
	R1-A5	15.7	26.3	27.7	54.0	39.6	91.0	230.4	16.5	25.0	31.5	31.9	12.9	49.6
	R1-A6	86.0	97.7	102.5	54.7	45.8	26.8	75.1	29.5	26.8	46.1	31.4	19.3	81.5
	R1-A7	114.3	72.7	44.4	80.9	57.6	22.8	1007.4	61.6	35.5	55.2	36.6	16.9	63.3
	R1-A8	80.9	47.8	42.8	40.2	30.4	22.1	59.5	10.7	16.0	28.9	15.7	20.6	59.7

Base: TEA

		R1-B1	R1-B2	R1-B3	R1-B4	R1-B5	R1-B6	R1-B7	R1-B8	R1-B9	R1-B10	R1-B11	R1-B12 (S)	R1-B12 (D)
DESI-MS	R1-A1	28.0	48.2	45.3	96.7	27.7	53.7	572.9	42.7	66.7	28.2	45.6	32.6	969.7
	R1-A2	26.3	41.0	62.3	29.3	47.2	24.2	19.9	54.5	7.5	38.0	44.2	29.1	328.1
	R1-A3	43.3	24.2	39.7	39.9	68.6	107.6	38.1	27.9	18.6	17.7	42.4	14.9	130.3
	R1-A4	253.5	88.7	149.5	656.1	159.9	611.1	573.4	29.8	29.0	47.5	19.0	38.4	185.6
	R1-A5	137.1	70.0	108.5	57.9	38.7	29.1	1862.1	19.6	24.4	27.0	49.2	22.2	101.1
	R1-A6	55.7	69.2	94.0	373.2	218.4	152.5	119.7	34.8	71.2	38.1	35.4	36.5	103.0
	R1-A7	183.4	220.4	353.6	264.8	68.9	99.1	2768.9	71.6	37.2	41.4	55.4	38.9	248.0
	R1-A8	102.1	2072.7	399.7	34.3	22.4	22.5	50.5	18.6	20.1	11.3	19.8	21.6	127.9
15 h heating	R1-A1	149.2	24.1	42.9	1579.2	53.8	91.9	4517.8	62.7	81.7	29.3	34.8	233.7	253.1
	R1-A2	31.9	62.9	64.6	118.1	23.8	22.6	25.6	174.7	42.6	99.3	141.5	43.1	230.8
	R1-A3	100.6	101.1	61.2	3364.5	216.8	571.2	74.1	39.6	20.5	17.8	479.3	70.4	128.2
	R1-A4	129.4	673.4	539.9	13179.8	1626.7	5754.4	1339.5	86.0	73.6	34.0	61.5	224.1	134.8
	R1-A5	107.7	133.5	29.1	167.5	38.9	34.5	6762.9	32.7	37.0	28.5	41.0	73.8	106.9
	R1-A6	52.1	90.3	75.4	224.3	137.1	128.0	339.7	36.5	51.4	24.6	136.6	122.4	129.9
	R1-A7	1486.9	425.0	535.5	9830.6	631.7	484.6	7931.6	88.6	55.6	81.0	65.8	66.5	143.6
	R1-A8	1964.7	1621.4	2018.3	54.6	66.9	18.6	597.6	18.4	13.4	38.6	111.8	49.7	80.9

Base: No base

		R1-B1	R1-B2	R1-B3	R1-B4	R1-B5	R1-B6	R1-B7	R1-B8	R1-B9	R1-B10	R1-B11	R1-B12 (S)	R1-B12 (D)
DESI-MS	R1-A1	30.0	50.6	31.9	45.4	20.6	30.9	676.5	66.9	47.7	29.9	32.8	101.6	673.3
	R1-A2	39.2	38.2	57.6	13.5	6.1	6.8	26.1	109.2	7.8	14.9	29.7	26.8	345.8
	R1-A3	49.3	42.3	55.8	83.5	43.2	37.1	40.2	21.0	14.0	10.8	19.4	18.0	54.2
	R1-A4	230.3	81.6	139.6	372.0	211.7	214.3	373.9	34.7	17.5	138.0	3.6	17.7	136.2
	R1-A5	190.7	109.8	122.9	52.9	33.0	52.9	278.5	19.5	25.3	24.1	24.4	9.4	64.8
	R1-A6	63.6	80.0	87.6	253.6	212.4	271.5	129.2	32.5	124.5	59.7	22.2	28.5	45.9
	R1-A7	128.7	212.1	454.8	47.9	28.4	35.5	1539.1	85.8	45.6	35.5	27.9	21.4	168.2
	R1-A8	1826.2	319.7	550.0	24.8	20.6	12.5	61.5	27.2	10.7	20.1	6.9	15.9	102.6
15 h heating	R1-A1	148.2	24.6	35.5	1429.4	21.6	72.7	1784.6	132.6	44.0	59.8	31.5	61.7	134.0
	R1-A2	56.5	74.9	255.8	88.8	6.4	6.9	144.0	314.4	11.7	35.4	19.7	12.7	210.0
	R1-A3	143.6	69.6	56.1	1681.9	96.6	464.0	22.0	35.3	13.9	22.0	373.6	19.9	44.5
	R1-A4	2030.4	455.3	643.6	7339.9	2065.5	6621.2	8273.6	59.7	49.6	241.1	36.2	55.3	50.0
	R1-A5	47.8	30.3	37.9	74.6	27.6	43.0	8215.1	34.1	28.4	24.8	31.9	23.2	79.0
	R1-A6	404.0	106.2	109.7	284.0	100.8	189.9	664.1	104.4	52.1	19.8	169.8	77.2	83.6
	R1-A7	1228.6	311.6	174.9	4752.6	349.3	686.4	8343.6	92.1	82.6	64.6	49.7	30.1	103.2
	R1-A8	890.4	545.5	793.8	86.9	14.4	21.7	846.6	147.3	31.2	31.6	13.9	60.2	78.5

Figure D1: Heat map of 1,536 reactions of R-1 S_NAr HTE using MeOH with 1% FA as spray solvent at 150 °C. A) reaction solvent: NMP; B) reaction solvent: 1,4-dioxane.

A)

Base: DIPEA

		R1-B1	R1-B2	R1-B3	R1-B4	R1-B5	R1-B6	R1-B7	R1-B8	R2-B9	R1-B10	R1-B11	R1-B12 (S)	R1-B12 (D)
DESI-MS	R2-A1	4.2	1.6	0.0	4.9	1.1	2.0	59.6	3.5	1.8	3.2	5.0	11.1	111.0
	R2-A2	5.5	3.6	7.5	12.7	7.9	12.4	0.6	9.7	8.8	11.8	5.0	146.2	239.2
	R2-A3	3.4	3.7	3.3	14.3	6.9	15.2	5.8	7.5	8.5	15.7	4.7	37.5	57.0
	R2-A4	1.6	1.7	1.9	5.4	2.7	2.5	609.9	3.9	1.4	2.1	77.6	8.9	34.5
	R2-A5	1.4	0.0	0.5	15.0	14.7	10.7	44.9	5.5	33.4	7.0	13.0	29.5	59.5
	R2-A6	20.1	4.6	2.0	284.7	1.1	6.4	879.2	4.5	3.9	3.2	4.3	55.3	325.5
	R2-A7	1.4	0.8	0.7	3.6	5.8	5.1	0.8	1.6	0.0	2.1	9.1	4.3	45.0
	R2-A8	10.8	9.5	16.1	9.1	4.2	5.1	9.3	15.8	15.1	15.5	5.5	9.6	25.0
1 h heating	R2-A1	7.0	4.2	1.7	13.8	3.0	11.1	56.7	4.4	5.1	4.0	3.8	7.7	72.8
	R2-A2	2.0	5.0	4.7	16.4	7.6	10.4	21.0	9.8	9.2	11.0	23.2	78.1	194.3
	R2-A3	5.1	6.8	3.7	13.0	5.5	10.6	18.4	23.1	41.6	16.5	2.8	20.0	43.7
	R2-A4	2.5	3.7	4.0	8.7	3.3	2.4	682.1	5.5	5.1	4.7	52.3	6.6	22.5
	R2-A5	18.8	2.0	6.9	26.6	9.9	18.7	1216.9	6.6	7.9	3.6	22.9	15.4	78.4
	R2-A6	530.9	27.4	98.9	895.2	180.6	264.4	4688.6	5.5	12.8	6.1	9.4	13.7	210.3
	R2-A7	2.2	1.8	2.9	6.6	4.4	12.9	7.6	11.3	2.2	1.3	4.0	4.4	48.6
	R2-A8	11.3	14.8	9.0	14.5	12.5	17.4	311.9	13.7	13.2	13.5	17.1	4.5	86.1
4 h heating	R2-A1	4.6	7.0	3.2	18.8	4.0	3.6	45.1	5.7	3.1	8.0	4.1	13.8	93.5
	R2-A2	2.3	5.6	4.4	15.4	8.9	13.5	26.9	10.2	13.7	7.2	34.0	100.1	189.3
	R2-A3	2.1	4.5	3.2	10.7	14.3	11.6	7.7	13.7	20.7	26.4	1.1	19.0	89.4
	R2-A4	1.3	3.1	2.8	8.5	2.0	4.3	595.4	3.7	2.7	4.2	50.0	15.9	33.5
	R2-A5	33.3	2.3	2.3	28.2	14.8	15.4	652.0	6.4	6.1	6.9	32.5	24.8	161.1
	R2-A6	612.2	30.4	65.6	1260.8	273.0	202.6	3237.5	12.1	10.4	5.5	6.8	6.4	305.5
	R2-A7	2.6	5.5	2.6	12.7	12.1	11.2	3.8	2.7	4.7	2.0	6.5	11.3	49.2
	R2-A8	10.2	10.3	13.7	18.3	8.8	13.3	250.1	10.4	13.1	14.1	10.4	3.0	72.6
15 h heating	R2-A1	1.6	11.4	13.1	21.7	4.9	7.3	38.5	4.5	2.6	5.5	6.1	19.2	58.4
	R2-A2	5.3	5.0	10.3	13.8	10.6	6.9	8.8	7.7	10.4	10.6	4.2	101.5	153.6
	R2-A3	5.2	2.7	3.9	14.4	9.8	10.2	10.4	13.4	17.2	9.8	4.5	21.8	74.9
	R2-A4	2.4	3.2	4.5	13.9	3.5	2.6	553.0	8.9	2.9	3.0	14.2	15.6	25.9
	R2-A5	63.3	1.9	4.3	32.5	12.1	14.5	971.1	11.4	7.7	4.0	26.3	15.5	49.7
	R2-A6	692.2	39.0	82.1	1208.8	24.2	123.6	3852.7	49.3	6.8	9.4	6.1	10.9	77.1
	R2-A7	1.7	1.6	3.4	9.0	10.4	12.2	9.8	3.9	4.0	1.1	4.3	15.6	83.5
	R2-A8	12.0	10.2	9.8	22.9	10.0	20.5	575.2	12.3	12.6	12.3	13.3	2.4	34.3

Base: NaO^{t}Bu

B)

		R1-B1	R1-B2	R1-B3	R1-B4	R1-B5	R1-B6	R1-B7	R1-B8	R2-B9	R1-B10	R1-B11	R1-B12 (S)	R1-B12 (D)
DESI-MS	R2-A1	6.8	5.1	13.9	10.5	5.5	9.4	54.7	4.1	2.9	4.3	7.8	18.2	165.8
	R2-A2	11.1	6.6	12.0	94.9	8.6	12.4	1.6	49.7	36.2	19.3	7.1	217.0	299.0
	R2-A3	14.5	8.9	13.8	9.2	10.4	18.0	8.4	12.0	7.6	18.8	4.1	17.9	80.8
	R2-A4	1.8	2.1	3.5	3.6	15.5	4.7	742.8	4.0	2.8	2.8	71.7	7.6	27.2
	R2-A5	0.6	2.7	3.3	12.8	27.9	12.4	40.0	8.7	13.8	8.8	31.2	28.4	115.5
	R2-A6	6.1	3.5	3.4	32.5	8.1	6.3	51.4	15.4	28.8	6.4	1.2	54.5	405.7
	R2-A7	1.5	18.8	13.5	10.3	42.3	39.7	8.0	6.2	5.2	1.7	10.7	6.0	38.2
	R2-A8	11.5	11.2	9.3	82.5	36.9	8.3	2.6	16.0	10.6	12.9	4.2	30.1	131.6
1 h heating	R2-A1	78.7	3.3	13.8	28.7	8.5	10.8	92.9	22.6	4.9	3.4	19.1	11.8	91.7
	R2-A2	29.2	8.0	10.9	114.6	24.1	29.9	15.7	19.3	25.0	29.4	5.6	227.4	280.7
	R2-A3	1.9	6.5	11.1	11.1	7.8	17.9	17.6	34.7	67.8	20.9	3.2	20.4	148.8
	R2-A4	3.8	4.4	4.2	13.5	19.3	17.6	734.7	7.7	8.4	26.6	13.5	6.5	44.5
	R2-A5	1.6	2.9	5.8	13.1	15.7	31.1	273.6	12.4	17.4	7.2	41.6	14.0	209.5
	R2-A6	183.8	18.7	21.9	315.7	37.8	13.5	23.5	13.5	13.7	10.6	5.5	63.1	545.6
	R2-A7	6.2	12.6	14.7	5.7	9.7	14.5	5.0	4.3	6.4	4.4	6.1	9.7	38.6
	R2-A8	67.5	55.1	60.8	72.3	49.3	15.9	103.7	21.2	15.7	18.5	15.6	12.9	102.8
4 h heating	R2-A1	169.5	4.7	8.7	15.6	6.5	14.6	17.7	22.3	9.9	8.5	18.2	14.0	147.5
	R2-A2	22.2	8.0	9.0	41.2	10.3	19.0	15.3	22.2	28.9	24.5	17.4	206.8	302.9
	R2-A3	3.5	4.2	10.5	11.0	10.3	16.8	17.6	15.9	35.1	13.6	3.7	20.2	85.7
	R2-A4	2.9	3.1	3.6	8.8	17.1	12.7	821.4	11.8	4.7	23.4	16.2	7.3	55.1
	R2-A5	1.2	6.0	3.5	10.2	14.7	25.8	171.8	18.0	17.1	11.6	34.3	31.4	178.6
	R2-A6	149.5	14.3	14.7	227.0	45.1	12.5	29.8	20.9	12.3	15.0	5.5	60.6	484.5
	R2-A7	1.3	19.6	6.9	9.6	11.2	17.3	8.7	2.9	3.7	4.6	8.9	5.8	57.2
	R2-A8	78.7	49.3	42.3	71.2	50.6	19.1	76.1	30.5	21.1	17.7	12.0	18.0	58.1
15 h heating	R2-A1	41.0	6.9	8.7	18.2	14.6	15.6	18.4	13.8	1.8	7.8	12.9	15.9	83.4
	R2-A2	12.4	8.5	12.5	22.2	15.3	12.7	8.3	19.6	12.4	7.5	4.8	187.5	239.2
	R2-A3	2.4	5.1	8.0	11.2	8.2	16.0	14.2	13.7	27.1	14.5	3.9	18.4	75.6
	R2-A4	3.1	4.3	5.5	10.9	14.4	14.3	867.5	8.6	5.2	19.8	12.7	5.6	33.4
	R2-A5	7.5	2.1	5.8	21.7	17.1	24.6	445.0	9.5	9.4	11.6	41.9	27.0	77.3
	R2-A6	496.3	17.1	30.1	356.2	53.2	9.1	70.0	16.7	3.4	9.2	6.8	10.2	307.6
	R2-A7	0.7	10.0	13.3	2.9	8.2	9.5	8.3	7.6	2.9	5.9	5.0	13.3	55.6
	R2-A8	84.8	45.3	47.9	57.2	31.5	14.6	94.3	17.8	25.4	30.7	12.8	23.6	30.7

Base: TEA

C)

		R1-B1	R1-B2	R1-B3	R1-B4	R1-B5	R1-B6	R1-B7	R1-B8	R2-B9	R1-B10	R1-B11	R1-B12 (S)	R1-B12 (D)
DESI-MS	R2-A1	9.6	1.2	1.8	1.7	1.9	0.0	42.5	4.3	2.5	2.2	2.1	13.0	120.7
	R2-A2	4.6	3.5	4.9	9.5	7.5	11.2	0.5	9.2	10.9	13.5	2.3	150.8	238.1
	R2-A3	1.4	3.1	1.8	12.6	16.5	15.1	2.9	7.4	5.0	8.4	3.1	34.8	151.0
	R2-A4	0.0	3.4	2.8	5.1	4.4	1.5	555.8	0.7	2.5	0.0	33.5	8.4	32.5
	R2-A5	2.6	0.6	0.0	144.1	92.5	153.5	86.3	12.5	9.1	8.1	23.6	45.3	66.9
	R2-A6	27.3	4.6	4.5	180.8	10.8	3.9	328.4	15.5	4.0	5.7	4.8	66.1	294.0
	R2-A7	2.0	1.1	1.3	9.3	2.6	2.0	1.8	1.9	1.9	0.6	9.7	4.5	43.6
	R2-A8	11.2	13.5	10.4	9.5	9.4	3.6	13.2	13.7	15.3	14.5	12.5	11.9	39.2
1 h heating	R2-A1	4.6	1.0	6.1	7.0	1.4	5.9	69.6	3.2	0.7	1.8	5.5	11.4	140.6
	R2-A2	2.7	4.1	5.6	16.4	6.3	7.1	1.4	10.7	20.2	18.9	3.1	178.0	188.7
	R2-A3	1.3	3.6	1.8	13.3	13.7	8.4	5.8	19.3	30.3	16.9	3.8	26.3	58.7
	R2-A4	0.6	6.9	3.7	5.0	1.3	3.5	557.5	3.7	3.0	2.7	23.8	4.7	25.5
	R2-A5	16.9	0.6	2.4	34.8	15.6	13.9	967.8	9.0	14.5	7.7	17.7	34.5	168.3
	R2-A6	256.9	26.8	46.2	1107.0	264.2	340.3	2758.4	14.3	4.4	4.7	3.7	5.4	795.6
	R2-A7	1.4	1.4	2.7	11.5	6.9	9.0	1.1	6.6	5.2	1.9	7.9	5.0	44.7
	R2-A8	6.8	11.8	8.3	9.6	13.1	10.8	123.1	11.5	12.6	14.3	9.3	4.5	106.2
4 h heating	R2-A1	2.4	0.6	3.1	13.7	0.5	4.5	44.8	0.0	1.5	2.8	5.9	12.4	110.7
	R2-A2	3.3	3.3	4.0	9.2	9.1	10.6	3.4	11.8	9.3	6.6	6.5	127.7	209.9
	R2-A3	2.2	2.2	1.7	12.8	11.6	9.9	9.1	26.0	35.5	13.9	3.9	13.2	61.9
	R2-A4	2.7	7.2	2.6	4.7	2.3	3.9	533.8	5.8	4.8	1.8	15.7	6.9	32.3
	R2-A5	25.9	4.0	4.1	36.3	17.7	16.1	404.2	9.2	10.7	14.9	26.5	20.5	174.7
	R2-A6	354.1	29.6	45.8	1285.1	277.9	249.2	2767.3	14.9	9.4	3.7	4.1	11.5	770.0
	R2-A7	2.4	2.9	2.1	11.2	17.4	10.6	2.8	5.7	3.5	4.6	10.5	4.3	47.1
	R2-A8	7.3	8.1	10.0	17.0	18.7	11.3	293.9	18.2	11.4	12.6	8.4	7.2	134.9
15 h heating	R2-A1	5.2	3.3	4.8	11.4	1.1	2.5	74.8	2.8	2.7	4.0	5.3	24.0	72.8
	R2-A2	2.1	3.0	5.9	14.0	5.6	8.4	1.9	14.6	13.7	9.2	6.1	139.4	255.2
	R2-A3	3.1	1.4	1.3	18.0	12.1	9.8	12.8	15.9	14.0	18.0	3.6	25.8	108.5
	R2-A4	1.2	2.3	3.5	11.4	3.7	4.3	547.7	2.0	8.1	3.1	29.3	6.8	22.1
	R2-A5	7.7	1.1	2.9	37.1	22.0	21.3	479.9	11.5	16.7	6.6	19.4	39.8	103.2
	R2-A6	366.9	33.1	67.0	1216.9	127.7	320.2	3017.0	63.6	6.6	6.0	7.7	4.2	239.0
	R2-A7	4.1	1.6	3.5	10.1	15.9	13.2	4.8	7.5	3.1	1.5	11.0	8.7	43.9
	R2-A8	16.4	12.0	13.7	19.6	17.2	20.8	620.3	14.4	11.6	13.8	18.4	5.7	83.3

Base: No base

D)

		R1-B1	R1-B2	R1-B3	R1-B4	R1-B5	R1-B6	R1-B7	R1-B8	R2-B9	R1-B10	R1-B11	R1-B12 (S)	R1-B12 (D)
DESI-MS	R2-A1	3.6	1.3	1.2	1.2	2.0	1.8	56.9	4.1	3.8	1.9	4.5	16.3	132.6
	R2-A2	1.9	7.7	4.1	5.5	13.0	12.0	0.6	13.0	10.4	11.6	3.4	244.6	451.9
	R2-A3	0.7	3.6	1.7	7.4	7.8	15.2	7.1	12.2	6.6	12.0	4.4	37.1	90.8
	R2-A4	1.2	3.0	1.4	4.5	3.2	4.6	844.5	5.1	0.7	0.8	44.1	5.2	24.2
	R2-A5	0.0	3.5	0.5	10.7	14.1	14.0	21.8	19.4	16.5	6.5	17.3	32.7	53.6
	R2-A6	8.4	7.5	3.4	48.8	3.5	4.7	50.0	7.8	2.6	4.1	2.8	43.3	115.3
	R2-A7	1.1	1.8	1.1	3.3	2.8	3.1	4.6	3.6	1.3	0.5	11.5	3.6	40.7
	R2-A8	8.4	8.3	9.8	5.2	4.2	2.4	9.8	21.2	14.2	17.5	8.3	11.3	39.7
1 h heating	R2-A1	0.0	1.1	5.9	5.6	1.2	3.8	63.9	8.4	1.7	4.0	1.9	14.0	142.8
	R2-A2	4.4	1.4	8.8	12.4	9.1	11.8	5.0	12.3	8.1	13.4	4.1	137.4	290.9
	R2-A3	0.0	4.8	7.6	11.1	6.6	23.3	6.7	16.1	16.5	14.5	2.7	10.4	87.2
	R2-A4	2.4	3.8	5.2	3.1	3.6	2.5	816.5	1.6	2.0	0.0	18.9	8.1	30.3
	R2-A5	1.8	1.7	0.0	19.6	12.6	19.4	514.2	8.1	8.3	3.5	20.7	17.5	140.9
	R2-A6	190.7	18.4	46.1	700.6	247.6	360.2	1515.5	4.4	5.7	2.5	3.8	5.0	715.0
	R2-A7	2.8	1.3	0.0	4.4	6.7	10.7	2.2	1.6	3.5	1.3	11.6	6.3	39.8
	R2-A8	5.9	10.3	12.3	7.5	16.2	8.2	241.4	14.2	18.4	13.9	9.0	6.1	113.7
4 h heating	R2-A1	1.2	1.0	3.4	11.1	0.6	5.3	43.4	2.7	3.6	2.6	5.7	17.1	147.2
	R2-A2	3.2	5.7	9.0	16.0	7.2	8.8	1.2	22.0	9.8	10.6	6.5	196.5	264.1
	R2-A3	8.0	3.6	6.6	11.0	7.4	14.2	9.3	39.8	38.1	17.3	4.8	12.6	122.6
	R2-A4	4.7	7.5	8.3	3.7	3.3	5.9	759.6	1.9	1.5	1.1	36.7	5.9	22.5
	R2-A5	34.5	2.6	4.8	12.4	11.0	16.0	1415.5	6.9	10.1	5.1	16.7	13.7	90.2
	R2-A6	242.2	36.1	48.9	982.0	138.9	211.7	1977.9	12.0	8.6	4.3	4.8	6.0	180.8
	R2-A7	1.3	1.4	1.6	2.8	5.9	5.6	12.8	4.0	1.7	5.2	6.6	3.6	49.2
	R2-A8	10.4	10.4	12.9	25.3	7.9	7.2	1112.9	16.4	14.7	15.5	17.5	11.7	92.8
15 h heating	R2-A1	1.1	1.8	2.4	20.5	2.4	5.0	11.1	3.9	2.7	1.8	2.0	27.0	98.4
	R2-A2	3.2	4.7	6.2	11.7	9.3	10.5	4.9	13.9	7.5	8.3	6.5	144.0	149.4
	R2-A3	0.0	8.0	3.0	6.3	8.0	17.9	8.2	30.5	21.4	17.0	4.4	8.0	124.8
	R2-A4	3.5	4.6	9.0	8.5	3.7	3.9	782.2	2.6	2.0	0.0	23.2	2.2	16.7
	R2-A5	38.8	3.0	4.9	13.9	10.8	9.5	1294.9	13.0	7.5	2.3	25.6	18.1	68.5
	R2-A6	266.0	70.4	112.4	850.7	67.6	138.9	3468.2	26.7	5.0	1.7	4.6	6.6	56.9
	R2-A7	3.3	2.3	2.7	4.0	4.8	9.0	32.9	3.8	5.5	5.4	8.2	3.4	40.4
	R2-A8	13.5	15.5	12.2	16.9	8.8	11.8	901.3	14.3	14.7	16.2	18.4	4.2	83.5

Figure D2: Heat map of 1,536 reactions of R-2 S_NAr HTE using MeOH with 1% FA as spray solvent at 150 °C using NMP as the reaction solvent. The four basic conditions are A) DIPEA B) NaO^{t}Bu C) TEA D) No base.

Base: DIPEA

A)

		R1-B1	R1-B2	R1-B3	R1-B4	R1-B5	R1-B6	R1-B7	R1-B8	R2-B9	R1-B10	R1-B11	R1-B12 (S)	R1-B12 (D)
DESI-MS	R2-A1	7.1	3.7	6.1	9.9	8.6	8.9	235.5	4.3	6.6	3.1	9.6	16.2	112.7
	R2-A2	13.2	3.0	5.3	30.9	32.1	29.9	3.7	5.4	21.9	10.8	4.1	32.1	79.6
	R2-A3	497.9	8.4	142.1	15.3	16.7	11.4	47.0	16.7	30.6	20.8	1.9	18.9	53.1
	R2-A4	24.4	4.0	9.6	3.1	2.6	2.2	49.6	14.4	15.4	10.2	30.0	9.3	22.0
	R2-A5	50.1	11.4	19.6	18.7	11.3	10.0	281.1	10.3	16.1	10.8	15.0	13.8	122.3
	R2-A6	90.5	8.2	11.8	320.0	4.9	2.7	584.1	21.4	11.9	12.2	3.6	252.0	346.2
	R2-A7	24.9	15.8	11.2	27.1	26.9	26.2	7.7	4.5	7.8	4.8	8.5	12.1	16.8
	R2-A8	19.5	53.1	11.7	10.9	18.1	19.2	23.0	7.6	13.1	6.0	9.5	34.5	79.8
1 h heating	R2-A1	55.7	36.7	45.2	26.6	14.4	16.6	141.3	7.6	12.4	10.6	4.8	13.4	47.7
	R2-A2	12.5	6.0	5.5	25.8	38.6	27.1	24.1	8.1	17.4	9.5	35.5	19.4	59.6
	R2-A3	27.2	11.3	15.6	14.5	12.3	9.8	10.8	21.2	23.4	28.5	3.0	21.5	36.6
	R2-A4	26.6	9.3	21.9	7.8	4.0	4.3	64.4	10.8	18.3	12.6	30.4	13.0	25.2
	R2-A5	153.2	7.2	27.6	39.4	18.9	17.8	1135.6	8.5	24.5	9.2	62.1	7.2	36.4
	R2-A6	3765.1	107.0	321.1	1438.5	196.3	142.4	4023.1	21.7	14.8	13.4	10.0	10.6	74.2
	R2-A7	26.8	14.8	13.5	25.7	23.5	25.9	8.1	7.8	6.8	9.1	7.0	13.9	33.5
	R2-A8	30.4	15.6	18.0	43.7	29.6	32.2	1123.6	10.4	11.4	7.4	35.9	5.7	65.5
4 h heating	R2-A1	21.7	15.5	16.4	32.6	15.8	20.5	68.8	6.8	10.2	7.6	6.2	15.8	48.9
	R2-A2	13.6	3.7	6.5	21.5	24.8	35.2	11.0	5.7	16.8	8.5	13.8	19.0	72.9
	R2-A3	22.4	12.0	11.1	17.3	13.9	13.8	21.3	17.8	18.5	21.7	2.6	22.1	56.2
	R2-A4	21.7	8.2	8.1	13.5	6.9	7.0	50.0	12.4	20.3	17.8	24.5	12.1	20.9
	R2-A5	318.1	8.9	13.8	28.4	17.9	18.8	910.8	6.9	9.7	10.9	24.3	8.2	35.6
	R2-A6	4585.7	171.0	272.4	340.5	38.8	38.5	2951.8	117.3	19.2	12.9	5.3	9.2	42.5
	R2-A7	31.0	11.1	10.0	24.8	35.5	23.8	12.8	4.9	7.3	6.0	9.4	14.9	39.4
	R2-A8	30.6	13.4	20.4	42.8	27.4	24.2	846.6	11.0	12.8	8.7	29.3	8.2	85.3
15 h heating	R2-A1	24.3	7.4	8.7	21.8	18.2	10.2	53.6	3.9	29.7	6.6	9.5	10.4	41.1
	R2-A2	23.2	11.4	21.9	26.4	30.1	24.2	48.5	4.8	11.2	10.7	13.7	21.0	49.9
	R2-A3	24.2	17.1	9.7	22.2	15.2	13.4	54.7	24.9	21.9	27.7	4.8	17.2	43.3
	R2-A4	24.3	5.6	7.9	28.0	13.0	11.0	81.2	13.9	18.8	14.9	12.8	9.3	17.5
	R2-A5	136.1	14.9	8.8	17.7	17.7	16.0	1120.3	7.6	13.4	10.5	11.4	14.7	25.8
	R2-A6	2838.4	225.7	334.8	25.1	14.3	10.7	1631.1	218.9	33.2	21.6	4.6	24.1	108.4
	R2-A7	40.5	15.8	14.1	38.7	36.1	30.6	7.4	2.4	3.0	3.6	29.1	15.7	17.5
	R2-A8	58.4	24.2	21.2	37.2	40.5	26.8	230.8	12.7	13.0	8.1	23.3	10.1	85.0

Base: NaO^{t}Bu

B)

		R1-B1	R1-B2	R1-B3	R1-B4	R1-B5	R1-B6	R1-B7	R1-B8	R2-B9	R1-B10	R1-B11	R1-B12 (S)	R1-B12 (D)
DESI-MS	R2-A1	24.6	25.4	18.7	40.7	17.8	7.8	14.1	5.1	7.8	7.8	6.5	16.9	137.2
	R2-A2	5.4	7.8	5.0	43.1	38.9	35.2	8.7	315.4	237.8	142.3	9.2	41.8	99.3
	R2-A3	48.7	34.4	52.0	18.3	20.5	15.6	5.1	19.6	28.4	19.0	5.6	26.4	88.7
	R2-A4	5.1	2.1	7.7	11.2	6.6	12.1	107.3	17.4	11.7	13.0	39.3	12.7	38.7
	R2-A5	2.8	8.3	6.5	47.3	11.2	12.7	26.7	8.6	13.7	6.9	39.1	15.9	90.7
	R2-A6	28.0	7.0	5.8	45.0	4.8	3.5	212.7	27.9	17.1	12.8	4.0	12.1	225.5
	R2-A7	44.0	40.8	31.2	25.7	24.2	32.5	5.3	7.2	9.8	4.0	1.7	17.6	27.1
	R2-A8	11.4	9.3	10.6	12.8	8.8	7.8	7.3	17.7	13.6	3.5	8.0	22.7	93.4
1 h heating	R2-A1	27.3	10.7	15.5	11.3	7.0	9.3	32.2	6.5	8.1	2.4	21.8	16.9	67.6
	R2-A2	37.2	19.1	25.5	19.6	23.3	26.1	9.6	24.5	18.6	8.1	14.9	36.4	68.1
	R2-A3	19.8	30.7	14.0	11.4	12.2	15.8	10.3	20.6	53.1	17.8	3.3	18.2	53.7
	R2-A4	11.8	6.7	7.0	11.9	11.6	8.4	108.3	18.8	13.9	10.8	5.2	11.6	30.6
	R2-A5	2.6	1.8	6.6	196.2	56.2	42.1	36.2	14.3	18.1	5.5	32.3	7.5	37.4
	R2-A6	100.3	31.9	31.3	162.2	13.3	9.6	628.2	20.4	15.8	5.1	7.8	18.8	87.8
	R2-A7	21.4	25.2	26.4	24.8	19.9	25.6	4.6	5.5	5.3	1.9	4.9	17.6	27.6
	R2-A8	45.2	25.4	26.3	17.2	15.5	13.3	22.8	22.2	11.6	10.7	3.4	8.0	82.8
4 h heating	R2-A1	6.6	8.6	11.9	18.2	12.4	18.2	37.6	10.5	6.4	6.8	14.5	16.9	52.2
	R2-A2	40.1	30.2	29.5	28.8	25.8	21.8	10.1	22.9	41.0	14.7	12.2	33.9	70.5
	R2-A3	16.5	29.7	19.0	14.4	9.7	11.0	9.9	21.7	42.7	17.9	3.0	21.9	70.6
	R2-A4	5.0	7.8	10.9	10.3	7.8	10.4	104.5	13.6	20.2	17.2	10.4	13.4	35.5
	R2-A5	5.7	3.9	6.8	18.8	14.0	16.0	26.7	15.4	20.8	12.9	27.2	10.1	33.9
	R2-A6	197.8	33.2	45.4	43.3	13.8	10.4	426.2	25.9	34.7	14.4	3.0	15.7	86.0
	R2-A7	21.5	21.8	28.5	25.5	16.8	31.6	8.4	9.8	7.2	4.5	5.3	20.9	39.4
	R2-A8	56.2	33.8	24.0	16.9	18.7	17.8	12.5	18.4	17.5	8.0	8.1	11.2	103.0
15 h heating	R2-A1	6.3	10.5	3.0	37.2	19.5	23.6	19.1	12.6	8.3	6.2	15.8	24.0	52.9
	R2-A2	42.0	30.7	26.7	26.5	15.7	20.4	13.3	29.2	40.7	7.5	10.7	28.6	68.6
	R2-A3	7.9	15.6	18.0	16.3	10.7	16.9	7.4	21.4	19.0	15.5	4.6	22.7	57.1
	R2-A4	13.0	12.5	11.3	9.3	5.4	9.5	103.3	14.6	15.2	11.4	13.5	7.2	29.7
	R2-A5	10.4	7.1	5.2	15.4	15.1	18.4	204.3	11.5	12.7	7.9	9.0	11.0	33.1
	R2-A6	245.5	25.2	31.8	15.2	9.9	7.2	713.3	89.0	76.7	9.7	5.5	31.3	105.1
	R2-A7	17.4	23.0	18.7	23.1	30.3	26.3	13.4	10.7	10.2	5.7	6.6	21.8	38.5
	R2-A8	39.8	18.4	29.6	18.7	23.9	24.1	32.8	26.0	30.1	16.0	30.0	10.4	87.6

Base: TEA

C)

		R1-B1	R1-B2	R1-B3	R1-B4	R1-B5	R1-B6	R1-B7	R1-B8	R2-B9	R1-B10	R1-B11	R1-B12 (S)	R1-B12 (D)
DESI-MS	R2-A1	8.0	2.5	5.1	8.1	9.0	5.5	290.3	6.1	42.4	7.1	5.1	9.1	75.5
	R2-A2	7.9	2.0	7.4	25.5	29.1	31.0	4.2	5.2	21.5	9.1	2.2	19.8	75.8
	R2-A3	132.9	5.6	9.8	17.5	18.0	13.4	26.5	21.0	27.3	29.8	1.8	29.3	59.6
	R2-A4	15.1	4.7	6.1	4.5	6.3	3.5	82.2	10.5	17.6	15.3	27.3	8.6	27.3
	R2-A5	38.5	4.7	8.9	139.5	58.8	147.0	434.3	12.7	16.4	26.2	7.9	13.2	123.7
	R2-A6	199.8	12.6	18.9	66.0	7.2	6.4	829.5	45.4	14.5	7.4	2.9	83.0	607.0
	R2-A7	34.9	14.3	16.7	31.9	25.3	20.8	2.9	4.8	6.7	5.2	3.2	21.7	23.2
	R2-A8	69.2	15.1	35.8	12.5	14.2	8.9	58.7	12.0	9.1	12.0	14.1	127.1	97.8
1 h heating	R2-A1	41.9	34.9	26.5	18.9	11.7	17.0	125.6	2.3	7.3	7.2	3.4	10.8	38.2
	R2-A2	22.4	3.7	10.1	22.0	29.3	23.4	4.1	3.0	12.8	11.2	27.1	18.6	52.5
	R2-A3	38.5	6.4	6.7	18.2	12.1	7.6	7.8	21.1	25.2	19.8	1.1	21.0	64.5
	R2-A4	15.3	4.2	7.2	8.0	7.2	6.0	57.5	13.5	12.0	15.0	51.5	8.0	28.5
	R2-A5	219.4	7.0	24.1	64.1	23.1	13.0	907.4	15.1	11.4	12.1	15.6	13.2	138.6
	R2-A6	3741.6	92.5	352.3	1544.5	256.6	191.2	3062.2	37.3	13.5	9.4	8.1	5.5	40.2
	R2-A7	24.9	14.4	13.2	30.2	24.4	23.6	8.3	18.9	25.6	19.6	4.2	15.0	55.7
	R2-A8	26.4	12.8	12.7	61.4	43.0	23.1	389.2	9.9	12.0	8.9	15.5	7.6	92.2
4 h heating	R2-A1	18.5	11.5	13.2	33.5	26.0	23.9	75.5	8.0	8.2	6.2	6.2	11.7	39.7
	R2-A2	13.1	6.2	6.2	28.6	29.7	27.1	9.0	4.2	7.7	6.8	10.2	22.1	66.6
	R2-A3	22.4	5.4	7.7	15.5	15.8	10.6	11.9	23.9	21.4	18.1	4.3	17.8	72.6
	R2-A4	19.8	4.8	6.7	24.8	13.0	8.7	71.9	10.5	18.8	14.2	20.4	9.2	22.9
	R2-A5	425.2	10.4	20.0	61.5	29.2	12.3	970.3	12.1	14.8	15.7	27.4	14.5	36.5
	R2-A6	2943.3	182.9	284.7	689.8	60.4	60.1	2932.4	93.4	17.8	11.3	25.9	4.1	37.4
	R2-A7	33.5	10.6	10.8	34.8	25.5	38.1	7.3	13.5	16.3	11.2	5.9	22.0	29.1
	R2-A8	26.9	4.9	9.0	32.2	16.8	8.1	121.8	5.5	7.9	4.8	15.1	10.5	112.4
15 h heating	R2-A1	13.9	6.6	6.5	59.3	22.8	18.2	36.1	2.6	26.3	6.3	4.0	10.7	46.0
	R2-A2	51.0	12.9	10.8	33.7	20.7	28.4	12.9	6.5	12.5	15.0	10.6	17.8	37.8
	R2-A3	27.7	6.3	22.7	19.3	15.7	7.7	29.6	22.8	23.4	23.1	4.5	15.0	88.3
	R2-A4	23.9	7.1	13.5	60.0	14.3	18.1	58.4	11.7	15.8	13.1	16.1	6.5	19.4
	R2-A5	332.7	9.8	32.9	13.6	16.4	18.7	965.4	10.1	12.5	11.5	23.2	11.6	29.0
	R2-A6	3186.7	172.9	428.9	72.2	18.1	14.8	2577.8	247.0	37.6	15.9	12.5	11.0	43.2
	R2-A7	45.1	13.4	13.8	43.4	39.1	38.3	10.1	10.6	10.8	8.1	12.5	17.0	25.7
	R2-A8	0.0	0.0	0.0	0.0	0.0	0.0	0.0	0.0	0.0	0.0	0.0	0.0	0.0

Base: No base

D)

		R1-B1	R1-B2	R1-B3	R1-B4	R1-B5	R1-B6	R1-B7	R1-B8	R2-B9	R1-B10	R1-B11	R1-B12 (S)	R1-B12 (D)
DESI-MS	R2-A1	1.6	3.2	2.7	7.0	11.0	7.5	277.6	6.7	4.0	5.3	4.1	21.3	91.8
	R2-A2	2.8	4.3	5.0	26.0	27.1	27.5	10.2	11.5	12.6	5.6	2.5	19.4	114.0
	R2-A3	230.9	61.7	6.4	14.5	12.1	13.0	62.9	20.2	22.7	17.4	3.6	47.7	115.1
	R2-A4	6.9	6.6	10.7	2.9	2.0	3.4	37.9	15.6	21.2	12.5	46.8	8.3	22.0
	R2-A5	8.5	35.8	6.8	11.7	7.4	7.4	160.3	13.7	15.0	9.7	29.1	18.6	43.4
	R2-A6	68.4	16.0	16.1	74.2	6.1	4.4	317.8	31.8	12.7	7.8	4.6	84.7	240.1
	R2-A7	14.8	14.1	22.3	26.0	27.1	25.2	3.2	6.2	6.0	5.0	4.6	18.6	25.9
	R2-A8	120.9	38.7	208.1	12.1	12.4	14.0	36.2	14.9	8.5	5.4	11.5	76.3	104.0
1 h heating	R2-A1	3.2	1.6	3.7	25.8	11.3	8.3	100.2	6.2	6.7	2.6	4.2	9.0	59.4
	R2-A2	3.9	2.6	4.0	27.1	28.0	32.3	7.6	6.6	10.5	3.8	48.4	32.1	91.0
	R2-A3	17.2	26.4	18.6	14.1	10.2	11.0	4.0	25.4	19.4	14.9	4.5	17.0	95.1
	R2-A4	28.1	19.1	16.4	3.2	6.3	4.3	62.2	16.5	17.1	9.4	49.8	7.8	19.5
	R2-A5	55.0	10.6	10.2	38.5	21.7	13.3	1579.9	14.9	12.0	6.7	17.4	7.8	35.6
	R2-A6	2387.9	107.9	174.9	2328.7	198.4	224.5	2402.8	41.9	13.7	5.4	10.0	10.8	52.1
	R2-A7	18.6	12.6	15.4	29.9	41.6	22.8	11.1	10.3	11.2	8.9	8.2	14.5	29.4
	R2-A8	17.3	12.1	11.9	53.2	22.2	20.7	1801.4	11.9	9.7	9.1	38.8	6.2	88.7
4 h heating	R2-A1	10.7	4.2	4.9	42.8	11.9	9.4	34.0	6.7	6.6	4.9	4.2	10.3	68.7
	R2-A2	2.9	2.6	3.8	22.0	28.0	23.8	6.7	6.7	13.4	4.3	22.8	18.9	80.0
	R2-A3	15.2	30.2	32.4	25.1	10.4	8.0	4.5	25.0	17.1	16.6	2.6	20.0	109.8
	R2-A4	14.3	13.6	11.6	17.3	7.9	3.4	39.5	15.9	20.2	13.4	38.1	8.7	22.5
	R2-A5	93.2	13.5	12.8	29.6	16.1	9.9	575.4	12.6	13.6	6.7	13.4	12.0	25.0
	R2-A6	2237.3	172.1	280.4	1281.3	138.2	93.8	1835.6	79.0	18.1	9.9	8.3	10.7	60.0
	R2-A7	14.0	9.8	17.2	27.6	25.6	22.5	15.8	9.7	12.1	3.8	25.0	15.2	32.0
	R2-A8	14.8	5.2	10.6	16.2	15.1	9.2	932.4	9.6	6.0	6.6	37.6	8.8	102.3
15 h heating	R2-A1	4.7	3.6	2.0	36.3	9.6	9.2	17.7	6.5	6.9	1.1	4.8	11.0	52.3
	R2-A2	5.7	3.6	4.6	26.2	22.8	26.3	6.7	7.2	9.5	5.7	9.3	32.6	88.0
	R2-A3	30.6	23.9	18.2	17.1	21.0	11.0	26.7	25.3	21.9	12.0	0.6	13.3	86.5
	R2-A4	10.7	5.5	8.3	24.7	11.6	7.5	59.0	14.3	14.0	11.4	14.0	10.7	24.8
	R2-A5	90.3	13.1	20.7	23.5	9.3	6.6	663.2	14.0	13.8	5.5	14.7	15.1	29.6
	R2-A6	1733.2	133.1	223.4	571.6	29.0	10.2	2109.0	294.6	24.8	9.4	10.8	5.7	43.1
	R2-A7	16.4	16.3	20.8	27.9	29.5	35.4	5.2	9.2	9.7	3.9	20.1	14.9	27.5
	R2-A8	0.0	0.0	0.0	0.0	0.0	0.0	0.0	0.0	0.0	0.0	0.0	0.0	0.0

Figure D3: Heat map of 1,536 reactions of R-2 S_NAr HTE using MeOH with 1% FA as spray solvent at 200 °C using NMP as the reaction solvent. The four basic conditions are A) DIPEA B) NaO^tBu C) TEA D) No base.

Continuous Flow Synthesis

Table D1: Chemtrix reactor chip: 3225, reactor volume:10 µL, pressure: ambient pressure

Amines µL/min	Aryl halides µL/min	Base µL/min	Residence Time T_r in Minutes	Temperature °C
6.67	6.67	6.67	0.5	100/150
3.33	3.33	3.33	1	100/150
1.11	1.11	1.11	3	100/150
0.67	0.67	0.67	5	100/150

"Yes" Reaction in Flow

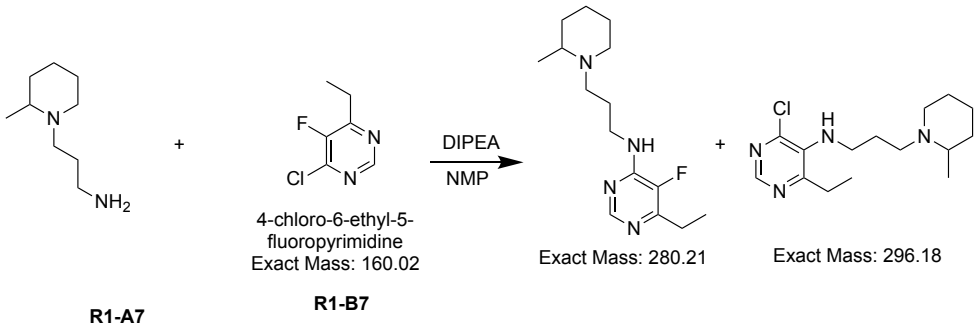

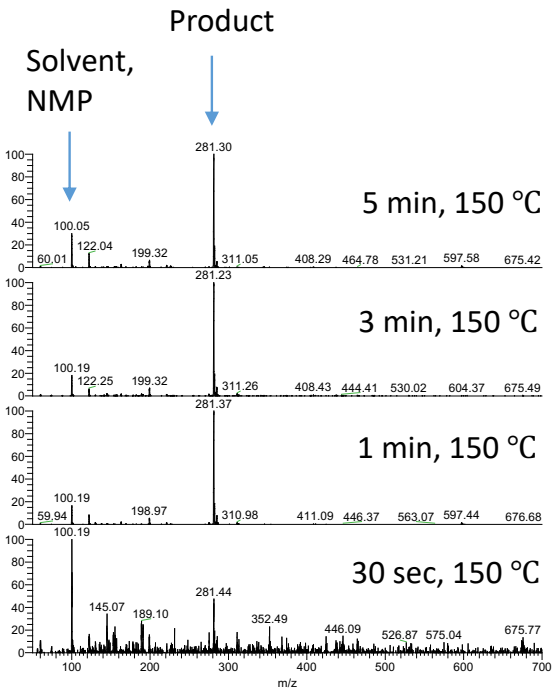

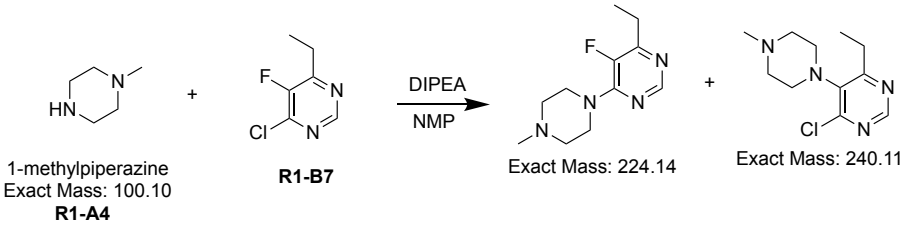

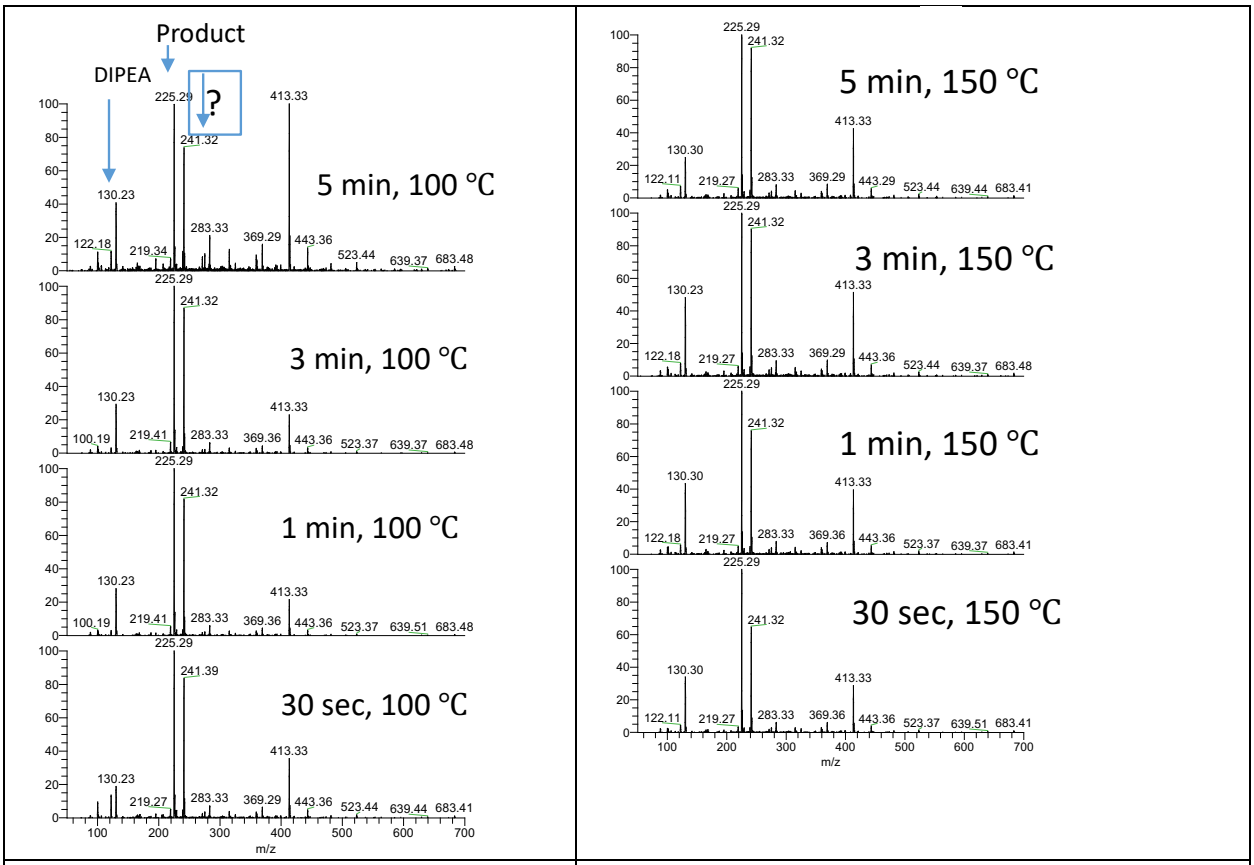

MS/MS of *m/z* = 225

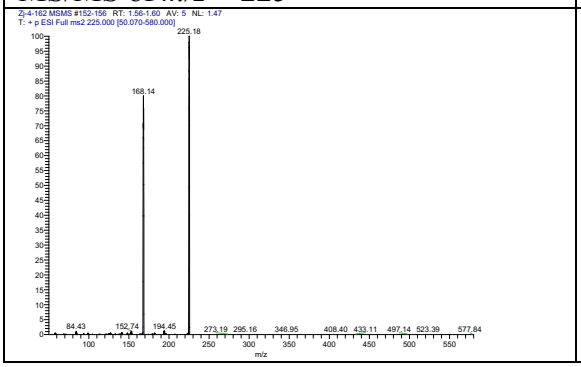

MS/MS of *m/z* = 241

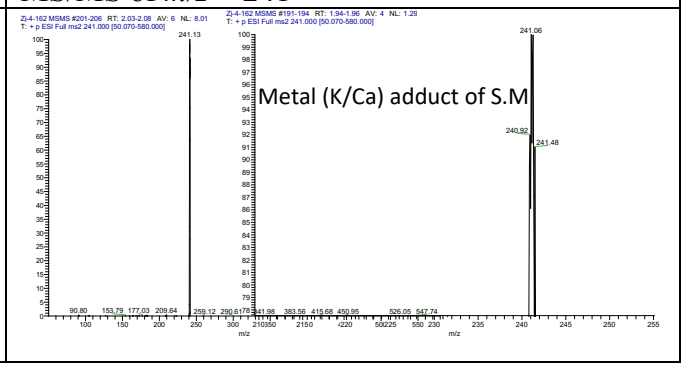

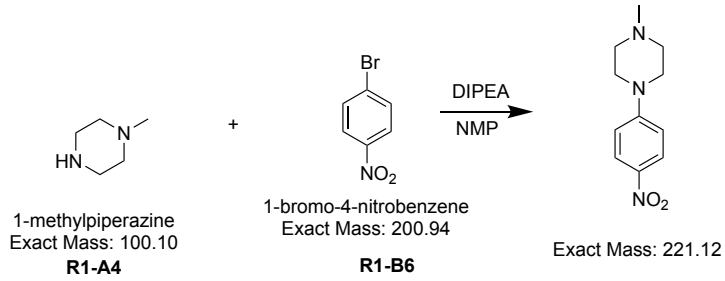

1-methylpiperazine
Exact Mass: 100.10
R1-A4

1-bromo-4-nitrobenzene
Exact Mass: 200.94
R1-B6

Exact Mass: 221.12

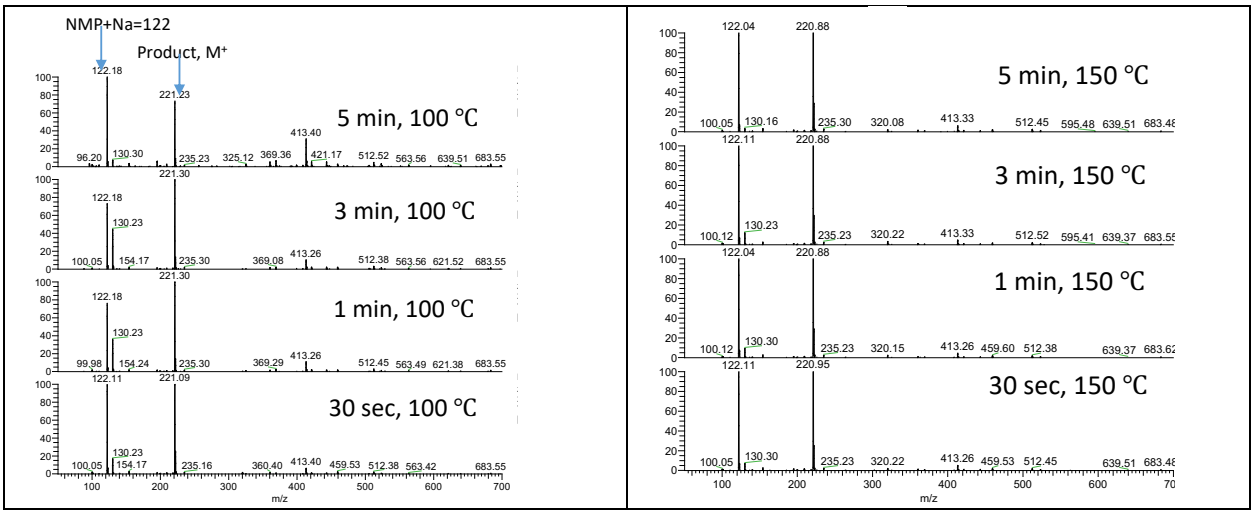

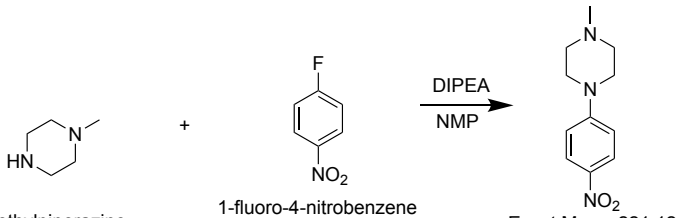

1-methylpiperazine
Exact Mass: 100.10
R1-A4

1-fluoro-4-nitrobenzene
Exact Mass: 141.02
R1-B4

Exact Mass: 221.12

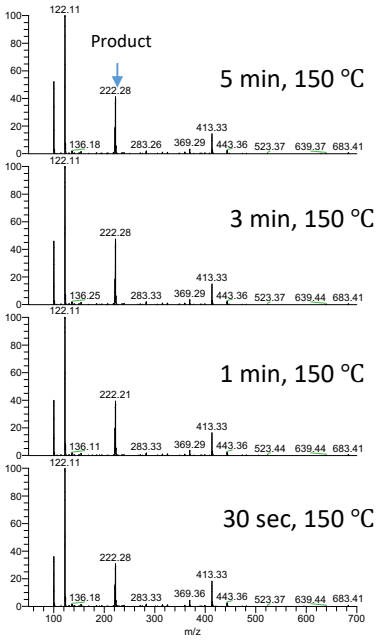

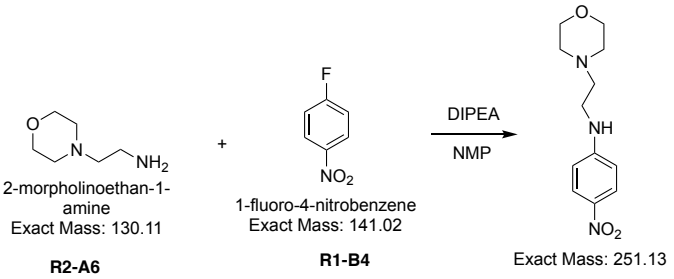
2-morpholinoethan-1-amine
Exact Mass: 130.11
R2-A6
1-fluoro-4-nitrobenzene
Exact Mass: 141.02
R1-B4
DIPEA
NMP
Exact Mass: 251.13

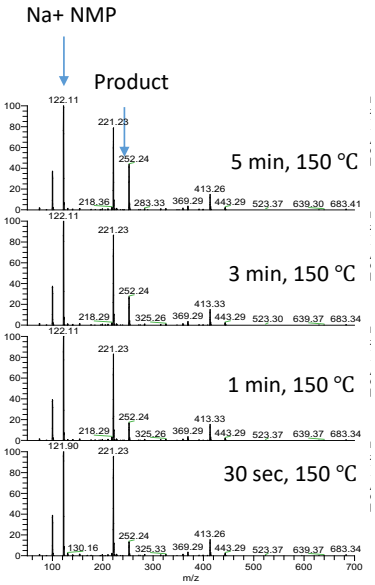
Na+ NMP
Product
5 min, 150 ℃
3 min, 150 ℃
1 min, 150 ℃
30 sec, 150 ℃
m/z

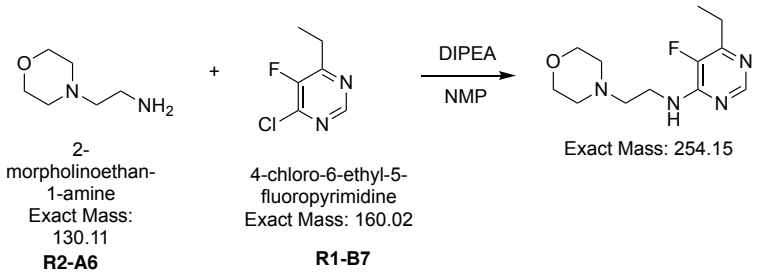
2-morpholinoethan-1-amine
Exact Mass: 130.11
R2-A6
4-chloro-6-ethyl-5-fluoropyrimidine
Exact Mass: 160.02
R1-B7
DIPEA
NMP
Exact Mass: 254.15

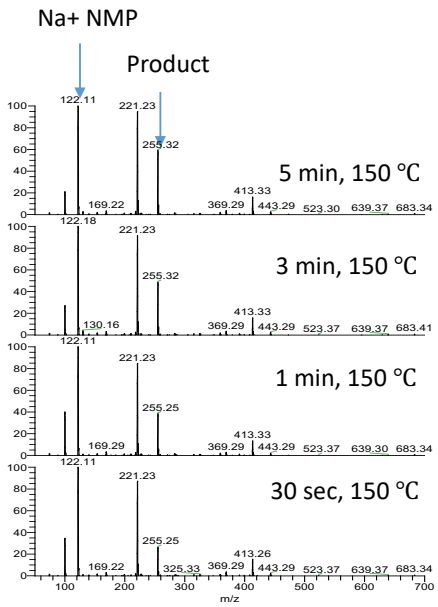

"No" Reaction in Flow

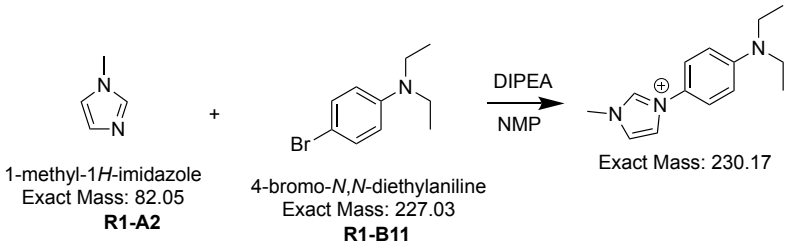

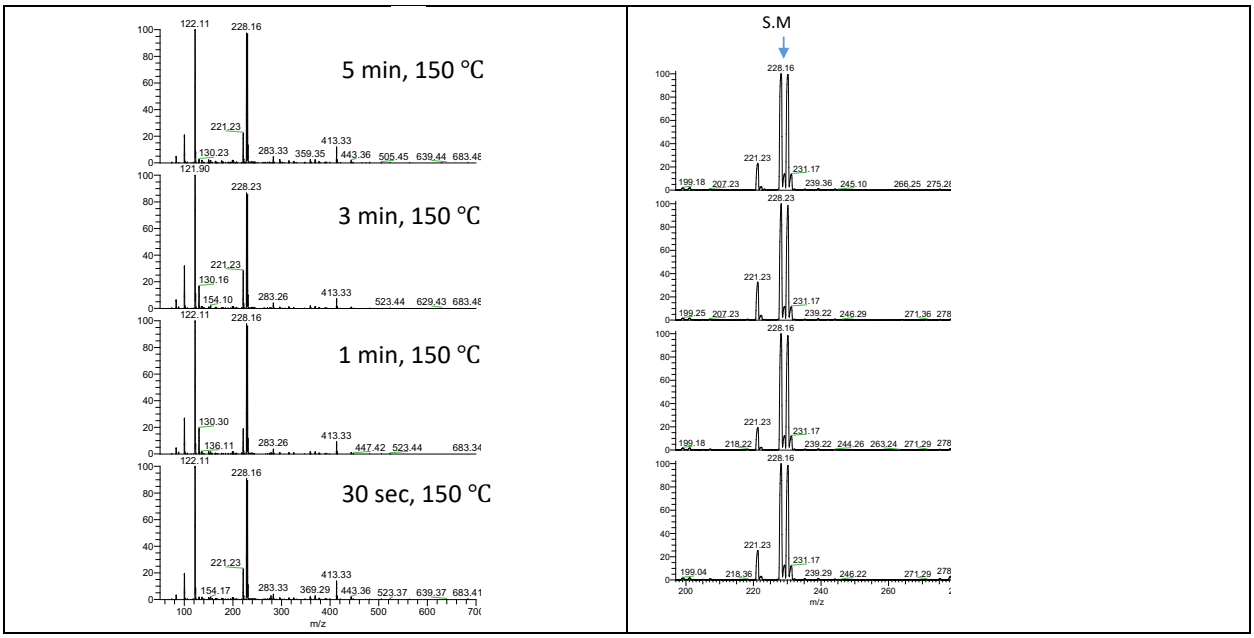

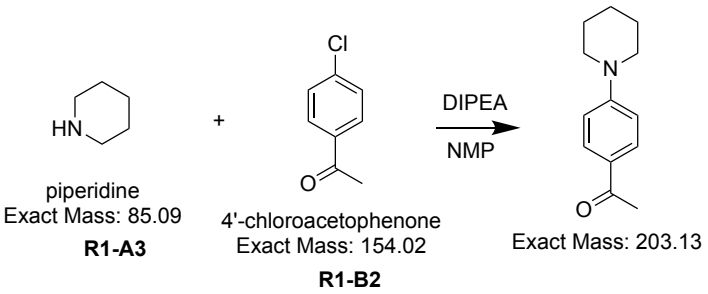
HN
+
Cl
O
DIPEA
NMP
N
O
piperidine
Exact Mass: 85.09
R1-A3
4'-chloroacetophenone
Exact Mass: 154.02
R1-B2
Exact Mass: 203.13

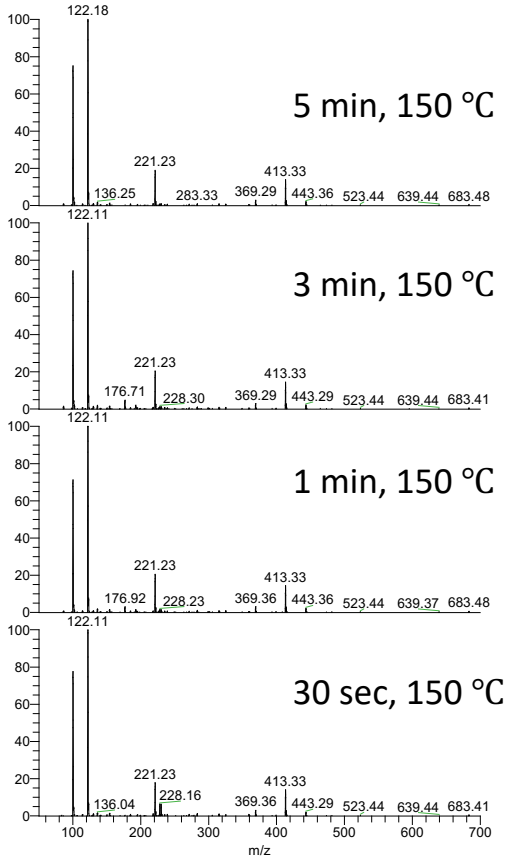
5 min, 150 °C
122.18
221.23
413.33
136.25
283.33
369.29
443.36
523.44
639.44
683.48
3 min, 150 °C
122.11
221.23
413.33
176.71
228.30
369.29
443.29
523.44
639.44
683.41
1 min, 150 °C
122.11
221.23
413.33
176.92
228.23
369.36
443.36
523.44
639.37
683.48
30 sec, 150 °C
122.11
221.23
413.33
136.04
228.16
369.36
443.29
523.44
639.44
683.41
m/z

VITA

Summary

- Highly motivated, and passionate synthetic organic and analytical chemist with a strong background of modern synthetic methodology such as small molecule synthesis both in continuous flow as well as in batch process for more than eight years leading to the successful publications of 8 journal papers.
- High-level strategic planner with experience in analyzing large scientific datasets as demonstrated by the optimization of 3 high-throughput methodologies, resulting in a new area of synthesis route screening that published in Analyst, Chem. Sci. and Chem. Eur. J.
- Excellent teamwork and collaboration skills established by managing a multidisciplinary team of chemists, analysts, engineers and computer scientists in a DARPA funded project, resulting in the development of 4 internal collaborations and 3 external collaborations.
- Highly skilled synthetic chemist in the area of methodology development and multistep synthesis with strong knowledge of techniques related to purification and characterization of organic compounds.
- Strong fundamental background in chemistry, as reflected from the excellent grades, knowledge of current industry trends and experience clearly communicating complex topics to diverse audiences, as evidenced by 6 award-winning scientific presentations.

Work Experience

Research Assistant, Prof. David H. Thompson, Purdue University--Aug/2014-present

- Lead chemist for automated robust continuous flow synthesis of active pharmaceutical ingredient (APIs) using catalysts, resulting in the publication of the projects in Analyst, Chem. Eur. J. and one patent
- Develop high throughput reaction screening technology both in batch and droplet reactor for the synthesis of molecules using liquid handling robots and identify the reaction hotspots in a collaborated project, published in Chem. Sci. and Chem. Eur. J.
- Investigate, design, develop, execute, and optimize APIs manufacturing efficiently and statistical analysis the data using various analytical tools including MS, DESI-MS, NMR, GC, UPLC, LC, HPLC-MS.

- Document work procedure timely, and demonstrate progress to technical and non-technical person, manage project deliverables with tight deadlines, and gained business acumen.

Research Assistant, Prof. Mohammad R. Karim, Tennessee State University--Aug/2012-Jul/2014

- Synthesized Schiff-bases and characterized the compounds using spectroscopic methods, subsequent publishing in Int. J. Org. Chem. as a first author
- Investigated the antibacterial activity of the Schiff-bases and determine minimum inhibitory concentration (MIC) of compounds, following in publication in Adv. Microbiol. as a first author.

MS Exchange Student, Prof. Takashi Sugimura, University of Hyogo, Japan Oct/2010-Mar/2011

- Methodological development of polyheterocyclic compounds and synthesized of precursors for heteropolycycles and studied of stereo-selectivity of synthesized compounds.

Research Assistant, Prof. Md. Giasuddin Ahmed, University of Dhaka, Bangladesh--Oct/2009-Sep/2010

- Synthesized and characterized of α,β-unsaturated cyanoesters with cyclic 1,3-diketones.

Education

Doctor of Philosophy, Organic Chemistry, Purdue University, West Lafayette, IN--May/2019

Dissertation: High Throughput screening guided continuous flow synthesis of active pharmaceutical ingredient (APIs) and optimization of the reaction conditions.

GPA: 4.00/4.00

Master of Science, Chemistry, Tennessee State University, Nashville, TN--Aug/2014

Dissertation: Synthesis and antibacterial study of Schiff Bases from 5-substituted-2, 9-dimethyl-1,10- phenanthroline dialdehyde and sulfur-containing amines

GPA: 4.00/4.00

Master of Science, Organic Chemistry, University of Dhaka, Dhaka, Bangladesh-- May/2011

Dissertation: Studies on the reactions of α,β-unsaturated cyanoesters with cyclic 1,3-diketones.

GPA: 4.00/4.00 (USA equivalent grade converted by WES)

Bachelor of Science, Chemistry, University of Dhaka, Dhaka, Bangladesh-- Jun/2009

GPA: 3.87/4.00 (USA equivalent grade converted by WES)

Techniques, Instrumentation & Software

- UV/VIS, IR, FTIR, GC, HPLC, UPLC, HPLC-MS, MS (EI and ESI), DESI-MS, DLS, NMR (1D and 2D)

- Chemtrix Labtrix S1 flow system, Bruker AV-III-400/500-HD NMR spectrometer, Biotage (Flash+), ThermoFisher TSQ QA MAX MS w/ Autosampler, ThermoFisher LTQ MS, Prosolia DESI 2D molecular imaging, Beckman Biomek FX and i-7, Agilent 1100 HPLC w/ Agilent MSD-TOF MS, Agilent 6410 NanoLC QQQ-MS, Agilent 6545 UPLC/Q-TOF MS, Thermo TSQ 8000 QQQ GC/MS/MS, DynaProTM DLS
- MS Office, ChemDraw, OriginPro, MestReNova, Perl, Xcalibur, BioMap, Sci-Finder, EndNote, Reaxys

Selected Publications (7 out of 9)

- Zinia Jaman, Tiago J. P. Sobreira, Ahmed Mufti, Christina R. Ferreira, R. Graham Cooks and David H. Thompson, "On-demand Rapid Synthesis of Lomustine Under Continuous Flow Conditions" accepted, *Org. Process Res. Dev*, **2019**, 23, 334–341
- Zinia Jaman, Samyukta Sah, Ahmed Mufti, Larisa Avramova, Tiago J. P. Sobreira, David H. Thompson, "High Throughput Experimentation and Continuous Flow Validation of Suzuki-Miyaura Cross-Coupling Reactions" *Chem. Eur. J* **2018**, 24, 9546-9554. (Citation:3)
- Michael Wleklinski‡, Bradley P. Loren‡, Christina R. Ferreira, Zinia Jaman, Larisa Avramova, Tiago J. P. Sobreira, David H. Thompson and R. Graham Cooks, "High Throughput Reaction Screening Using Desorption Electrospray Ionization Mass Spectrometry" *Chem. Sci* **2018**, 9, 1647-1653. (Citation:7)
- Zinia Jaman‡, Caitlin E. Falcone‡, Michael Wleklinski, Andy Koswara, David H. Thompson, R. Graham Cooks, "Reaction screening and optimization of continuous-flow atropine synthesis by preparative electrospray mass spectrometry" *Analyst* **2017**, 142, 2836-2845. (Citation:6)
- Michael Wleklinski, Caitlin E. Falcone, Bradley P. Loren, Zinia Jaman, Kiran Iyer, H. Samuel Ewan, Seok-Hee Hyun, David H. Thompson, and R. Graham Cooks, "Can Accelerated Reactions in Droplets Guide Chemistry at Scale?", *Eur. J. Org. Chem.* **2016**, 2016, 5480-5484. (Citation:14)
- Zinia Jaman, Mohammad R. Karim, Korsi Dumenyo, Aminul H. Mirza, "Antibacterial activities of new Schiff bases and intermediate Silyl compounds sythesized from 5-substituted-1,10-phenanthroline-2,9-dialdehyde". *Adv Microbiol*, **2014**, 4, 1140-1153. (Citation:5)
- Zinia Jaman, Mohammad R. Karim, Tasneem A. Siddiquee, Aminul H. Mirza, Mohamad A. Ali, "Synthesis of 5-Substituted 2, 9-Dimethyl-1,10-Phenanthroline Dialdehydes and Their

Schiff bases with Sulfur-containing Amines". *Int J Org Chem*, **2013**, Vol 3, 214-219. (Citation:6)

Selected Presentations (9 out of 14)

- Oral Presentation, Bangladesh Student Association, Purdue University, IN, 2018
- Oral Presentation, Cal Meyers Memorial Organic Chemistry Symposium, Southern Illinois University, Carbondale, IL, 2017
- Oral Presentation, 36th Annual University-Wide Research Symposium, Tennessee State University, TN, 2014.
- Poster Presentation, Flow Chemistry Congress, Miami, FL, 2018.
- Poster Presentation, H.C Brown Symposium, Purdue University, IN, 2018.
- Poster Presentation, 9th Chicago Organic Symposium, Northwestern University, IL, 2018.
- Poster Presentation, Flow Chemistry Europe, Cambridge, UK, 2018.
- Poster Presentation, 247th ACS National Meeting, Dallas, TX, 2014.
- Poster Presentation, 35th Annual University-Wide Research Symposium, Tennessee State University, TN, 2013.

Selected Fellowship, Awards and Honors (11 out of 16)

- Best Poster Award, Flow Chemistry Congress, Miami, FL, 2018.
- First Prize, Poster presentation, H.C Brown Symposium, Purdue University, IN, 2018.
- Poster Award, 9th Chicago Organic Symposium, Northwestern University, IL, 2018
- Cagiantas Fellowship, College of Science, Purdue University, IN, 2017-2018.
- H.C Brown Organic Travel Grant, Department of Chemistry, Purdue University, IN, 2017.
- Best Poster, Ei-ichi Negishi 80th Birthday Symposium and 8th Negishi- Brown Lectures, Department of Chemistry, Purdue University, IN, 2015.
- Outstanding (Masters) Graduate Student, College of Agriculture, Human and Natural Sciences, Tennessee State University, Nashville, TN, 2014.
- First Place, Oral presentation at 36th Annual University-Wide Research Symposium, Tennessee State University, Nashville, TN, 2014.
- Second Place, Poster presentation at 35th Annual University-Wide Research Symposium, Tennessee State University, Nashville, TN, 2013.
- Gold Medal, First Place in Graduate Study (M.S), University of Dhaka, Bangladesh, 2011.

- Dean's award, Undergraduate Study (B.S), University of Dhaka, Bangladesh, 2009.

Outreach and Engagement Activities

- Bindley Ambassador, Discovery Park, 2018-2019, Purdue University
- Volunteer, National Chemistry Week, 2017 & 2016, Purdue University
- Community Volunteer, Winterization, 2017, Fund Raising, 2016, Purdue University-BoilerLink
- Social Correspondent, Bangladesh Student Association, 2016-2017, Purdue University
- Member: Toastmaster, Flow Chemistry Society, American Chemical Society; Bangladesh Student Association at Purdue (BDSA)

LIST OF PUBLICATIONS

1. **Zinia Jaman**, Tiago J. P. Sobreira, Ahmed Mufti, Christina R. Ferreira, R. Graham Cooks and David H. Thompson, "On-demand Rapid Synthesis of Lomustine Under Continuous Flow Conditions" *Org. Process Res. Dev* **2019**, 23, 334–341.

2. **Zinia Jaman**, Samyukta Sah, Ahmed Mufti, Larisa Avramova, Tiago J. P. Sobreira, David H. Thompson, "High Throughput Experimentation and Continuous Flow Validation of Suzuki-Miyaura Cross-Coupling Reactions" *Chem. Eur. J* **2018**, 24, 9546-9554.

3. Michael Wleklinski[‡], Bradley P. Loren[‡], Christina R. Ferreira, **Zinia Jaman**, Larisa Avramova, Tiago J. P. Sobreira, David H. Thompson and R. Graham Cooks, "High Throughput Reaction Screening Using Desorption Electrospray Ionization Mass Spectrometry" *Chem. Sci.* **2018**, 9, 1647-1653.

4. **Zinia Jaman**[‡], Caitlin E. Falcone[‡], Michael Wleklinski, Andy Koswara, David H. Thompson, R. Graham Cooks, "Reaction screening and optimization of continuous-flow atropine synthesis by preparative electrospray mass spectrometry" *Analyst* **2017**, 142, 2836-2845.

5. Michael Wleklinski, Caitlin E. Falcone, Bradley P. Loren, **Zinia Jaman**, Kiran Iyer, H. Samuel Ewan, Seok-Hee Hyun, David H. Thompson, and R. Graham Cooks, "Can Accelerated Reactions in Droplets Guide Chemistry at Scale?", *Eur. J. Org. Chem.* **2016**, 2016, 5480-5484.

ORGANIC PROCESS RESEARCH & DEVELOPMENT
OPR&D
Article
Cite This: Org. Process Res. Dev. XXXX, XXX, XXX−XXX
pubs.acs.org/OPRD

Rapid On-Demand Synthesis of Lomustine under Continuous Flow Conditions

Zinia Jaman,[†] Tiago J. P. Sobreira,[†] Ahmed Mufti,[‡] Christina R. Ferreira,[†] R. Graham Cooks,[†] and David H. Thompson*,[†]

[†]Department of Chemistry, Purdue University, Bindley Bioscience Center, 1203 West State Street, West Lafayette, Indiana 47907, United States

[‡]School of Chemical Engineering, Purdue University, 480 West Stadium Avenue, West Lafayette, Indiana 47907, United States

Supporting Information

ABSTRACT: Lomustine, an important agent for treatment of brain tumors and Hodgkin's lymphoma, has been synthesized using continuous flow methodology. Desorption electrospray ionization mass spectrometry (DESI-MS) was used to quickly explore a large number of reaction conditions for one of the reaction steps and guide the efficient translation of optimized conditions to continuous lomustine production. Using only four inexpensive commercially available starting materials and a total residence time of 9 min, lomustine was prepared via a linear sequence of two chemical reactions performed separately in two telescoped flow reactors. Sequential offline extraction and filtration resulted in a 63% overall yield of pure lomustine at a production rate of 110 mg/h. The primary advantages of this approach are the rapid manufacture of lomustine with two telescoped steps to avoid isolation and purification of a labile intermediate and the mild conditions used in the nitrosylation step, thereby significantly increasing the purity and yield of this active pharmaceutical ingredient.

KEYWORDS: *Lomustine, continuous synthesis, reaction telescoping, desorption electrospray ionization mass spectrometry (DESI-MS), high throughput experimentation*

INTRODUCTION

Lomustine, a widely used anticancer agent, is a highly lipophilic alkylating agent that produces chloroethyl carbenium ions and carbamylating intermediates *in vivo*.[1,2] These electrophilic compounds attack the nucleophilic sites on DNA to form alkylated products.[1] Other anticancer agents such as mitomycin C, streptonigrin, bleomycin, and the anthracyclines require bioactivation to react with their cellular targets, whereas lomustine does not require preactivation.[3] Unlike alkylating agents that form adducts at the most reactive N^7 position of guanine, chloroethylating compounds like lomustine form adducts at O^6, leading to interstrand DNA cross-linking. If DNA repair does not occur, this cross-linking can cause double strand breaks during DNA replication, eventually leading to cell death via apoptosis.[4]

Lomustine, 1-(2-chloroethyl)-3-cyclohexyl-l-nitroso-urea (commercial names: CCNU, CeeNU, Gleostine), is used as an oral antineoplastic agent that is administered every 6 weeks. It was first evaluated in clinical trials in the late 1960s[5] and approved by the US FDA in 1976[6] for primary and metastatic brain tumors as well as Hodgkin's lymphoma.[4] Bristol-Myers Squibb originally held the patent for the agent under the brand name CeeNu. In 2014, Next Source Biotechnology LLC was approved by the FDA for the rebranding of lomustine under the trade name Gleostine.[6] The average wholesale price for one dose of rebranded Gleostine has recently experienced a substantial price increase,[5] in part due to the new regulatory challenges of handling carcinogenic compounds of this type.[1,4] Unfortunately, this situation has created patient access problems, thus motivating our effort to develop a lomustine synthesis using continuous flow methods.

Flow chemistry approaches have been reported as an efficient methodology and have recently been explored in both industry and academic laboratories.[7−18] Compared to traditional batch synthesis processes, flow transformations provide better control over reaction conditions and selectivity owing to rapid mixing and precise control of reaction parameters such as temperature, stoichiometry, pressure, and residence time. The enhanced heat and mass transfer capabilities also provide safer operational conditions.[8,19−25] Generally, these aspects of continuous flow synthesis contribute to improved chemical reaction efficiency[25,26] and shorter reaction times, enabling process intensification,[19] and more facile scale-up, with improved quality and consistency in production. Motivated by these factors, continuous flow synthesis of active pharmaceutical ingredients has recently become more attractive.[23,27−39] Efficient execution of multistep reactions in a telescoped manner, however, still remains a challenge due to issues arising from workup conditions,[32,40,41] solvent switches,[42,43] and flow rate differences.[42,44] Moreover, optimization of continuous flow conditions and analysis require significant investments in time and material.[32,45−50]

Recently, our group reported a robust high throughput experimentation method using desorption electrospray ionization mass spectrometry (DESI-MS) to explore reaction conditions for scalable synthesis in continuous flow reactors

Received: November 19, 2018

ACS Publications © XXXX American Chemical Society

DOI: 10.1021/acs.oprd.8b00387
Org. Process Res. Dev. XXXX, XXX, XXX−XXX

Scheme 1. Synthesis Plan for Lomustine in Continuous Flow, Where 4 = $NaNO_2/HCO_2H$ and 5 = ^tBuONO

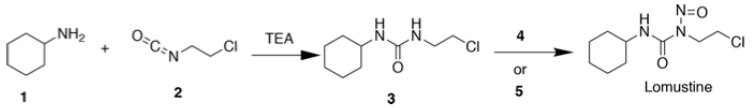

at scale.[49] Herein, we report the continuous flow synthesis of lomustine using an optimization protocol that was guided by DESI-MS. The final method consists of two reactions telescoped without isolation of the reaction intermediate. This approach can reduce production costs radically by using a simple reactor setup and inexpensive starting materials (Scheme 1). To the best of our knowledge, this is the first synthesis of lomustine telescoped in continuous flow using an approach that does not interrupt the flow sequence due to intermediate workup requirements.

■ RESULTS AND DISCUSSION

Continuous Synthesis of 1-(2-Chloroethyl)-3-cyclohexylurea, 3. The first step in the synthesis of lomustine (Scheme 1) is a fast reaction at room temperature. This transformation was optimized in continuous flow as a function of temperature, solvent, and stoichiometry to discover the conditions for maximum product yield. The reactions were monitored by TLC and MS using a triple quadrupole mass spectrometer operating in positive ion mode to afford rapid investigation of full mass spectra and product ion distributions for each reaction condition.

A cascade method was designed to reveal the best conditions for the first step. Cyclohexylamine, **1**, 1-chloro-2-isocyanato-ethane, **2**, and triethylamine (TEA) solutions were pumped through a Chemtrix 3225 SOR chip with automatic collection of the products in vials via an autosampler (Figure 1). The

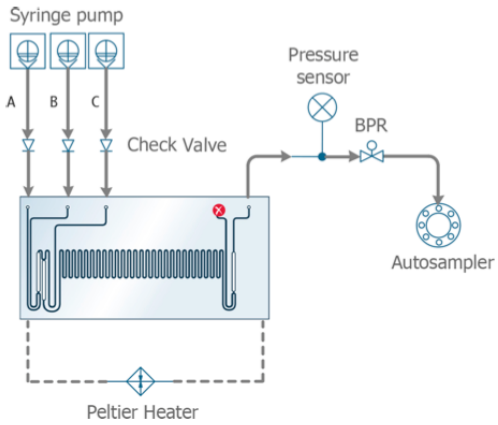

Figure 1. Microfluidic synthesis of intermediate **3** in a glass reactor chip (SOR 3225). A = **1** in THF; B = **2** in THF, C = TEA in THF.

individual reaction mixtures were evaporated, and the white solid was washed with cold Et_2O before drying under vacuum for overnight prior to analysis by TLC, MS, MS/MS, and NMR (^1H and ^{13}C).

Parameters such as residence time (τ), reaction temperature (T), and 1-chloro-2-isocyanatoethane/cyclohexylamine ratio were investigated systematically under continuous flow conditions. As shown in Table 1, product yields dropped sharply in EtOH at longer residence times (entries 1−3) due

Table 1. Reaction Conditions Evaluated for the Synthesis of 3 in Flow Using a Chemtrix S1 Glass System Fitted with a 3225 SOR Reactor Chip

entry	solvent	**2** (equiv)	temp (°C)	residence time (s)	isolated yield (%)
1	EtOH	1	50	10	42.8
2	EtOH	1	50	30	0.00
3	EtOH	1	50	60	0.00
4	ACN	1	50	10	56.2
5	ACN	1	50	30	clogged
6	ACN	1	25	30	clogged
7	toluene	1	50	10	clogged
8	ether	1	50	10	clogged
9	THF	1	25	10	50.0
10	THF	1	25	30	56.4
11	THF	1	50	10	59.5
12	THF	1	50	30	62.1
13	THF	1	65	10	47.5
14	THF	1	65	30	29.1
15	THF	1.2	50	10	61.2
16	THF	1.2	50	30	64.8
17	THF	1.2	50	60	71.3
18	THF	1.4	50	10	67.1
19	THF	1.4	50	30	82.0
20	THF	1.4	50	60	91.7
21	THF	1.4	50	180	82.8

to ethanolysis of the 1-chloro-2-isocyanato-ethane starting material. Though the yield of **3** in ACN was significant, its low solubility in this solvent led to significant chip clogging (entries 4−6). Similar clogging problems were found for toluene and Et_2O, even at low concentrations (entries 7−8). The yield increased to 50−62% with longer residence times (entries 9−14) in THF, reaching a maximum when τ = 30 s at 50 °C and decayed rapidly with increased temperature (entries 13, 14) due to increased product decomposition at elevated temperatures. The yield of **3** was also found to increase with proportions of **2** ratio (entries 15−21), whereas longer residence times promoted product decomposition (entry 21). Consequently, a maximum yield of intermediate **3** (92%) was achieved under conditions of τ = 60 s, T = 50 °C, and 1.4 equivalents of 1-chloro-2-isocyanatoethane (entry 20).

Synthesis of Lomustine, Guided by DESI-MS High Throughput Experimentation. We employed DESI-MS to evaluate the impact of solvent, concentration, and nitrosation reagent type on the efficiency of lomustine production. DESI-MS was originally applied to the surface analysis of intact samples such as biological tissues for cancer diagnosis or human fingerprints for drug detection,[51,52] although, more recently, the DESI-MS approach has been used for chemical reaction analysis.[49] This approach is thought to involve the phenomenon of reaction acceleration that occurs within

DOI: 10.1021/acs.oprd.8b00387
Org. Process Res. Dev. XXXX, XXX, XXX−XXX

confined volumes such as microdroplets that originate from spray-based MS ionization processes.[51] MS analysis speeds approaching 10^4 reaction spots/h can be achieved by this technique.[49]

As shown in Scheme 1 (second step), two nitrosation methods were investigated. First, the efficiency of sodium nitrite, **4**, in formic acid as the nitrosation reagent toward the conversion of **3** to lomustine was evaluated. This conversion was then compared with *tert*-butyl nitrite (TBN, **5**) as the nitrosation reagent. DESI-MS was used to evaluate the $NaNO_2/HCO_2H$ transformation under different reactant concentrations and solvents. The expected m/z 234 value for lomustine was not observed. Analysis of a commercial lomustine sample yielded a very similar MS, suggesting that fragmentation occurs readily during the ionization process. Triple quadrupole MS with electrospray ionization, as well as ion trap mass spectrometry coupled with DESI, revealed the presence of a stable lomustine fragment ion at m/z 169. This was further confirmed by the fact that the lomustine fragments from this reaction matched with commercially available lomustine (see Supporting Information for details, Figures S10 and S11). Reactions for all $NaNO_2$ concentrations in THF/H_2O worked better than in the case of ACN/H_2O (Figure 2A). Also, the fragments from **3** were most abundant

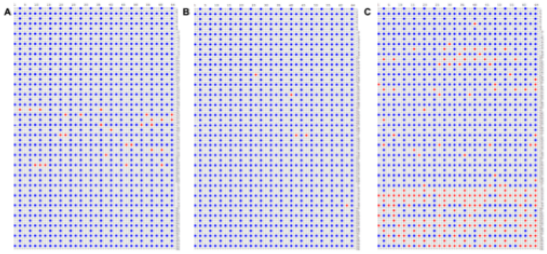

Figure 2. DESI-MS plate maps showing the presence or absence of expected ions at each spot where the nitrosation reaction conditions were tested using different stoichiometries and with commercially available standards. Blue dots indicate the presence of the m/z 169 expected stable fragment for the reaction product (successful reaction). Red dots indicate that the expected m/z for the reaction product was not present at the reaction spot (unsuccessful reaction condition). (A) Concentration screening using the lomustine ion (m/z 169) intensity and $NaNO_2$ as nitrosation reagent. (B) Solvent screening using the lomustine ion (m/z 169) intensity and $NaNO_2$ as nitrosation reagent. (C) Solvent screening using the lomustine ion (m/z 169) intensity and ^{t}BuONO as nitrosation reagent.

in the ACN/H_2O reactions compared to reactions in THF/H_2O, suggesting that the conversion of starting material was comparatively sluggish in ACN/H_2O. Next, eight different solvents (EtOH, MeOH, DCM, ACN, toluene, DMSO, THF, and EtOAc) were compared to optimize the continuous flow synthesis. All eight solvents produced similar outcomes using **4** as the nitrosation reagent (Figure 2B). When **5** was used, lomustine was detected in all solvents except THF and EtOAc (Figure 2C).

Nitrosation Reaction Optimization in Continuous Flow. We utilized the reaction conditions emerging from the DESI-MS high throughput experiments to optimize the flow synthesis and also check whether unsuccessful reactions identified by DESI-MS would negatively translate under flow conditions. From the DESI-MS experiments, THF was identified as the best solvent for nitrosation using **4**. Excess **4** was also used to maximize conversion of **3** to lomustine since the nitrosation reagents are hygroscopic and readily oxidize to nitrate.[53,54] Overall, the DESI-MS experiments were in excellent agreement with the outcomes of flow reaction conditions in terms of stoichiometry, reagents, and solvents.

A series of reactions (Table 2) were performed to maximize the conversion of **3** to lomustine under continuous synthesis

Table 2. Isolated Yields of Lomustine under Different Reaction Conditions Using 4 as the Nitrosation Reagent[a]

entry	residence time (min)	isolated yield (%) (Method 1)	isolated yield (%) (Method 2)	isolated yield (%) (Method 3)
1	0.5	26.8	–	43.7
2	1	48.8	–	50.6
3	3	51.6	41.2	63.1
4	5	79.0	54.4	74.5
5	8	59.0	–	68.7
6	10	50.2	–	65.3

[a]Temperature = 0 °C, solvent = $MeOH/H_2O$ (4:1).

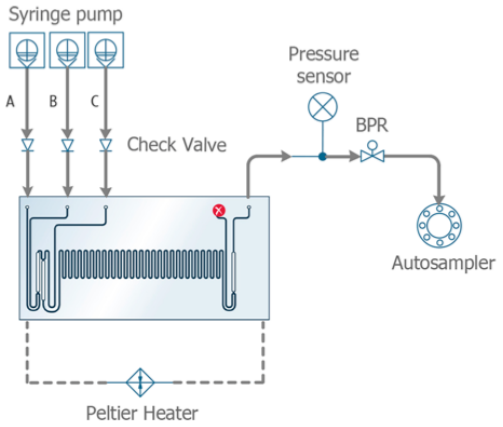

Figure 3. Microfluidic synthesis of lomustine using $NaNO_2/HCO_2H$ as nitrosation reagent in a Chemtrix 3225 SOR glass reactor chip. A = **3** in THF; B = HCO_2H (neat), C = $NaNO_2$ in $MeOH/H_2O$ (4:1).

conditions (Figure 3). Initially, we examined the reaction at 0 °C with a residence time of 30 s using TLC and MS to monitor the reaction progress. Gratifyingly, lomustine was obtained through this very short reaction time, albeit in low conversion (Table 2, entry 1). A systematic evaluation of residence times led to good lomustine yields and starting material conversions; however, longer residence times appeared to enhance the decomposition of lomustine (Table 2, entries 2–6). Consequently, we kept the temperature constant at 0 °C to avoid $NaNO_2$ decomposition to the diazonium salt that occurs at higher temperatures.[54]

Different purification methods were evaluated to isolate pure lomustine. Initially, the product was extracted with Et_2O (3 times) to exploit the low solubility of **3** in this solvent (Method 1). Unfortunately, TLC analysis revealed the presence of **3** in the organic layer as well as in the aqueous layer. Therefore, the combined organic extracts were dried over anhydrous Na_2SO_4

DOI: 10.1021/acs.oprd.8b00387
Org. Process Res. Dev. XXXX, XXX, XXX−XXX

and concentrated in vacuo to produce a yellowish oil that was redissolved in Et_2O, heated, and cooled in an ice bath to precipitate **3** from the mixture. NMR analysis of the filtrate revealed that 22% of **3** remained in the isolated lomustine product. Next, we purified the product by recrystallization from ACN (Method 2). Although we obtained very pure lomustine as determined by NMR analysis, recovery using this approach was low. Finally, we found that hot filtration from petroleum ether removed the insoluble **3** impurity (Method 3). Concentration of the filtrate after drying gave pure lomustine without a detectable amount of **3** by NMR. Using this method, we obtained a 74% isolated yield of pure lomustine under the conditions of 0 °C reaction and a residence time of 5 min using 3 equivalents of **4**.

The reaction was also optimized with respect to residence time, temperature, and solvent using **5** as the nitrosation agent (Figure 4 and Table 3). This optimization process led to the finding that an elevated residence time (8 min), lower temperature (25 °C), and increased **5** ratio (3 equiv) resulted in the most efficient conversion to lomustine (91% isolated yield) after Method 3 purification (Table 3, entry 11).

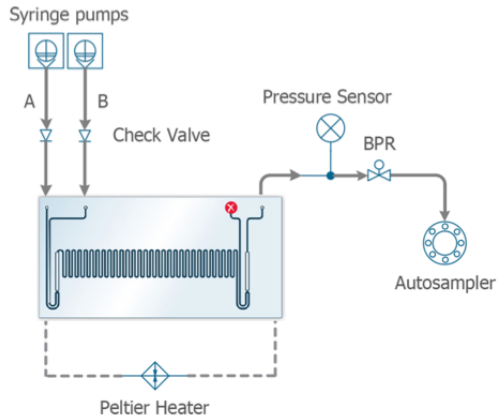

Figure 4. Microfluidic synthesis of lomustine using **5** as nitrosation reagent in a Chemtrix 3223 SOR glass reactor chip. A = **3** in ACN/EtOH (3.7:1); B = **5** in ACN.

Table 3. Synthesis of Lomustine under at Different Reaction Conditions Using 5 as the Nitrosation Reagent

entry	solvent (3.7:1)	temp (°C)	residence time (min)	isolated lomustine yield (%)
1	ACN/EtOH	50	0.5	68.3
2	ACN/EtOH	50	1	69.8
3	ACN/EtOH	50	3	60.0
4	ACN/EtOH	50	5	58.8
5	ACN/EtOH	50	8	51.9
6	ACN/EtOH	50	10	49.4
7	ACN/EtOH	25	0.5	48.8
8	ACN/EtOH	25	1	54.1
9	ACN/EtOH	25	3	66.5
10	ACN/EtOH	25	5	79.3
11	ACN/EtOH	25	8	91.2
12	ACN/EtOH	25	10	89.8
13	THF (100%)	25	3	36.5

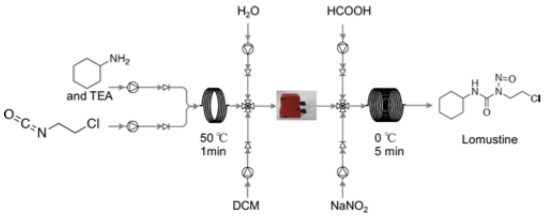

Figure 5. Schematic for the telescoped synthesis of lomustine using $NaNO_2/HCO_2H$ (**4**) as nitrosation reagent.

Table 4. Lomustine Synthesis Yields for Telescoped Reactions under Different Reagents, Residence Time, Stoichiometry, and Temperature Conditions

entry	nitrosation reagent	step 1	step 2	TEA (equiv)	isolated lomustine yield (%)
1	**4**	1 min, 50 °C	5 min, 0 °C	1	51.8
2	**4**	2 min, 50 °C	5 min, 0 °C	1	44.2
3	**4**	10 min, 50 °C	5 min, 0 °C	1	38.6
4	**4**	10 min, 50 °C	3 min, 0 °C	1	24.0
5	**5**	1 min, 50 °C	5 min, 50 °C	1	41.5
6	**5**	1 min, 50 °C	5 min, 25 °C	1	21.8
7	**5**	1 min, 50 °C	8 min, 25 °C	1	24.6
8	**5**	1 min, 50 °C	8 min, 25 °C	0.1	55.5
9	**5**	1 min, 50 °C	8 min, 25 °C	0.01	63.7

Telescoped Synthesis of Lomustine. The next step was to adapt the two-step sequence to a continuous flow setup. We sought to telescope the carbamylation and nitrosation reactions using the Chemtrix reactor chips. However, an extraction was required between the steps to remove the TEA present in the first reaction to avoid competitive consumption of the nitrosation reagent in the second step. We achieved this objective by incorporating a commercially available Zaiput liquid−liquid extractor to remove the base before the nitrosation step and by reoptimizing the synthesis using a FEP tubing reactor (Figure 5). In the beginning, the best reaction conditions included a 1 min residence time at 50 °C for the first step and a 5 min residence time at 0 °C for the second step, yielding 43 mg (51.8% overall yield) of pure lomustine (Table 4, entry 1). Efforts to improve the lomustine yield by changing the residence times of either the first or second steps were unsuccessful in the FEP tubing reactor using **4** as the nitrosation reagent (Table 4, entries 1−4).

DOI: 10.1021/acs.oprd.8b00387
Org. Process Res. Dev. XXXX, XXX, XXX−XXX

Subsequent telescoping experiments indicated that **5** was a better nitrosation reagent than **4** for the efficient synthesis of lomustine in flow. This is also true when the synthesis of lomustine was performed separately in glass reactor chips (Table 2 and 3). The final optimized conditions included a 1 min reaction time at 50 °C for the first step and an 8 min reaction time at 25 °C for the second step (Figure 6). As the small amount of extracted TEA from the first step negatively impacted TBN activity, lowering the amount of TEA used led to an increased production of lomustine (Table 4, entries 7−9) such that 1% TEA produced 110 mg (63%) of pure isolated lomustine via this reaction setup (Table 4, entry 9). TLC, NMR (^{1}H and ^{13}C), MS, and MS/MS data of lomustine obtained by this telescoped continuous route were a direct match with values measured for a commercially available lomustine sample.

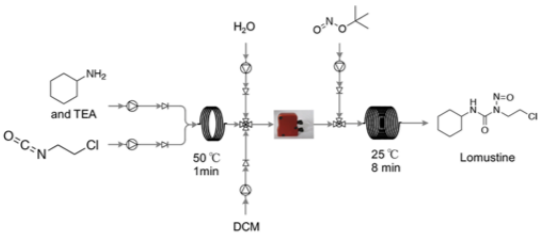

Figure 6. Schematic for the final telescoped synthesis of lomustine using **5** as a nitrosation reagent.

HPLC-MS was used to certify the purity of the synthesized lomustine and compare the total ion chromatogram (TIC) values of this material with a commercial lomustine standard. The TIC profile fully overlapped with the commercial standard without the appearance of any new byproducts (Figure 7).

■ CONCLUSION

In summary, we have developed a rapid continuous synthesis of lomustine using DESI-MS to guide the selection of reaction conditions in the second step of the two-step overall transformation. A total residence time of 9 min was employed to produce pure lomustine in 63% overall isolated yield compared to over 2 h to generate a lower product yield using batch conditions.[2,3,55,56] The two synthetic steps were optimized separately in glass chips and then translated using FEP tubing for telescoped scaling of the whole process. Only one in-line workup step was required for the two-step reaction sequence. Mixed solvents were used in the telescoped reaction to avoid clogging due to the low solubility of **3**. *tert*-Butyl nitrite, **5**, was found to be a milder and more efficient nitrosation reagent in this process to enable the isolation of pure lomustine via simple extraction, filtration, and washing. This synthesis is a faster and greener process that affords a significant reduction in reaction time, lower waste production, and avoidance of any chromatographic steps. Using this method, 110 mg/h of lomustine can be produced, equivalent to one dose/2 h for an agent that is administered orally every 6 weeks. Scale up and in-line recrystallization of lomustine are in progress.

■ EXPERIMENTAL SECTION

All chemicals and reagents were purchased from Sigma-Aldrich (St Louis, Missouri) and used without any purification. Intermediate **3** standard was purchased from 1Click Chemistry, Inc. (Kendall Park, NJ). Lomustine was purchased from ApexBio (Houston, TX).

Liquid Handling Robot. Assay plate setup and sample preparation steps for DESI-MS were done using a Biomek i7 (Beckman Coulter, Inc., Indianapolis, IN) dual-bridge liquid handling robot. A 384-tip head was employed to enable simultaneous transfer of 384 samples under the same conditions (speed of aspiration and dispensing, height of pipetting at source and destination positions, pattern of pipetting, etc.). An 8-channel head was used to provide more flexibility in terms of volumes transferred, layout of source and destination places, pipetting height, speed, and reaction stoichiometry. The high capacity deck accommodated all labware (robotic tips, plates, reservoirs) needed for assembling one reaction step. All robotic tips were made of chemically resistant polypropylene and disposable. Polypropylene multi-well plates and reservoirs, as well as custom-made Teflon reservoirs, were used during the experiments for reagent solutions. Methods were developed and validated using the Biomek point-and-click programming tool. Standard pipetting techniques used in this software were modified to optimize accurate transfer of highly volatile liquids.

Mass Spectrometry. Samples were analyzed using a Thermo Fisher TSQ Quantum Access MAX mass spectrometer that was connected with a Dionex Ultimate 3000 Series Pump and WPS-3000 Autosampler (Thermo Fisher Scientific, Waltham, MA). Electrospray ionization (ESI) analysis in full scan mode was used to monitor each reaction in both positive and negative ion modes. These data were recorded using optimized parameters for the ESI source and MS as follows: spraying solvent, ACN; spray voltage +3.5 kV (positive mode) and −4.0 kV (negative mode); capillary temperature, 250 °C;

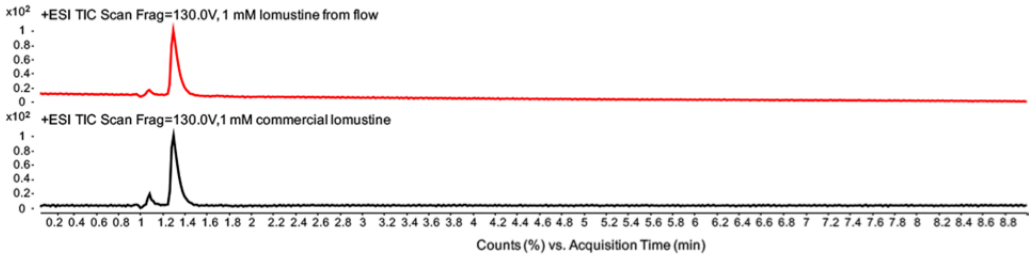

Figure 7. Total ion chromatogram (TIC) from HPLC-MS/MS and comparison between flow synthesized lomustine (top, red) and commercially available lomustine (bottom, black).

DOI: 10.1021/acs.oprd.8b00387
Org. Process Res. Dev. XXXX, XXX, XXX−XXX

sheath gas pressure, 10 psi; scan time, 1 s; Q1 peak width (fwhm), 0.70 Th; micro scans, 3. The autosampler settings were as follows: MS acquire time, 2 min; sample injection volume, 10 μL. Thermo Fisher Xcalibur software was used to process the data from the MS spectrometer.

NMR Analysis. ^{1}H NMR and ^{13}C NMR were acquired using a Bruker AV-III-500-HD NMR spectrometer (Billerica, MA, USA). Samples for NMR were prepared by dissolving ~5 mg of sample in $CDCl_3$. MestReNova 10.0 software was used to analyze the ^{1}H NMR and ^{13}C NMR.

Optimization in Microfluidic Glass Chips. The first and second steps of the lomustine synthesis were individually optimized using a Labtrix S1 (Chemtrix, Ltd., Netherlands) fitted with a glass microreactor containing staggered oriented ridges (SOR). Microchips 3223 (three inlets and one outlet, volume = 10 μL) or 3225 (four inlets and one outlet, volume = 10 μL) having channel widths of 300 μm and channel depth 120 μm were used. The S1 unit is able to independently drive five syringes connected to the microreactor mounted on a Peltier heating and cooling stage. All the gastight glass syringes used were obtained from Hamilton Company (Hamilton, Reno, NV). FEP tubing and fittings were used to connect the syringes with the selected connection port on the microreactor. All operations were controlled using a ChemTrix GUI software installed on a laptop that was connected to the Labtrix S1 via an USB cable.

Liquid−Liquid Separator. All the liquid−liquid separations were performed using a SEP-10 unit (Zaiput Flow Technologies, Cambridge, MA). The separator uses a porous hydrophobic PTFE membrane (OB-900) which allows flow of the organic phase through the membrane. The organic phase wets the membrane while the aqueous phase does not. A built-in pressure controller is used to maintain the appropriate pressure differential that is required of the flow for both sides of the membrane.

DESI-MS Analysis. The DESI-MS evaluation was done following the previously published method of Wleklinski et al.,[49] except that the density of reaction spots was 1536 spots/plate instead of 6144 spots/plate using reagents that were pipetted into standard polypropylene 384-well plates via the liquid handling robot. DESI-MS slides were fabricated from porous PTFE sheets (EMD, Millipore Fluoropore, Saint-Gobain, France) glued onto a glass support (Foxx Life Sciences, Salem, NH). The PTFE sheet was cut with scissors and bonded to the glass slides using spray adhesive (Scotch Spray mount) (see Supporting Information for details).

HPLC-MS Analysis. HPLC/MS analysis was performed using an Agilent 6545 UPLC/quadrupole time-of-flight (Q-TOF) mass spectrometer (Palo Alto, CA), fitted with an Agilent XDB-C18 column (3.5 μm, 150 mm × 2.1 mm i.d.) and a 5 μL injection volume. A binary mobile phase, consisting of solvent systems A and B, was used. Solvent A was 0.1% formic acid (v/v) in ddH_2O, and Solvent B was 0.1% formic acid (v/v) in ACN. Isocratic elution of A/B at 95:5 was used, with a column flow rate of 0.3 mL/min. Following separation, the column effluent was introduced by positive mode electrospray ionization (ESI) into the mass spectrometer. High mass accuracy spectra were collected between 70 and 1000 m/z. Mass accuracy was improved by continuously infusing Agilent Reference Mass Correction Solution (G1969−85001). The MS detection conditions were as follows: ESI capillary voltage, 3.5 kV; nebulizer gas pressure, 30 psig; gas temp, 325 °C; drying gas flow rate, 8.0 L/min; fragmentor voltage, 130 V; skimmer, 45 V; and OCT RF V, 750 V.

Carbamylation of Cyclohexylamine in Flow. ***CAUTION:*** *The 1-chloro-2-isocyanatoethane (**1**) starting material and cyclohexylurea product (**3**) are potent alkylating agents. Appropriate chemical inhalation masks and impermeable gloves must be worn while handling all reaction operations and product analyses in a ventilated hood.* A solution of cyclohexylamine (**1**, 500 mmol, 1 equiv) in THF was loaded into a 1 mL Hamilton gastight glass syringe. Triethylamine (TEA) (500 mmol, 1 equiv) and 1-chloro-2-isocyanatoethane (**2**, 700 mmol, 1.4 equiv) solutions in THF were individually loaded into another two 1 mL Hamilton gastight glass syringes. Each solution was simultaneously dispensed into the SOR 3225 reactor to engage the reactants. The syringe containing **2** was protected from light by covering it with aluminum foil. The reactions were run at 25, 50, and 65 °C, with each temperature condition run at residence times of 10, 30, 60, and 180 s. The reactions were monitored by TLC and ESI-MS. Product **3** was collected after evaporation and washing with cold Et_2O. The white solid product was stored in the dark at 4 °C. The subsequent TLC, ESI-MS, MS/MS, and NMR (^{1}H and ^{13}C) analyses were performed after purification (see Supporting Information for details).

DESI-MS Screening. ***CAUTION:*** *The cyclohexylurea starting material (**3**) and lomustine product are potent alkylating agents. Appropriate chemical inhalation masks and impermeable gloves must be worn while handling all reaction operations and product analyses in a ventilated hood.* Stock solutions of **3** and nitrosation reagents were made at four different concentrations (50, 100, 150, 200 mmol) in THF and ACN (see Supporting Information, Figure S2). Each reagent solution was also prepared (0.1 M) in eight different solvents (EtOAc, THF, DMSO, toluene, ACN, DCM, EtOH, and MeOH; see Supporting Information, Figure S3). Initially, 20 μL of **3** solution were dispensed into a 384-well master plate and then the corresponding nitrosation reagents were added to the plate in a 1:1 stoichiometry using a Beckman i7 liquid handling robot, resulting in a final volume of 40 μL in each well. Moreover, a master plate was made using only commercially available **3** and lomustine to compare the data (see Supporting Information, Figure S4). Rhodamine was dissolved in ACN (0.25 mg/mL) and transferred to a reservoir. A pin tool fitted with 50 nL pins was used to transfer solutions from the master plates as well as from the rhodamine reservoir onto the DESI-MS substrates. The master plate was pinned three times in separate locations with reaction mixtures and rhodamine once, resulting in 1536 density on the microtiter plate used as the DESI-MS substrate (see Supporting Information for details).

Nitrosation of 3 in Flow. ***CAUTION:*** *The cyclohexylurea starting material (**3**) and lomustine product are potent alkylating agents. Appropriate chemical inhalation masks and impermeable gloves must be worn while handling all reaction operations and product analyses in a ventilated hood.* A solution of **3** (245 mmol, 1 equiv) in 98% formic acid was loaded into a 1 mL Hamilton gastight glass syringe. A $NaNO_2$ (735 mmol, 3 equiv) solution in MeOH/H_2O (4:1) was separately loaded into another 1 mL Hamilton gastight glass syringe and dispensed into the SOR 3225 reactor to engage the reactants. The reactions were run at 0 °C, using residence times of 30 s, 1, 3, 5, 8, and 10 min. For nitrosation with **5**, solutions of **3** in ACN/EtOH (3.7:1) (200 mmol, 1 equiv) and **5** in ACN (600 mmol, 3 equiv, protected from light by covering the syringe

DOI: 10.1021/acs.oprd.8b00387
Org. Process Res. Dev. XXXX, XXX, XXX−XXX

with aluminum foil) were loaded into two separate 1 mL Hamilton gastight glass syringes and dispensed into the SOR 3223 reactor. All the reactions were monitored at two different temperatures (50 and 25 °C) at residence times of 30 s, 1, 3, 5, 8, and 10 min. Reaction progress was monitored by TLC and ESI-MS. The reaction mixtures were extracted by Et_2O, evaporated, and dried over anhydrous Na_2SO_4. The crude oily product was purified by dissolving it in hot petroleum ether, hot filtering the solution, and evaporating the filtrate to dryness under reduced pressure to give the yellowish solid lomustine that was stored at −20 °C. TLC, ESI-MS, MS/MS, NMR (^{1}H and ^{13}C), and yield analyses were performed after purification (see Supporting Information for details).

Telescoped Synthesis of Lomustine in Flow. *CAUTION: The starting material (**2**), intermediate (**3**), and lomustine product are potent alkylating agents. Appropriate chemical inhalation masks and impermeable gloves must be worn while handling all reaction operations and product analyses in a ventilated hood.* A solution of a 1:1 mixture of **1** (0.5 M, 1 equiv) and TEA (0.05 M, 0.01 equiv) in DCM was loaded into a 5 mL Hamilton gastight glass syringe. A solution of **2** in THF (0.7 M, 1.2 equiv) was separately loaded into another 5 mL Hamilton gastight glass syringe. Each solution was simultaneously dispensed through a T-connector into a 0.8 mm diameter chemically resistant fluorinated ethylene propylene (FEP) tube reactor at 50 °C for 1 min. The output from the first reactor was connected to a four-way connector where H_2O and DCM were added from two additional syringes. This mixture was introduced into a Zaiput liquid−liquid separator (Cambridge, MA), and the organic phase was fed to another four-way connector where a formic acid and sodium nitrite (1.5 M, 3 equiv) solution in MeOH/H_2O (4:1) was added via another two 5 mL Hamilton gastight glass syringes. This mixture was passed through a second FEP tube reactor at 0 °C for 5 min. In the telescoped reactions using **5**, a three-way connector was connected to the organic phase emerging from the Zaiput separator using doubled concentrations of all starting materials (**1**, 1 M; **2**, 1.4 M). An ACN solution of **5** (3 M, 3 equiv) was introduced from a 5 mL Hamilton gastight syringe. Two separate syringe pumps and three/four syringe pumps integrated into the Chemtrix system were used to dispense all solutions and solvents. The reactions were monitored by TLC and ESI-MS. The purification and analyses were conducted as described above, except that HPLC-MS analysis was performed to evaluate the purity of the product (see Supporting Information for details).

■ ASSOCIATED CONTENT

Supporting Information

The Supporting Information is available free of charge on the ACS Publications website at DOI: 10.1021/acs.oprd.8b00387.

Details of the experimental outline, DESI-MS analysis, summary of DESI-MS experimental findings, flow rates for the continuous flow synthesis, impurity analysis, and spectral data (PDF)

■ AUTHOR INFORMATION

Corresponding Author

*E-mail: davethom@purdue.edu.

ORCID

R. Graham Cooks: 0000-0002-9581-9603

David H. Thompson: 0000-0002-0746-1526

Notes

The authors declare no competing financial interest.

■ ACKNOWLEDGMENTS

We thankfully acknowledge the financial support from the Department of Defense: Defense Advanced Research Projects Agency (Award No. W911NF-16-2-0020) and NIH Grant P30 CA023168 of the Purdue University Center for Cancer Research (NMR, MS, and MPF Shared Resources). The efforts of Samyukta Sah, Yuta Moriuchi, Deborah M. Aremu, Ryan Hilger (Amy Facility at Purdue University, Department of Chemistry, Teflon reservoir fabrication), Larisa Avramova, and Andy Koswara are also noted with great appreciation.

■ REFERENCES

(1) Chakkath, T.; Lavergne, S.; Fan, T. M.; Bunick, D.; Dirikolu, L. Alkylation and carbamylation effects of lomustine and its major metabolites and MGMT expression in canine cells. *Vet. Sci.* **2015**, *2*, 52−68.

(2) Dirikolu, L.; Chakkath, T.; Fan, T.; Mente, N. R. Synthesis of trans-and cis-4′-hydroxylomustine and development of validated analytical method for lomustine and trans-and cis-4′-hydroxylomustine in canine plasma. *J. Anal. Toxicol.* **2009**, *33*, 595−603.

(3) Lown, J. W.; Chauhan, S. M. S. Synthesis of specifically nitrogen-15- and carbon-13-labeled antitumor (2-haloethyl)nitrosoureas. The study of their conformations in solution by nitrogen-15 and carbon-13 nuclear magnetic resonance electronic control in their aqueous decomposition. *J. Org. Chem.* **1981**, *46*, 5309−5321.

(4) Kaina, B.; Christmann, M.; Naumann, S.; Roos, W. P. MGMT: Key node in the battle against genotoxicity, carcinogenicity and apoptosis induced by alkylating agents. *DNA Repair* **2007**, *6*, 1079−1099.

(5) Lee, F. Y.; Workman, P.; Roberts, J. T.; Bleehen, N. M. Clinical pharmacokinetics of oral CCNU (lomustine). *Cancer Chemother. Pharmacol.* **1985**, *14*, 125−131.

(6) Funaro, J.; Friedman, H.; Weant, M. A costly "rebranding" of an old drug comes with a 700% price increase. *Cancer Lett.* **2017**, 13−14.

(7) Webb, D.; Jamison, T. F. Continuous flow multi-step organic synthesis. *Chem. Sci.* **2010**, *1*, 675−680.

(8) Wegner, J.; Ceylan, S.; Kirschning, A. Ten key issues in modern flow chemistry. *Chem. Commun.* **2011**, *47*, 4583−4592.

(9) Yoshida, J. I.; Kim, H.; Nagaki, A. Green and sustainable chemical synthesis using flow microreactors. *ChemSusChem* **2011**, *4*, 331−340.

(10) Yoshida, J.-i.; Takahashi, Y.; Nagaki, A. Flash chemistry: flow chemistry that cannot be done in batch. *Chem. Commun.* **2013**, *49*, 9896−9904.

(11) Hessel, V.; Kralisch, D.; Kockmann, N.; Noël, T.; Wang, Q. Novel process windows for enabling, accelerating, and uplifting flow chemistry. *ChemSusChem* **2013**, *6*, 746−789.

(12) Jensen, K. F.; Reizman, B. J.; Newman, S. G. Tools for chemical synthesis in microsystems. *Lab Chip* **2014**, *14*, 3206−12.

(13) Gutmann, B.; Cantillo, D.; Kappe, C. O. Continuous-flow technology-a tool for the safe manufacturing of active pharmaceutical ingredients. *Angew. Chem., Int. Ed.* **2015**, *54*, 6688−728.

(14) Cambié, D.; Bottecchia, C.; Straathof, N. J. W.; Hessel, V.; Noël, T. Applications of continuous-flow photochemistry in organic synthesis, material science, and water treatment. *Chem. Rev.* **2016**, *116*, 10276−10341.

(15) Poh, J. S.; Makai, S.; von Keutz, T.; Tran, D. N.; Battilocchio, C.; Pasau, P.; Ley, S. V. Rapid asymmetric synthesis of disubstituted allenes by coupling of flow-generated diazo compounds and propargylated amines. *Angew. Chem., Int. Ed.* **2017**, *56*, 1864−1868.

(16) Yu, Z.; Ye, X.; Xu, Q.; Xie, X.; Dong, H.; Su, W. A fully continuous-flow process for the synthesis of p-cresol: impurity analysis and process optimization. *Org. Process Res. Dev.* **2017**, *21*, 1644−1652.

(17) Britton, J.; Raston, C. L. Multi-step continuous-flow synthesis. *Chem. Soc. Rev.* **2017**, *46*, 1250−1271.
(18) Berton, M.; Huck, L.; Alcázar, J. On-demand synthesis of organozinc halides under continuous flow conditions. *Nat. Protoc.* **2018**, *13*, 324−334.
(19) Hessel, V. Novel process windows − gate to maximizing process intensification via flow chemistry. *Chem. Eng. Technol.* **2009**, *32*, 1655−1681.
(20) Zaborenko, N.; Bedore, M. W.; Jamison, T. F.; Jensen, K. F. Kinetic and scale-up investigations of epoxide aminolysis in microreactors at high temperatures and pressures. *Org. Process Res. Dev.* **2011**, *15*, 131−139.
(21) Wiles, C.; Watts, P. Recent advances in micro reaction technology. *Chem. Commun.* **2011**, *47*, 6512−6535.
(22) Wegner, J.; Ceylan, S.; Kirschning, A. Flow chemistry − a key enabling technology for (multistep) organic synthesis. *Adv. Synth. Catal.* **2012**, *354*, 17−57.
(23) Snead, D. R.; Jamison, T. F. End-to-end continuous flow synthesis and purification of diphenhydramine hydrochloride featuring atom economy, in-line separation, and flow of molten ammonium salts. *Chem. Sci.* **2013**, *4*, 2822−2827.
(24) Len, C.; Bruniaux, S.; Delbecq, F.; Parmar, V. Palladium-catalyzed Suzuki−Miyaura cross-coupling in continuous flow. *Catalysts* **2017**, *7*, 146.
(25) Lummiss, J. A. M.; Morse, P. D.; Beingessner, R. L.; Jamison, T. F. Towards more efficient, greener syntheses through flow chemistry. *Chem. Rec.* **2017**, *17*, 667−680.
(26) Morse, P. D.; Jamison, T. F. Synthesis and utilization of nitroalkyne equivalents in batch and continuous flow. *Angew. Chem., Int. Ed.* **2017**, *56*, 13999−14002.
(27) Gustafsson, T.; Ponten, F.; Seeberger, P. H. Trimethylaluminium mediated amide bond formation in a continuous flow microreactor as key to the synthesis of rimonabant and efaproxiral. *Chem. Commun.* **2008**, 1100−1102.
(28) Hopkin, M. D.; Baxendale, I. R.; Ley, S. V. An expeditious synthesis of imatinib and analogues utilising flow chemistry methods. *Org. Biomol. Chem.* **2013**, *11*, 1822−39.
(29) Deadman, B. J.; Hopkin, M. D.; Baxendale, I. R.; Ley, S. V. The synthesis of Bcr-Abl inhibiting anticancer pharmaceutical agents imatinib, nilotinib and dasatinib. *Org. Biomol. Chem.* **2013**, *11*, 1766−1800.
(30) Murray, P. R. D.; Browne, D. L.; Pastre, J. C.; Butters, C.; Guthrie, D.; Ley, S. V. Continuous flow-processing of organometallic reagents using an advanced peristaltic pumping system and the telescoped flow synthesis of (e/z)-tamoxifen. *Org. Process Res. Dev.* **2013**, *17*, 1192−1208.
(31) Zhang, P.; Russell, M. G.; Jamison, T. F. Continuous flow total synthesis of rufinamide. *Org. Process Res. Dev.* **2014**, *18*, 1567−1570.
(32) Snead, D. R.; Jamison, T. F. A three-minute synthesis and purification of ibuprofen: pushing the limits of continuous-flow processing. *Angew. Chem., Int. Ed.* **2015**, *54*, 983−7.
(33) Adamo, A.; Beingessner, R. L.; Behnam, M.; Chen, J.; Jamison, T. F.; Jensen, K. F.; Monbaliu, J. C.; Myerson, A. S.; Revalor, E. M.; Snead, D. R.; Stelzer, T.; Weeranoppanant, N.; Wong, S. Y.; Zhang, P. On-demand continuous-flow production of pharmaceuticals in a compact, reconfigurable system. *Science* **2016**, *352*, 61−7.
(34) Lin, H.; Dai, C.; Jamison, T. F.; Jensen, K. F. A rapid total synthesis of ciprofloxacin hydrochloride in continuous flow. *Angew. Chem., Int. Ed.* **2017**, *56*, 8870−8873.
(35) Zhang, P.; Weeranoppanant, N.; Thomas, D. A.; Tahara, K.; Stelzer, T.; Russell, M. G.; O'Mahony, M.; Myerson, A. S.; Lin, H.; Kelly, L. P.; Jensen, K. F.; Jamison, T. F.; Dai, C.; Cui, Y.; Briggs, N.; Beingessner, R. L.; Adamo, A. Advanced continuous flow platform for on-demand pharmaceutical manufacturing. *Chem. - Eur. J.* **2018**, *24*, 2776−2784.
(36) Falcone, C. E.; Jaman, Z.; Wleklinski, M.; Koswara, A.; Thompson, D. H.; Cooks, R. G. Reaction screening and optimization of continuous-flow atropine synthesis by preparative electrospray mass spectrometry. *Analyst* **2017**, *142*, 2836−2845.
(37) Loren, B. P.; Wleklinski, M.; Koswara, A.; Yammine, K.; Hu, Y.; Nagy, Z. K.; Thompson, D. H.; Cooks, R. G. Mass spectrometric directed system for the continuous-flow synthesis and purification of diphenhydramine. *Chem. Sci.* **2017**, *8*, 4363−4370.
(38) Wleklinski, M.; Falcone, C. E.; Loren, B. P.; Jaman, Z.; Iyer, K.; Ewan, H. S.; Hyun, S.-H.; Thompson, D. H.; Cooks, R. G. Can accelerated reactions in droplets guide chemistry at scale? *Eur. J. Org. Chem.* **2016**, *2016*, 5480−5484.
(39) Ewan, H. S.; Iyer, K.; Hyun, S.-H.; Wleklinski, M.; Cooks, R. G.; Thompson, D. H. Multistep flow synthesis of diazepam guided by droplet-accelerated reaction screening with mechanistic insights from rapid mass spectrometry analysis. *Org. Process Res. Dev.* **2017**, *21*, 1566−1570.
(40) Riva, E.; Rencurosi, A.; Gagliardi, S.; Passarella, D.; Martinelli, M. Synthesis of (+)-dumetorine and congeners by using flow chemistry technologies. *Chem. - Eur. J.* **2011**, *17*, 6221−6226.
(41) Ahmed-Omer, B.; Sanderson, A. J. Preparation of fluoxetine by multiple flow processing steps. *Org. Biomol. Chem.* **2011**, *9*, 3854−3862.
(42) Newton, S.; Carter, C. F.; Pearson, C. M.; Alves, L. D.; Lange, H.; Thansandote, P.; Ley, S. V. Accelerating spirocyclic polyketide synthesis using flow chemistry. *Angew. Chem., Int. Ed.* **2014**, *53*, 4915−4920.
(43) Peeva, L.; Da Silva Burgal, J.; Heckenast, Z.; Brazy, F.; Cazenave, F.; Livingston, A. Continuous consecutive reactions with inter-reaction solvent exchange by membrane separation. *Angew. Chem., Int. Ed.* **2016**, *55*, 13576−13579.
(44) Brasholz, M.; Macdonald, J. M.; Saubern, S.; Ryan, J. H.; Holmes, A. B. A gram-scale batch and flow total synthesis of perhydrohistrionicotoxin. *Chem. - Eur. J.* **2010**, *16*, 11471−11480.
(45) Jensen, K. F. Silicon-based microchemical systems: Characteristics and applications. *MRS Bull.* **2006**, *31*, 101−107.
(46) Geyer, K.; Gustafsson, T.; Seeberger, P. H. Developing continuous-flow microreactors as tools for synthetic chemists. *Synlett* **2009**, *2009*, 2382−2391.
(47) Kim, H.; Min, K. I.; Inoue, K.; Im, D. J.; Kim, D. P.; Yoshida, J. Submillisecond organic synthesis: Outpacing Fries rearrangement through microfluidic rapid mixing. *Science* **2016**, *352*, 691−694.
(48) Troshin, K.; Hartwig, J. F. Snap deconvolution: An informatics approach to high-throughput discovery of catalytic reactions. *Science* **2017**, *357*, 175−181.
(49) Wleklinski, M.; Loren, B. P.; Ferreira, C. R.; Jaman, Z.; Avramova, L.; Sobreira, T. J. P.; Thompson, D. H.; Cooks, R. G. High throughput reaction screening using desorption electrospray ionization mass spectrometry. *Chem. Sci.* **2018**, *9*, 1647−1653.
(50) Jaman, Z.; Mufti, A.; Sah, S.; Avramova, L.; Thompson, D. H. High throughput experimentation and continuous flow validation of Suzuki−Miyaura cross-coupling reactions. *Chem. - Eur. J.* **2018**, *24*, 9546−9554.
(51) Yan, X.; Bain, R. M.; Cooks, R. G. Organic reactions in microdroplets: reaction acceleration revealed by mass spectrometry. *Angew. Chem., Int. Ed.* **2016**, *55*, 12960−12972.
(52) Ifa, D. R.; Manicke, N. E.; Dill, A. L.; Cooks, R. G. Latent fingerprint chemical imaging by mass spectrometry. *Science* **2008**, *321*, 805−805.
(53) Freeman, E. S. The kinetics of the thermal decomposition of sodium nitrate and of the reaction between sodium nitrite and oxygen. *J. Phys. Chem.* **1956**, *60*, 1487−1493.
(54) Fox, J. B.; Suhre, F. B. The determination of nitrite: a critical review. *Crit. Rev. Anal. Chem.* **1985**, *15* (3), 283−313.
(55) Johnston, T. P.; McCaleb, G. S.; Montgomery, J. A. Synthesis of chlorozotocin, the 2-chloroethyl analog of the anticancer antibiotic streptozotocin. *J. Med. Chem.* **1975**, *18*, 104−106.
(56) Baracu, I.; Niculescu-Duvaz, I. Potential anticancer agents. XXVIII. Synthesis of Some Cyclohexanone Derived N-Nitrosoureas. *J. Prakt. Chem.* **1985**, *327*, 675−681.

DOI: 10.1021/acs.oprd.8b00387
Org. Process Res. Dev. XXXX, XXX, XXX−XXX

ChemPubSoc Europe
DOI: 10.1002/chem.201801165
CHEMISTRY A European Journal
Full Paper

Flow Reactions

High Throughput Experimentation and Continuous Flow Validation of Suzuki–Miyaura Cross-Coupling Reactions

Zinia Jaman,[a] Ahmed Mufti,[b] Samyukta Sah,[a] Larisa Avramova,[a] and David H. Thompson*[a]

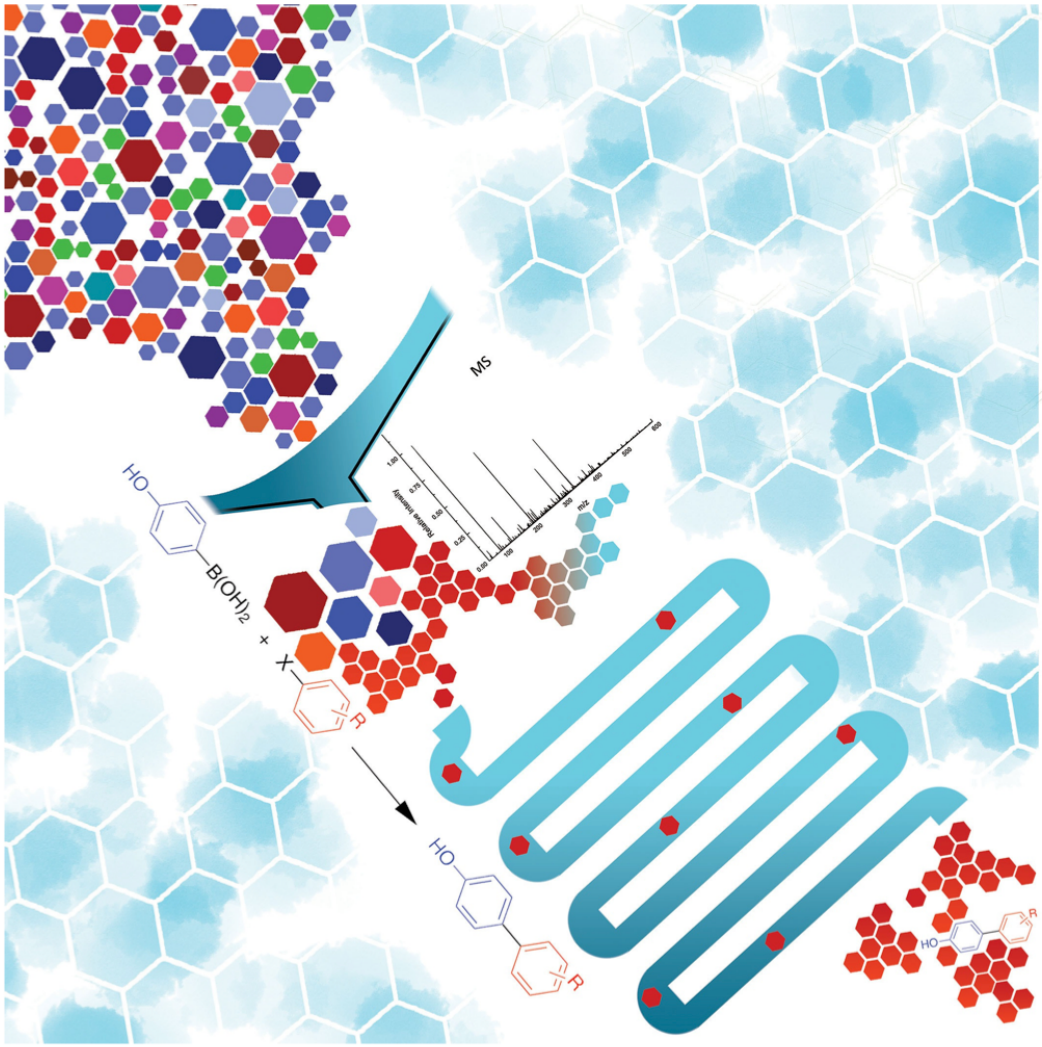

© 2018 Wiley-VCH Verlag GmbH & Co. KGaA, Weinheim

ChemPubSoc Europe

CHEMISTRY A European Journal
Full Paper

Abstract: Traditional methods to discover optimal reaction conditions for small molecule synthesis is a time-consuming effort that requires large quantities of material and a significant expenditure of labor. High-throughput techniques are a potentially transformative approach for reaction condition screening, however, rapid validation of the reaction hotspots under continuous flow conditions remains necessary to build confidence in high throughput screening hits. Continuous flow technology offers the opportunity to upscale the screening hotspots and optimize their output of the target compounds due to the exceptional heat and mass transfer ability of flow reactions that are conducted in a smaller and safer reaction volume. We report a robotic high throughput technique to execute reactions in multi-well plates that were coupled with fast mass spectrometric analysis using an autosampler to accelerate the reaction screening process. Palladium-catalyzed Suzuki–Miyaura cross-coupling reactions were screened in this system and a heat map was generated to identify the best reaction conditions for downstream scale-up under continuous flow. Here, high throughput experimentation reactions in 96-well plates were performed for 1 h at 50 °C, 100 °C, 150 °C, and 200 °C before diluting them into 384-well plates for mass analysis. With the aid of high throughput tools, 648 unique experiments were conducted in duplicate. The cross-coupling reactions were evaluated as a function of stoichiometry, temperature, concentration, order of addition, and substrate type. The hotspots from high throughput experimentation were examined using a microfluidic Chemtrix system that confirmed the positive reaction leads as true positives. Negative outcomes identified by these experiments were found to be true negatives by microfluidic reaction evaluation. Quantitation of product yields was performed using high-performance liquid chromatography-mass spectrometry (HPLC/MS-MS).

Introduction

The development of automated high throughput experimentation (HTE) methods has been shown to boost lab productivity by rapid generation of comprehensive reaction data that enriches our understanding of reaction scope and limitations.[1] HTE across a range of settings have impacted many areas of biology, drug discovery, medicinal chemistry,[2] and catalysis.[4] Automated reactions can often be run in parallel, but the downstream analysis is typically a bottleneck due to relatively slow chromatographic separation and/or quantitation methods. HTE coupled with rapid mass spectrometry (MS) analysis can accelerate both the discovery and optimization of reaction conditions, particularly in the cases of chemical process development[3a,4] and (bio)pharmaceutical drug development where pressures to shorten the time to market are increasing.[5] HTE has been challenging in the case of organic reaction optimization, especially for catalytic reactions that may employ solid catalysts or volatile organic solvents.[3b,4a]

The central goal in HTE for reaction optimization is the discovery of the best experimental conditions for a given set of precursors to identify the most prominent reaction hotspots. After HTE, a quick validation of these hotspots is used to build confidence in the reaction hits identified by the HTE process. Microfluidic reaction evaluation of the HTE hits are an essential step for validating organic transformations[6] under continuous flow conditions. This has been shown to be especially true for catalytic reactions that can be achieved under faster and greener conditions.[7] Moreover, fast microfluidic synthesis of small organic molecules, coupled with continuous reaction monitoring using electrospray ionization mass spectrometry (ESI-MS), shows even greater promise for rapid optimization of continuous production methodology.[8] Here, we report a study of the Suzuki–Miyura (S-M) cross-coupling reaction as a test bed for HTE reaction optimization using ESI-MS as a readout tool. The S-M reaction was chosen because carbon-carbon bond formation via palladium-catalyzed S-M cross-coupling is an important reaction for small molecule synthesis[9] that has been widely used.[10] Recently Perera et al. and Santanilla et al. have reported[3b,6] high throughput S-M cross-coupling reactions in both flow and batch mode with demonstration of the ability to screen reactions quickly on the nanomole-scale under different conditions. These efforts encouraged us to explore the S-M cross-coupling reactions in the synthesis of precursor compounds of importance in biological, pharmaceutical, and materials applications.

A simple and efficient technique for identifying and optimizing S-M reaction conditions with different functional group tolerance is described. Important biphenyl intermediates (Figure 1) were synthesized using S-M cross-coupling reactions without protecting the functional groups. Our HTE effort was focused on identifying the preferred reaction parameters that would enable faster optimization of microfluidic reactions by eliminating failed reaction conditions from the flow chemistry search process. Decreasing the number of unsuccessful transformations will focus efforts on the rapid discovery of compound leads whose syntheses are more robust and economical in a shorter period of time.

[a] *Z. Jaman, S. Sah, L. Avramova, Prof. D. H. Thompson*
Department of Chemistry, Bindley Bioscience Centre
Purdue University
1203 W State St
West Lafayette, IN 47906 (USA)
E-mail: davethom@purdue.edu

[b] *A. Mufti*
School of Chemical Engineering
Purdue University
480 W Stadium Ave
West Lafayette, IN 47907 (USA)

Supporting information and the ORCID identification number(s) for the author(s) of this article can be found under: https://doi.org/10.1002/chem.201801165.

 © 2018 Wiley-VCH Verlag GmbH & Co. KGaA, Weinheim

ChemPubSoc Europe
CHEMISTRY A European Journal
Full Paper

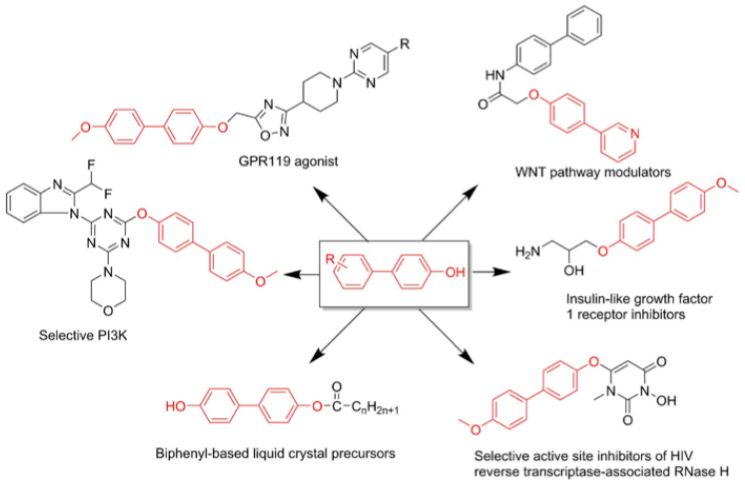

Figure 1. [1,1′-Biphenyl]-4-ol synthon and its use in some important biological, pharmaceutical, and materials science target compounds.

The S-M reaction has already been reported under some limited ranges of flow conditions,[7,11] nonetheless, we explored its utility toward the synthesis of important synthons[12] in a microfluidic reactor using EtOH as solvent to broadly explore the utility of this transformation.[7,10c]

Automated HTE of S-M reactions was performed in 96-well plates using 4-hydroxyphenylboronic acid and 11 different aryl halides (Scheme 1) with order of addition, stoichiometry, temperature, and concentration as independent variables. These experiments led to the discovery of optimized batch conditions from hundreds of different reaction conditions using XPhosPdG3 as catalyst and 1,8-diazabicyclo[5.4.0]undec-7-ene (DBU) as the base. Small scale microfluidic reactions employing the best conditions from the batch reaction screening produced up to 98% yield of S-M coupled products by HPLC/MS-MS analysis, thus validating our findings from HTE.

Results and Discussion

High Throughput Experimentation: A high-precision Biomek FX robot was used for the preparation of nanoliter scale reaction mixtures for automated HT screening of S-M reaction conditions with downstream MS analysis. The reactions were performed in glass vials sealed within four 96-well aluminum blocks and the outcome monitored with a highly sensitive triple quadrupole MS coupled to an autosampler for rapid determination of the reaction product distribution. Full mass spectra in negative ion mode were recorded for each reaction mixture.

The S-M cross-coupling reactions were evaluated in EtOH using 4-hydroxyphenylboronic acid (**1**), various aryl halides, and XPhosPdG3 as palladium catalyst (Scheme 1), to explore the impact of different aryl halide substrates on reaction efficiency without the use of additional protection/deprotection steps. Reaction mixtures (45 µL of total volume of each well) were deposited in duplicate within four 96 glass-lined Al well plates and the reactions heated at either 50, 100, 150, or 200 °C for 1 h before quenching to 20 °C, centrifuging, and diluting into 384 well plates for MS analysis. Each square in Figure 2 represents a unique reaction condition. The first two columns and last four columns are negative controls. Although the ionization efficiencies vary for each compound, the outcomes are reported based on reaction product peak intensity to enable a simple and uniform comparison (see Supporting Information for details).

Our initial HTE experiments explored the S-M reaction by adding in sequence a mixture of **1**, base, and catalyst solution in EtOH, followed by aryl halide (**2**–**12**) addition. Unfortunately, no product peak was detected in MS, although a prominent peak corresponding to the hydrolyzed boronic acid product was observed. These findings suggest that the catalyst was poisoned by the base while sitting idle at 20 °C during subsequent robotic reagent transfers over the intervening period (20 min) before the reaction was initiated by heating. When the order of addition was changed to aryl halide and **1**, followed by base and catalyst in sequence, the product peak was observed in the resulting MS, although the product yields were not satisfactory (Figure 2, top). We attribute these finding to the consumption of **1** by base before catalyst addition such that insufficient boronic acid was available to participate in the catalytic cycle. This hypothesis was further supported by the observation of predominantly product ions in the MS under conditions of excess boronic acid (e.g., at 20:1–2:1 stoichiometries). Nonetheless, when the base solution was added after the catalyst, a significant increase in product conversion was observed (Figure 2, bottom), with the accompanying detection of self-coupled **1**-**1** product by MS (see Supporting Information for detail results).

 © 2018 Wiley-VCH Verlag GmbH & Co. KGaA, Weinheim

ChemPubSoc Europe
CHEMISTRY A European Journal
Full Paper

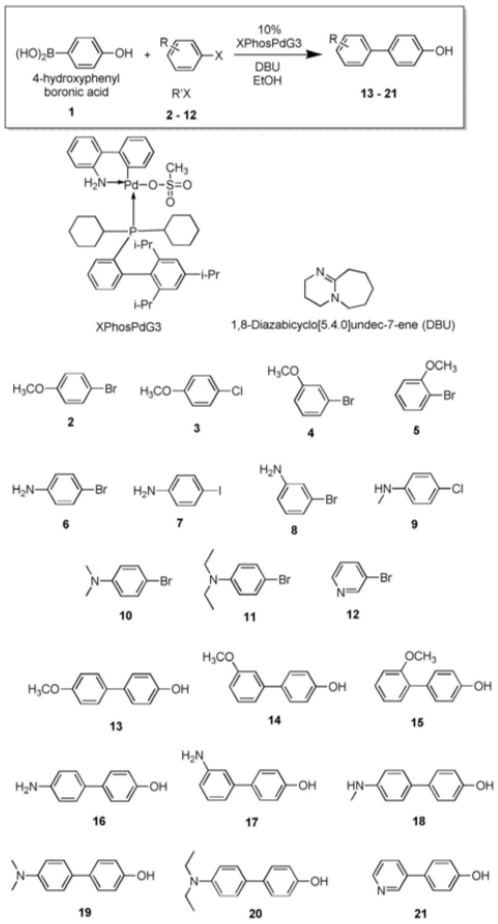

Scheme 1. Substrate scope evaluated in high-throughput experimentation of S-M cross-coupling reactions to generate various biphenyl products.

We subsequently utilized the optimal conditions identified in Figure 2 for a broader screen of aryl halide substrates. Our results show that both electron-rich and electron-deficient aryl halides (**2**–**12**) were tolerated to produce cross-coupled products in moderate to good yield as assessed by product peak intensities (Figure 3 A–D). Comparison of the anisole family of precursors (**2**–**5**) revealed that the *meta*-positioned methoxy group (**4**, Figure 3 C) provided more desired product than *ortho* (**5**, Figure 3 D) or *para* (**2**&**3**, Figure 3 A&B) due to the reduced electron donating contribution from the *meta* placement of this substituent.[13]

Haloanilines (**6**–**11**) were also transformed into the corresponding biphenyl products, yielding moderate peak intensities for the cross-coupled products (Figure 4 A–G). As seen in the anisole family of compounds, the *meta* product, **17** (**1**+**8**, Figure 4 C), produced a higher peak intensity than *para*, **16** (**1**+**6**/**7**, Figure 3 A&B), for the primary amine substrates. When aniline- and anisole-derived products were compared, higher product peak intensities were observed for the anisole family of compounds, **13**–**15** than the anilines series, **16**–**20** (Figures 3 and 4). We attribute these finding to the greater electron donating property of the amine versus methoxy substituents such that formation of the aminophenyl palladium intermediate is less favorable in the rate limiting oxidation addition step of the catalytic cycle in the aniline series.

The product peak intensities for secondary and tertiary substrates were higher than those observed for the primary amines (Figure 4 A–C vs. Figure 4 D–F), consistent with the observation that primary amines are known to more readily coordinate with palladium catalysts than secondary or tertiary amines due to steric hindrance.[14] In the case of the pyridine derivative, a higher product peak intensity was observed due to the comparative electron deficiency of the pyridine ring relative to the aniline series (**1**+**12**, Figure 4 G vs. Figure 4 A–F; see Supporting Information for detail results).

Figure 5 shows the product peak intensities for 504 unique Suzuki–Miyaura reactions, employing one of 11 different aryl halides and 4-hydroxyphenyl boronic acid in the presence of DBU and 10% XPhosPdG3. Since some low level peak intensities were observed in the negative control reactions that we attributed to noise during acquisition of the MS data, we used >50% peak intensity as the selection criterion to choose reaction hotspots in this map for subsequent evaluation in a series of microfluidic reactions.

Microfluidic evaluation of HT experimentation leads

After identifying reaction hotspots from the HTE campaign, we proceeded to test one of the favorable conditions for each reaction to determine the confidence level that could be assumed for the two different reaction formats (i.e., batch 96-well vs. continuous flow). For all microfluidic reactions, the reactions employing a 1:1 ratio of 4-hydroxyphenylboronic acid and aryl halide were evaluated for 0.5, 1, 3 and 6 min residence times at either 100 or 150 °C. Reactions using 10% XPhosPdG3 catalyst loadings were complicated by chip clogging problems shortly after initiating the reaction (see Supporting Information for details). This problem was obviated by reducing the catalyst loading to 0.5% since prior work has shown that S-M transformations are more efficient in continuous flow than under traditional bulk reaction conditions due to superior mass and heat transfer and greater mixing efficiency in the narrow reactor channels. The order of addition did not matter in the microfluidic synthesis since all the reagents come into contact within the same mixing region (Figure 6). The formation of the expected products was confirmed by TLC and MS. As the data in Figure 7 show, the results from microfluidic continuous reactions were comparable to the findings from bulk screening.

The data in Figure 7 shows that the S-M reaction tolerates electron donating substitutes in the aryl halide substrate to

© 2018 Wiley-VCH Verlag GmbH & Co. KGaA, Weinheim

ChemPubSoc Europe
CHEMISTRY A European Journal
Full Paper

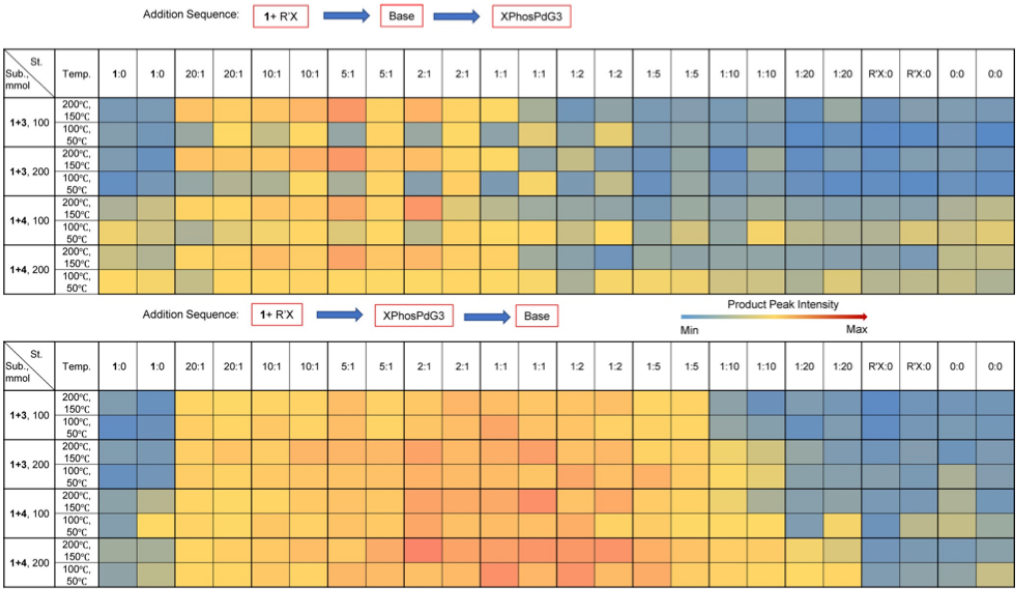

Figure 2. HT reaction outcomes as a function of reagent addition order and substrate concentration in the reaction mixture. Each quantity is an average of two experimental measurements. Each set of similar substrates and stoichiometries appears as a set of four conditions wherein the top left, top right, bottom left and bottom right entries are reactions run at 200 °C, 150 °C, 100 °C and 50 °C, respectively. The first two columns (St. = **1**:0) and last four columns (St. = R'X:0 and 0:0) are the negative controls. Sub = substrates; St = stoichiometry.

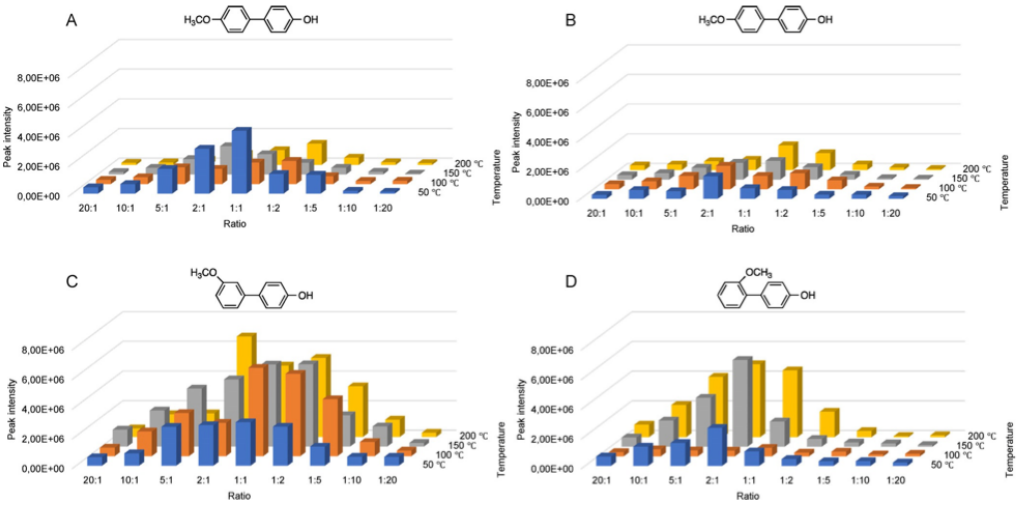

Figure 3. Comparative coupling efficiencies for anisole-type biphenyl products formed under different temperature and stoichiometric conditions. Reactant concen- trations were 200 mmol, except for **1** + **5** that was run at 100 mmol, 400 mmol DBU, and 10% XPhosPdG3. A = **1** + **2**; B = **1** + **3**; C = **1** + **4**; D = **1** + **5**.

afford the cross coupled products with varying efficiency. In both bulk and microfluidic experiments, *meta* (**1** + **4**) directed anisole biphenyl products showed higher product conversion than *ortho* (**1** + **5**), but in continuous flow processes, *para* (**1** + **2** & **1** + **3**) also showed higher product peak intensities (Figure 4 and 7). Similarly, bulky tertiary amine (**1** + **9**) and pyri-

© 2018 Wiley-VCH Verlag GmbH & Co. KGaA, Weinheim

ChemPubSoc Europe
CHEMISTRY A European Journal
Full Paper

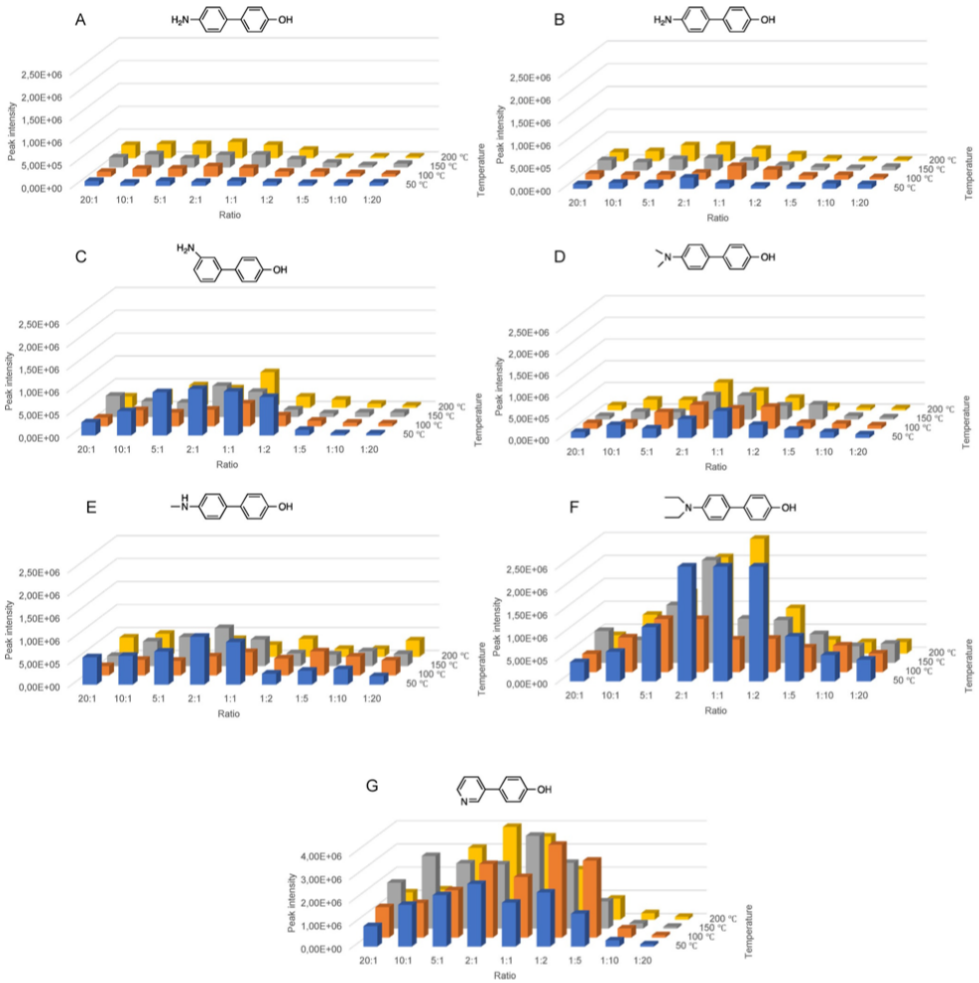

Figure 4. Comparative coupling efficiencies for aniline-type biphenyl products formed under different temperature and stoichiometric conditions. Reactant concentrations were 200 mmol, 400 mmol DBU, and 10% XPhosPdG3. A = **1** + **6**; B = **1** + **7**; C = **1** + **8**; D = **1** + **10**, E = **1** + **9**, F = **1** + **11**, G = **1** + **12**.

dine (**1** + **12**) precursors generated higher product peak intensities in both the bulk screening and flow synthesis formats.

We also investigated the negative results obtained from HTE and evaluated those reaction conditions under continuous flow (Figure 8). In both cases, almost no product peak was observed, even at extended residence times (e.g., 15 min at 150 °C in the case of **1** + **8**).

Next, we focused on testing the validity of using product ion intensities as a measure of reaction progress. The anisole and pyridine reaction products were selected for evaluation by HPLC/MS-MS since these products showed high peak intensities in both bulk screening and microfluidic reactions. A general trend of increasing product yield was observed for all anisoles (**2**–**5**) and pyridine **12** starting materials (Table 1). High yields were observed for **14** and **21** as was expected from the screening results. In most cases, there was good agreement between peak intensities and quantitative product yield. A low yield for **15** was observed due to the steric demands of the *o*-MeO substituent that requires more energy to drive the reaction.[12e, 13]

© 2018 Wiley-VCH Verlag GmbH & Co. KGaA, Weinheim

ChemPubSoc Europe
CHEMISTRY A European Journal
Full Paper

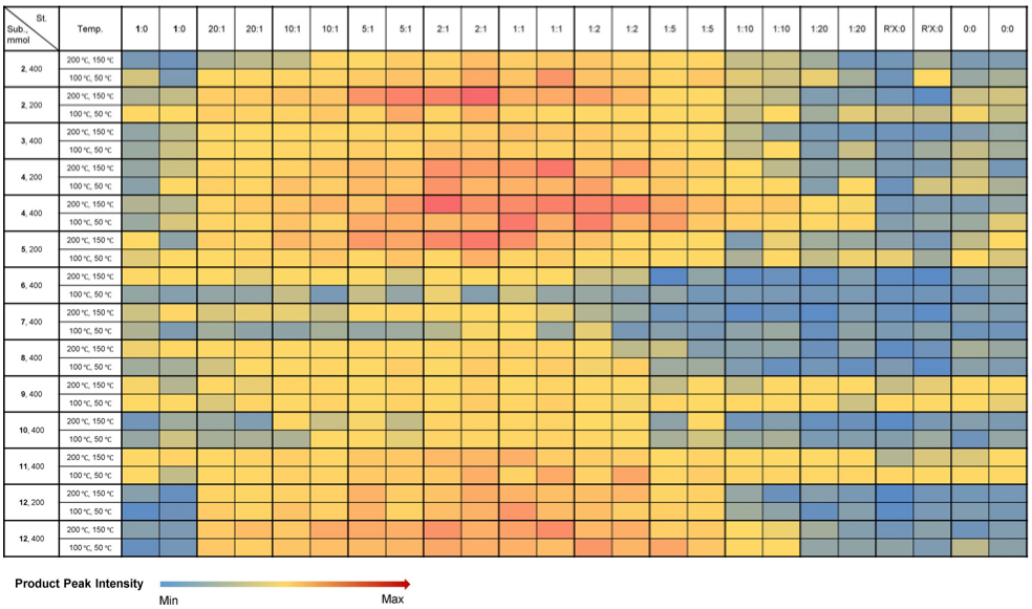

Figure 5. Product peak intensities observed for 504 unique S-M reactions run in bulk mode with the order of addition of base solution after the catalyst. Each quantity is an average of two experimental measurements. The product peak intensity data is normalized across the entire matrix. Each row indicates reactions of nine ratios of substrates including the control reactions at two different temperatures. Each set of similar substrates and stoichiometries appears as a set of four conditions, wherein the top left, top right, bottom left and bottom right entries are reactions run at 200, 150, 100 and 50 °C, respectively (see Supporting Information for details). The first two columns (St. = 1:0) and last four columns (St. = R'X:0 and 0:0) are the negative controls. Sub = substrates; St = stoichiometry.

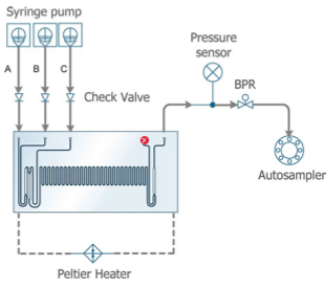

Figure 6. Chemtrix reactor and fluid handling for continuous flow synthesis of S-M cross coupling reactions. A = 1:1 mixture of 4-hydroxyphenylboronic acid and aryl halide; B = DBU, C = XPhosPdG3.

Conclusions

This investigation explored the use of a robotic HTE technique to execute reactions in 96-well arrays that were subsequently coupled with fast MS analysis using an autosampler. Palladium catalyzed S-M cross-coupling reactions were screened in this system to generate a heat map of reactivity to inform conditions for the downstream scale up in continuous flow. A total of 648 unique experiments using 4-hydroxyphenylboronic acid and 11 different aryl halides were explored in duplicate and the results reported as a function of MS peak intensity. The comparison of some successful reactions from HTE were run under microfluidic conditions; these experiments confirmed that the positive conditions identified by HTE were true positives. Furthermore, negative reaction conditions identified by this method also produced negative results under microfluidic conditions, even after long residence times at higher temperature. Moreover, quantitative analysis by HPLC/MS-MS provided evidence of a good correlation between HT reaction screening and microfluidic reactions.

This HTE and microfluidic validation approach may be equally applicable to other catalytic and noncatalytic reactions to rapidly reveal vast reactivity landscapes to guide reaction optimization efforts. This method might also be applied to the identification of optimal conditions for challenging substrates or the discovery of new routes for the production of bioactive molecules. Further investigation along these lines will be needed to assess the robustness of this correlation.

Experimental Section

All chemicals and reagents were purchased from Sigma–Aldrich (St. Louis, MO) and used without purification. All standards for quantitation were purchased from Combi-Blocks, Inc. (San Diego, CA).

© 2018 Wiley-VCH Verlag GmbH & Co. KGaA, Weinheim

ChemPubSoc Europe
CHEMISTRY A European Journal
Full Paper

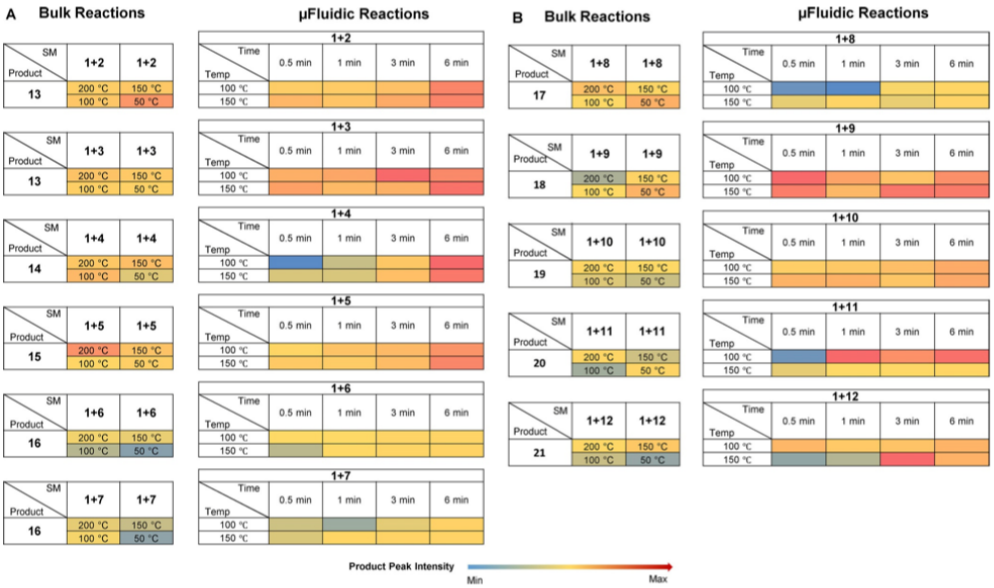

Figure 7. Comparison of microfluidic and bulk screening outcomes for S-M reactions performed under similar conditions using 200 mmol substrate loading and a 1:1 4-hydroxyphenylboronic acid:aryl halide stoichiometry.

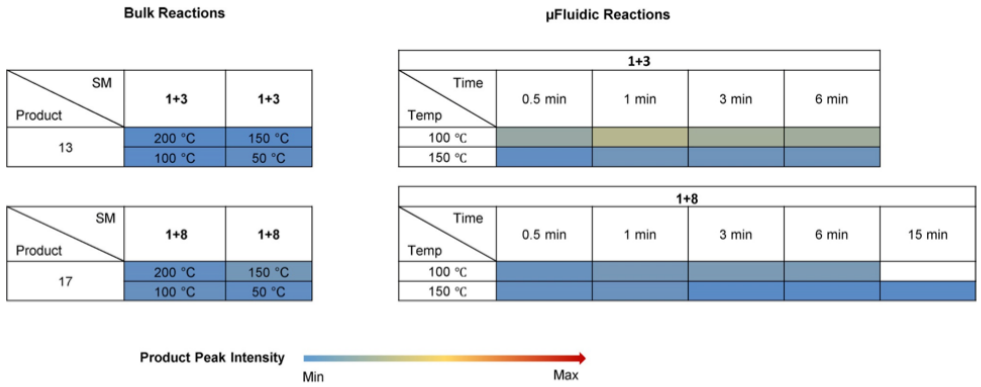

Figure 8. Comparison of microfluidic and bulk screening outcomes for S-M reactions that gave negative bulk reaction results. The same reaction conditions were used in each case with 200 mmol substrate loading and 1:20 4-hydroxy- phenylboronic acid:aryl halide stoichiometry.

High throughput bulk experimentation: High-throughput experiments of palladium catalyzed S-M reactions were performed in 96-well parallel synthesis metal block assemblies (Analytical Sales and Services, Inc., Flanders, NJ). The reaction mixtures in each glass vial insert of the 96-well metal block were prepared using a Beckman Coulter FX liquid handling robot. 4-Hydroxyphenylboronic acid (**1**, 400 mmol) and aryl halide (**2**–**12**, 400 mmol) in EtOH were pipetted via the Span 8 arm into a master plate and then distributed equally into another set of three 96-well plates using the 96-tip head. A master plate was made containing nine different ratios of boronic acid, **1**, and aryl halide **2**–**12**. Next, DBU (800 mmol) was dispensed separately into each plate followed by XPhosPdG3 (40 mmol) solutions in EtOH using the 96-tip head. The top of the metal block was pressure sealed with a sheet of perfluoroalkoxy (PFA) film and two silicone rubber mats that fully covered the reaction vials. The metal blocks were heated without stirring at 50 °C, 100 °C, 150 °C or 200 °C using a home built block heater for 1 h. Extensive testing revealed that the reactor is sealed well enough to heat above the solvent boiling point with less than 5% solvent loss and no cross talk between wells. After 1 h heating, the plates were cooled to

© 2018 Wiley-VCH Verlag GmbH & Co. KGaA, Weinheim

ChemPubSoc Europe

CHEMISTRY A European Journal Full Paper

Table 1. Quantified yields of some S-M microfluidic reactions using HPLC/MS-MS. The same reaction conditions were used in each case (i.e., 200 mmol substrate loading and 1:1 4-hydroxyphenylboronic acid:aryl halide stoichiometry). Peak intensity values are multiples of 1×10^6.

Reaction conditions		13 (1+2)		13 (1+3)		14 (1+4)		15 (1+5)		21 (1+12)	
		Peak intensity	Yield [%]	Peak intensity	Yield [%]	Peak intensity	Yield [%]	Peak intensity	Yield [%]	Peak intensity	Yield [%]
100 °C	0.5 min	1.1	3.4	3.1	13.8	1.3	46.8	0.6	3.5	6.1	23.2
1 °C	1 min	1.1	4.6	3.5	24.5	2.6	54.0	1.6	6.5	4.7	37.7
100 °C	3 min	1.8	6.1	7.6	27.8	3.7	70.9	2.1	15.1	5.1	47.7
100 °C	6 min	5.2	10.5	5.6	48.1	6.1	95.5	4.3	17.6	6.3	48.1
150 °C	0.5 min	2.3	8.0	4.4	48.7	2.8	61.9	1.2	5.6	1.8	45.8
150 °C	1 min	1.6	12.5	2.2	71.2	2.8	93.9	1.1	15.1	2.3	68.6
150 °C	3 min	3.2	35.4	2.8	71.8	3.9	95.6	2	17.1	12.2	70.5
150 °C	6 min	5.3	77.8	7.1	73.1	5.8	97.9	5.2	20.8	6.5	95.6

room temperature, centrifuged, and loaded back onto the deck of the liquid handling robot. Samples for MS autosampling were prepared in 384-well plates by robotic pipetting and diluted by 1000-fold in EtOH. The MS analysis method includes pre-wash and post-wash of the needle to avoid contamination between sample analyses.

Microfluidic experiments: A 1:1 mixture of **1** (400 mmol, 1 equiv) and aryl halide (**2**–**12**, 400 mmol, 1 equiv) in EtOH was loaded into a 1 mL ILS gas tight glass syringe. DBU (800 mmol, 2 equiv) and XPhosPdG3 (2 mmol, 0.5 %) solutions in EtOH were individually loaded into two additional 1 mL ILS gastight glass syringes. Each solution was successively dispensed into the SOR 3225 reactor to engage the reactants. All cross-coupling reactions were run at either 100 °C or 150 °C, with residence times of 0.5, 1, 3, or 6 min unless otherwise noted. The reaction mixtures were collected after quenching and stored at −80 °C. The subsequent ESI-MS and HPLC/MS-MS analyses were performed without further purification.

Acknowledgements

We gratefully acknowledge the financial support from the Department of Defense: Defense Advanced Research Projects Agency (Award no. W911NF-16-2-0020). The efforts of R. Graham Cooks, Ryan Hilger (Amy Facility at Purdue University, Department of Chemistry, heating block fabrication), Tiago J. P. Sobreira, Michael Wleklinski and Andy Koswara are also noted with great appreciation. We also want to thank Shorf Afza for drawing the cover art.

Conflict of interest

The authors declare no conflict of interest.

Keywords: bulk screening · cross-coupling · mass spectrometry · microfluidic evaluation · Suzuki–Miyaura

[1] J. A. Selekman, J. Qiu, K. Tran, J. Stevens, V. Rosso, E. Simmons, Y. Xiao, J. Janey, *Annu. Rev. Chem. Biomol. Eng.* **2017**, *8*, 525–547.

[2] a) R. Macarron, M. N. Banks, D. Bojanic, D. J. Burns, D. A. Cirovic, T. Garyantes, D. V. S. Green, R. P. Hertzberg, W. P. Janzen, J. W. Paslay, U. Schopfer, G. S. Sittampalam, *Nat. Rev. Drug Discovery* **2011**, *10*, 188; b) M. Liu, K. Chen, D. Christian, T. Fatima, N. Pissarnitski, E. Streckfuss, C. Zhang, L. Xia, S. Borges, Z. Shi, P. Vachal, J. Tata, J. Athanasopoulos, *ACS Comb. Sci.* **2012**, *14*, 51–59.

[3] a) P. Chen, *Angew. Chem. Int. Ed.* **2003**, *42*, 2832–2847; *Angew. Chem.* **2003**, *115*, 2938–2954; b) A. B. Santanilla, E. L. Regalado, T. Pereira, M. Shevlin, K. Bateman, L.-C. Campeau, J. Schneeweis, S. Berritt, Z.-C. Shi, P. Nantermet, Y. Liu, R. Helmy, C. J. Welch, P. Vachal, I. W. Davies, T. Cernak, S. D. Dreher, *Science* **2015**, *347*, 49–53.

[4] a) K. Troshin, J. F. Hartwig, *Science* **2017**, *357*, 175–181; b) M. Wleklinski, B. P. Loren, C. R. Ferreira, Z. Jaman, L. Avramova, T. J. P. Sobreira, D. H. Thompson, R. G. Cooks, *Chem. Sci.* **2018**.

[5] a) H. Kim, K. I. Min, K. Inoue, D. J. Im, D. P. Kim, J. Yoshida, *Science* **2016**, *352*, 691–694; b) D. R. Snead, T. F. Jamison, *Angew. Chem. Int. Ed.* **2015**, *54*, 983–987; *Angew. Chem.* **2015**, *127*, 997–1001.

[6] D. Perera, J. W. Tucker, S. Brahmbhatt, C. J. Helal, A. Chong, W. Farrell, P. Richardson, N. W. Sach, *Science* **2018**, *359*, 429–434.

[7] C. Len, S. Bruniaux, F. Delbecq, V. Parmar, *Catalysts* **2017**, *7*, 146.

[8] a) C. E. Falcone, Z. Jaman, M. Wleklinski, A. Koswara, D. H. Thompson, R. G. Cooks, *Analyst* **2017**, *142*, 2836–2845; b) B. P. Loren, M. Wleklinski, A. Koswara, K. Yammine, Y. Hu, Z. K. Nagy, D. H. Thompson, R. G. Cooks, *Chem. Sci.* **2017**, *8*, 4363–4370; c) H. S. Ewan, K. Iyer, S.-H. Hyun, M. Wleklinski, R. G. Cooks, D. H. Thompson, *Org. Process Res. Dev.* **2017**, *21*, 1566–1570; d) M. Wleklinski, C. E. Falcone, B. P. Loren, Z. Jaman, K. Iyer, H. S. Ewan, S.-H. Hyun, D. H. Thompson, R. G. Cooks, *Eur. J. Org. Chem.* **2016**, 5480–5484.

[9] S. D. Roughley, A. M. Jordan, *J. Med. Chem.* **2011**, *54*, 3451–3479.

[10] a) M. Brambilla, M. Tredwell, *Angew. Chem. Int. Ed.* **2017**, *56*, 11981–11985; *Angew. Chem.* **2017**, *129*, 12143–12147; b) A. Suzuki, *Angew. Chem. Int. Ed.* **2011**, *50*, 6722–6737; *Angew. Chem.* **2011**, *123*, 6854–6869; c) A. Chatterjee, T. R. Ward, *Catal. Lett.* **2016**, *146*, 820–840.

[11] a) B. J. Reizman, Y.-M. Wang, S. L. Buchwald, K. F. Jensen, *React. Chem. Eng.* **2016**, *1*, 658–666; b) T. Noël, A. J. Musacchio, *Org. Lett.* **2011**, *13*, 5180–5183; c) T. Noël, S. Kuhn, A. J. Musacchio, K. F. Jensen, S. L. Buchwald, *Angew. Chem.* **2011**, *123*, 6065–6068.

[12] a) S. Fukumoto, O. Ujikawa, S. Morimoto, Y. Asano, S. Mikami, N. Tokunaga, M. Kori, T. Imaeda, K. Fukuda, S. Nakamura in Sulfonamide derivative and use thereof, Vol. Google Patents, **2012**; b) S. Fu, W. Xiang, J. Chen, L. Ma, L. Chen, *Chem. Biol. Drug Des.* **2017**, *89*, 815–819; c) M. Sánchez-Peris, J. Murga, E. Falomir, M. Carda, J. A. Marco, *Chem. Biol. Drug Des.* **2017**, *89*, 577–584; d) V. E. Gregor in Tricyclic compound derivatives useful in the treatment of neoplastic diseases, inflammatory disorders and immunomodulatory disorders, Vol. Google Patents, **2014**; e) M. Sánchez-Peris, E. Falomir, J. Murga, M. Carda, J. A. Marco, *Bioorg. Med. Chem.* **2016**, *24*, 3108–3115; f) P. R. D. Murray, D. L. Browne, J. C. Pastre, C. Butters, D. Guthrie, S. V. Ley, *Org. Process Res. Dev.* **2013**, *17*, 1192–1208; g) K.-S. Jang, *Mol. Cryst. Liq. Cryst.* **2016**, *633*, 123–128.

[13] B. Schmidt, M. Riemer, *J. Org. Chem.* **2014**, *79*, 4104–4118.

[14] M. A. Düfert, K. L. Billingsley, S. L. Buchwald, *J. Am. Chem. Soc.* **2013**, *135*, 12877–12885.

Manuscript received: March 7, 2018
Revised manuscript received: April 21, 2018
Version of record online: June 19, 2018

 © 2018 Wiley-VCH Verlag GmbH & Co. KGaA, Weinheim

Chemical Science

EDGE ARTICLE

View Article Online
View Journal | View Issue

Check for updates

Cite this: *Chem. Sci.*, 2018, **9**, 1647

High throughput reaction screening using desorption electrospray ionization mass spectrometry†

Michael Wleklinski,‡ Bradley P. Loren,‡ Christina R. Ferreira, Zinia Jaman, Larisa Avramova, Tiago J. P. Sobreira, David H. Thompson and R. Graham Cooks *

Received 24th October 2017
Accepted 28th December 2017

DOI: 10.1039/c7sc04606e

rsc.li/chemical-science

We report the high throughput analysis of reaction mixture arrays using methods and data handling routines that were originally developed for biological tissue imaging. Desorption electrospray ionization (DESI) mass spectrometry (MS) is applied in a continuous on-line process at rates that approach 10^4 reactions per h at area densities of up to 1 spot per mm^2 (6144 spots per standard microtiter plate) with the sprayer moving at *ca.* 10^4 microns per s. Data are analyzed automatically by MS using in-house software to create ion images of selected reagents and products as intensity plots in standard array format. Amine alkylation reactions were used to optimize the system performance on PTFE membrane substrates using methanol as the DESI spray/analysis solvent. Reaction times can be <100 μs when reaction acceleration occurs in microdroplets, enabling the rapid screening of processes like *N*-alkylation and Suzuki coupling reactions as reported herein. Products and by-products were confirmed by on-line MS/MS upon rescanning of the array.

Introduction

Pharmaceutical discovery depends on screening large numbers ("libraries") of compounds against biological targets of therapeutic interest. In some cases, this involves evaluation of large collections of natural products and their derivatives for biological activity.[1–4] Current estimates suggest that there are more than 10^{60} drug-like molecules of pharmaceutical interest and over 10^7 possible reaction conditions for a single metal-catalyzed reaction used to build a drug scaffold.[5–8] This reality underscores the need for rapid reaction screening and optimization, particularly with the introduction of automated synthesis techniques and the use of combinatorial methods to generate large numbers of closely related compounds.[9] An illustration of the current bottleneck is given by the fact that compound library sizes of a million are common, requiring two years of continuous operation even at conventional UPLC sampling rates of 1 min per sample. Clearly, multiplexing of the sample transfer, reaction, and/or product analysis is essential to remove this bottleneck. The first two of these steps are readily multiplexed using microtiter well plate formats. The analysis step can also be multiplexed in a variety of ways, including fluorescence analysis with 2D imaging detection. Unfortunately, fluorescence techniques require orthogonal labels and have limited molecular specificity, while label-free approaches like mass spectrometry (MS) are serial analytical tools.[10] State of the art LC-MS high throughput methods require roughly 10 s per sample.

In this paper, we describe an MS method that analyses product outcomes in reaction droplets within about 1 s. If proven to be sufficiently rugged and reliable, this approach will reduce the analysis time for 10^5 reactions from 2 months to about a day. Furthermore, the traditional process of route design, reaction optimization, and scaling can take years to successfully implement for many target compounds. The use of high throughput experimental methods to guide scalable syntheses such as continuous-flow reactors has the potential to drastically improve the speed at which an optimized process can be achieved at scale. Accelerated reactions in microdroplets have been previously shown capable of guiding optimization of continuous-flow syntheses of multiple targets,[11] including diphenhydramine,[12] atropine,[13] and diazepam.[14] The overall goal of this work is the development of a system that can leverage rapidly acquired information on reaction acceleration from a high throughput format and use the output data to inform downstream scaling.

The combination of rapid reaction screening and reaction product analysis described here is based on two well-established analytical technologies: (i) the use of desorption electrospray ionization (DESI) in surface analysis[15–17] and (ii) the occurrence of accelerated chemical reactions in microdroplets.[18–20] DESI is an ambient ionization method (*i.e.*,

Department of Chemistry, Purdue University, West Lafayette, IN 47907, USA. E-mail: cooks@purdue.edu

† Electronic supplementary information (ESI) available. See DOI: 10.1039/c7sc04606e

‡ These authors contributed equally to this work.

analysis is performed on unmodified samples in the open air) using charged microdroplets to extract analytes from complex samples. It does so with ~200 μm spatial resolution and with rapid data acquisition (typically < 1 s per spot).[21,22] The combination of another ambient method, paper spray, with *in situ* analysis has also been reported.[23]

The workflow for the automated high throughput reaction screening experiment with DESI-MS is described in Fig. 1. Upon selection of the reactions, a Beckman-Coulter Biomek FX liquid handling robot is used to prepare the reaction mixtures in a 384 well plate (20 μL per well). The liquid handling robot then transfers nL volumes of each reaction mixture to the DESI plate (porous PTFE) with a magnetic pin tool. The small spot sizes achieved by the transfer pins allow for the preparation of high density plates, which are subjected to DESI-MS immediately following their preparation. In-house software is then used to generate a reactivity heat map capable of guiding MS/MS experiments for structural confirmation of both products and byproducts.

The center-to-center reaction mixture spot distance in a 6144 array is 1125 microns, thus easily accommodating one full MS scan. The DESI-extracted analytes are released from the surface in the form of microdroplets. High throughput DESI-MS reaction screening is based, in part, on the occurrence of accelerated chemical reactions in these microdroplets.[24–27] This forms the temporal basis for an experiment wherein an array of reaction mixtures (for example on a microtiter plate) is examined by rastering a DESI spray across the surface. Previous studies indicate that there is good correlation between microdroplet chemistry and more traditional batch or continuous chemistries.[11–14] This study focuses on the development of a high throughput screening system with amine alkylation and Suzuki cross-coupling transformations to further test this expectation. In both cases, reagent screening was also evaluated.

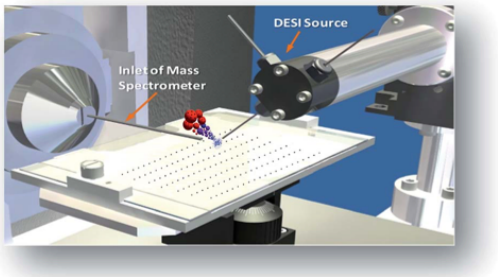

Fig. 2 Reaction (in secondary droplets) and MS product analysis of reaction mixtures presented in microtiter plate format. Automated acquisition of DESI mass spectra occurs at a rate of 1 reaction mixture per s.

The phenomena involved in reaction screening are similar to those taking place in DESI-MS tissue imaging, so the same instrumentation and software can be used to gather and process the data. Fig. 2 illustrates the high throughput DESI analysis of an array of reaction mixtures. Note that a mixture of reagents is deposited at each well, with the DESI spray potentially accelerating both the reaction and facilitating the analysis of the reaction mixture. Earlier work[6] on high throughput HPLC-MS analysis using the microtiter format represents an alternative approach with analysis times of 5–22 s per sample while commercial SPE MS systems, such as the RapidFire 365 system, allow rates of up to 8 s per sample.[8] The use of DESI-MS to evaluate reactions in a high-throughput fashion suited our overall objective to develop and demonstrate a novel, fast, and reliable system for solution-phase reaction screening. The novelty of this study is to seek to extend the speed with which large numbers of microdroplet reactions can be carried out and their products analyzed.

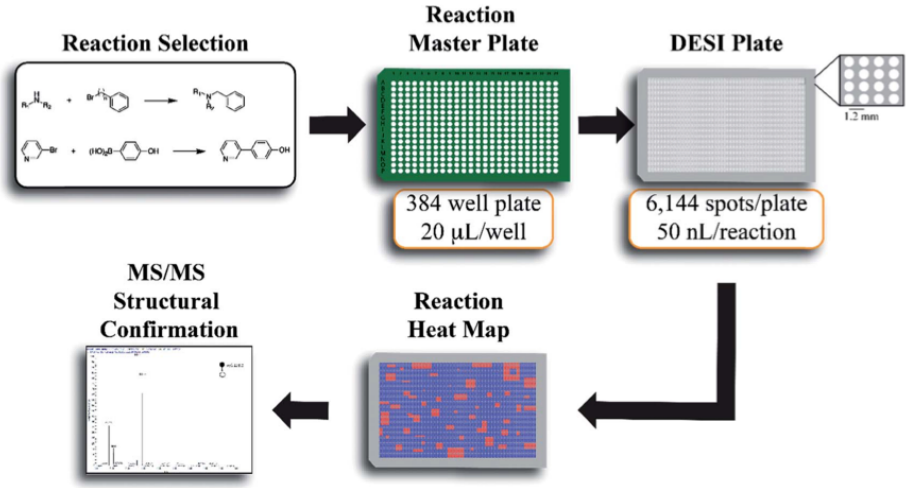

Fig. 1 Summary of the high throughput reaction screening experiment workflow with DESI-MS. Both the master plate and the DESI plate are prepared in an automated fashion with a liquid handling robot. The DESI plate (porous PTFE) is prepared with a 50 nL pin tool.

This journal is © The Royal Society of Chemistry 2018

The system was intended to provide a rapid answer to the yes/no question of whether or not a particular set of reagents produces a desired product. If a reaction occurs under DESI-MS conditions, it is considered a candidate for further investigation as a scaled-up version of the reaction for process optimization. If not, this possible route to a particular product under those conditions is discarded. In roughly the same amount of time that it takes to record data for a single product, one can collect MS data on by-products, reaction intermediates, and residual starting material in the same mass scan. Full mass spectra, therefore, were recorded on each spot of reagent mixture at a target throughput of 10 000 reactions per h. Software was written to automatically screen for ion *m*/*z* values corresponding to reagents, reaction products and simple by-products. For selected target ions, re-analysis at particular locations was performed using MS/MS data acquisition to allow product confirmation while retaining the advantages of high throughput imaging.

Results

N-Alkylation reactions

The ultimate goal of this effort is to develop screening capabilities across a broad range of reaction conditions for synthetic optimization and reaction discovery. This led us to evaluate the capability of screening different reaction classes such as *N*-alkylation and Suzuki cross-coupling given their importance in medicinal chemistry transformations.[28]

Fig. 3 shows selected data from an experiment wherein a set of 16 alkylation reactions (Schemes 1, S1, and S2†) was studied by spotting mixtures of eight amines (benzylamine, **1**; 1-aminohexane, **2**; *N*,*N*-dihexylamine, **3**; 2-methoxyaniline, **4**; 3-methoxyaniline, **5**; 4-methoxyaniline, **6**; piperidine, **7**; *N*-methylbenzylamine, **8**) and two alkyl bromides (benzyl bromide,

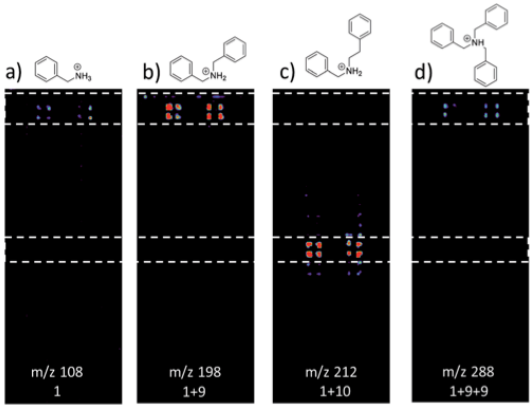

Fig. 3 Selected ion images for reactions between amines and alkyl bromides. Images are (a) *m*/*z* 108, benzylamine; (b) *m*/*z* 198, alkylation product for reaction of **1** and **9**; (c) *m*/*z* 212, alkylation product for reaction of **1** and **10**; (d) *m*/*z* 288, double alkylation product for reaction of **2** and **9**.

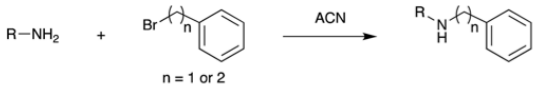

Scheme 1 *N*-Alkylation reactions.

9; 2-(bromoethyl)benzene, **10**) in a 1 : 1 molar ratio on a porous PTFE substrate at the density of a 1536-well microtiter plate. Spotting was done using a Beckman-Coulter Biomek FX liquid handling system equipped with small (typically 50 nL) slotted delivery pins. Fig. 3 illustrates the data for the reaction between **1** and **9** as well as **1** and **10**, each panel showing the location of spots which display ions corresponding to particular reagents or products. The brighter colors indicate higher ion intensity. A series of mass spectra was continuously recorded while covering the entire plate by scanning row by row at a slightly faster scan speed of 6250 μm s^{-1}, but with a lower spot density and averaging 3 mass spectra per array spot and achieving a screening rate of 1284 reactions per h. Note that this time includes reaction and analysis times, but not the time required for sample preparation.

Note also that rhodamine B (*m*/*z* 443) was used as a positional reference. Significant features of the experiment are: (i) starting materials were often, but not always visible; (ii) product formed readily with **9** and much less readily with **10**; (iii) there is no evidence of an elimination reaction with **10**; (iv) double alkylation reactions are commonly observed with **9**; (v) there is little sign of sample carry-over, a desirable feature that is also true of tissue imaging by DESI-MS; and (vi) there is some variability in signal when replicates are examined. Experimental details are in the ESI† (Section 2) and results for the other reactions are detailed in Table 1. The reaction was successful for 7 out of 8 amines with benzyl bromide and 3 out of 8 amines with 2-(bromoethyl)benzene, the difference reflecting the known difference in bromoalkane reactivity.

These reactions may be accelerated in the droplets, or even earlier, since the 50 nL reaction mixtures containing less than 0.5 μg of each reagent (Table S4†) may evaporate on the PTFE plate. They may occur in the master plate well for very fast reactions. In any event, the DESI screen answers affirmatively in this case the yes/no question being asked and conversion rates (CR) can be calculated in order to estimate the reaction completeness (Table S3†). Product characterization (Tables S3 and S4†) was by tandem mass spectrometry, as discussed below.

Suzuki cross-coupling reactions

Suzuki cross-coupling between phenylboronic acid precursors and aryl halides using a commercially available palladium catalyst (XphosPD G3) was also screened (Scheme 2). All of the reactions were run in ethanol, and the effect of base on the reaction was explored with EtONa, EtOK, CH_3ONa, and CH_3OK using rhodamine as a fiducial marker. Reaction mixtures were prepared in a 384 well master plate (20 μL per well) and spotted onto a porous PTFE substrate using 6 nL slotted pins. All of the reaction mixtures were prepared in quadruplicate wells and the entire master plate was spotted in quadruplicate to achieve 1536 density on the final DESI plate.

Table 1 Summary of results from *N*-alkylation DESI reaction screen

Amine	Product *m/z*	Alkylation product?	*m/z*	Double alkylation product?
Amine + Benzyl bromide				
Benzylamine	198	✓	288	✓
Hexylamine	192	✓	282	✓
Dihexylamine	276	✓	366	✗
o-Anisidine	214	✓	304	✓
m-Anisidine	214	✓	304	✗
p-Anisidine	214	✓	304	✓
Piperidine	176	✓	266	✓
N-Benzylmethylamine	212	✓	302	✓
Amine + 2-(bromoethyl)benzene				
Benzylamine	212	✓	316	✗
Hexylamine	206	✓	310	✗
Dihexylamine	290	✗	394	✗
o-Anisidine	228	✗	332	✗
m-Anisidine	228	✗	332	✗
p-Anisidine	228	✗	332	✗
Piperidine	190	✓	294	✗
N-Benzylmethylamine	226	✗	330	✗

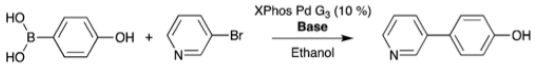

Scheme 2 Palladium-catalyzed Suzuki cross-coupling reaction. Bases used include EtONa, EtOK, MeONa, and MeOK.

In this experiment, one sees the boronic acid starting material in negative ion mode (*m/z* 137), aryl bromide starting material in positive ion mode (*m/z* 159), and cross-coupled product in both modes (*m/z* 170 and 172, respectively). The reaction proceeds well in 3 of the 4 bases, namely CH_3OK, EtOK, and EtONa (Fig. 4 and S8, Table S6†).

Optimization of pinning and DESI analysis

Porous PTFE has been chosen as a reaction substrate due to the high ion intensities for the reaction product, low background and high chemical compatibility compared to non-porous PTFE, Nylon, cellulose, and DMF (data not shown). A standard porous PTFE plate containing a single mine alkylation reaction mixture (benzylamine, **1** and benzyl bromide, **9**) was used to develop an understanding of the experiment, including (i) achievable number of reactions per h and (ii) the effects of mechanical instabilities on data quality. Considering these points in turn: (i) under the solvent and instrument setting conditions used for the experiments at 6144-well microtiter plate spot density, the fastest analysis speed achieved was 6004 reactions per h with a lateral spray velocity of 8333 μm s^{-1} (Fig. S10†). (ii) Distinct spots can be deposited at densities as high as 24 457 per standard plate, as confirmed by fluorescence (Fig. S11†), but the spots blur at DESI analysis speeds above 10 000 reaction mixtures per h.

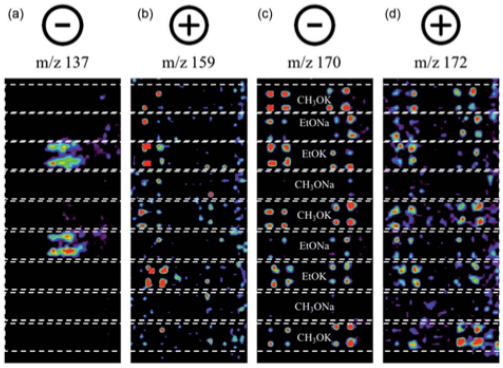

Fig. 4 Selected ion images for reactions between **11** and **12**. Images. (a) Negative ion mode *m/z* 137, **11**; (b) positive ion mode *m/z* 159, **12**; (c) negative ion mode *m/z* 170, **13**; (d) positive ion mode *m/z* 172, **13**.

Furthermore, it is notable that there is variation in intensity across the plate surface as well as small variations in spot placement. Two possible causes for the decrease in signal intensity are that the pins do not deliver the appropriate volume of solution to the substrate and that DESI-MS analysis performance drops due to surface roughness or non-planarity. Fluorescence imaging and DESI-MS were used to explore these factors. Pins used in these experiments differed in diameter, shape, length, and prior use history. Pins (6 nL) that were heavily used in earlier screening experiments produced spots with variation in fluorescence intensity, indicating the inability to deliver a constant volume of sample to the substrate. When thicker pins calibrated to 50 nL were used, the intensity was relatively uniform. With optimized equipment and spotting procedures, the variation in signal intensity is low. Fig. 5 details an experiment in which 50 nL pins were used to deposit a single reaction mixture of **1** and **9** at 6144 density. The reactions were screened at varying speeds of the moving stage. We found that data quality increases with decreasing speed of the moving stage. The optimized rate was calculated by eliminating the

This journal is © The Royal Society of Chemistry 2018

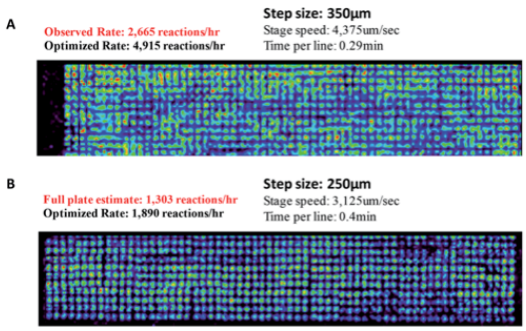

Fig. 5 DESI analysis of the reaction between benzylamine (**1**) and benzyl bromide (**9**) at different speeds of the moving stage.

time for line transitions on the moving stage. It is noteworthy that even at four times higher density (6144 *vs.* 1536), DESI-MS showed similar performance to fluorescence (compare Fig. S9–S11†) while giving much more information.

Point-to-point DESI MS/MS

We next sought to develop the capability for rapid structural confirmation by MS/MS immediately following the DESI reaction screen on the same substrate. To accomplish this, we first needed to determine whether a plate could be re-analyzed without blurring the sample on the surface or causing significant depletion of material. This was done for the entire *N*-alkylation plate (Fig. S2–S6). The reaction between **1** and **9** is shown in Fig. 6A. In all eight replicates shown, there is clearly no significant blurring or sample depletion. With this established, we were then able to confidently move forward with the development of an MS/MS methodology on the same reaction plate. The data shown in Fig. 6B utilizes the point-to-point feature of the DESI system. Once the reaction hits are determined, a spreadsheet is uploaded into the commercial 2D DESI platform software (Prosolia Inc. Indianapolis, IN, US) with their *x* and *y* positions. The DESI sprayer then oscillates four times over each location while the mass spectrometer is collecting the desired MS/MS spectra for the products and by-products. This methodology is detailed in Fig. S7 and the data is summarized in Tables S4 and S5.†

This was done for all of the *N*-alkylation reactions with **9** for both the single alkylation product and the double alkylation byproduct. The mass spectrum for the reaction between **1** and **9** (Fig. S12A†) shows several products, including the target dibenzylamine *m*/*z* 198, confirmed as such by on-line by MS/MS and comparison with a standard (Fig. 6). The MS/MS shows elimination of NH_3 to give the *o*-benzyl benzyl cation (*m*/*z* 181) through benzyl rearrangement. The ion pair *m*/*z* 475/477 (Fig. S17†) is a brominated by-product while the ion *m*/*z* 288, corresponds to a by-product, assigned after independent synthesis and MS/MS characterization as tribenzylamine (Fig. S14–S17; Scheme S3†).

Reanalysis of a plate typically gives high quality data in both MS and MS/MS modes (ESI, Fig. S18 and S19†). Reaction

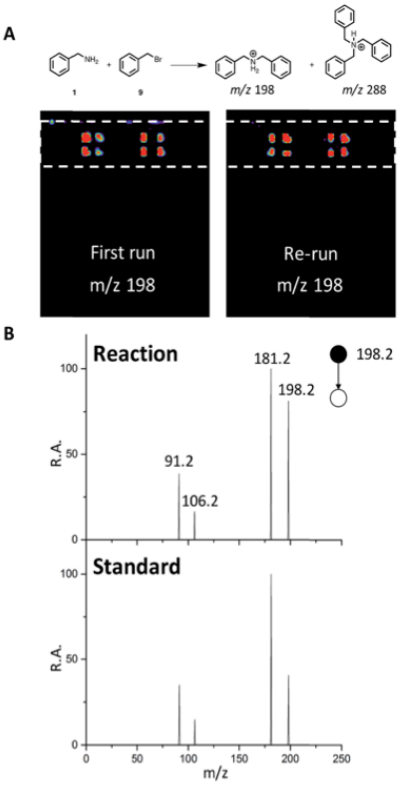

Fig. 6 (A) DESI-MS images for reaction between **1** and **9** for the first run and a re-run of the same plate. (B) MS/MS of reaction product (*m*/*z* 198) and a dibenzylamine standard.

product structural analysis can be interrogated beyond MS^2 and this capability will be incorporated in the ongoing automation of mass spectra interpretation. As an example, the reaction of dihexylamine and benzyl bromide has been used to acquire MS^3 and MS^5 data directly from the PTFE plate spotted at 6144 density. The alkylation product of *m*/*z* 276, yielded the most intense fragment of *m*/*z* 184, which has been further isolated for examination by MS^3 (Fig. S19†). For the double alkylation product of *m*/*z* 366, after MS^2 the most intense fragment is *m*/*z* 274 due the loss of alkene (C_7H_8), which fragments further (MS^3) to yield *m*/*z* 204 due to another alkene loss (C_5H_{10}). MS^4 of *m*/*z* 204 was followed by another alkene loss (C_5H_{10}) to yield *m*/*z* 134, which was intense enough to be isolated for MS^5 (Fig. S20†). The ion C_7H_7 (*m*/*z* 91) is observed as a fragment at MS^3 through MS^5 stages. MS^3 of *m*/*z* 276 and MS^5 of *m*/*z* 366 in point-analysis experiments provided data of similar quality (data not shown).

Automation of MS analysis

Commercial software (Prosolia, Inc.) was used to operate the DESI system. Data were acquired using a commercial instrument (Thermo, LTQ) and converted into images using

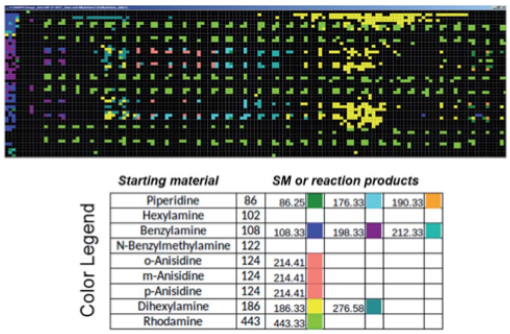

Fig. 7 Output of the software intended to automatically perform data analysis during high-throughput reaction screening by DESI-MS. The output depicted shows starting materials (SM) and reaction products in different colors for the sixteen different *N*-alkylation reactions described in Schemes S1 and S2,† and for which ion images have been recorded using the imaging software BioMAP in Fig. S2–S6.†

commercial software (Prosolia, Inc.). The total ion current plots simply represent images of the array. The question of what specific data to examine in the high spatial resolution full mass spectral data space is addressed using in-house software to automate MS data analysis. Fig. 7 shows application of this methodology to plotting starting materials and potential reaction products of all the alkylation reactions in a compact format. One function of the in-house software is to automatically search the captured data for *m*/*z* values that correspond to reactants and products to generate a yes/no report. Known intermediates, products and by-products can also be identified by rules-based input. Another function is to display the output as an *x*, *y* image of this search as shown in Fig. 7. A third feature of the software is that it displays the mass spectrum at any coordinate position upon clicking the image (as shown in the TOC). Computational approaches to the more challenging problem of identification of unknowns and by-products are being evaluated in an extension of the program using MS/MS data, taken either on-line or during a repeat scan.

Conclusions

Initial development of this DESI-MS screening methodology (i) holds promise for high speed reaction screening while using minute amounts of chemicals/(low μg level); (ii) provides information valuable in scaled-up synthesis including solvent and pH optimization; and (iii) gives good qualitative reproducibility although this suffers at the highest speeds. Our results indicate that the engineering requirements for the highest speed screens will be demanding in terms of quality of reaction mixture spotting, the planarity of the plate, accurate sample positioning on the plate and spray reproducibility. Development of automation and integration methodology for high-throughput reaction screening by DESI-MS is underway. Software to allow automated and near real-time analysis of MS and MS/MS data is under development. We show initial data obtained using this tool (Fig. 7) but do not explore details in this manuscript. Innovations in fluid handling are under development in order to allow preparation of reaction mixtures at speeds to match the time taken for reaction and analysis. The strategy of using accelerated reactions has already been adapted to synthetic route screening and is currently being extended to optimization. As shown, it allows structural confirmation and identification of targets using MS/MS. Translation of results from high throughput DESI reaction screens to continuous-flow reactions is underway.

Experimental methods

Preparation of reaction mixtures

All chemicals and reagents were purchased from Sigma Aldrich and used without further purification. Stock solutions (0.1 M) were prepared in appropriate solvents as indicated. Master 384-well microtiter plates were prepared either by hand pipetting appropriate mixtures of chemicals or by robotic pipetting with a Biomek FX liquid handling system. Once the master plate was prepared, a 384-pin tool from V&P Scientific, Inc. was used to deliver mixtures from the master plate to the DESI-MS substrate. Transfer was repeated multiple times in order to generate the desired titer plate density (1536-well, 6144-well, *etc.*). Details for each individual experiment are provided in the ESI.†

DESI-MS substrates

A variety of DESI-MS substrates were tested including regenerated cellulose (Membrane Filtration Products, Inc.), PTFE (EMD, Millipore Fluoropore, Saint-Gobain), glass fiber (Foxx Life Sciences), and nylon (Foxx Life Sciences). The substrates were cut with scissors and adhered to glass slides using a spray adhesive (Scotch Spray mount). No signs of interference from the glue was observed.

Mass spectrometer parameters

A commercial DESI source from Prosolia, Inc. was used for the *N*-alkylation experiments and MS/MS analysis. A homebuilt DESI ion source similar to the commercial source available from Prosolia, Inc. was used for the Suzuki experiments. A Thermo LTQ linear ion trap was used to acquire data. DESI-MS experiments were performed in both positive and negative ion mode over the range *m*/*z* 50–500. The ion source parameters are detailed in the ESI.† Membrane substrates were scanned horizontally at a rate between 5000 and 10 000 μm s^{-1} using vertical steps of 500 μm. The MS injection time was set so as to produce square pixels of 500 by 500 μm. Data were first converted using a in-house software into a format compatible with Biomap. Biomap (freeware, https://ms-imaging.org/wp/biomap/) was used to generate the selected ion images by choosing appropriate ion thresholds.

Conflicts of interest

There are no conflicts to declare.

This journal is © The Royal Society of Chemistry 2018

Acknowledgements

Financial Support is acknowledged from the Department of Defense: Defense Advanced Research Projects Agency (award no. W911NF-16-2-0020). We thank Zoltan Nagy, Andy Koswara and Caitlin Falcone for contributions to the larger study of which this work is a part.

References

1 L. M. Mayr and D. Bojanic, *Curr. Opin. Pharmacol.*, 2009, **9**(5), 580–588.
2 F. E. Koehn, in *Natural Compounds as Drugs*, ed. F. Petersen and R. Amstutz, Birkhäuser Basel, Basel, 2008, vol. I, pp. 175–210.
3 W. P. Janzen, *Chem. Biol.*, 2014, **21**(9), 1162–1170.
4 A. Syahir, K. Usui, K.-y. Tomizaki, K. Kajikawa and H. Mihara, *Microarrays*, 2015, **4**(2), 228–244.
5 P. M. Murray, S. N. G. Tyler and J. D. Moseley, *Org. Process Res. Dev.*, 2013, **17**(1), 40–46.
6 A. Buitrago Santanilla, E. L. Regalado, T. Pereira, M. Shevlin, K. Bateman, L. C. Campeau, J. Schneeweis, S. Berritt, Z. C. Shi, P. Nantermet, Y. Liu, R. Helmy, C. J. Welch, P. Vachal, I. W. Davies, T. Cernak and S. D. Dreher, *Science*, 2015, **347**(6217), 49–53.
7 T. Cernak, Synthesis in the Chemical Space Age, *Chem*, 2016, **1**(1), 6–9.
8 G. C. Adam, J. Meng, J. M. Rizzo, A. Amoss, J. W. Lusen, A. Patel, D. Riley, R. Hunt, P. Zuck, E. N. Johnson, V. N. Uebele and J. D. Hermes, *J. Biomol. Screening*, 2014, **20**(2), 212–222.
9 K. D. Collins, T. Gensch and F. Glorius, *Nat. Chem.*, 2014, **6**(10), 859–871.
10 C. J. Henrich and J. A. Beutler, *Nat. Prod. Rep.*, 2013, **30**(10), 1284–1298.
11 M. Wleklinski, C. E. Falcone, B. P. Loren, Z. Jaman, K. Iyer, H. S. Ewan, S.-H. Hyun, D. H. Thompson and R. G. Cooks, *Eur. J. Org. Chem.*, 2016, **33**, 5480–5484.
12 B. P. Loren, M. Wleklinski, A. Koswara, K. Yammine, Y. Hu, Z. K. Nagy, D. H. Thompson and R. G. Cooks, *Chem. Sci.*, 2017, **8**(6), 4363–4370.
13 C. E. Falcone, Z. Jaman, M. Wleklinski, A. Koswara, D. H. Thompson and R. G. Cooks, *Analyst*, 2017, **142**, 2836–2845.
14 H. S. Ewan, K. Iyer, S.-H. Hyun, M. Wleklinski, R. G. Cooks and D. H. Thompson, *Org. Process Res. Dev.*, 2017, **21**(10), 1566–1570.
15 R. G. Cooks, Z. Ouyang, Z. Takats and J. M. Wiseman, *Science*, 2006, **311**(5767), 1566.
16 P. Nemes and A. Vertes, *Trends Anal. Chem.*, 2012, **34**(suppl. C), 22–34.
17 M. E. Monge, G. A. Harris, P. Dwivedi and F. M. Fernández, *Chem. Rev.*, 2013, **113**(4), 2269–2308.
18 X. Yan, R. M. Bain and R. G. Cooks, *Angew. Chem., Int. Ed.*, 2016, **55**(42), 12960–12972.
19 S. Banerjee and R. N. Zare, *Angew. Chem., Int. Ed.*, 2015, **54**(49), 14795–14799.
20 E. A. Crawford, C. Esen and D. A. Volmer, *Anal. Chem.*, 2016, **88**(17), 8396–8403.
21 C. Wu, A. L. Dill, L. S. Eberlin, R. G. Cooks and D. R. Ifa, *Mass Spectrom. Rev.*, 2013, **32**(3), 218–243.
22 S. N. Nguyen, A. V. Liyu, R. K. Chu, C. R. Anderton and J. Laskin, *Anal. Chem.*, 2017, **89**(2), 1131–1137.
23 S. Chen, Q. Wan and A. K. Badu-Tawiah, *Angew. Chem., Int. Ed.*, 2016, **55**(32), 9345–9349.
24 R. D. Espy, M. Wleklinski, X. Yan and R. G. Cooks, *Trends Anal. Chem.*, 2014, **57**(suppl. C), 135–146.
25 A. K. Badu-Tawiah, L. S. Eberlin, Z. Ouyang and R. G. Cooks, *Annu. Rev. Phys. Chem.*, 2013, **64**(1), 481–505.
26 R. M. Bain, C. J. Pulliam, F. Thery and R. G. Cooks, *Angew. Chem., Int. Ed.*, 2016, **55**(35), 10478–10482.
27 S. Banerjee, E. Gnanamani, X. Yan and R. N. Zare, *Analyst*, 2017, **142**(9), 1399–1402.
28 S. D. Roughley and A. M. Jordan, *J. Med. Chem.*, 2011, **54**(10), 3451–3479.

This journal is © The Royal Society of Chemistry 2018

Analyst

PAPER

View Article Online
View Journal | View Issue

Check for updates

Cite this: *Analyst*, 2017, **142**, 2836

Reaction screening and optimization of continuous-flow atropine synthesis by preparative electrospray mass spectrometry†

Caitlin E. Falcone,‡[a] Zinia Jaman,‡[a] Michael Wleklinski,[a] Andy Koswara,[b] David H. Thompson*[a] and R. Graham Cooks *[a]

Preparative electrospray (ES) exploits the acceleration of reactions in charged microdroplets to perform a small scale chemical synthesis. In combination with on-line mass spectrometric (MS) analysis, it constitutes a rapid screening tool to select reagents to generate specific products. A successful reaction in preparative ES triggers a refined microfluidic reaction screening procedure which includes the optimization for stoichiometry, temperature and residence time. We apply this combined approach for refining a flow synthesis of atropine. A successful preparative ES pathway for the synthesis of the phenylacetyl ester intermediate, using tropine/HCl/phenylacetyl chloride, was optimized for solvent in both the preparative ES and microfluidics flow systems and a base screening was conducted by both methods to increase atropine yield, increase percentage conversion and reduce byproducts. In preparative ES, the first step yielded 55% conversion (judged using MS) to intermediate and the second step yielded 47% conversion to atropine. When combined in two discrete steps in continuous-flow microfluidics, a 44% conversion of the starting material and a 30% actual yield of atropine were achieved. When the reactions were continuously telescoped in a new form of preparative reactive extractive electrospray (EES), atropine was synthesized with a 24% conversion. The corresponding continuous-flow microfluidics experiment gave a 55% conversion with an average of 34% yield in 8 min residence time. This is the first in depth study to utilize telescoped preparative ES and the first use of dual ESI emitters for multistep synthesis.

Received 13th April 2017,
Accepted 20th June 2017

DOI: 10.1039/c7an00622e

rsc.li/analyst

Introduction

Continuous flow reactors are gaining attention in the pharmaceutical and fine chemical industries for the preparation of small and large molecules including active pharmaceutical ingredients (APIs).[1,2] Key advantages of continuous flow are increased mass transfer, controlled flow, ease of integration, and precise control of the reaction temperature and reaction time, as well as high efficiency and safety.[3,4] Generally, reaction optimization and screening require significant investments in time and material.[5,6] Pharmaceutical production still utilizes a supply chain network where reagent shortage often occurs due to the use of multipurpose batch reactors which are operated in cycles, and lengthy experiments may be required to identify and optimize the intermediates in each of the several reaction steps while minimizing carry-through of by-products.[7] Microreactors, used in conjunction with on-line nESI-MS analysis, speed up reaction optimization[8] and lower the costs due to low material requirements and reduced waste generation.[9,10] The reduced channel widths, together with the exceptional mass-and heat-transfer capacity of these reactors, are responsible for decreasing reaction times.[11] With all of these advantages, it is expected that continuous flow processes should emerge as an important technique for API synthesis.[12,13] Indeed, many APIs have been synthesized continuously by incorporating small-scale work up techniques and formulations. Continuous flow synthesis of the APIs efaproxial, rimonabant,[14] imatinib,[15,16] ibuprofen,[8] rufinamide,[17] diphenhydramine hydrochloride,[18] and (*E*/*Z*)-tamoxifen[19] have been reported. Two MS experiments are investigated here to further facilitate the development of continuous flow synthesis: (i) rapid screening using accelerated reactions in microdroplets or thin films and (ii) on-line continuous MS monitoring of the microfluidic reaction using inductive ESI.†[20] The methodology

[a]*Department of Chemistry, Purdue University, 560 Oval Drive, West Lafayette, IN 47907, USA. E-mail: cooks@purdue.edu, davthom@purdue.edu*
[b]*Chemical Engineering, Purdue University, 480 W Stadium Ave., West Lafayette, IN 47907, USA*
†Electronic supplementary information (ESI) available. See DOI: 10.1039/c7an00622e
‡These authors contributed equally to this work.

This journal is © The Royal Society of Chemistry 2017

differs from but can be compared to the use of drop-based microfluidics for screening analytes.[21]

In preparative electrospray, accelerated chemical reactions occur in charged microdroplets, reducing the reaction times.[22] Accelerated reactions in microdroplets have been studied using desorption electrospray ionization (DESI),[23–25] nanoDESI,[26] paper spray[27] and electrospray ionization (ESI)[28] as well as in a levitated form.[29] These reactions have been employed to derivatize analytes for improved MS analysis,[22] in mechanistic studies,[30–32] to identify reaction intermediates[24,33,34] and to perform microscale synthesis.[35,36] Accelerated droplet reactions can be monitored by on-line MS analysis and they can be used to prepare milligram quantities of material in minutes.[35] In preparative ES a reaction mixture is optimized for product formation by on-line MS analysis and then electrosprayed off-line onto a collector surface. The material deposited is subsequently analyzed by extraction with solvent and off-line chemical analysis.

Extractive electrospray ionization (EESI) is an alternative spray ionization technique that utilizes two ESI emitters to allow collisions between droplets from two separate streams. One emitter nebulizes the sample and the other produces charged microdroplets of the solvent.[37–44] Liquid–liquid extraction of analytes from the sample during microdroplet collisions leads to extraction of the analyte into a solvent that is amenable to on-line mass spectrometric analysis. As used here, the second spray contains a reagent which can react with the intermediate products of the first sprayer to yield the desired final product. Note that a technique similar to EESI, droplet fusion, uses two separate ESI emitters to collide microdroplet reagents to form fused droplets containing both reagents. The reagents mix in the fused droplets and the reaction proceeds. Microdroplet fusion has been used to study the kinetics of phenolindophenol reduction by ascorbic acid, acid-induced cytochrome c unfolding, and HDX in bradykinin.[45] In a third multi ESI emitter technique, multichannel rotating electrospray ionization, ESI emitters nebulize volatile reagents that induce reactions in the gas phase and the resulting products are extracted by droplets from another ESI emitter.[46] Among these three methods, only EESI was used in this study.

Atropine is traditionally manufactured industrially by natural product extraction.[47] Atropine, the natural tropane alkaloid, exists as a racemic mixture of D-hyoscyamine and L-hyoscyamine and has both anticholinergic and anti-parasympathetic properties.[48] The drug is included in the WHO list of essential medicines and the U.S. Food and Drug Administration (FDA) has reported it to be among drugs which were in short supply during 2011–2014.[49] The total synthesis of atropine has previously been published using a batch process[50–52] and more recently using continuous flow.[49] This previous continuous flow process required multiple steps of purification by liquid–liquid extraction due to a variety of byproducts and this reduced the overall yield of atropine.[49,53] Reported here is a rapid screening technique that utilizes preparative ES to screen pathways and microfluidics with on-line MS to optimize selected pathways.

Experimental

All chemicals and solvent were purchased from Sigma-Aldrich (St Louis, Missouri) and used without any purification. pH = 10 buffer was purchased from Macron (Avantor Performance Materials, Center Valley, PA).

Mass spectrometry

Samples were analyzed using a Thermo LTQ linear ion trap mass spectrometer (ThermoFisher Scientific, San Jose, CA, USA). NanoESI analysis in both positive and negative ion modes was performed using 2.0 kV spray voltage. Other experimental parameters were: capillary temperature: 200 °C; tube lens (V): −85 V; capillary voltage: −20 V for positive ion mode and tube lens (V): 85 V; capillary voltage: 20 V for negative ion mode. Tandem mass spectrometry was performed using an isolation window of 1.5 (m/z units) and 25% collision energy. The spectra were acquired with automatic gain control while averaging 3 micro-scans for each spectrum. Samples were prepared for nanoESI by diluting them 100-fold in acetonitrile.

Microfluidics

All microfluidic syntheses were performed using a Labtrix S1 (Chemtrix, Ltd, Netherlands). A home-built Peltier-controlled system coupled with the Chemtrix microfluidic platform allowed for multi-step reactions to be performed with control over the temperature in each chip.

HPLC-MS analysis

Separations were performed on an Agilent 1100 HPLC system (Palo Alto, CA) using a Varian C18 Amide column (3 μm, 150 × 2.1 mm id) and 10 μL injection volume. Following the separation, the column effluent was introduced by positive mode electrospray ionization (ESI) into an Agilent MSD-TOF mass spectrometer. The percentage conversion was calculated as the product signal divided by the sum of all the peaks in the spectra.

RP-UPLC analysis

An isocratic reverse-phase ultra-high performance liquid chromatography method (RP-UPLC) using the PATROL UPLC Process Analysis System (Waters Corp.) was used to determine the yield of atropine in continuous flow. The detection of eluted atropine was accomplished using a dual-channel PDA detector at 190 and 225 nm in conjunction with ApexTrack analysis for integrating the atropine peak that was matched with an atropine standard chromatogram. Quantification was then performed *via* interpolation using a standard calibration curve at 225 nm. Three standard stock solutions of atropine sulfate were prepared.

NMR analysis

^{1}H-NMR and ^{13}C-NMR samples were prepared by dissolving ~10 mg of samples in $CDCl_3$ and spectra were acquired using a Bruker AV-III-500-HD NMR spectrometer (Billerica,

Massachusetts, USA). The NMR data were analyzed using the MestReNova 10.0 software.

Preparative electrospray

A home-built electrospray source was enclosed in a polypropylene tube (15 mL Falcon tube) with a small piece of glass wool for deposition. The reaction mixture was pumped through fused silica capillary at a rate of 10 μL min^{-1} and a high voltage of 5 kV was applied through the stainless steel needle of the 250 μL Hamilton gastight syringe. A nitrogen sheath gas was used at 100 Psi. The sprayed droplets were collected on glass wool and washed with a solvent for analysis by nanoESI or to be telescoped for the next step in the reaction.

Preparative reactive EES

Two home-built electrospray sources were angled at 22.5° with the intersection of the spray plumes occurring at a distance of 4 cm. The deposition surface of glass wool in a polypropylene tube was placed at varying distances from the intersection point. Each ES emitter was connected to two syringes *via* tubing and mixed in line with a mixing T. Each syringe had a flow rate of 5 μL min^{-1} with a total flow rate of 10 μL min^{-1} for each ES emitter. The high voltage was applied through a platinum electrode in a T junction. A nitrogen sheath gas was used at 100 Psi. The sprayed droplets were collected on the gas wool and washed with a solvent for analysis by nanoESI.

Synthesis of intermediates in preparative ES

For the synthesis of intermediate **4**, 0.1 mmol of solid tropine **2** and 0.1 mmol of phenyl acetic acid or phenylacetyl chloride **5** were added to 100 μL of aqueous 3 M HCl or 100 μL of 4 M HCl in dioxane and sprayed for 5 minutes. For the synthesis of intermediate **4**, 0.1 mmol of solid tropine **2** and 0.1 mmol of phenyl acetic acid or phenylacetyl chloride **5** were added to 100 μL of solvent and sprayed for 5 minutes. All deposited products were washed with 500 μL ACN and analyzed *via* nanoESI-MS.

Synthesis of intermediates in microfluidics

A DMF solution of tropine **2** HCl in dioxane and phenylacetyl chloride **6** were individually loaded onto 1 mL ILS gas tight glass syringes. Each solution was in turn dispensed onto the SOR 3225 reactor to react and produce intermediate **4**. Similarly, a DMA solution of tropine **2** and phenylacetyl chloride **5** were loaded into a pair of 1 mL syringes and reacted onto the SOR 3227 reactor to prepare for intermediate **4**. The esterification reaction was run at 100 °C, 150 °C and 200 °C in residence times of 1 min, 2 min, 5 min, and 8 min. The intermediate was collected without quenching. The subsequent nESI-MS and HPLC-MS analyses were performed without further purification. By contrast, NMR analysis was performed after neutralization and extraction of the reaction mixture.

Synthesis of atropine in preparative ES

The first step product of the atropine synthesis was achieved by preparative ES spraying of 200 μL 1 : 1 0.5 M tropine in DMA : 0.5 M phenylacetyl chloride in DMA and then washing the deposited product from the glass wool with 500 μL DMA. The second step of the atropine synthesis was performed by spraying 50 μL of the following solution: 10 μL Step 1 product, 30 μL 36–37% formaldehyde solution in water and 30 μL 1 M base in DMA. The sample on the glass wool was quenched with 500 μL water and the product was extracted with 100 μL DCM. The preparative ESI product was analyzed *via* nanoESI.

Synthesis of atropine by reactive preparative EES

The first ES emitter sprayed the step 1 reagents to form the intermediate and the first syringe contained 0.1 M tropine in DMA and the second syringe contained 0.1 M phenylacetyl chloride in DMA. The second ES emitter sprayed the second step reagents and the first syringe contained 1 M 1,5-diazabicyclo[4.3.0] in DMA and the second syringe contained 36–37% formaldehyde solution in water. A total of 100 μL of each reagent was sprayed for 20 minutes. The glass wool was quenched with 2 mL water and the product was extracted with 100 μL DCM. For analysis by nanoESI, 10 μL of the DCM extract was diluted in 90 μL of ACN.

Synthesis of atropine by microfluidics using two chips

DMA solution of intermediate **4** and aqueous formaldehyde solution with each of the nine bases in turn were loaded onto a pair of 1 mL glass syringes and delivered at temperatures starting from room temperature to 200 °C. All the bases were diluted in DMA. The residence times of the reactions also varied from 10 s to 8 minutes, depending on the base, in a Labtrix SOR reactor, such as the 3227, 3225, 3223 or 3222 reactor. Deionized water was loaded into the last 1 mL glass syringe and delivered to quench the reaction (see ESI† for details).

Continuous microfluidic synthesis of atropine

The DMA solutions of tropine **2** (1.0 equiv.) and phenylacetyl chloride **5** (1.0 equiv.) were loaded into a pair of 1 mL glass syringes and delivered to SOR 3221 at 100 °C in 2 min residence time. The solution from SOR 3221 was poured into the first inlet of SOR 3223. A DMA solution of 1,5-diazabicyclo [4.3.0] base and formaldehyde solutions (4.0 equiv.) and water were loaded onto a pair of 1 mL glass syringes and delivered to SOR 3223 at 70 °C in 6 min residence time.

Results and discussion

Preparation of intermediate ester 4 by electrospray

Multiple reaction pathways for the synthesis of atropine (**1**) were explored using preparative ES with off-line product collection (Fig. 1). In its simplest form, preparative ES gives a binary response as to whether a synthetic route does or does not yield product. A successful reaction in spray guides the choice of possible reactions to pursue in microfluidics. Four synthetic routes (Scheme 1) were screened by preparative ES for the formation of the atropine intermediate **4**. The first pathway

This journal is © The Royal Society of Chemistry 2017

Fig. 1 Preparative ES. A high voltage is applied to the dissolved reaction mixture in a syringe and nitrogen assists in nebulizing the solution. Spray droplets containing product and unconverted reagent are deposited on glass wool for analysis.

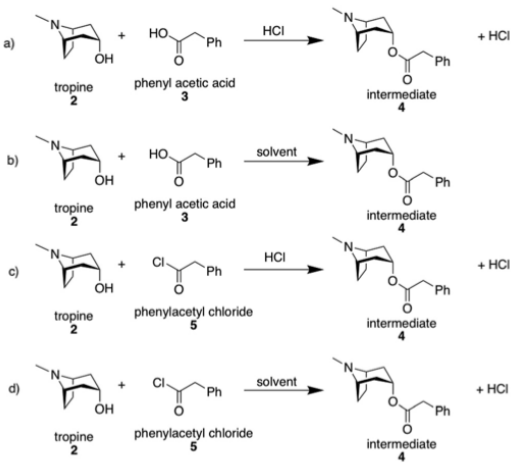

Scheme 1 Routes to intermediate **4**.

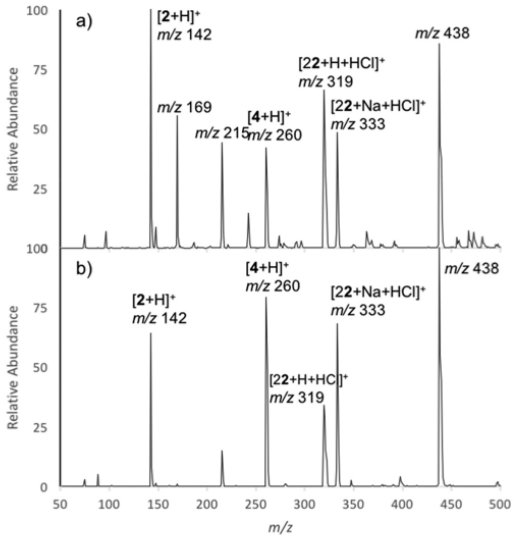

Fig. 2 Mass spectra of ES deposited material. (a) Full scan positive ion mode spectrum of the deposited material from the preparative ES reaction of tropine **2**, phenylacetyl chloride **5** and HCl in dioxane yielding intermediate **4** (30% conversion). (b) Full scan positive ion mode spectrum of the deposited material from the preparative ES reaction of tropine **2**, and phenylacetyl chloride **5** in DMA yielding intermediate **4** (55% conversion). **22** indicates the dimer of **2**.

(Scheme 1a) explored the use of tropine **2**, phenyl acetic acid **3** and HCl in both water and dioxane. The use of aqueous HCl yielded no observable intermediate **4** in the full scan MS; however, the presence of product in low abundance was evident from the MS/MS spectrum recorded for ions of *m*/*z* 260, of the value corresponding to the protonated intermediate. The use of HCl in dioxane yielded a low but measurable signal for intermediate **4** in the full scan MS with a conversion of 1.4% (conversion is defined as the abundance of the product ion divided by the sum of the abundances of the reagent, product, and byproduct ions). The second pathway (Scheme 1b) involving tropine **2** and phenyl acetic acid **3** again yielded no intermediate **4** in the full scan MS in a solvent screening that included acetonitrile (ACN), dichloromethane (DCM), dimethylacetamide (DMA), dimethylformamide (DMF), dimethyl sulfoxide (DMSO), ethanol, methanol, tetrahydrofuran (THF), and toluene. By contrast, the third pathway (Scheme 1c) using tropine **2**, phenylacetyl chloride **5** and HCl in dioxane yielded **4** in 30% conversion (Fig. 2a). The fourth pathway (Scheme 1d) eliminated the use of acid, with only tropine **2** and phenylacetyl chloride **5** in the solvent. A solvent screening using the nine previously used solvents was conducted for this pathway to the esterification of tropine **2** with phenylacetyl chloride **5**. The intermediate **4** was produced in DMA, DMF, ethanol and methanol, with the highest percentage conversion (55%) being shown in DMA (Fig. 2b). This pathway to the synthesis of intermediate **5** has not been published in the bulk and was first described in a preliminary communication on the utilization of this screening methodology.[54] The conversion varied in different permutations of the pathway with the finding that tropine **2** and phenylacetyl chloride **5** in DMA produced the highest conversion of the four pathways. This is a promising pathway to carry forward microfluidics testing. Because the solvents ethanol and methanol are expected to lead to aldol condensation byproducts, only DMA and DMF were examined in microfluidics.

Preparation of intermediate 4 in flow

The two best pathways (Scheme 1c and d) and solvents, DMA and DMF, for the synthesis of the intermediate ester **4** in preparative ES were examined in microfluidics. The flow reaction between tropine **2** (1 equivalent) and phenylacetyl chloride **5** (1.1 equivalents) in the presence of HCl in dioxane in DMA (Scheme 1c) gave 91% conversion as judged using LC-MS of the intermediate salt **4** at 100 °C in 9.16 minutes (ESI Table 1†). The second pathway used tropine **2** (1 equivalent) and phenylacetyl chloride **5** (1.1 equivalent) (Scheme 1d) in DMA and at 150 °C in 4 minutes gave 94% conversion of the intermediate **4** along with quaternary ammonium salt bypro-

ducts (ERI Scheme 1 and ESI Table 2†). The quaternary ammonium salts were produced from a reaction between the ester intermediate and phenyl acetyl chloride. The presence of solvent associated byproducts was noted at 150 °C and 200 °C (ESI Scheme 2†). The microfluidic reaction using DMF as the solvent showed more solvent associated byproduct than did DMA. For neither of these processes was reaction quenching performed.

Reducing the amounts of the quaternary ammonium salt byproducts is important because it decreases the probability of producing further byproducts in the next step of the atropine synthesis. To achieve this, equimolar (1 : 1) amounts of tropine **2** and phenylacetyl chloride **5** were used: this gave 89% conversion of intermediate **4** with less quaternary ammonium byproducts at 100 °C in 2 minutes (ESI Table 2†). The latter route eliminates the step of producing the tropine salt using hydrochloric acid and both routes have similar conversions to intermediate **4**. This route is 3.8 fold faster than the reported flow synthesis of atropine.[49] Preparative ES and microfluidics data both show that the highest conversion pathway for the production of intermediate **4** was tropine **2** and phenylacetyl chloride **5** in DMA.

Synthesis of atropine by preparative electrospray

The second step in the synthesis of atropine is a base-catalyzed aldol condensation with the addition of formaldehyde and a base to the intermediate **4**. The crude product from the preparative ES reaction of tropine **2** and phenylacetyl chloride **5** in DMA was telescoped with aqueous formaldehyde (37%) and 1 M base in DMA to form atropine. Twenty-two bases were screened in preparative ES to determine which base yielded the highest conversion to atropine with the least amount of byproduct. This methodology allowed quick screening of different bases to determine which base yielded the highest conversion to atropine and simultaneously allowed examination of the byproducts produced by each base. Of the 22 bases screened (ESI Table 3†), seven showed conversions to atropine of more than 5%. The percentage conversion included accounting for byproducts previously identified in the continuous flow synthesis by aldol condensation of atropine and aqueous formaldehyde in both sodium hydroxide and pH 10 buffer. Seven bases successfully produced atropine; therefore, the best bases for the aldol condensation were judged from both high conversion to atropine and low conversion to byproducts. The bases 1,8-diazabicyclo[5.4.0]undec-7-ene, potassium ethoxide, potassium methoxide, sodium ethoxide, sodium hydroxide and sodium methoxide had a higher percentage conversion to apoatropine **6**, the E1 elimination byproduct, than atropine. The base 1,5-diazabicyclo[4.3.0]non-5-ene was the screened base with the highest conversion (44.5%) to atropine; moreover, it was the only base with only a nominal production of byproducts. The preparative ES data therefore indicate that the best base for the synthesis of atropine in microfluidics is likely to be 1,5-diazabicyclo[4.3.0]non-5-ene.

Telescoped synthesis of atropine in flow using two chips

The hydroxymethylation step (aldol condensation, 2nd step) was examined under different reaction conditions using the intermediate from the first step in microfluidics without any further purification (Fig. 3). Nine bases were screened, which encompassed both successful and unsuccessful reactions in preparative ES and their conversions to product are summarized in Table 1. Apoatropine **6** (E1 elimination byproduct) was produced under all the conditions as E1 elimination is accelerated by the temperature and the base. Sodium ethoxide in ethanol produced a solid during the microfluidic reaction leading to a clogged chip because the byproduct (sodium chloride) has a low solubility in ethanol. The pH 10 buffer led to an overall conversion to atropine of 30% and this condition produced byproducts **6** and **8** (Scheme 2) (ESI Table 4†). Increasing the temperature led to more elimination byproduct **7**, the higher temperatures driving water elimination from atropine. Increasing the amount of formaldehyde or the residence time increased the second aldol byproduct **8**. Decreasing the temperature did not lead to the production of atropine. Sodium methoxide and potassium methoxide gave 24% overall conversions, again as measured by MS. However, increasing the residence time and temperature increased the production of byproducts **6** (ESI Table 5†). A new byproduct, **7**, arose from a Michael addition of the methanol present in the base and in formaldehyde solutions. Trimethylamine and DABCO showed poor conversion to atropine even at higher temperature and longer residence time.

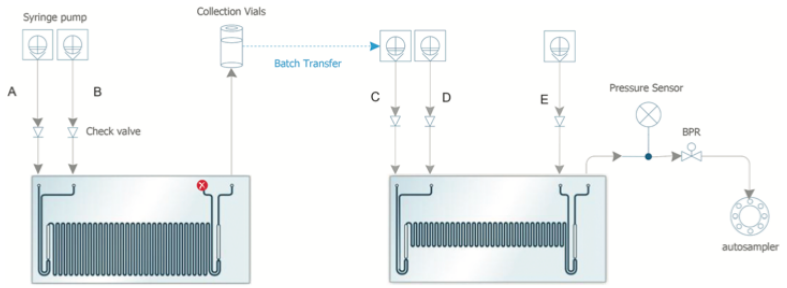

Fig. 3 Synthesis of atropine in flow in two chips A = tropine; B = phenylacetyl chloride, C = crude product from first chip; D = base + formaldehyde; E = water.

This journal is © The Royal Society of Chemistry 2017

Table 1 Conversion of crude intermediate **4** to atropine (1) and to byproducts

Base	Maximum conversion of atropine (%)	Reaction conditions	Byproducts in flow	Preparative ES conversion (%)	Byproducts in ES
pH 10 buffer	30	150 °C, 2 min	**7**, **9**	1.6	**7**
Sodium methoxide in methanol (CH_3ONa)	24	150 °C, 2.9 min	**7**, **8**	9.9	**7**
Potassium methoxide in methanol (CH_3OK)	24*	70 °C, 2 min	**7**, **8**	7.6	**7**, **9**
Tetramethyl ammonium hydroxide	36*	100 °C, 21.4 s	**7**, **8**	1.6	**7**, **9**
Sodium hydroxide	23	70 °C, 2 min	**7**, **9**	15.4	**7**
1,5-Diazabicyclo[4.3.0]non-5-ene	44*	70 °C, 6 min	**7**	47.5	**7**

Maximum percentage conversion of atropine in two steps in two different chips. The percentage conversion was determined by nESI-MS unless asterisked (*) in which case conversion was determined by LC-MS. The reaction conditions describe the temperature and residence time in the second chip.

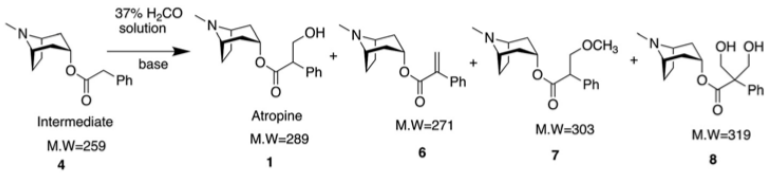

Scheme 2 Possible byproducts from the second step reaction.

Tetramethylammonium hydroxide took less than a minute to convert all intermediates to products and byproducts. The maximum conversion to atropine (36%) was associated with large amounts of byproducts **6**, **7**. The best conditions for tetramethylammonium hydroxide with the highest conversion (32%) and the lowest conversion to byproducts were found at 100 °C in 8.6 seconds (ESI Table 5†). Sodium hydroxide showed 23% maximum overall conversion of atropine in 6 minute residence time with hydrolyzed tropine and byproducts **6** and **8** (ESI Table 7†).

1,5-Diazabicyclo[4.3.0]non-5-ene was the most effective base for the aldol condensation reaction in microfluidics, which correlates to the preparative ES data. The maximum overall conversion of atropine using 1,5-diazabicyclo[4.3.0]non-5-ene base was 44% (Table 1) at 70 °C in 4 and 6 min residence time and it showed minimum amounts of byproduct **6**. Increasing the residence time and temperature increased the amount of byproduct **6**. The maximum atropine yield (not conversion) measured quantitatively by NMR was 30% at 70 °C using 6 min residence time.

The reaction conditions (chip 3227, 4 equiv. of formaldehyde, 4 equiv. base, 70 °C, P = 9 bar) for the highest conversion of 1,5-diazabicyclo[4.3.0]non-5-ene were used to compare the relative conversion of atropine in 1,5-diazabicyclo[4.3.0]non-5-ene, potassium methoxide, sodium hydroxide and pH 10 buffer (ESI Table 7†). The overall conversion of atropine using 1,5-diazabicyclo[4.3.0]non-5-ene in two steps was almost identical in 4 and 6 minutes. Atropine conversion decreased with increasing residence time for both potassium methoxide and sodium hydroxide bases. The pH 10 buffer did not lead to the production of atropine under these reaction conditions.

Table 2 Conversion to byproducts in different bases

		Percentage conversion of byproducts (%)		
Byproduct	Method	1,5-Diazabicyclo[4.3.0]non-5-ene	CH_3OK	NaOH
6	ES	11.4	45.1	40.3
	Flow	3.8	20.2	65.8
7	ES	<1	<1	<1
	Flow	<1	44.8	<1
8	ES	2.2	31.1	1.4
	Flow	1.5	4.1	13.4

The base 1,5-diazabicyclo[4.3.0]non-5-ene gave the smallest conversion to byproducts and showed only 3.8% of byproduct **6** in 6 min residence time (Table 2). The best base for the aldol condensation was 1,5-diazabicyclo[4.3.0]non-5-ene in both preparative ES and microfluidics.

Telescoped synthesis of atropine by extractive electrospray

The multi-step synthesis of atropine was performed continuously using a variant of extractive electrospray (EES) (Fig. 4). This technique utilized two electrospray emitters where the first ESI emitter produced the intermediate **4** and the second ESI emitter nebulized the hydroxymethylation reagents for the second and final steps of the atropine synthesis. The reactive EES setup used differs from traditional EES. In traditional EES the angle of intersection of the two ES emitters is 90 degrees, with some experiments using angles of 40–60 degrees.[38,40] For these reactive EES experiments, the angle of intersection is <22.5%, which allows for more interaction of the droplets

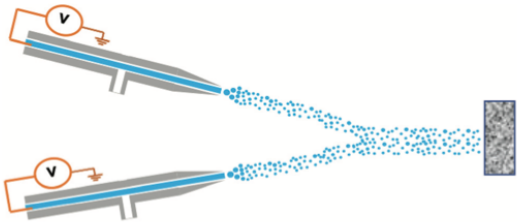

Fig. 4 Preparative reactive EES. A high voltage is applied to the solvent through a platinum electrode and nitrogen gas assists in nebulizing the solution. The ES emitters are positioned at an angle of 22.5° and the point of intersection of the spray plumes is 4 cm from the glass wool collection surface.

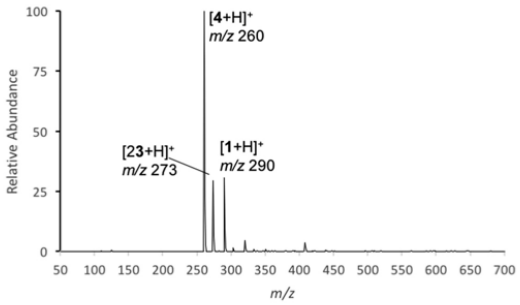

Fig. 5 Mass spectrum (positive ion mode) of the material deposited using preparative reactive EES, showing the atropine product **1** and intermediate **4**.

from the ES emitters. This was also favored by increasing the distance of their intersection point to the collecting surface by 4 cm. This allows for an adequate reaction time for the first step of the reaction to proceed before interacting with droplets from the second step reagents. The setup was optimized using different angles of emitters, distances of the emitters to droplet intersection and droplet intersection to the glass wool, and applied polarities (ESI Fig. 30–33†). When the ES emitters were orthogonal, as in traditional EES, the ratio of product to intermediate was low. The highest ratio of product to intermediate occurred when the emitters were placed at an angle of *ca.* 22.5°. Higher ratios of product to intermediate occurred when the point of intersection of the plume from both emitters and the distance from the intersection to the collection surface was greater; however, there was a trade-off in quantity of material deposited on the glass wool. In preparative reactive EES, the unreacted phenylacetyl chloride reacted with the water in aqueous formaldehyde to form the phenyl acetic acid seen in MS as the protonated dimer $[2M + H]^+$. This was expected as phenylacetyl chloride is highly reactive with water. Despite this, the percentage conversion to atropine was 24% which is similar to the total conversion from both steps in the preparative ES of 26% (Fig. 5). Therefore, telescoped preparative EES is a viable approach to microscale synthesis with similar conversions to telescoped preparative ES.

Continuous microfluidic synthesis of atropine

Telescoping in a 3224 reactor caused more byproduct formation and gave less control over the reaction conditions, so this encouraged us to telescope the atropine synthesis in two separate reactors (Fig. 6). The optimized conditions using 1,5-diazabicyclo[4.3.0]non-5-ene base in separate steps (1st step: 2 min, 100 °C and 2nd step: 6 min, 70 °C) allowed telescoped atropine synthesis in 55.1% conversion by nanoESI-MS. The average quantified yield was 33.5% by RP-UPLC.

Comparison of preparative ES and microfluidics

Preparative ES is a rapid method which successfully predicted the reaction pathway, solvent and base with the highest percentage conversion in microfluidics. Naturally, there were noticeable differences between the results of the two techniques in both the conversion to products and the production of byproducts. The conversion from the starting material to product was somewhat higher in microfluidics than in pre-

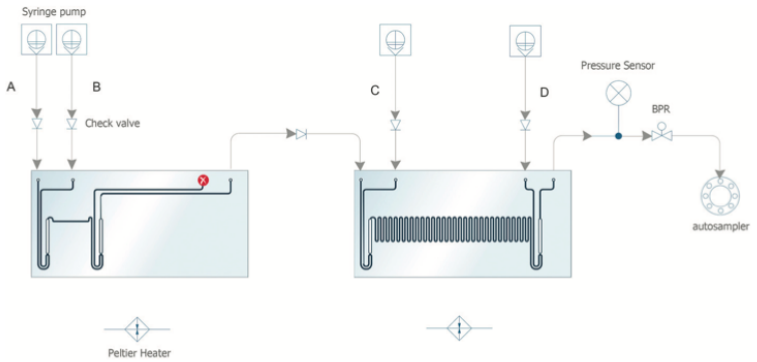

Fig. 6 Continuous flow synthesis of atropine in separate reactors. A = tropine; B = phenylacetyl chloride, C = base + formaldehyde; D = water.

This journal is © The Royal Society of Chemistry 2017

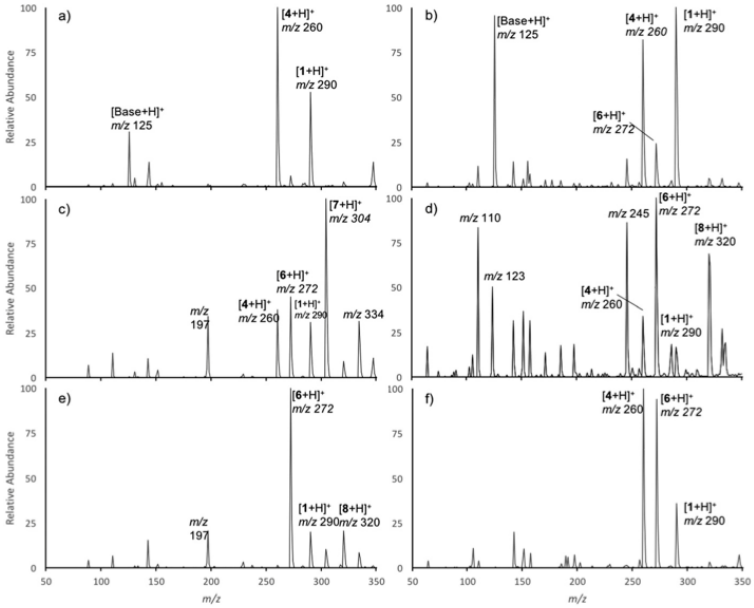

Fig. 7 Full scan positive ion mode spectra of atropine synthesized using (a) 1,5-diazabicyclo[4.3.0]non-5-ene in microfluidics, (b) 1,5-diazabicyclo[4.3.0]non-5-ene in preparative ES, (c) potassium methoxide in microfluidics, (d) potassium methoxide in preparative ES, (e) sodium hydroxide in microfluidics, and (f) sodium hydroxide in preparative ES.

parative ES. This can be attributed to the larger scale, the longer time, the greater ability to control reactions in microfluidics and the use of elevated temperatures. Elevated temperatures have been used for preparative ES experiments[54,55] but the successful synthesis of the intermediate at room temperature showed that heat was unnecessary for the binary reaction screening. However, elevated temperatures may be useful for screening other reactions. Another differentiating factor is the open atmosphere in preparative ES. In microfluidics, the reaction occurs in a closed pressurized system which limits interfaces to glass/solution interfaces unlike the air/solution interfaces in preparative ES. A third factor affecting the difference in conversion is the vapor pressure of both the reagents and solvents. Reaction acceleration in preparative ESI relies heavily on solvent evaporation from the charged droplets.[22] Volatile reagents may leave the droplets rather than remain in the (presumably) highly reactive interfacial positions on its surface.

There were differences in the formation of byproducts for the second step of the atropine synthesis in preparative ES and microfluidics (Fig. 7). While both techniques heavily favored the E1 eliminated byproduct, **6**, major difference lie in the production of byproducts **7** and **8**. In preparative ES, **7** was not produced and conversion to byproduct **8** occurred to give more than 5% conversion in every successful base with the exception of 1,5-diazabicyclo[4.3.0]non-5-ene, sodium hydroxide and sodium methoxide. Conversely, byproduct **7** was produced in microfluidics with the bases sodium methoxide, potassium methoxide and tetramethyl ammonium hydroxide. The only bases to produce byproduct **8** with a conversion greater that 5% were sodium hydroxide and pH 10 buffer. Byproduct **8** is formed when two formaldehyde molecules react with the intermediate **4**, while byproduct **7** is the Michael addition product of methanol to **6** at high temperature. Byproduct **7** was not formed in preparative ES due to the lack of heat necessary for the Michael addition.

Conclusion

This is the first investigation of spray reactions guiding microfluidic synthesis where preparative ES has been explicitly used for route screening, solvent screening and acid/base screenings on a large scale. Preparative ES was used as a rapid way to discover new synthetic pathways and this methodology led to faster optimization of microfluidic reactions by determining and eliminating unsuccessful reaction pathways from further consideration. Pathway discovery to determine new and faster reactions for formulation from raw materials can improve current manufacturing workflows in the pharmaceutical and chemical industries.

This investigation led to a highly efficient first step esterification of tropine to intermediate without the use of a tropine salt or an added acid. The first step was optimized in flow utili-

zing the information obtained in the charged microdroplets. The intermediate from the first step in preparative ES was used to screen 22 unique bases for the base-catalyzed aldol condensation to form the final product, atropine. Seven bases were shown to yield atropine and with the exception of transient solids, all led to the production of atropine in flow. In both preparative ES and continuous microfluidics the base with the highest conversion and lowest conversion to byproducts was 1,5-diazabicyclo[4.3.0]non-5-ene. In preparative ES, the first step yielded conversion to intermediate **4** of 55% and the second step yielded atropine in 47% conversion, with an overall conversion of 26%. In flow, the atropine yield was 30% using NMR (44% conversion using nanoESI-MS). Atropine was continuously synthesized in both preparative EES and microfluidics with a conversion of 24% in preparative EES (by nanoESI-MS) and 34% yield in flow (by RP-UPLC). The correlation of the data between preparative ES and microfluidics provides evidence that accelerated reactions in droplets can guide microfluidics.

Acknowledgements

Financial support from the Department of Defense's Defense Advanced Research Projects Agency (award no. W911NF- 16-2-0020) is acknowledged.

Notes and references

1 V. Hessel, D. Kralisch, N. Kockmann, T. Noël and Q. Wang, *ChemSusChem*, 2013, **6**, 746–789.
2 J.-I. Yoshida, Y. Takahashi and A. Nagaki, *Chem. Commun.*, 2013, **49**, 9896–9904.
3 J. Wegner, S. Ceylan and A. Kirschning, *Chem. Commun.*, 2011, **47**, 4583–4592.
4 D. Webb and T. F. Jamison, *Chem. Sci.*, 2010, **1**, 675–680.
5 K. Geyer, T. Gustafsson and P. H. Seeberger, *Synlett*, 2009, 2382–2391.
6 K. F. Jensen, *MRS Bull.*, 2006, **31**, 101–107.
7 A. Adamo, R. L. Beingessner, M. Behnam, J. Chen, T. F. Jamison, K. F. Jensen, J. C. Monbaliu, A. S. Myerson, E. M. Revalor, D. R. Snead, T. Stelzer, N. Weeranoppanant, S. Y. Wong and P. Zhang, *Science*, 2016, **352**, 61–67.
8 D. R. Snead and T. F. Jamison, *Angew. Chem., Int. Ed.*, 2015, **54**, 983–987.
9 D. Kralisch and G. Kreisel, *Chem. Eng. Sci.*, 2007, **62**, 1094–1100.
10 R. L. Hartman and K. F. Jensen, *Lab Chip*, 2009, **9**, 2495–2507.
11 H. Kim, K. I. Min, K. Inoue, D. J. Im, D. P. Kim and J. Yoshida, *Science*, 2016, **352**, 691–694.
12 L. Malet-Sanz and F. Susanne, *J. Med. Chem.*, 2012, **55**, 4062–4098.
13 I. R. Baxendale, R. D. Braatz, B. K. Hodnett, K. F. Jensen, M. D. Johnson, P. Sharratt, J. P. Sherlock and A. J. Florence, *J. Pharm. Sci.*, 2015, **104**, 781–791.
14 T. Gustafsson, F. Ponten and P. H. Seeberger, *Chem. Commun.*, 2008, 1100–1102.
15 M. D. Hopkin, I. R. Baxendale and S. V. Ley, *Org. Biomol. Chem.*, 2013, **11**, 1822–1839.
16 B. J. Deadman, M. D. Hopkin, I. R. Baxendale and S. V. Ley, *Org. Biomol. Chem.*, 2013, **11**, 1766–1800.
17 P. Zhang, M. G. Russell and T. F. Jamison, *Org. Process Res. Dev.*, 2014, **18**, 1567–1570.
18 D. R. Snead and T. F. Jamison, *Chem. Sci.*, 2013, **4**, 2822–2827.
19 P. R. D. Murray, D. L. Browne, J. C. Pastre, C. Butters, D. Guthrie and S. V. Ley, *Org. Process Res. Dev.*, 2013, **17**, 1192–1208.
20 X. Yan, E. Sokol, X. Li, G. Li, S. Xu and R. G. Cooks, *Angew. Chem., Int. Ed.*, 2014, **53**, 5931–5935.
21 J. J. Agresti, E. Antipov, A. R. Abate, K. Ahn, A. C. Rowat, J.-C. Baret, M. Marquez, A. M. Klibanov, A. D. Griffiths and D. A. Weitz, *Proc. Natl. Acad. Sci. U. S. A.*, 2010, **107**, 4004–4009.
22 R. D. Espy, M. Wleklinski, X. Yan and R. G. Cooks, *TrAC, Trends Anal. Chem.*, 2014, **57**, 135–146.
23 M. Girod, E. Moyano, D. I. Campbell and R. G. Cooks, *Chem. Sci.*, 2011, **2**, 501–510.
24 G. Xu, B. Chen, B. Guo, D. He and S. Yao, *Analyst*, 2011, **136**, 2385–2390.
25 A. K. Badu-Tawiah, L. S. Eberlin, Z. Ouyang and R. G. Cooks, *Annu. Rev. Phys. Chem.*, 2013, **64**, 481–505.
26 J. Laskin, P. A. Eckert, P. J. Roach, B. S. Heath, S. A. Nizkorodov and A. Laskin, *Anal. Chem.*, 2012, **84**, 7179–7187.
27 R. M. Bain, C. J. Pulliam, S. A. Raab and R. G. Cooks, *J. Chem. Educ.*, 2015, **93**, 340–344.
28 R. M. Bain, C. J. Pulliam and R. G. Cooks, *Chem. Sci.*, 2015, **6**, 397–401.
29 E. A. Crawford, C. Esen and D. A. Volmer, *Anal. Chem.*, 2016, **88**, 8396–8403.
30 D. Schröder, *Acc. Chem. Res.*, 2012, **45**, 1521–1532.
31 R. H. Perry, T. J. Cahill, J. L. Roizen, J. Du Bois and R. N. Zare, *Proc. Natl. Acad. Sci. U. S. A.*, 2012, **109**, 18295–18299.
32 D. N. Mortensen and E. R. Williams, *J. Am. Chem. Soc.*, 2016, **138**, 3453–3460.
33 R. H. Perry, M. Splendore, A. Chien, N. K. Davis and R. N. Zare, *Angew. Chem.*, 2011, **123**, 264–268.
34 R. H. Perry, K. R. Brownell, K. Chingin, T. J. Cahill, R. M. Waymouth and R. N. Zare, *Proc. Natl. Acad. Sci. U. S. A.*, 2012, **109**, 2246–2250.
35 T. Müller, A. Badu-Tawiah and R. G. Cooks, *Angew. Chem., Int. Ed.*, 2012, **51**, 11832–11835.
36 S. Banerjee, E. Gnanamani, X. Yan and R. N. Zare, *Analyst*, 2017, **142**, 1399–1402.
37 H. Chen, A. Venter and R. G. Cooks, *Chem. Commun.*, 2006, 2042–2044.
38 L. Zhu, G. Gamez, H. W. Chen, H. X. Huang, K. Chingin and R. Zenobi, *Rapid Commun. Mass Spectrom.*, 2008, **22**, 2993–2998.

This journal is © The Royal Society of Chemistry 2017

39 K. Chingin, G. Gamez, H. Chen, L. Zhu and R. Zenobi, *Rapid Commun. Mass Spectrom.*, 2008, **22**, 2009–2014.
40 H. Chen, S. Yang, M. Li, B. Hu, J. Li and J. Wang, *Angew. Chem., Int. Ed.*, 2010, **49**, 3053–3056.
41 H. Chen and R. Zenobi, *Nat. Protoc.*, 2008, **3**, 1467–1475.
42 H. Chen, A. Wortmann and R. Zenobi, *J. Mass Spectrom.*, 2007, **42**, 1123–1135.
43 H. Chen, A. Wortmann, W. Zhang and R. Zenobi, *Angew. Chem., Int. Ed.*, 2007, **46**, 580–583.
44 L. Zhu, G. Gamez, H. Chen, K. Chingin and R. Zenobi, *Chem. Commun.*, 2009, 559–561.
45 J. K. Lee, S. Kim, H. G. Nam and R. N. Zare, *Proc. Natl. Acad. Sci. U. S. A.*, 2015, **112**, 3898–3903.
46 R. Qiu, C. Zhang, Z. Qin and H. Luo, *RSC Adv.*, 2016, **6**, 36615–36622.
47 G. Grynkiewicz and M. Gadzikowska, *Pharmacol. Rep.*, 2008, **60**, 439–463.
48 M. Gadzikowska and G. Grynkiewicz, *Acta Pol. Pharm.*, 2002, **59**, 149–160.
49 C. H. Dai, D. R. Snead, P. Zhang and T. F. Jamison, *J. Flow Chem.*, 2015, **5**, 133–138.
50 R. Robinson, *J. Chem. Soc., Trans.*, 1917, **111**, 762–768.
51 G. C. Schmidt, T. E. Eling and J. C. Drach, *J. Pharm. Sci.*, 1967, **56**, 215–221.
52 J. R. Pfister, *J. Org. Chem.*, 1978, **43**, 4373–4374.
53 A.-C. Bédard, A. R. Longstreet, J. Britton, Y. Wang, H. Moriguchi, R. W. Hicklin, W. H. Green and T. F. Jamison, *Bioorg. Med. Chem.*, 2017, in press.
54 M. Wleklinski, C. E. Falcone, B. P. Loren, Z. Jaman, K. Iyer, H. S. Ewan, S. H. Hyun, D. H. Thompson and R. G. Cooks, *Eur. J. Org. Chem.*, 2016, **2016**, 5480–5484.
55 H. Chen, L. S. Eberlin, M. Nefliu, R. Augusti and R. G. Cooks, *Angew. Chem., Int. Ed.*, 2008, **47**, 3422–3425.

This journal is © The Royal Society of Chemistry 2017

ChemPubSoc Europe
DOI: 10.1002/ejoc.201601270
EurJOC European Journal of Organic Chemistry
Communication

Mass Spectrometry

Can Accelerated Reactions in Droplets Guide Chemistry at Scale?

Michael Wleklinski,[a] Caitlin E. Falcone,[a] Bradley P. Loren,[a] Zinia Jaman,[a] Kiran Iyer,[a] H. Samuel Ewan,[a] Seok-Hee Hyun,[a] David H. Thompson,*[a] and R. Graham Cooks*[a]

Abstract: Mass spectrometry (MS) is used to monitor chemical reactions in droplets. In almost all cases, such reactions are accelerated relative to the corresponding reactions in bulk, even after correction for concentration effects, and they serve to predict the likely success of scaled-up reactions performed in microfluidic systems. The particular chemical targets used in these test studies are diazepam, atropine and diphenhydramine. In addition to a yes/no prediction of whether scaled-up reaction is possible, in some cases valuable information was obtained that helped in optimization of reaction conditions, minimization of by-products, and choice of catalyst. In a variant on the spray-based charged droplet experiment, the Leidenfrost effect was used to generate larger, uncharged droplets and the same reactions were studied in this medium. These reactions were also accelerated but to smaller extents than in microdroplets, and they gave results that correspond even more closely to microfluidics data. The fact that MS was also used for online reaction monitoring in the microfluidic systems further enhances the potential role of MS in exploratory organic synthesis.

Introduction

This study is part of a larger project, the overall goal of which is to develop an automated scalable and continuous synthesis system. A key objective is to test possible synthetic pathways quickly on a small scale seeking a go/no-go result. We "spot-test" particular routes using a chemical pruning step, which employs reaction acceleration in droplets with independent mass spectrometric analysis. A simple yes/no answer to product or (in multistep reactions) intermediate formation is sought using the charged droplet reactor. We use electrospray (ESI) for both synthesis and analysis with careful control of parameters to avoid unwanted reaction during analysis.[1]

Charged microdroplets are produced by ESI. It is known that reaction rates increase as the solvent evaporates because of changes in concentration, pH, surface/volume ratios, and interfacial effects.[1b,1c,2] The acceleration factors can be remarkably large.[3] A recent review covers the topic of accelerated reactions in droplets, including evidence that partial solvation of reagents at interfaces contributes to the orders of magnitude reaction rate acceleration that can be seen.[1a] The hypothesis investigated here is that the accelerated reactions that occur in droplets might assist in rapidly evaluating reactivity in microfluidic systems.

A second method of producing droplets is based on the Leidenfrost effect.[4] It has recently been shown that accelerated organic reactions occur in Leidenfrost droplets.[5] These droplets differ from ESI-based droplets in that they are (i) larger, (ii) net-neutral, and (iii) involve elevated temperatures. The difference in droplet size means that larger amounts of reagent can be studied, but the surface/volume ratio is greatly decreased. The measured reaction acceleration factors for three previously studied Leidenfrost reactions, hydrazone formation, Katritzky pyrylium → pyridinium conversion and Claisen–Schmidt condensation, are about an order of magnitude.[5]

Note that we do not expect to be able to transfer optimized conditions exactly from the droplet scale to the microfluidics scale, in part because of uncertainty about the origins of acceleration effects in the two systems. We do expect that these optimized conditions will represent a starting point for efficient optimization of the conditions in the microfluidics reactor. We also expect that information on reaction intermediates and mechanisms might be acquired from the study of droplet reactions. This information is already being obtained in experiments in which the degree of desolvation of the initial droplets is varied by changing the distance that the droplets travel before analysis.[1b] Information obtained from the droplet reactor on experimental parameters including solvent, catalyst, pH, etc. is also readily acquired, and we examine how transferable this information is in optimizing the microfluidics reactor.

The identification of suitable pathways to target molecules is just one step towards an online, automated flow-through synthesizer, for which the groundwork has been laid by several groups. Notable are the mol-scale, end-to-end, continuous manufacturing pilot plant developed by MIT/Novartis,[6] the refrigerator-sized, reconfigurable, on-demand synthesizer of pharmaceuticals of MIT,[7] the nanomol-scale robotic high-throughput synthesizer of Merck,[8] and the automated synthesis labo-

[a] Department of Chemistry, Purdue University
560 Oval Drive, West Lafayette, IN 47907, USA
E-mail: davethom@purdue.edu
cooks@purdue.edu
http://aston.chem.purdue.edu
Supporting information and ORCID(s) from the author(s) for this article are available on the WWW under http://dx.doi.org/10.1002/ejoc.201601270.

© 2016 Wiley-VCH Verlag GmbH & Co. KGaA, Weinheim

ChemPubSoc Europe
EurJOC European Journal of Organic Chemistry
Communication

ratory of Eli Lilly.[9] The mol-scale MIT synthesizer was used to produce aliskiren hemifumarate in tablet form, from a complex intermediate in a continuous fashion.[6] The Merck nanomol system was used to screen 1500 reactions per day to identify potential candidate reactions for large-scale syntheses. The Lilly system combined automated synthesis with analysis performed remotely controlled in real-time, to produce products on a gram-scale.

The main question underlying this study is whether droplet reactions may be used to predict chemical reactivity in flow chemistry systems, in particular in microfluidics. The mechanism for acceleration observed in microdroplets is certainly different from that in microfluidics in that evaporation is not significant in microfluidics; however, interfacial effects may still play an important role, especially in droplet microfluidics.[10] The speed of data acquisition in droplets makes this approach attractive. Note that false negatives (predict no reaction, but reaction can be observed) is not expected to be a serious problem, because there are usually many available routes to test. On the other hand, a false positive result will lead to wasted effort in seeking an analogous flow reaction. Note, too, that use of droplets for a simple yes/no regarding occurrence of reaction represents only one level of enquiry, even though it is the most important one. As will be seen in the results now to be discussed, information on reaction conditions is also obtained, although the quality of this information remains to be evaluated further by studying more cases.

Results and Discussion

The charged-droplet- and microfluidic-based synthesis of amide **3**, generated by *N*-acylation of **1** with the 2-haloacetyl chloride **2**, was examined due to its importance as a synthetic step in the pathway to diazepam (Scheme 1). An electrospray droplet reactor was used to evaluate potential solvents for the *N*-acylation reaction using chloroacetyl chloride. Offline charged-droplet reactions were performed using a mixture of **1** and **2** (X = Cl) in various solvents, and conversion to product as analyzed by ESI MS was compared to a 30 min batch reaction (Figure S1). Before analysis, samples are quenched in order to ensure no further reaction by diluting the collected product into the solvent used in the prior step. The results indicate that there is significant acceleration of the reaction when the solvent is DMF, ACN, or toluene. Acceleration in microdroplets is associated with evaporation and is proposed to be due, in part, to intrinsic rate acceleration at the interface.[2c] These initial results encouraged a more extensive reaction screening, where the effect of the chosen 2-haloacetyl chloride (Cl or Br) and the solvent (ACN, toluene) was investigated using a droplet reactor. Interestingly, the droplet reactor data indicated nearly complete conversion of starting materials to product for both the chloro and bromo starting materials in acetonitrile (Figure 1) and in toluene (Figure S2). Starting material **1** is observed at m/z = 246, and product **3** appears in either its protonated (X = Cl: m/z = 322–326; X = Br: m/z = 366–370) or sodiated (X = Cl: m/z = 344–348; X = Br: m/z = 388–392) form. A small amount of S_N2 product (m/z = 322) was observed for bromoacetyl chloride in ACN but not in toluene. In the case of the chloro starting material (**2**), the S_N2 and acylation products have identical molecular formulae and are not differentiable; however, the presence of only small amounts of the S_N2 product using the bromo starting material, provides evidence that the chloro compound reacts mainly to form the desired acylation product.

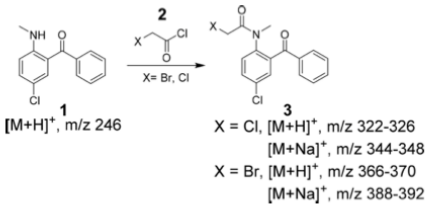

Scheme 1. Reaction of **1** and **2** (X = Cl, Br) to form amide **3**.

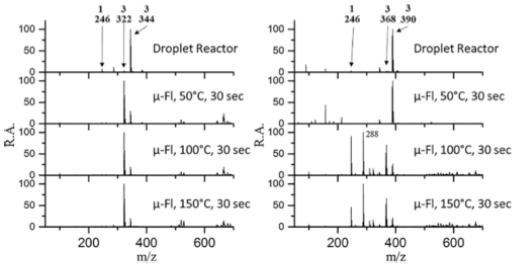

Figure 1. Synthesis of **3** in ACN using (a) chloroacetyl chloride and (b) bromoacetyl chloride in a droplet reactor and in microfluidics (μ-Fl).

Flow experiments were performed using the same concentrations as in the droplet reactor while screening the effect of temperature for a fixed residence time of 30 s. High conversion to **3** was observed with chloroacetyl chloride in both solvents at 50 °C. More interestingly, a major difference was observed with bromoacetyl chloride in ACN, wherein a major amount of S_N2 reaction product was observed, especially at higher temperatures (100 and 150 °C). The presence of a by-product (ion m/z = 288) arising from the initial S_N2 reaction product was confirmed by NMR spectroscopy and MS/MS (data not shown). The droplet reactor predicted formation of the desired intermediate, which was observed in flow. However, under higher-temperature conditions in flow, the proportion of S_N2 product increased. This difference can be explained by the fact that evaporative cooling occurs during flight in the droplet reaction at room temperature, thus reducing the reaction temperature.[11] Nonetheless, the droplet reaction demonstrated reaction feasibility and showed that specific solvents (ACN, toluene) are better than others, a fact reiterated under microfluidic conditions for this transformation.

The ability of droplet reactivity to guide chemistry at scale was investigated for another important drug, diphenhydramine. The flow-based synthesis of diphenhydramine was demonstrated by the reaction of 2-(dimethylamino)ethanol (DMAE) with chlorodiphenylmethane.[12] This synthesis featured 100 % atom economy; however, chlorodiphenylmethane is an expen-

 © 2016 Wiley-VCH Verlag GmbH & Co. KGaA, Weinheim

ChemPubSoc Europe
EurJOC European Journal of Organic Chemistry
Communication

sive starting material, which motivated an effort to develop a more cost-effective process by replacing chlorodiphenylmethane using a commodity starting material, benzhydrol (**4**). To synthesize diphenhydramine (**5**), benzhydrol (**4**) was converted into the corresponding mesyl ester, which was subsequently treated with DMAE to produce **5** (Scheme 2). The droplet-reactor synthesis of **5** was demonstrated by performing two sequential charged-droplet reactions in either a toluene or acetonitrile solvent system. First benzhydrol and mesyl chloride were sprayed to produce the mesyl ester. This material was recovered and redissolved before introduction of the second reagent, DMAE (20 equiv.) and repetition of the spray process (Figure 2). The MS analysis of the two-step spray product indicated that ACN is overall a better solvent for the synthesis of diphenhydramine, (**5**) (m/z = 256) than toluene. Unreacted DMAE (m/z = 90), mesylated DMAE (m/z = 168), and a dimer of DMAE with methanesulfonic acid (m/z = 275) were observed with the charged microdroplets. A similar trend was observed in flow (Figures S3 and S4), where optimized conditions gave diphenhydramine in 35 % and <1 % yield in ACN and toluene, respectively, using 1 equiv. of 2-(dimethylamino)ethanol. Good agreement is observed between the charged droplet reactor and flow in this synthesis.

Scheme 2. Mesylation of **4** followed by reaction with 2-(dimethylamino)-ethanol (DMAE) to form diphenhydramine (**5**).

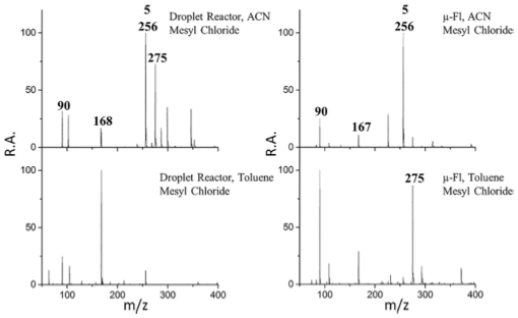

Figure 2. Charged-microdroplet (a, c) and microfluidic (b, d) reaction telescoping for the diphenhydramine synthesis in two solvents (ACN, toluene).

The charged-droplet and microfluidic synthesis of atropine also was achieved by telescoping two reaction steps. The intermediate ester **8** (Scheme 3) was prepared from the commercially available starting materials tropine (**6**) and phenylacetyl chloride (**7**). The intermediate **8** was used without further purification for the aldol condensation reaction to produce the final product, atropine. The first step was optimized for solvent and reactant stoichiometry. The droplet reactor indicated *N,N*-dimethylacetamide (DMA) as the best solvent, and this was confirmed in microfluidics (data not shown). Using the unpurified intermediate ester **8** (m/z = 260), a base screen with the droplet reactor determined the effectiveness of three bases in synthesizing atropine (**9**) (m/z = 290). Each base was successful in the droplet reactor, producing significant amounts of atropine (and byproducts), with 1,5-diazabicyclo[4.3.0]dec-5-ene being the most effective (Figure 3 and Figure S5). In flow, each base produced atropine (and byproducts) with 1,5-diazabicyclo[4.3.0]-dec-5-ene again being the most efficient. There is also some agreement between flow and charged droplets on the type and extent of byproduct formation. For example, using 1,5-diazabicyclo[4.3.0]dec-5-ene, atropine and its dehydration product **10** (m/z = 272) are observed. However, with MeOK the same type of byproducts could be observed, but their proportions were quite different (Scheme 3). The major byproduct in flow, **11** (characterized by m/z = 304) is barely formed in charged droplets. One possible reason for this difference is that formaldehyde with its high vapor pressure escapes the droplets rapidly obviating formation of this byproduct. Finally, good agreement between the two methods was observed with NaOH, where the α,β-unsaturated product **10** (m/z = 272) is the major byproduct for both droplet reactor and microfluidics. Thus, for the synthesis of atropine, the charged-droplet reactor was useful in guiding the choice of solvent and base.

The occurrence of accelerated organic reactions in Leidenfrost droplets[5] is at least in part a surface property (partial solvation of reagent molecules at the surface reduces activation energies). Consistent with this and the smaller surface/volume ratios of Leidenfrost droplets, acceleration factors are smaller than in electrosprayed microdroplets. However, the larger droplets (0.5 mL volume) mean that conditions in the Leidenfrost droplets are closer to those in microfluidic solutions and in bulk, so the predictive power of Leidenfrost droplet reactions might be even greater than that of electrospray-generated droplets.

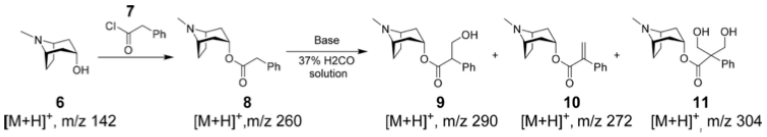

Scheme 3. Esterification reaction of **6** with **7** to synthesize **8** followed by base-catalyzed aldol condensation with formaldehyde to synthesize atropine (**9**).

 © 2016 Wiley-VCH Verlag GmbH & Co. KGaA, Weinheim

ChemPubSoc Europe
EurJOC European Journal of Organic Chemistry
Communication

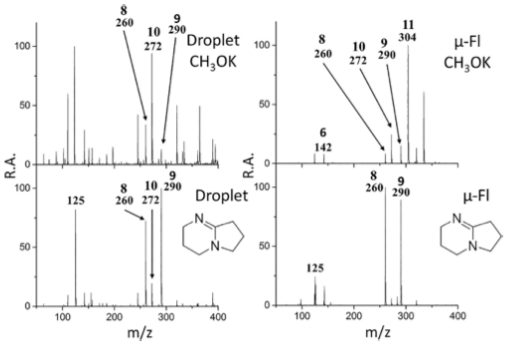

Figure 3. Charged-microdroplet (a, c) and microfluidic (b, d) reaction telescoping for the atropine synthesis using potassium methoxide or 1,5-diazabicyclo[4.3.0]dec-5-ene.

The lack of a formal charge also strengthens the expected analogy with scaled-up chemistry.

This expectation is met when one considers data for the first step of the diazepam synthesis using bromoacetyl chloride and chloroacetyl chloride. First, consider the mass spectra recorded for charged droplets in ACN and in toluene vs. those for Leidenfrost droplets in the same two solvents (Figure 4 and Figure S6). The assignment of *m/z* values is the same as in Figure 1 and Scheme 1. The conversion in the Leidenfrost experiment is not as great (more starting material seen) as in the charged-droplet reactions, but both methods give almost exclusively the desired acylation intermediate as opposed to the S_N2 product. There is not a large difference in the results for ACN vs. toluene as solvent, except that the conversion is slightly higher in ACN. If we now consider the difference between microfluidic flow and Leidenfrost droplet data, we find remarkable similarities. Microfluidic synthesis at 50 °C results primarily in the desired acylation product as is the case in the Leidenfrost droplets. One difference is in the formation of a minor species seen at *m/z* = 260 in the Leidenfrost case.

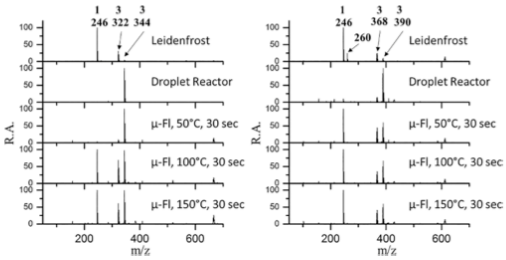

Figure 4. Synthesis of **3** (in two forms) in toluene using chloroacetyl chloride (a) and bromo acetylchloride (b) in Leidenfrost, charged-microdroplets and microfluidics.

The ion *m/z* = 260 is believed to be due to a ring-closure product resulting from acylation. The uncharged Leidenfrost droplets closely mirror the chemistry in microfluidics, except when the temperature in the microfluidics reaction is greatly elevated. Under these circumstances different byproducts are generated as S_N2 becomes more competitive.

The complete synthesis of diazepam in Leidenfrost droplets was demonstrated by adding 7 or 70 equiv. of NH_3 to intermediate **3** (not isolated) in a telescoped reaction. The chloro intermediate was unable to produce diazepam in quantity. However, the bromo intermediate produced diazepam (confirmed by MS/MS) in agreement with a reported flow synthesis.[7]

Conclusions

This study provides evidence for the importance of MS, not only in the traditional sense as an analytical method, but as a fast, predictive means to perform small-scale continuous synthesis. The data encourage the use of spray ionization as a method of screening for successful reaction pathways in flow reactions. At a secondary level, we find some parallels in the favored catalysts, solvents, mol ratios of reagents, and other operating conditions. However, little is known of droplet reaction mechanisms (an important topic in its own right), so extrapolation from conditions that favor reactions in nanodroplets to microfluidic chemistry may not be simple or universal. Nevertheless, as we show in this study, a useful guide to the global aspects of flow chemistry is obtained in these cases.

Limitations in further extending this approach to reaction screening (and to online reaction monitoring) are to be found in the size, cost and complexity of commercial mass spectrometers, many of the features of which are unnecessary for this type of study. What is needed for the purposes described here is a small, portable, unit-resolution, low mass/charge range (to *m/z* = 1000) instrument, which has ambient ionization and tandem mass spectrometry capabilities. A recent review of miniature MS instruments[13] describes a few systems of this type.

Experimental Section

Droplet-Reactor Experiments: These experiments used electrospray ionization (ESI) by spraying the reaction mixture either directly into the MS (Figure 5a) or onto a collection surface (Figure 5b) before taking up the residue in solvent and performing ESI-MS product analysis. Figure 5 illustrates these two options, which are distinguished by the fact that (a) is virtually instantaneous (10–15 s), while (b) can take a few minutes, but (b) is more versatile in that

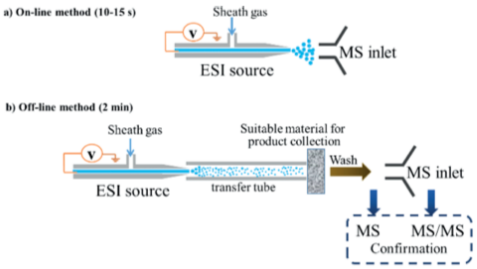

Figure 5. Methods used to perform microdroplet reactions, based on ESI either (a) with online product analysis by MS or (b) with sprayed droplet deposition and subsequent offline MS product analysis.

© 2016 Wiley-VCH Verlag GmbH & Co. KGaA, Weinheim

ChemPubSoc Europe
EurJOC European Journal of Organic Chemistry
Communication

the reaction and analysis occur in separate steps, more product is formed, and the procedure allows temperature and other conditions to be varied and optimized. In both cases, the primary question being asked is whether the desired reaction occurs or not. Products, byproducts and residual reagents were identified from mass spectra recorded at unit resolution, while tandem mass spectrometry (MS/MS) was used to confirm identifications.

Offline-Droplet Reactor: Offline-droplet experiments were performed using a homebuilt electrospray ionization source. In the cases of atropine and diazepam, the reagents were premixed and subjected to offline electrospray at 10 µL/min with +5 kV voltage and 100 psi N_2. For diphenhydramine, reagents were mixed inline using a mixing tee and offline electrospray was performed under the same conditions. After the electrospray deposition was complete, the reaction product was rinsed from the collection surface and then analyzed by nanoESI. Samples were diluted at least 100-fold before analysis in order to quench the reaction and ensure no further reaction could occur during the analysis step. For two-step reactions, the washed material was drawn back into a syringe and mixed with the second-step reagent and then electrosprayed, collected, and washed as before.

Leidenfrost-Droplet Experiments: Reactions in Leidenfrost droplets[5] differ in that these are (i) larger, (ii) net-neutral, and (iii) involve elevated temperatures. Reaction mixtures were added in aliquots over a 2 min period to maintain a constant droplet volume (Figure S7). The droplet (ca. 2 mm diameter) was levitated in a petri dish atop a heater with a surface temperature of 400–500 °C (***CARE!***). Reactions occurred at temperatures close to, but below, the boiling point of the solvent.[14]

Mass Spectrometry: Mass spectral analysis of reaction products was performed using an LTQ ion trap mass spectrometer (Thermo Fisher Scientific, San Jose, CA) with nanoESI ionization. All product samples (spray, Leidenfrost, or flow reactions) were diluted 1:100 into acetonitrile before analysis, unless otherwise noted. The distance between the tip of the spray emitter and ion transfer capillary to the MS was kept constant at ca. 1 mm. Experiments were performed using borosilicate glass pulled to a ca. 1–3 µm aperture. A spray voltage of either positive or negative 2.0 kV was used for all analyses. Positive-ion mode was used for all chemical analyses, unless otherwise noted. Product ion (MS/MS) spectra were recorded using collision-induced dissociation (CID) with a normalized collision energy of 25 (manufacturer's unit).

Synthesis of Diazepam Precursor: Reactions were performed with 100 mM 5-chloro-2-(methylamino)benzophenone and 100 mM 2-haloacetyl chloride (halo = Cl, Br) dissolved in either toluene or acetonitrile. Solutions were either mixed prior to use (droplet reactor, Leidenfrost) or mixed online (microfluidics) to give a final reaction concentration of 50 mM. Other conditions were explored as indicated in the results section.

Diphenhydramine: Reactions were performed in a two-step manner. First, 500 mM benzhydrol was mixed with 500 mM mesyl chloride, then in the second step 20 equiv. of 2-(dimethylamino)ethanol was used in the droplet reactor, while 1 equiv. was used for microfluidics. Other conditions were explored as indicated in the Results section.

Atropine: The atropine intermediate was first synthesized by allowing 1 M phenylacetyl chloride to react with 1 M tropine dissolved in DMA. For the second step, 7 equiv. of base in DMA and 7 equiv. of formaldehyde in H_2O were used. Other conditions were explored as indicated in the Results section.

Microfluidics: Microfludic reactions were performed using a Labtrix S1 system from Chemtrix, Ltd. The Labtrix S1 system is comprised of syringe pumps to deliver reagents, microfluidic chips, a Peltier element, back-pressure regulator, and a collection carousel. For the synthesis of diphenhydramine a homebuilt Peltier-controlled system coupled with the Chemtrix microfluidic platform was used to allow for multi-step reactions to be performed with control over the temperature of each step.

Chemicals and Reagents: All chemicals were purchased from Sigma Aldrich and used without further purification.

Acknowledgments

Support is acknowledged from the Department of Defense: Defense Advanced Research Projects Agency (award no. W911NF-16-2-0020).

Keywords: Kinetics · Mass spectrometry · Reaction acceleration · Flow chemistry · Leidenfrost effect

[1] a) X. Yan, R. M. Bain, R. G. Cooks, *Angew. Chem. Int. Ed.* **2016**, *55*, 12960–12972; *Angew. Chem.* **2016**, *128*, 13152–13156; b) R. M. Bain, C. J. Pulliam, R. G. Cooks, *Chem. Sci.* **2015**, *6*, 397–401; c) R. M. Bain, C. J. Pulliam, S. T. Ayrton, K. Bain, R. G. Cooks, *Rapid Commun. Mass Spectrom.* **2016**, *30*, 1875–1878.
[2] a) J. K. Lee, S. Kim, H. G. Nam, R. N. Zare, *Proc. Natl. Acad. Sci. USA* **2015**, *112*, 3898–3903; b) R. M. Bain, C. J. Pulliam, S. A. Raab, R. G. Cooks, *J. Chem. Educ.* **2016**, *93*, 340–344; c) Y. Li, X. Yan, R. G. Cooks, *Angew. Chem. Int. Ed.* **2016**, *55*, 3433–3437; *Angew. Chem.* **2016**, *128*, 3494.
[3] S. Banerjee, R. N. Zare, *Angew. Chem. Int. Ed.* **2015**, *54*, 14795–14799; *Angew. Chem.* **2015**, *127*, 15008.
[4] C. Josserand, S. T. Thoroddsen, *Annual Rev. Fluid Mechanics* **2016**, *48*, 365–391.
[5] R. M. Bain, C. J. Pulliam, F. Thery, R. G. Cooks, *Angew. Chem. Int. Ed.* **2016**, *55*, 10478–10482; *Angew. Chem.* **2016**, *128*, 10634–10638.
[6] S. Mascia, P. L. Heider, H. Zhang, R. Lakerveld, B. Benyahia, P. I. Barton, R. D. Braatz, C. L. Cooney, J. M. B. Evans, T. F. Jamison, K. F. Jensen, A. S. Myerson, B. L. Trout, *Angew. Chem. Int. Ed.* **2013**, *52*, 12359–12363; *Angew. Chem.* **2013**, *125*, 12585.
[7] A. Adamo, R. L. Beingessner, M. Behnam, J. Chen, T. F. Jamison, K. F. Jensen, J.-C. M. Monbaliu, A. S. Myerson, E. M. Revalor, D. R. Snead, T. Stelzer, N. Weeranoppanant, S. Y. Wong, P. Zhang, *Science* **2016**, *352*, 61–67.
[8] A. Buitrago Santanilla, E. L. Regalado, T. Pereira, M. Shevlin, K. Bateman, L.-C. Campeau, J. Schneeweis, S. Berritt, Z.-C. Shi, P. Nantermet, Y. Liu, R. Helmy, C. J. Welch, P. Vachal, I. W. Davies, T. Cernak, S. D. Dreher, *Science* **2015**, *347*, 49–53.
[9] A. G. Godfrey, T. Masquelin, H. Hemmerle, *Drug Discovery Today* **2013**, *18*, 795–802.
[10] a) H. Song, D. L. Chen, R. F. Ismagilov, *Angew. Chem. Int. Ed.* **2006**, *45*, 7336–7356; *Angew. Chem.* **2006**, *118*, 7494; b) K. Jähnisch, V. Hessel, H. Löwe, M. Baerns, *Angew. Chem. Int. Ed.* **2004**, *43*, 406–446; *Angew. Chem.* **2004**, *116*, 410.
[11] S. C. Gibson, C. S. Feigerle, K. D. Cook, *Anal. Chem.* **2014**, *86*, 464–472.
[12] D. R. Snead, T. F. Jamison, *Chem. Sci.* **2013**, *4*, 2822–2827.
[13] D. T. Snyder, C. J. Pulliam, Z. Ouyang, R. G. Cooks, *Anal. Chem.* **2016**, *88*, 2–29.
[14] R. Abdelaziz, D. Disci-Zayed, M. K. Hedayati, J.-H. Pöhls, A. U. Zillohu, B. Erkartal, V. S. K. Chakravadhanula, V. Duppel, L. Kienle, M. Elbahri, *Nat. Commun.* **2013**, *4*, 2400.

Received: October 10, 2016
Published Online: November 3, 2016

 © 2016 Wiley-VCH Verlag GmbH & Co. KGaA, Weinheim